Effect of Lead-Lag Dynamics on Command Filtered Incremental Adaptive Backstepping

Hingeless Rotorcraft

M.D.C. Arons

Technische Universiteit Delft

TU Delft

This report can be regarded confidential

Front cover: helicopter flying in fjord Norway, taken from https://heliwing.no/en/home/flyfoto-og-film/flyfoto-av-hytta/galleriet/attachment/helikopter-as350-ideell-i-norske-fjell

Effect of Lead-Lag Dynamics on Command Filtered Incremental Adaptive Backstepping

Hingeless Rotorcraft

by

M.D.C. Arons (4306511)

to obtain the degree of Master of Science
at the Delft University of Technology,
to be defended publicly on Friday July 3, 2020 at 10:00 AM.

Student number :	4306511	
Thesis committee:	Dr. ir. M.D. Pavel,	TU Delft, supervisor
	Dr. ir. E. van Kampen,	TU Delft
	Dr. ir. E. Mooij,	TU Delft

An electronic version of this report is available at `http://repository.tudelft.nl/`.

TU Delft

Preface

M.D.C. Arons
Delft, June 2020

First, I would like to express my gratitude to my daily supervisor, Dr. Ir. Marilena Pavel from the faculty of Aerospace Engineering at Delft University of Technology. I am very grateful for being involved in a thesis subject that was both challenging and interesting at the same time. Moreover, I also appreciate our weekly conversations, which were very helpful. Secondly, I also would like to express my gratitude to Dr. Ir. Ping Chu from the faculty of Aerospace Engineering at Delft University of Technology for helping me with advanced flight control. You really managed to let me understand the fundamental aspects related to this topic. Lastly, I also would like to thank my friends and family for their continuous and unconditional support.

Contents

List of Figures

List of Tables

List of Symbols

List of Symbols

Roman Symbol

a	Acceleration	[m/s^2]
a	lift curve slope	[rad$^-$1]
c	Blade cord	[m]
c	Backstepping gain	[-]
C_{l_a}	Lift slope	[rad^{-1}]
c_{d0}	blade profile drag coefficient	[-]
C_T	Thrust coefficient	[-]
d	local blade drag per unit length	[N/m]
D	Helicopter parasite drag	[N]
e	Error	[-]
e	Fraction hinge offset to the rotor radius	[-]
G	Control effectiveness matrix	[-]
f	flat plate drag are	[m^2]
F	System dynamics	[-]
F_β	force per unit length, perpendicular to blade and also perpendicular to direction of rotation	[N/m]
g	Gravitational acceleration	[ms^{-2}]
H	State dynamics	[-]
h	Hub height	[m]
i, j, k	Counter	[-]
I_{bl}	Blade inertia	[kgm^2]
K	Scalar gain	[-]
K_β	Flapping stiffness	[N/m]
K_ζ	Lead-lag stiffness	[N/m]
L,M,N	Moment around x,y,z body axes respectively	[Nm]
L	Total rotor blade length from hinge	[m]
l	Local blade lift per unit length	[N/m]
M_a	Aerodynamic moment on the blade	[Nm]
M_I	Inertial moment on the blade	[Nm]
M_ζ	Lead-lag moment on the blade	[Nm]
M_β	Flapping moment on the blade	[Nm]
M_{bl}	Blade mass	[kg]
m	Blade mass per unit length of rotor blade	[kg/m]
p	roll rate	[rad/s]
Q	Torque	[Nm]
Q_I	Inertial moment	[Nm]
Q_A	Aerodynamic moment	[Nm]
q	Pitch rate	[rad/s]
R	Rotor radius	[m]
r	Rotor element distance w.r.t center of rotation	[m]
r	Yaw rate	[rad/s]
T	Thrust force	[N]
t	Time	[s]
t_s	Sample time	[s]
u,v,w	Velocity components in body axis	[m/s]
u	Control vector	[-]
U	Total velocity of blade section relative to air	[m/s]

U_p	Local perpendicular blade velocity relative to air	[m/s]
U_t	Local tangential blade velocity relative to air	[m/s]
V	Control Lyapunov function	[-]
V	Velocity	[m/s]
x	State vector	[-]
x,y,z	Position	[m]
X, Y,Z	Force components in x,y,z direction respectively	[N]
y	Output vector	[-]
y_r	Signal reference	[-]
z	Altitude	[m]
z_*	Tracking error	[-]
Greek Symbol		
β	Flapping angle	[rad]
γ	Lock number	[-]
γ	Multi-blade coordinates	[-]
ϵ	Hinge offset	[m]
ζ	Damping ratio	[-]
ζ	Lagging angle	[rad]
θ	Pitch angle	[rad]
λ	Inflow ratio	[-]
ν	Virtual control input	[-]
μ	Advance ratio	[-]
ρ	Air density	[kg/m^3]
ϕ	Roll angle	[rad]
σ	Rotor solidity	[-]
τ	Time delay	[-]
ψ	Rotor azimuth	[rad]
ψ	Yaw angle	[rad]
Ω	Rotor speed	[rad/s]
ω	Angular rate vector	[rad/s]
ω_n	Natural frequency	[-]
ω_β	Non-dimensional non-rotating flap frequency	[-]
ω_ζ	Non-dimensional non-rotating lag frequency	[-]

List of Abbreviations

List of Abbreviations

ABS	Adaptive Backstepping
ACAH	Attitude Command/Attitude Hold
AFCS	Automatic Flight Control System
AIAA	American Institute of Aeronautics and Astronautics
BF	Body-Flap
BFL	Body-Flap-Lag
BS	Backstepping
CFBS	Command-Filtered Backstepping
CG	center of gravity
CLF	Control Lyapunov Function
CP	Control Plane
CSER	Center Spring Equivalent Rotor
DOF	Degree of Freedom
EOM	Equations Of Motion
FBL	Feedback Linearisation
FCS	Flight Control System
IABS	Incremental Adaptive Backstepping
IBS	Incremental Backstepping
IO	Input-Output
INDI	Incremental Nonlinear Dynamics Inversion
LHP	Left Half-Plane
MBC	Multi-Blade Coordinates
MIMO	Multiple-Input Multiple-Output
NDI	Nonlinear Dynamics Inversion
P	Proportional
PD	Proportional Derivative
PI	Proportional Integral
PID	Proportional-Integral-Derivative
RHP	Right Half-Plane
RK4	Runge-Kutta 4
RL	Root Locus
RMS	Root Mean Square
RMSE	Root Mean Square Error
ROC	Region of Convergence
SAS	Stability Augmentation System
SCAS	Stability and Control Augmentation System
SISO	Single-Input Single-Output
SP	Shaft Plane
TSS	time-scale separation
VTOL	Vertical Take-Off and Landing

1
Introduction

1.1. Background

Nowadays there is a great desire to design highly augmented rotorcraft with tight stabilisation of all commanded states using robust control systems to meet high performance criteria [36]. This can be regarded as a tedious task, because of the higher-order rotor dynamics by which the rotorcraft is associated with [10–12, 18, 55]. The aforementioned can be regarded as the main point of departure for this research. The necessity of conducting research regarding the effects of higher-order rotor dynamics on control design does find its roots in linear control design. In [3, 9, 10, 40, 44] it was found that rotor dynamics is of great concern when considering high-gain and high-bandwidth linear control systems as they yield a limitation on the allowable design space. In [10] it was found that lead-lag dynamics did have a dominant effect on body rate gain limitations, whereas flapping dynamics did affect body attitude feedback gains. In this research a hingeless rotorcraft with a soft-in-plane rotor system will be considered. In [40] it was mentioned that soft-in-plane rotors are susceptible to inadequate designed linear feedback controllers as they may can trigger the air-resonance mode. This shows that higher-order rotor dynamics should not be overlooked when designing linear control systems. Incorporating linear control strategies can be favourable, because of the ease by which these controllers can be analysed and due to the well-developed linear control methods [53]. However, this does come at cost of depending on local linearisation of the system and being unable of adequately capturing non-linearities in system dynamics or control action [57]. With the advance of control design, non-linear control strategies have become available. The *Lyapunov*-based and *feedback-linearisation* method can be regarded as the two most attractive non-linear control strategies available [1]. With the existence of such control strategies it is a natural choice to investigate whether these are capable of circumventing some of the shortcomings of linear controllers. *Lyapunov*-based controllers are of great interest as these are based upon *Lyapunov* stability concepts such that stability can be easily proven [21, 28, 29].

In this research the main focus shall be on the rate-command/attitude-hold (RCAH) mode, for which the stabilising control law is established by means of IBS, making it less reliant on model knowledge [18, 46, 47, 55]. Such a control strategy would require a first-order *Taylor* series of the angular accelerations and the assumption of TSS to diminish dependency on system dynamics. In [55] it is actually found that the TSS condition is violated, because system dynamics cannot be neglected. In particular the coupling between the angular body dynamics and flapping dynamics is significant. In order to circumvent this problem, the *method of residualised dynamics* [48] was incorporated by van der Goot [55] to diminish state-dependency and increase control-dependency. This would yield a modified control effectiveness, which was substantially greater than the control effectiveness without modification. However, a counter measure was required to account for the difference by which the IBS control law was established, which shall be designated as the *idealised* model, and the *actual* rotorcraft model. The problem lies therein that the feedback of the actuator measurements does see the *idealised* rotorcraft model and the angular acceleration measurements come from the *actual* rotorcraft model. Both are needed in the IBS control law, but do come from different rotorcraft models. This is problematic, because adequate synchronisation of the actuator and angular acceleration measurement is needed to assure adequate closed-loop stability [24, 53, 55, 57]. In [57] it was found that closed-loop stability cannot be assured when actuator and state derivative measurements are not well-synchronised with each other. To be more specific, when the angular acceleration measurement is delayed with respect to the actuator measurement, closed-loop stability will be significantly harmed [57]. This is the main point of concern when establishing the IBS control law using the *method of residualised dynamics*, because it yields an *idealised* rotorcraft model for which rotor dynamics is (partially) not present. This means that the angular acceleration measurements lag behind the actuator measurements, which can harm closed-loop stability. A

rotor synchronisation filter would be required to assure that the difference between the *idealised* and *actual* rotorcraft model is compensated for. This can be regarded as the adaptive nature of the controller, because it changes the feedback of the actuator measurements. In this research "*adaptive*" does therefore refer to the the synchronisation filter. This filter accounts for the delaying nature of rotor dynamics. The main purpose of this filter is to delay the actuator measurements by the same amount by which the angular acceleration measurements are being delayed with due to rotor dynamics and in particular lead-lag and flapping dynamics.

1.2. Research Objectives and Research Questions

In order to perform research, it is deemed necessary to present a main research question and a set of sub-research questions related to the research topic. The research will be conducted on an existing hingeless rotorcraft model from van der Goot [55], therefore the questions provided below are related to this model.

- (MRQ 1) What are the effects of rotor dynamics, and in particular lead-lag and flapping dynamics, on (command-filtered) incremental adaptive backstepping regarding controller robustness, performance and construction when using a hingeless rotorcraft model?
  - (SRQ 1.1) How robust is (command-filtered) incremental adaptive backstepping with and without the inclusion of lead-lag dynamics to the rotor synchronisation filter?
  - (SRQ 1.2) What are the limitations and/or implications on the construction of a (command-filtered) incremental adaptive backstepping controller due to the inclusion of lead-lag dynamics to the rotor synchronisation filter?
  - (SRQ 1.3) Does the inclusion of lead-lag dynamics affect the assumptions used to enable incremental backstepping?
- (MRQ 2) What equivalent rotor blade model shall be incorporated for mimicking elastic rotor blade behaviour of a hingeless rotor?
  - (SRQ 2.2) Is it deemed necessary to account for body-lag coupling to adequately mimic the open-loop frequency response of the angular body rates?
- (MRQ 3) What are the required rotorcraft performance criteria for aggressive agility given a hingeless rotorcraft for near hover and forward flight?

The main research objective of this thesis is:

" *Determining the effects of rotor dynamics, and in particular lead-lag and flapping dynamics, on the robustness, performance and construction of a (command-filtered) incremental adaptive backstepping controller* ***by*** *analysing rotorcraft behaviour using predefined ADS-33E-PRF performance criteria.*".

Answer to MRQ 1 shall be provided in the conclusion of this thesis. Moreover, answer to MRQ 2 shall be provided in Chapter 2 and answer to MRQ 3 shall be given in Chapter 5. It should also be noted that the main focus shall not be on command-filtered incremental adaptive backstepping, but rather on incremental adaptive backstepping. The main rotorcraft model that shall be analysed, incorporates the former control strategy, therefore it is also necessary to account for the command-filters. On the other hand, the adaptive nature by which signal synchronisation is achieved will be of prime concern.

1.3. Thesis outline

This report consists of two parts, in which Part I does present a scientific paper. Moreover, Part II provides fundamental background information about the rotorcraft simulation models used as well as non-linear control design. This part does consists of a set of chapters, which shall be discussed below. In Chapter 2 the main BO-105 helicopter simulation model is provided along with a set of simplified rotorcraft models. The theoretical basis for *Lyapunov*-based control design is provided in Chapter 3. Methods for establishing a modified rotorcraft model from which the controller can be established will be considered in Chapter 4. In Chapter 5 IBS will be applied to the simplified rotorcraft models from Chapter 2. The control modes used by the main rotorcraft model shall be introduced in Chapter 6, with a main focus on the angular rate controller of the rotorcraft. Lastly, the conclusions and recommendations will be provided in chapter 7.

Part I
Scientific Paper

Understanding the Effects of Rotor Dynamics on Incremental Backstepping Control Design

M.D.C. Arons *
Delft University of Technology, 2629HS Delft, The Netherlands

This paper provides fundamental understanding on the effects of rotor dynamics, and in particular flapping and lead-lag dynamics, on incremental backstepping (IBS) control design, performance and robustness. This particular control strategy is being used by the angular rate controller of a rotorcraft. Accounting for rotor dynamics in IBS control design is found to be of great importance to assure that the fundamental assumption pertaining time-scale separation (TSS) is not being violated. This can be realised by making use of an *idealised* rotorcraft model, which is being established by means of the *method of residualised dynamics* that assumes steady-state condition of the rotor dynamics. However, this will yield a difference with respect to the *actual* rotorcraft model, which needs to be accounted for in control design. This can be achieved by means of a so-called rotor synchronisation filter, which assures synchronisation of actuator and angular acceleration measurements. This is needed, because the former does see the *idealised* rotorcraft model, whereas the latter is obtained from the *actual* rotorcraft model. This paper will show that the *method of residualised dynamics* must be applied to flapping dynamics in order to have a well-established IBS control law that is less likely of violating the TSS condition. This is due to the fact that it sufficiently diminishes state-dependency, while substantially increases control-dependency in the first-order *Taylor* series for the angular accelerations. The aforementioned does not hold for lead-lag dynamics, which was also apparent from the insufficient change in controller performance. This shows that the IBS controller with synchronisation filter is robust to uncertainties in lead-lag dynamics.

Nomenclature

Subscripts

CL	=	closed-loop
com	=	commanded
CP and cp	=	control plane
des	=	desired
ideal	=	idealised
interm	=	intermediate
F	=	flap
filt	=	filter
FL	=	flap-lag
max	=	maximum
min	=	minimum
ref	=	reference
res	=	residualised
SP and sp	=	shaft plane
SS	=	steady-state
sync	=	synchronisation

I. Introduction

In this research the main focus shall be on the angular rate controller, for which the stabilising control law is established by means of IBS, making it less reliant on model knowledge [1–4]. IBS requires a first-order *Taylor* series of the

*Graduate student, Control and Simulation Division, Faculty of Aerospace Engineering, Kluyverweg 1, 2629HS Delft, the Netherlands

angular accelerations and the assumption of TSS to diminish dependency on system dynamics. In [4] it is actually found that the TSS condition is violated, because system dynamics cannot be neglected. In particular the coupling between the angular body dynamics and flapping dynamics is significant. In order to account for this problem, the *method of residualised dynamics* [5] was incorporated by van der Goot [3] to diminish state-dependency and increase control-dependency. This would yield a modified control effectiveness matrix, which was substantially greater than the control effectiveness matrix from the original rotorcraft model. However, a counter measure was required to account for the difference by which the IBS control law was established, which shall be designated as the *idealised* model, and the *actual* rotorcraft model. The problem lies therein that the feedback of the actuator measurements does see the *idealised* rotorcraft model, whereas the angular acceleration measurements come from the *actual* rotorcraft model. Both are needed in the IBS control law, but do come from different rotorcraft models. This is problematic, because adequate synchronisation of the actuator and angular acceleration measurement is needed to assure closed-loop stability [3, 6–8]. In [8] it was found that closed-loop stability cannot be assured when actuator and state derivative measurements are not well-synchronised with each other. To be more specific, when the angular acceleration measurement is delayed with respect to the actuator measurement, closed-loop stability will be significantly harmed [8]. This is exactly the main point of concern when establishing the IBS control law using the *method of residualised dynamics*, because it yields an *idealised* rotorcraft model for which rotor dynamics is (partially) not present. This means that angular acceleration measurements will be lagging behind actuator measurements, which can harm closed-loop stability.

In this paper the main focus shall be on understanding the effects of flapping and lead-lag dynamics on IBS control design and robustness. Although, research from van der Goot [3] has shown that a modified control effectiveness and rotor synchronisation filter are required to enable a well-defined IBS controller for controlling the angular rates of the rotorcraft, it is still not yet clear how it affects closed-loop stability and controller robustness. On top of this, van der Goot [3] did also not consider the effects of lead-lag dynamics on IBS control design and robustness. It was therefore a natural choice to consider the effects of lead-lag and flapping dynamics on IBS control design and robustness in more depth. First, in Section II the rotorcraft models used in the research will be provided. There after, in Section III the main crux in control design for rotorcraft control is shortly discussed, where after information about the IBS controller with synchronisation filter is provided. In Section IV the procedure for identifying the effects of rotor dynamics on IBS is outlined. In Section V and VI the results of the analysis are provided for simplified rotorcraft models from Section II. Next to this, in Section VII results of the analysis on the main simulation model are provided. Lastly, in Section VIII a conclusion is given.

II. Rotorcraft models

To assess the effects of rotor dynamics on IBS control design and performance, it will be necessary to establish a well-defined rotorcraft model. In this section a set of simplified first-order body-flap (BF) and body-flap-lag (BFL) models shall be introduced. These models represent the first few instants during the transition from hover to forward flight without building up horizontal speed. First, a first-order BF model shall be introduced, which considers longitudinal flapping and angular body dynamics. There after, four first-order BFL models shall be introduced. These models are established by combining the BFL model proposed by Pavel [9] with the BFL model from Tod et al. [10]. Lastly, the main MBB Bo 105 simulation model from van der Goot [3] shall also be introduced. For a more in-depth explanation of this model, the reader is referred to the work from van der Goot [3] and Simplício et al. [2].

A. First-order body-flap model in hover condition

The first model to be considered is the 2-DOF longitudinal BF model in hover condition with first-order flapping dynamics. The model is associated with a dimensionless parameter that indicates disc-tilt quickness, namely τ_β ($=\frac{16}{\gamma}$), with γ being the lock number. A large value of τ_β indicates slow disc-tilt motion. In Eq. 1 the first-order flap model is provided, wherein β_{1c} represents the longitudinal disc tilt angle [9]. The expression for $\dot{q}$ is provided in Eq. 2, which depends on K_{lon} that is equal to $(\frac{N}{2}K_\beta + Th)/I_{yy}$ (T=W) [9]. The numerator can be identified as the moment exerted on the rotorcraft body per unit flapping angle M_β, which depends on flap centre-spring rotor stiffness K_β, number of rotor blades N, weight W and height h of rotorcraft hub above center of gravity [9]. Body and flapping dynamics can be identified from Fig. 1, wherein the angle between the disc and shaft plane is β_{1c} from Eq. 1 (this angle is not identical to the one provided in Fig. 1, which shows that counterclockwise cyclic control input is associated with clockwise disc-tilt motion). Moreover, Eq. 2 does also directly depend on θ_{1s}, which has been added to the original expression given in [9]. The improtance of the artificial control effectiveness coefficient α_{G_q} shall be considered later on.

$$\dot{\beta}_{1c} = -\frac{\Omega}{\tau_\beta}\beta_{1c} + \frac{16q}{\gamma\tau_\beta} - \frac{\Omega}{\tau_\beta}\theta_{1s} \qquad (1)$$

$$\dot{q} = -\frac{\frac{N}{2}K_\beta + Th}{I_{yy}}\beta_{1c} + \alpha_{G_q}K_{\text{lon}}\theta_{1s} \qquad (2)$$

$$\text{with } 0 \leq \alpha_{G_q} \leq 1$$

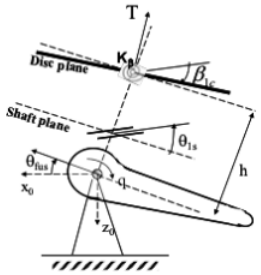

Fig. 1 Rotorcraft transitioning from hover to forward flight [9].

B. First-order body-flap(-lag) rotorcraft models specified in hover condition

Next, a set of BF(L) models shall be introduced, which have been established by combining the BFL model from Tod et al. [10] with the BFL model from Pavel [9]. To be more specific, the BFL model from Pavel [9] has been used with corrections obtained from Tod et al. [10]. The BFL model from Pavel [9] does not account for the coupling between the angular body dynamics and lead-lag dynamics. This means that the body-lag coupling from Tod et al. [10] has been incorporated to account for this discrepancy. The following body-lag term was incorporated: $\boldsymbol{F}_{p,\zeta}$ (=$[F_{p,\zeta_{1c}}\ F_{p,\zeta_{1s}}]$). Moreover, the control-depended term for lead-lag dynamics $\boldsymbol{H}_\zeta$ (= $[H_{\zeta_{1c}}\ H_{\zeta_{1s}}]^T$) was also taken from Tod et al. [10], because it accounts for more main rotor and individual blade parameters, yielding a better estimate of this term. Only lateral body dynamics shall be considered, because the model from Tod et al. [10] does not account for longitudinal body dynamics. Moreover, lead-lag dynamics can also be easier identified from the roll-rate-to-lateral-cyclic transfer function [11, 12]. Lastly, the first-order BFL model from Tod et al. [10] was not considered as main BFL model, because it did not account for flap-roll $\boldsymbol{F}_{\beta,p}$ and lag-roll $\boldsymbol{F}_{\zeta,p}$ coupling. The following BF(L) models will be considered:

I 5-DOF BFL model given in [9] with $\boldsymbol{F}_{p,\zeta}$ and $\boldsymbol{H}_\zeta$ given in [10].
II 3-DOF BF-model given in [9].
III 5-DOF BFL-model given in [9] with $\boldsymbol{H}_\zeta$ given in [10].
IV 5-DOF BFL model given in [9] with $\boldsymbol{F}_{p,\zeta}$ and $\boldsymbol{H}_\zeta$ given in [10] ($\boldsymbol{F}_{\beta,\zeta}$, $\boldsymbol{F}_{\zeta,\beta}$, $\boldsymbol{F}_{p,\zeta}$, $\boldsymbol{H}_\zeta$ being enhanced).

The above mentioned numbering shall be used for identifying the models used in an analysis provided in Section VI. Model III does not account for body-lag coupling ($\boldsymbol{F}_{p,\zeta} = \boldsymbol{0}_{1x2}$). Model IV was established by multiplying the original value of coning angle β_0 with 1.25 as it would also scale $\boldsymbol{F}_{\beta,\zeta}$, $\boldsymbol{F}_{\zeta,\beta}$, $\boldsymbol{F}_{p,\zeta}$ and $\boldsymbol{H}_\zeta$ with that factor. Most importantly $\boldsymbol{F}_{p,\beta}$ does not change when doing the aforementioned, which implies that $\boldsymbol{F}_{p,\zeta}$ becomes relatively greater than this term. Models I,III and IV incorporate two regressive flapping states β_{1c} and β_{1s}, two regressive lead-lag states ζ_{1s} and ζ_{1c} and lateral body states p and ϕ. The flapping states can be identified as the longitudinal and lateral disc-tilt motion respectively. Moreover, ζ_{1s} and ζ_{1c} indicate lateral and longitudinal shift of the rotor center of gravity respectively.

The flap-lag (FL) EOM are provided in Eq. 3 with corresponding matrices in Eq. 4 [9]. After solving Eq. 3, corrective terms will replace the original terms in the EOM. In other words, $F_{p,\zeta_{1c}}$, $F_{p,\zeta_{1s}}$, $H_{\zeta_{1c}}$ and $H_{\zeta_{1s}}$ obtained from [10] shall replace the original coupling and control-depended terms. The expression for roll rate is provided in Eq. 5 [9], with K_{lat} being equal to $(\frac{N}{2}K_\beta + Th)/I_{xx}$ (T=W). Roll angle can be obtained by integrating roll rate.

$$\boldsymbol{C}_{NR}\begin{bmatrix}\dot{\boldsymbol{\beta}}\\ \dot{\boldsymbol{\zeta}}\end{bmatrix} = \Omega\boldsymbol{K}_{NR}\begin{bmatrix}\boldsymbol{\beta}\\ \boldsymbol{\zeta}\end{bmatrix} + \Omega\boldsymbol{F}_{NR}, \quad \text{with } \boldsymbol{\beta} = [\beta_{1c},\ \beta_{1s}]^T \text{ and } \boldsymbol{\zeta} = [\zeta_{1c},\ \zeta_{1s}]^T. \qquad (3)$$

$$\mathbf{C}_{NR} = \begin{bmatrix}-2 & \gamma/8 & 0 & -2\beta_{ss}\\ \gamma/8 & 2 & -2\beta_{ss} & 0\\ 0 & 2\beta_{ss} & -2 & C_\zeta\\ 2\beta_{ss} & 0 & C_\zeta & 2\end{bmatrix},\ \mathbf{K}_{NR} = \begin{bmatrix}\gamma/8 & 1-\lambda_\beta^2 & -2\beta_{ss} & 0\\ 1-\lambda_\beta^2 & -\gamma/8 & 0 & 2\beta_{ss}\\ 2\beta_{ss} & 0 & C_\zeta & 1-\lambda_\zeta^2\\ 0 & -2\beta_{ss} & 1-\lambda_\zeta^2 & -C_\zeta\end{bmatrix} \text{ and } \mathbf{F}_{NR} = \begin{bmatrix}\frac{\gamma}{8}\bar{p} - 2\bar{q} + \frac{\gamma}{8}\theta_{1s}\\ 2\bar{p} + \frac{\gamma}{8}\bar{q} + \frac{\gamma}{8}\theta_{1c}\\ \frac{\gamma}{6}\lambda_i(1-2C_{D1})\theta_{1s}\\ \frac{\gamma}{6}\lambda_i(1-2C_{D1})\theta_{1c}\end{bmatrix} \qquad (4)$$

$$\dot{p} = -\frac{\frac{N}{2}K_\beta + Th}{I_{xx}}\beta_{1s} \qquad (5)$$

Terms $F_{p,\zeta_{1c}}$, $F_{p,\zeta_{1s}}$, $H_{\zeta_{1c}}$ and $H_{\zeta_{1s}}$ given in [10] are a function of: number of blades N, rotor radius R, blade root eccentricity e_{bl}, lock number γ, rotor angular velocity Ω, coning angle β_0 (=β_{ss}), rotor blade static moment m_s, rotor blade inertia I_{bl}, rotor blade mass m_{bl}, lag damper stiffness K_ζ, lead-lag damping coefficient C_ζ, roll inertia I_{xx}, vehicle mass M and height h of rotorcraft hub above center of gravity. More in-depth information regarding the corrective terms can be found in [10]. Next to this, the matrices from Eq. 4 depend on lock number, coning angle, lead-lag damping coefficient, non-dimensional lagging frequency λ_ζ, non-dimensional flapping frequency λ_β, non-dimensional inflow velocity λ_i and drag coefficient C_{D1} (from $C_d = C_{d_0} + C_{d1}\alpha^2$). Lastly, $\bar{p}$ and $\bar{q}$ are equal to p/Ω and q/Ω respectively.

C. Main rotorcraft simulation model of the MBB Bo 105

The main rotorcraft simulation model is a 22-DOF non-linear simulation model including 6-DOF body motion, 6-DOF first and second order flapping dynamics, 6-DOF first and second order lead-lag dynamics, 3-DOF *Pitt-Peters* inflow and 1-DOF quasi-dynamic tail rotor inflow. The 6-DOF lead-lag model was obtained from previous work from Nguyen [13], whereas the remaining part of the simulation model originates from previous work from van der Goot [3]. The simulation model can be divided into a main rotor, tail rotor, fuselage and empennage. In this section, the main focus shall be on the main rotor. For a more in-depth explanation of the simulation model, the reader is referred to the work from van der Goot [3] and Simplício et al. [2].

The main rotor model includes a second-order flapping model, modelled up to the first harmonic of the rotor frequency, with coning β_0, regressive flap and advancing flap modes β_{1s} and β_{1c}. Flapping angles are defined as the angle between shaft and disc plane. The second-order lead-lag model is associated with lead-lag coning ζ_0, regressive lag and advancing lag states ζ_{1s} and ζ_{1c}. The inflow model is a first-order *Pitt-Peters* unsteady model, modelled up to the first harmonic of the rotor frequency. Main rotor forces and moments can be calculated using the approach outlined in [14]. Hub roll and pitch moments given in Eq. 6 and Eq. 7 are modelled as center-spring moments.

$$L_h = -\frac{N}{2} K_\beta \beta_{1s} \tag{6}$$

$$M_h = -\frac{N}{2} K_\beta \beta_{1c} \tag{7}$$

In this research, the main focus is on the angular accelerations of the vehicle, therefore it is of prime concern to have fundamental understanding of the relation between the moments introduced at the hub, as given in Eq. 6 and Eq. 7, and the angular accelerations. In Eq. 8 the expression for the rotational dynamics is provided, wherein the angular accelerations are governed by the applied hub moments and gyroscopic precession [14]. The resistance in control action of the rotorcraft is indicated by $\boldsymbol{J}$, being the moment of inertia tensor.

$$\dot{\boldsymbol{\omega}} = \boldsymbol{J}^{-1} \left(\boldsymbol{M} - \boldsymbol{\omega} \times \boldsymbol{J}\boldsymbol{\omega} \right) \tag{8}$$

From Eq. 8 it can be observed that angular accelerations depend on the total moments $\boldsymbol{M}$ introduced. For roll and pitch accelerations this would mean that dependency on cyclic flapping angles is significant. To be more specific, roll and pitch accelerations would be more governed by cyclic flapping angles than by cyclic control inputs [3]. In the next section, it will be explained that this is the main problem in control design for rotorcraft control. On the other hand, lead-lag dynamics is not accounted for when establishing the forces and moments due to the main rotor, therefore the coupling between angular body dynamics and lead-lag dynamics will be absent. The total state vector is given in Eq. 9.

$$\boldsymbol{X} = [\underbrace{u\ v\ w}_{\boldsymbol{V}}\ \underbrace{x\ y\ z}_{\boldsymbol{P}}\ \underbrace{p\ q\ r}_{\boldsymbol{\omega}}\ \underbrace{\phi\ \theta\ \psi}_{\boldsymbol{\theta}}\ \underbrace{\lambda_{0,\mathrm{mr}}\ \lambda_{1\mathrm{s}}\ \lambda_{1\mathrm{c}}\ \lambda_{0,\mathrm{tr}}}_{\boldsymbol{\lambda}}\ \underbrace{\beta_0\ \beta_{1\mathrm{s}}\ \beta_{1\mathrm{c}}}_{\boldsymbol{\beta}}\ \underbrace{\dot{\beta}_0\ \dot{\beta}_{1\mathrm{s}}\ \dot{\beta}_{1\mathrm{c}}}_{\dot{\boldsymbol{\beta}}}\ \underbrace{\zeta_0\ \zeta_{1\mathrm{c}}\ \zeta_{1\mathrm{s}}}_{\boldsymbol{\zeta}}\ \underbrace{\dot{\zeta}_0\ \dot{\zeta}_{1\mathrm{c}}\ \dot{\zeta}_{1\mathrm{s}}}_{\dot{\boldsymbol{\zeta}}}]^T \tag{9}$$

The body-fixed linear velocity and position in the North-East-Down (NED) reference frame are indicated by $\boldsymbol{V}$ and $\boldsymbol{P}$ respectively. Body angular rates and attitude angles are given by $\boldsymbol{\omega}$ and $\boldsymbol{\theta}$ respectively. Next to this, $\boldsymbol{\lambda}$ contains the non-dimensional inflow components. Vectors $\boldsymbol{\beta}$ and $\dot{\boldsymbol{\beta}}$ contain the flapping angles and flapping derivatives respectively. Lastly, $\boldsymbol{\zeta}$ and $\dot{\boldsymbol{\zeta}}$ are the lead-lag angles and associated derivatives. When linearising the 22-DOF simulation model, the state-space system given in Eq. 10 can be identified. It can be considered a Linear Time-Variant (LTV) system. The BFL model from Nguyen [13] did incorporate a quasi-dynamic inflow model, therefore $\boldsymbol{F}_{\zeta\lambda_{1c}}$, $\boldsymbol{F}_{\zeta\lambda_{1s}}$, $\boldsymbol{F}_{\dot{\zeta}\lambda_{1c}}$ and $\boldsymbol{F}_{\dot{\zeta}\lambda_{1s}}$ are equal to $\boldsymbol{0}_{3x1}$. Moreover, since the current implementation did not take into account the effect of lead-lag dynamics on forces and moments, coupling terms $\boldsymbol{F}_{\omega,\zeta}$ and $\boldsymbol{F}_{\omega,\dot{\zeta}}$ must be equal to $\boldsymbol{0}_{3x3}$. On the other hand, the flap-lag and lag-flap (LF) coupling terms are present in the model. The control vector of the rotorcraft is also given in Eq. 10, which consists of main rotor collective $\theta_{0,\mathrm{mr}}$, longitudinal cyclic θ_{1s}, lateral cyclic θ_{1c} and tail rotor collective $\theta_{0,\mathrm{tr}}$.

$$\dot{\boldsymbol{X}} = \begin{bmatrix} \boldsymbol{F}_{V,V} & \boldsymbol{F}_{V,P} & \boldsymbol{F}_{V,\omega} & \boldsymbol{F}_{V,\theta} & \boldsymbol{F}_{V,\lambda} & \boldsymbol{F}_{V,\beta} & \boldsymbol{F}_{V,\dot{\beta}} & \boldsymbol{F}_{V,\zeta} & \boldsymbol{F}_{V,\dot{\zeta}} \\ \boldsymbol{F}_{P,V} & \boldsymbol{F}_{P,P} & \boldsymbol{F}_{P,\omega} & \boldsymbol{F}_{P,\theta} & \boldsymbol{F}_{P,\lambda} & \boldsymbol{F}_{P,\beta} & \boldsymbol{F}_{P,\dot{\beta}} & \boldsymbol{F}_{P,\zeta} & \boldsymbol{F}_{P,\dot{\zeta}} \\ \boldsymbol{F}_{\omega,V} & \boldsymbol{F}_{\omega,P} & \boldsymbol{F}_{\omega,\omega} & \boldsymbol{F}_{\omega,\theta} & \boldsymbol{F}_{\omega,\lambda} & \boldsymbol{F}_{\omega,\beta} & \boldsymbol{F}_{\omega,\dot{\beta}} & \boldsymbol{F}_{\omega,\zeta} & \boldsymbol{F}_{\omega,\dot{\zeta}} \\ \boldsymbol{F}_{\theta,V} & \boldsymbol{F}_{\theta,P} & \boldsymbol{F}_{\theta,\omega} & \boldsymbol{F}_{\theta,\theta} & \boldsymbol{F}_{\theta,\lambda} & \boldsymbol{F}_{\theta,\beta} & \boldsymbol{F}_{\theta,\dot{\beta}} & \boldsymbol{F}_{\theta,\zeta} & \boldsymbol{F}_{\theta,\dot{\zeta}} \\ \boldsymbol{F}_{\lambda,V} & \boldsymbol{F}_{\lambda,P} & \boldsymbol{F}_{\lambda,\omega} & \boldsymbol{F}_{\lambda,\theta} & \boldsymbol{F}_{\lambda,\lambda} & \boldsymbol{F}_{\lambda,\beta} & \boldsymbol{F}_{\lambda,\dot{\beta}} & \boldsymbol{F}_{\lambda,\zeta} & \boldsymbol{F}_{\lambda,\dot{\zeta}} \\ \boldsymbol{F}_{\beta,V} & \boldsymbol{F}_{\beta,P} & \boldsymbol{F}_{\beta,\omega} & \boldsymbol{F}_{\beta,\theta} & \boldsymbol{F}_{\beta,\lambda} & \boldsymbol{F}_{\beta,\beta} & \boldsymbol{F}_{\beta,\dot{\beta}} & \boldsymbol{F}_{\beta,\zeta} & \boldsymbol{F}_{\beta,\dot{\zeta}} \\ \boldsymbol{F}_{\dot{\beta},V} & \boldsymbol{F}_{\dot{\beta},P} & \boldsymbol{F}_{\dot{\beta},\omega} & \boldsymbol{F}_{\dot{\beta},\theta} & \boldsymbol{F}_{\dot{\beta},\lambda} & \boldsymbol{F}_{\dot{\beta},\beta} & \boldsymbol{F}_{\dot{\beta},\dot{\beta}} & \boldsymbol{F}_{\dot{\beta},\zeta} & \boldsymbol{F}_{\dot{\beta},\dot{\zeta}} \\ \boldsymbol{F}_{\zeta,V} & \boldsymbol{F}_{\zeta,P} & \boldsymbol{F}_{\zeta,\omega} & \boldsymbol{F}_{\zeta,\theta} & \boldsymbol{F}_{\zeta,\lambda} & \boldsymbol{F}_{\zeta,\beta} & \boldsymbol{F}_{\zeta,\dot{\beta}} & \boldsymbol{F}_{\zeta,\zeta} & \boldsymbol{F}_{\zeta,\dot{\zeta}} \\ \boldsymbol{F}_{\dot{\zeta},V} & \boldsymbol{F}_{\dot{\zeta},P} & \boldsymbol{F}_{\dot{\zeta},\omega} & \boldsymbol{F}_{\dot{\zeta},\theta} & \boldsymbol{F}_{\dot{\zeta},\lambda} & \boldsymbol{F}_{\dot{\zeta},\beta} & \boldsymbol{F}_{\dot{\zeta},\dot{\beta}} & \boldsymbol{F}_{\dot{\zeta},\zeta} & \boldsymbol{F}_{\dot{\zeta},\dot{\zeta}} \end{bmatrix} \boldsymbol{X} + \begin{bmatrix} \boldsymbol{H}_V \\ \boldsymbol{H}_P \\ \boldsymbol{H}_\omega \\ \boldsymbol{H}_\theta \\ \boldsymbol{H}_\lambda \\ \boldsymbol{H}_\beta \\ \boldsymbol{H}_{\dot{\beta}} \\ \boldsymbol{H}_\zeta \\ \boldsymbol{H}_{\dot{\zeta}} \end{bmatrix} \boldsymbol{U}, \quad \text{with } \boldsymbol{U} = \begin{bmatrix} \theta_{0,\mathrm{mr}} \\ \theta_{1s} \\ \theta_{1c} \\ \theta_{0,\mathrm{tr}} \end{bmatrix} \tag{10}$$

III. Controlling rotorcraft angular rates using incremental backstepping

In this research the focus shall be on establishing a well-defined angular rate controller using IBS. In order to realise this, it is necessary to determine which methods are available to define a modified control effectiveness such that the TSS condition is less likely violated. First, it will be necessary to shortly touch upon the main crux in control design for rotorcraft control. Next, the methods available for obtaining a modified control effectiveness matrix will be considered. Lastly, the IBS and command filtered IBS (CFIBS) control laws will be provided respectively.

A. Main crux in control design for rotorcraft control

First, the main crux in control design for rotorcraft control shall be considered, which does has its roots in establishing the stabilising control law for the angular rate subsystem. Since the angular rate dynamics of a rotorcraft does depend upon complex aerodynamics, it is a natural choice to consider IBS [1, 3, 4]. A condition to have a well-established IBS control law that is robust to uncertainties in system dynamics, is TSS. This condition is violated when establishing the IBS control law for p and q and shall be demonstrated below. The angular accelerations $\dot{p}$ and $\dot{q}$ ($\dot{\boldsymbol{\omega}}_{pq}$) can be written as

$$\dot{\boldsymbol{\omega}}_{pq} = \boldsymbol{F}_{\omega_{pq}}(\boldsymbol{X}) + \boldsymbol{H}_{\omega_{pq}}(\boldsymbol{X},\boldsymbol{U}), \text{ with } \boldsymbol{F}_{\omega_{pq}}(\boldsymbol{X}) = \boldsymbol{J}^{-1}\left[\boldsymbol{M}(\boldsymbol{X}) - \boldsymbol{\omega}\times\boldsymbol{J}\boldsymbol{\omega}\right] \text{ and } \boldsymbol{H}_{\omega_{pq}}(\boldsymbol{X},\boldsymbol{U}) = \boldsymbol{J}^{-1}\left[\boldsymbol{M}(\boldsymbol{X},\boldsymbol{U})\right], \quad (11)$$

wherein $\boldsymbol{F}_{\omega_{pq}}(\boldsymbol{X})$ and $\boldsymbol{H}_{\omega_{pq}}(\boldsymbol{X},\boldsymbol{U})$ indicate state- and control-dependency of the angular accelerations respectively [1]. A *Taylor* series expansion around a previous point t_0 can be considered for $\dot{\boldsymbol{\omega}}_{pq}$, which is provided in Eq. 12.

$$\dot{\boldsymbol{\omega}}_{pq} = \dot{\boldsymbol{\omega}}_{pq,0} + \underbrace{\left(\frac{\partial \mathbf{F}_{\omega_{pq}}(\boldsymbol{X})}{\partial \mathbf{X}} + \frac{\partial \mathbf{H}_{\omega_{pq}}(\mathbf{X},\mathbf{U})}{\partial \mathbf{X}}\right)\Bigg|_{\substack{\mathbf{X}=\mathbf{X}_0\\ \mathbf{U}=\mathbf{U}_0}}}_{\mathbf{F}_{\omega_{pq},0}} (\mathbf{X}-\mathbf{X}_0) + \underbrace{\frac{\partial \mathbf{H}_{\omega_{pq}}(\mathbf{X},\mathbf{U})}{\partial \mathbf{U}}\Bigg|_{\substack{\mathbf{X}=\mathbf{X}_0\\ \mathbf{U}=\mathbf{U}_0}}}_{\mathbf{H}_{\omega_{pq},0}} (\mathbf{U}-\mathbf{U}_0) + \mathcal{O}\left((\mathbf{X}-\mathbf{X}_0)^2, (\mathbf{U}-\mathbf{U}_0)^2\right) \quad (12)$$

The previous expression can be written into the following simplified form

$$\dot{\boldsymbol{\omega}}_{pq} = \dot{\boldsymbol{\omega}}_{pq,0} + \boldsymbol{F}_{\omega_{pq},0}\Delta\mathbf{X} + \boldsymbol{H}_{\omega_{pq},0}\Delta\mathbf{U} + \mathcal{O}\left(\Delta\mathbf{X}^2, \Delta\mathbf{U}^2\right). \quad (13)$$

The *Taylor* series expansion from Eq. 13 can be simplified by assuming TSS, wherein $\Delta\boldsymbol{X}$ is significantly smaller than $\Delta\boldsymbol{U}$ and state derivative $\Delta\dot{\boldsymbol{X}}$ [1, 15–17]. This would imply that $\Delta\boldsymbol{X}$ and higher-order terms can be omitted from Eq. 13 [1, 15–17], yielding the following first-order *Taylor* series expression

$$\dot{\boldsymbol{\omega}}_{pq} = \dot{\boldsymbol{\omega}}_{pq,0} + \boldsymbol{H}_{\omega_{pq},0}\Delta\mathbf{U}. \quad (14)$$

Arriving at Eq. 14 is important when establishing the IBS control law. If the TSS condition does not hold, increments in system dynamics cannot be neglected. Based on Eq. 11, Eq. 8, Eq. 6 and Eq. 7, it can be stated that there will be large body-flap coupling terms $F_{p,\beta_{1s}}$ and $F_{q,\beta_{1c}}$. From this it follows that $\boldsymbol{F}_{\omega_{pq},0}\Delta\mathbf{X} > \boldsymbol{H}_{\omega_{pq},0}\Delta\mathbf{U}$, yielding violation of the TSS condition. This is the main crux in control design for rotorcraft control and was also pointed out in [4].

B. Control strategies for establishing a well-defined IBS control law for the angular rate subsystem

The *method of residualised dynamics* incorporated by van der Goot [3] and *flapping angle equivalence method* are interesting methods for establishing the control effectiveness of the angular rate subsystem. Both methods opt for defining a modified control effectiveness matrix, such that the TSS condition is less likely violated. The method introduced by Howitt [4] and the method from Simplício [1] are less attractive, because they require measurements of flapping angles and body moments respectively, which cannot be (accurately) measured.

First, the *method of residualised dynamics* will be considered, wherein the objective is to establish an *idealised* model associated with a diminished system and enhanced input matrix. The method does set the derivatives related to the fast modes equal to zero, which implies that these states are continuously at steady-state [5]. The method can be considered for all rotor dynamics. For a BF model with second-order flapping dynamics, this means that $\dot{\boldsymbol{\beta}}$ and $\ddot{\boldsymbol{\beta}}$ are $\mathbf{0}_{3x1}$, leaving only steady-state flapping angles $\boldsymbol{\beta}_{ss}$. The differential equation for flapping dynamics is

$$\ddot{\boldsymbol{\beta}} = \boldsymbol{F}_{\dot{\beta},X_{\text{res}}}\boldsymbol{X}_{\text{res}} + \boldsymbol{F}_{\dot{\beta},\beta}\boldsymbol{\beta} + \boldsymbol{F}_{\dot{\beta},\dot{\beta}}\dot{\boldsymbol{\beta}} + \boldsymbol{H}_{\dot{\beta}}\boldsymbol{U}, \quad (15)$$

wherein $\boldsymbol{X}_{\text{res}} = \left[\boldsymbol{\omega}_{pq}^T, ...\right]^T$ is the residualised state vector, which contains all states except for the flapping states and flapping state derivatives. Setting $\ddot{\boldsymbol{\beta}} = \dot{\boldsymbol{\beta}} = 0$ and rewriting Eq. 15 yields

$$\boldsymbol{\beta}_{ss} = -\boldsymbol{F}_{\dot{\beta},\beta}^{-1}\boldsymbol{F}_{\dot{\beta},X_{\text{res}}}\boldsymbol{X}_{\text{res}} - \boldsymbol{F}_{\dot{\beta},\beta}^{-1}\boldsymbol{H}_{\dot{\beta}}\boldsymbol{U}. \quad (16)$$

This means that the *idealised* model, using the previous expression, can be written as follows

$$\dot{\boldsymbol{X}}_{\text{res}} = \underbrace{\left\{ \boldsymbol{F}_{X_{\text{res}},X_{\text{res}}} - \boldsymbol{F}_{X_{\text{res}},\beta}\boldsymbol{F}^{-1}_{\dot{\beta},\beta}\boldsymbol{F}_{\dot{\beta},X_{\text{res}}} \right\}}_{\text{diminished system matrix}} \boldsymbol{X}_{\text{res}} + \underbrace{\left\{ \boldsymbol{H}_{\text{X}_{\text{res}}} - \boldsymbol{F}_{\text{X}_{\text{res}},\beta}\boldsymbol{F}^{-1}_{\dot{\beta},\beta}\boldsymbol{H}_{\dot{\beta}} \right\}}_{\boldsymbol{G_R}} \boldsymbol{U}. \tag{17}$$

It should be noted that $\boldsymbol{G}_R$ can be identified as the residualised control effectiveness matrix. From this, the control effectiveness matrix for $\dot{\boldsymbol{\omega}}_{pq}$ can be isolated, namely $\boldsymbol{G}_{\omega_{pq},R}$. The method does diminish state-dependency and enhances control-dependency [5]. The validity of the *method of residualised dynamics* greatly depends on whether the *idealised* and *actual* rotorcraft model do have the same natural response (modes of motion/transfer function). A countermeasure is needed to compensate for the difference in *idealised* and *actual* rotorcraft model, which shall be discussed later on.

Next, the *flapping angle equivalence method* shall be considered, which can be regarded a novel approach for establishing $\boldsymbol{G}_{\omega_{pq},R}$. The approach does purely account for the fact that $\dot{\omega}_{pq}$ is primarily governed by cyclic flapping angles, which is generally true [3, 4, 18]. Moreover, it includes a transformation, that transforms cyclic flapping angles into an equivalent form wherein the cyclic control inputs explicitly appear. Rotorcraft models introduced in Section II incorporate flapping models for which the flapping angles are defined between the disc plane and shaft plane. These angles are provided in Fig. 2, wherein reference plane can be identified as the shaft plane and the tip-path plane (TPP) as disc plane. The flapping angles with respect to the shaft plane (sp) can be transformed into flapping angles with respect to the control plane (cp), also known as the no-feathering plane (NFP), and cyclic control inputs. The longitudinal and lateral flapping angle equivalence are provided in Eq. 18 and Eq. 19 respectively [19].

$$\beta_{1c,sp} = \beta_{1c,cp} - \theta_{1s}, \tag{18}$$

$$\beta_{1s,sp} = \beta_{1s,cp} + \theta_{1c}. \tag{19}$$

This transformation holds for a positive *Fourier* series when transforming from the rotating to the non-rotating frame of reference when establishing the flapping EOM (this is equivalent to the Multiblade Coordinate Transformation (MCT)) [19]. The cyclic flapping angles and control inputs can be written into the compact form given below.

$$\boldsymbol{\beta}_{SP} = \boldsymbol{\beta}_{CP} + \boldsymbol{\theta}_{C_F}, \quad \text{with } \boldsymbol{\theta}_{C_F} = [-\theta_{1s}\ \theta_{1c}]^T \ \ \boldsymbol{\beta}_{CP} = [\beta_{1c}\ \beta_{1s}]^T_{co} \text{ and } \boldsymbol{\beta}_{SP} = [\beta_{1c}\ \beta_{1s}]^T_{sp}. \tag{20}$$

(a) Longitudinal flapping angle equivalence. **(b) Lateral flapping angle equivalence.**

Fig. 2 Equivalence between longitudinal and lateral flapping angles with respect to the shaft plane and control plane [19].

In the first expression of Eq. 21 the first-order *Taylor* series for the angular accelerations is provided, which holds for a BF model for which the flapping angles are defined with respect to the shaft plane. In the first expression it can be observed that $\dot{\boldsymbol{\omega}}_{pq}$ does depend on the flapping angles with respect to the shaft plane. In the second expression, it has been transformed into an equivalent form, wherein the cyclic control inputs and flapping angles with respect to the control plane explicitly appear. Moreover, the last term from Eq. 21 is neglected, because $\boldsymbol{F}_{\omega_{pq},\beta_{SP}} >> \boldsymbol{H}_{\omega_{pq}}$. Moreover, $\boldsymbol{F}_{\omega_{pq},\beta_{SP}}$ does primarily depend on K_β, as can be seen from Eq. 6 and Eq. 7, which is generally well-known.

$$\begin{aligned} \dot{\boldsymbol{\omega}}_{pq} &= \dot{\boldsymbol{\omega}}_{pq,0} + \boldsymbol{F}_{\omega_{pq},\beta_{SP}}\Delta\boldsymbol{\beta}_{SP} + \boldsymbol{H}_{\omega_{pq}}\Delta\boldsymbol{\theta}_C \\ &= \dot{\boldsymbol{\omega}}_{pq,0} + \boldsymbol{F}_{\omega_{pq},\beta_{SP}}\Delta\left[\boldsymbol{\theta}_{C_F} + \boldsymbol{\beta}_{CP}\right] \\ &= \dot{\boldsymbol{\omega}}_{pq,0} + \boldsymbol{F}_{\omega_{pq},\beta_{SP}}\Delta\boldsymbol{\beta}_{CP} + \boldsymbol{F}_{\omega_{pq},\beta_{SP}}\Delta\boldsymbol{\theta}_{C_F} \end{aligned} \tag{21}$$

When using Eq. 21 for establishing the IBS control law, it would depend on $\Delta\boldsymbol{\beta}_{CP}$, which is rather small and can therefore be neglected. This means that $\boldsymbol{F}_{\omega_{pq},\beta_{SP}}\Delta\boldsymbol{\beta}_{CP}$ could be obviated from Eq. 21. The approach does therefore assume TSS between flapping and angular body dynamics, because cyclic control inputs have become identical to the rotor disc-tilt angles, which can only happen when neglecting rotor disc-tilt dynamics [20]. Moreover, control effectiveness has been enhanced, which means that the TSS condition will be less likely violated. Moreover, the *flapping angle equivalence method* considers steady-state flapping dynamics, therefore a counter measure will be needed to compensate for the difference in *idealised* and *actual* model.

C. Adjustments to feedback-loop of actuator measurements

A technique called *rotor synchronisation* is required to compensate for the difference in *idealised* and *actual* rotorcraft model. The IBS control law will depend on the feedback of the actuator measurements, which do see the *idealised* model, and the angular acceleration measurements which do come from the *actual* model. The angular acceleration measurements will be delayed with respect to the actuator measurements, because the latter measurements assume steady-state condition of the residualised dynamics. This is problematic, because angular acceleration measurements are used in a negative feedback in the IBS control law, which could yield quicker closed-loop instability [8].

In order to establish the rotor synchronisation filter, it is first necessary to determine the *idealised* and *actual* expressions for $\dot{\boldsymbol{\omega}}_{pq}$. For the derivation only first-order flapping dynamics shall be considered. For flap residualisation, there will be a flap synchronisation filter. The *actual* expression for $\dot{\boldsymbol{\omega}}_{pq}$ is

$$\dot{\boldsymbol{\omega}}_{pq} = \boldsymbol{F}_{\omega_{pq},\beta}\boldsymbol{\beta}_{\text{sync}} + \boldsymbol{H}_{\omega_{pq}}\boldsymbol{\theta}_{C,\text{meas}}, \tag{22}$$

wherein $\boldsymbol{\theta}_{C,\text{meas}}$ are the cyclic actuator measurements after being fed through a second-order washout filter by which the angular accelerations are also being obtained with. This filter shall be discussed later on. Moreover, $\boldsymbol{F}_{\omega_{pq},\beta}$ and $\boldsymbol{H}_{\omega_{pq}}$ are the body-flap coupling and control-depended term of the angular accelerations respectively. The *idealised* rotorcraft model is purely governed by cyclic control inputs, therefore $\dot{\boldsymbol{\omega}}_{pq}$ can be written as

$$\dot{\boldsymbol{\omega}}_{pq} = \boldsymbol{G}_{\omega_{pq},R}\boldsymbol{\theta}_{C,\text{sync}}. \tag{23}$$

It should be noted that $\boldsymbol{G}_{\omega_{pq},R}$ was established by means of the *method of residualised dynamics*, wherein steady-state flapping dynamics was considered. The synchronised control inputs can there after be obtained by inverting Eq. 23 and substituting the expression from Eq. 22 into it. The synchronised cyclic control inputs are

$$\boldsymbol{\theta}_{C,\text{sync}} = \boldsymbol{G}^{-1}_{\omega_{pq},R}\left[\boldsymbol{F}_{\omega_{pq},\beta}\boldsymbol{\beta}_{\text{sync}} + \boldsymbol{H}_{\omega_{pq}}\boldsymbol{\theta}_{C,\text{meas}}\right]. \tag{24}$$

From Eq. 24 it can be observed that $\boldsymbol{\beta}_{\text{sync}}$ is also required, which can be considered the synchronised flapping angles. These synchronised flapping angles will differ from the *actual* flapping angles and can be determined using Eq. 25. It can be observed that $\dot{\boldsymbol{\beta}}_{\text{sync}}$ is purely governed by measured cyclic control inputs.

$$\dot{\boldsymbol{\beta}}_{\text{sync}} = \boldsymbol{F}_{\beta,\beta}\boldsymbol{\beta}_{\text{sync}} + \boldsymbol{H}_{\beta}\boldsymbol{\theta}_{C,\text{meas}}. \tag{25}$$

The synchronisation filter defined in the *Laplace*-domain is provided in Eq. 26.

$$\boldsymbol{H}_{\text{sync}}(s) = \frac{\boldsymbol{\theta}_{C,\text{sync}}(s)}{\boldsymbol{\theta}_{C,\text{meas}}(s)} = \frac{\boldsymbol{G}^{-1}_{\omega_{pq},R}\boldsymbol{F}_{\omega_{pq},\beta}\boldsymbol{H}_{\beta} + \boldsymbol{G}^{-1}_{\omega_{pq},R}\boldsymbol{H}_{\omega_{pq}}s - \boldsymbol{G}^{-1}_{\omega_{pq},R}\boldsymbol{F}_{\beta,\beta}\boldsymbol{H}_{\omega_{pq}}}{s\boldsymbol{I}_{2x2} - \boldsymbol{F}_{\beta,\beta}}. \tag{26}$$

From Eq. 26 it can be observed that model knowledge is required for the synchronisation filter. This shows that when establishing the control effectiveness by means of the *method of residualised dynamics*, there must also be sufficient model knowledge. In Fig. 3 the flapping synchronisation filter is provided.

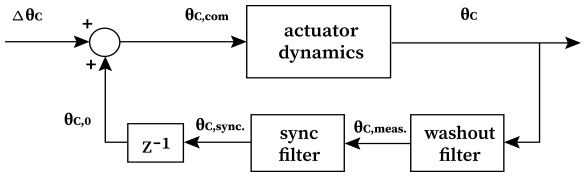

Fig. 3 Synchronisation filter placed in feedback-loop of cyclic actuator measurement.

D. Stabilising control law for angular rate subsystem using standard IBS procedure

Next, it will be of great interest to determine the stabilising control law for the angular rate subsystem. This shall be considered for the main simulation model only, as the stabilising control laws for the simple first-order body-flap(-lag) models shall be considered in the sections that follow here after, which incorporate IBS. On the other hand, the stabilising control law of the angular rate subsystem for the main MBB Bo 105 simulation model was established by means of CFIBS. First the IBS control law for the main simulation model shall be considered. The IBS procedure provided in [15] was followed to derive the stabilising control law. The main objective is to let the angular rates follow a desired angular rate signal. The actual angular rates, desired angular rates, and control input can be identified as

$$\boldsymbol{\omega} = [p, q, r]^T, \quad \boldsymbol{\omega}_{\text{ref}} = [p, q, r]^T_{\text{ref}} \text{ and } \quad \boldsymbol{U} = [\theta_{1s}, \theta_{1c}, \theta_{0,\text{tr}}]^T. \tag{27}$$

It should be noted from Eq. 27 that the vector containing the control inputs differs from the complete control vector of the main rotorcraft model. The control effectiveness based upon the *method of residualised dynamics* shall be used for this derivations and shall be designated as $\boldsymbol{G}_{\omega,R}$. When $\boldsymbol{G}_{\omega,R}$ is associated with uncertainties, then it will be designated as $\hat{\boldsymbol{G}}_{\omega,R}$. In Section VII, the expression for $\hat{\boldsymbol{G}}_{\omega,R}$ will be provided. The stabilising control has been established by making use of a quadratic CLF $\mathcal{V}_\omega(z_\omega)$. The final stabilising control law was obtained by making $\dot{\mathcal{V}}_\omega$ become negative definite along the trajectories of the error dynamics. The stabilising control law is found to be equal to

$$\boldsymbol{U} = \boldsymbol{U}_0 + \hat{\boldsymbol{G}}^{-1}_{\omega,R}\left[-\dot{\boldsymbol{\omega}}_0 - \boldsymbol{c}_\omega \boldsymbol{z}_\omega + \dot{\boldsymbol{\omega}}_{\text{ref}}\right], \tag{28}$$

wherein z_ω, $\dot{\omega}_0$ and $\boldsymbol{c}_\omega$ are the tracking error, angular acceleration measurements and IBS gain respectively. The stabilising control law would yield the following expression for $\dot{\mathcal{V}}_\omega$

$$\dot{\mathcal{V}}_\omega = -\boldsymbol{z}^T_\omega \boldsymbol{c}_\omega \boldsymbol{z}_\omega. \tag{29}$$

Equilibrium $z_\omega = \boldsymbol{0}_{3x1}$ is globally uniformly asymptotically stable when $\boldsymbol{c}_\omega > \boldsymbol{0}_{3x3}$, such that the desired angular rates $\boldsymbol{\omega}_{\text{ref}}$ can be tracked for time going to infinity. This is in accordance with the theorem of *LaSalle-Yoshizawa* [21].

E. Command-filtered IBS approach for imposing limits on commanded signals

The CFIBS procedure provided in [15] was incorporated to derive the stabilising control law and to proof stability. Instead of directly applying the previous stabilising control law, a new raw reference signal could be defined and led through a command filter. This will enable to impose rate, magnitude and bandwidth limitations on a raw reference signal $\boldsymbol{U}^0$, yielding command $\boldsymbol{U}$ and command derivative $\dot{\boldsymbol{U}}$. Since an incremental-based control strategy is being adopted for the angular rate subsystem, it is necessary to apply the command filter to the total raw reference signal in order to limit sensitivity to delays [15]. The effect of the command filter on z_ω is estimated by means of a stable linear filter $\dot{\boldsymbol{\chi}}_\omega$ given in Eq. 30 [15]. Moreover, the compensated tracking errors used for the derivation are also provided in Eq. 30. The second-order command filter with initial condition from Eq. 31 will be incorporated.

$$\dot{\boldsymbol{\chi}}_\omega = -\boldsymbol{c}_\omega \boldsymbol{\chi}_\omega + \hat{\boldsymbol{G}}_{\omega,R}(\boldsymbol{U} - \boldsymbol{U}^0), \quad \text{with} \quad \bar{z}_\omega = z_\omega - \boldsymbol{\chi}_\omega \tag{30}$$

$$\begin{bmatrix} \dot{\boldsymbol{U}} \\ \ddot{\boldsymbol{U}} \end{bmatrix} = \begin{bmatrix} \dot{\boldsymbol{U}} \\ 2\zeta\omega_n\left(\boldsymbol{S}_R\left\{\frac{\omega_n^2}{2\zeta\omega_n}\left[\boldsymbol{S}_M\left(\boldsymbol{U}^0\right) - \boldsymbol{U}\right]\right\} - \dot{\boldsymbol{U}}\right) \end{bmatrix}, \quad \text{with} \quad \begin{matrix} \boldsymbol{U}(0) = \boldsymbol{U}\left(z_\omega(0)\right) \\ \dot{\boldsymbol{U}}(0) = 0 \end{matrix} \tag{31}$$

The filter is characterised with damping ratio ζ_n (= 1) and natural frequency ω_n (= 100 rad/s). Magnitude and rate limitations are given in Eq. 32 and Eq. 33 respectively (see Table 8 for limits).

$$\boldsymbol{S}_M(\boldsymbol{U}^0) = \begin{cases} \boldsymbol{U}_{\max} & \text{if} \quad \boldsymbol{U}^0 \geq \boldsymbol{U}_{\max} \\ \boldsymbol{U}^0 & \text{if} \quad \boldsymbol{U}_{\min} < \boldsymbol{U}^0 < \boldsymbol{U}_{\max} \\ \boldsymbol{U}_{\min} & \text{if} \quad \boldsymbol{U}^0 \leq \boldsymbol{U}_{\min} \end{cases} \tag{32}$$

$$\boldsymbol{S}_R\left[\left(\frac{\omega_n^2}{2\zeta\omega_n}\right)\left(\boldsymbol{S}_M\left(\boldsymbol{U}^0\right) - \boldsymbol{U}\right)\right] = \begin{cases} \dot{\boldsymbol{U}}_{\max} & \text{if} \quad \dot{\boldsymbol{U}}^0 \geq \dot{\boldsymbol{U}}_{\max} \\ \dot{\boldsymbol{U}}^0 & \text{if} \quad \dot{\boldsymbol{U}}_{\min} < \dot{\boldsymbol{U}}^0 < \dot{\boldsymbol{U}}_{\max} \\ \dot{\boldsymbol{U}}_{\min} & \text{if} \quad \dot{\boldsymbol{U}}^0 \leq \dot{\boldsymbol{U}}_{\min} \end{cases} \tag{33}$$

The stabilising control law will make the derivative of the quadratic CLF $\dot{\mathcal{V}}_\omega$ negative definite along the trajectories of the compensated tracking errors. The final expression for $\dot{\mathcal{V}}_\omega$ is given in Eq. 34 when making use of Eq. 28.

$$\dot{\mathcal{V}}_\omega = -\bar{\boldsymbol{z}}^T_\omega \boldsymbol{c}_\omega \bar{\boldsymbol{z}}_\Omega \tag{34}$$

In accordance with the theorem of *LaSalle-Yoshizawa*, equilibrium $\bar{\boldsymbol{z}}_\Omega = \boldsymbol{0}_{3x1}$ can be regarded uniformly asymptotically stable for time going to infinity [21]. In Fig. 4 the angular rate control mode is provided with synchronisation filter and washout filter. For CFIBS, it should be augmented with command-filters in the appropriate place.

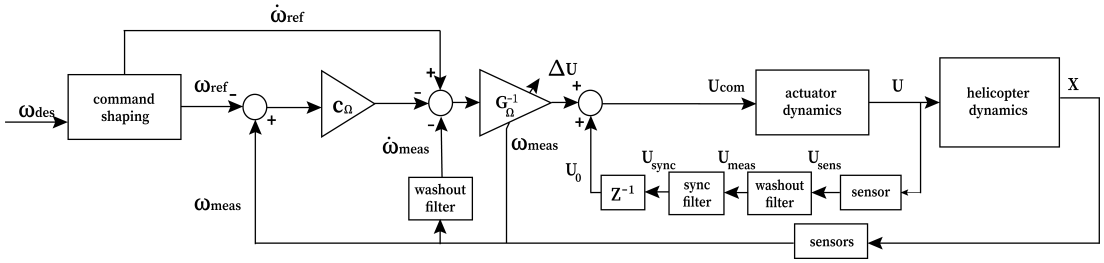

Fig. 4 Angular rate subsystem based on IBS with synchronisation and washout filter.

F. Actuator and sensor dynamics

Having established the (CF)IBS control law, it is also necessary to define the dynamics of the actuators and sensors. All models incorporate the same sensors and actuator dynamics. Moreover, sensor and actuator dynamics shall be the same for all angular rates and control inputs of the main MBB Bo 105 simulation model. The expression for the actuator dynamics is provided in Eq. 35, wherein τ_{act} is equal to 0.1 s [3]. Angular accelerations can be obtained using the second-order washout filter provided in Eq. 36 [3]. This filter characterised with damping ratio ζ_{filt}, natural frequency $\omega_{\text{n,filt}}$ and zero-mean noise signal $\mathcal{N}\left(0, \sigma^2_{\text{filt}}\right)$, which were set equal to 1, 100 rad/s and $0.006°/s$ respectively [3].

$$H_{\text{act}}(s) = \frac{1}{\tau_{\text{act}} s + 1} \tag{35}$$

$$\dot{\boldsymbol{\omega}}_{\text{meas}} = s\boldsymbol{H}_{\text{filt}}(s)\left(\boldsymbol{\omega} + \mathcal{N}(0, \sigma^2_{\text{filt}})\right) = \frac{\boldsymbol{\omega}^2_{n,\text{filt}} s}{s^2 + 2\zeta_{\text{filt}}\omega_{n,\text{filt}} s + \omega^2_{n,\text{filt}}}\left(\boldsymbol{\omega} + \mathcal{N}(0, \sigma^2_{\text{filt}})\right) \tag{36}$$

IV. Procedure for identifying the effects of rotor dynamics on IBS

In order to understand the effects of rotor dynamics on IBS, and in particular the angular rate controller, it will be necessary to outline the main procedure for determining this. The complete analysis shall be considered for all models introduced in Section II with the exception of the main MBB Bo 105 simulation model. For the latter model, a separate robustness analysis shall be considered, which is explained in more detail in Section VII.

The first step is to to identify the difference between the *idealised* and *actual* rotorcraft model, by considering the modes of motion and open-loop frequency response without the controller for both models. The next step is to establish the first-order *Taylor* series based upon the *idealised* and *actual* rotorcraft model. From this, the IBS control law and TSS condition can be defined. Important to understand is that, when the *idealised* and *actual* modes of motion and open-loop frequency significantly differ from each other, a counter measure must be considered. The counter measure will come in the form of a rotor synchronisation filter, for which the frequency response must be analysed. Next, a tracking task shall be executed, wherein tracking performance will be correlated with adequate synchronisation of actuator and angular acceleration measurements. On top of this, the effects of having a modified control effectiveness matrix, using the the *idealised* rotorcraft model, on tracking performance shall also be considered. The performance can be determined using the Root Mean Square Error (RMSE), for which the expression is provided in Eq. 37. Herein, ϵ_j is the residual, which is the difference between the target value and actual value of an angular rate (e.g. p_{ref} and p). Moreover, n is the number of residuals.

$$RMSE = \sqrt{\frac{\sum_{j=1}^{n}\left(\epsilon_j\right)^2}{n}} \tag{37}$$

There after, the closed-loop frequency response shall be considered, wherein actuator and sensor dynamics will be accounted for. Important points of interest are the bandwidth and resonance peak of the closed-loop frequency response. Below, the procedure is summarised, for which a closed-loop system is considered for steps IV, V and VI with (CF)IBS controller, actuator and sensor dynamics.

I identifying the difference between *idealised* and *actual* rotorcraft model, by considering the modes of motion and open-loop frequency response.

II determine the TSS condition and IBS control law for the *idealised* and *actual* rotorcraft model.

III assess the frequency response of the rotor synchronisation filter.

IV analyse controller performance by incorporating an ADS-33E-PRF tracking task for aggressive agility given in [22] and using the performance criteria from Eq. 37. Reference signal is generated by means of three hyperbolic tangent functions. Moreover, simulations are performed using fourth order Runge-Kutta (RK4) integration at 100 Hz. Likewise, the (CF)IBS controller operates at 100 Hz.

V analyse closed-loop frequency behaviour, given it is stable, by considering bandwidth, resonance peak etc.

VI analyse closed-loop stability using the *Routh-Hurwitz* stability criterion. Closed-loop system is asymptotically stable if and only when real parts of the closed-loop eigenvalues are situated in the left-half-plane (LHP) [23].

V. Analysing the effects of flapping dynamics on IBS using first-order BF model

In this section, the effects of flapping dynamics on IBS shall be considered. Use is made of the first-order BF model described by Eq. 1 and Eq. 2. Moreover, the MBB Bo 105 rotorcraft is used for the analysis, for which data has been

provided in the Appendix. First, the difference in *idealised* and *actual* rotorcraft model shall be determined by means of the modes of motion and open-loop frequency response. There after, synchronisation filter frequency response shall be touched upon. Lastly, tracking performance will be assessed along with closed-loop frequency response.

A. Modes of motion for varying K_β and τ_β

First, the modes of motion of the τ_β-based model without controller will be considered for the *idealised* and *actual* BF model, wherein the former was obtained by means of the *method of residualised dynamics*. The modes of motion for the *actual* rotorcraft model are situated at

$$\lambda_{1,2} = -\frac{\Omega}{2\tau_\beta} \pm \sqrt{\frac{1}{4}\left(\frac{\Omega}{\tau_\beta}\right)^2 - \frac{16K_{\text{lon}}}{\gamma\tau_\beta}} \tag{38}$$

and will couple for $\tau_\beta K_{\text{lon}} > \frac{\gamma\Omega^2}{64}$. The *idealised* pitch mode of motion is decoupled from flapping and situated at $-\frac{16K_{\text{lon}}}{\gamma\Omega}$. In Fig. 5 the modes of motion for the *idealised* and the *actual* model are provided for two instances of τ_β and $K_\beta \in [10, 30, ..., 150]$ kNm/rad. It can be observed that the modes of motion for the *idealised* and *actual* rotorcraft model differ for large τ_β, therefore the dynamic response of q will be different for both models.

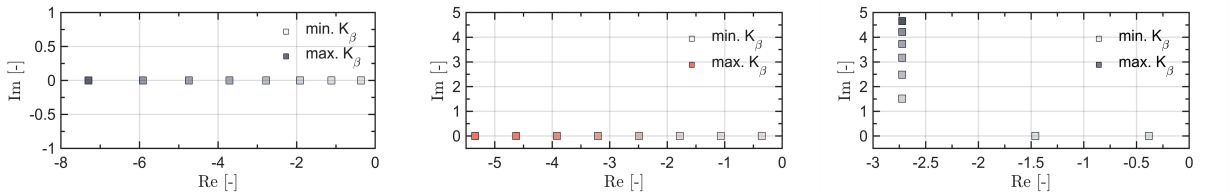

(a) *Actual* for τ_β = 1.0. **(b) *Idealised*.** **(c) *Actual* for τ_β = 5.0.**

Fig. 5 Modes of motion of *actual* (coupled pitch-flap) and *idealised* (decoupled pitch) rotorcraft model.

B. Open-loop Frequency response of angular body dynamics

Before assessing the effects of rotor dynamics on control design, it is necessary to consider the angular body dynamics without controller. The transfer function in standard *Bode* form for $\alpha_{G_q} = 0$ is provided in Eq. 39.

$$H_q(s) = \frac{\left(\frac{\gamma\Omega}{16}\right)}{\left(\frac{\gamma\tau_\beta}{16K_{\text{lon}}}s^2 + \frac{\Omega\gamma}{16K_{\text{lon}}}s + 1\right)} \tag{39}$$

In Fig. 6 the frequency response of $H_q(s)$ is provided for varying τ_β, three instances of K_β and $\alpha_{G_q} = 0$. It can be observed that for smaller τ_β the difference in frequency response between *idealised* (steady-state, $\tau_\beta = 0$) and *actual* model becomes less. This is in line with expectation as decreasing τ_β does yield quicker disc-tilt response. Moreover, adjusting K_β did not influence the difference between *actual* and *idealised* rotorcraft model.

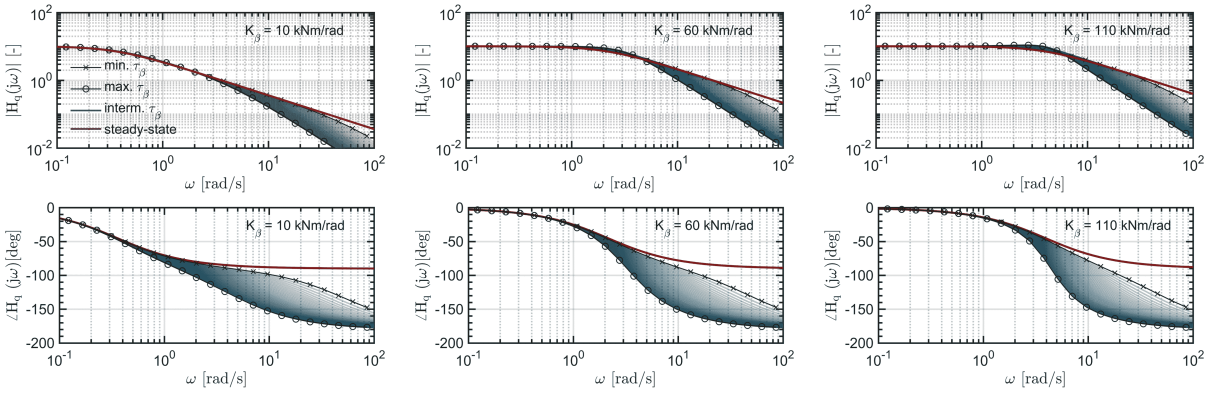

Fig. 6 *Bode* frequency response of $H_q(s)$ for $\tau_\beta \in [0.5, 0.6, ..., 5.5]$, $K_\beta \in [10, 60, 110]$ kNm/rad and α_{G_q} = 0.

C. Control effectiveness established using flapping angle equivalence method or method of residualised dynamics

The control effectiveness using the *flapping angle equivalence method* only requires knowledge of $F_{q,\beta_{1c}}$, which is $-K_{\text{lon}}$, and the IBC to MBC transformation. Since a positive *Fourier* series was incorporated for establishing the body-flap EOM ($\beta_{1c_{SP}} = \beta_{1c_{CP}} - \theta_{1s}$), the control effectiveness G_q must be equal to K_{lon}. Using the *method of residualised dynamics*, the control effectiveness must be equal to the following

$$G_q = H_q - F_{q,\beta_{1c}} F^{-1}_{\beta_{1c},\beta_{1c}} H_{\beta_{1c}} = \alpha_{G_q} K_{\text{lon}} - -K_{\text{lon}} \cdot -\frac{\tau_\beta}{\Omega} \cdot -\frac{\Omega}{\tau_\beta} = K_{\text{lon}} \left(1 + \alpha_{G_q}\right). \tag{40}$$

It can be observed from Eq. 40 that G_q is approximately the same as the control effectiveness when using the *flapping angle equivalence method*. For the proceeding analysis it will be assumed that there is inaccurate knowledge of control effectiveness, which implies that $\hat{G}_q = \gamma_q G_q$, wherein γ_q is the control effectiveness mismatch factor.

D. Stabilising control law for angular rate subsystem using IBS

A *Taylor* series must be used for defining the control law. The first-order *Taylor* series for the *idealised* model based upon the *method of residualised dynamics* and *actual* rotorcraft model are given in Eq. 41 and Eq. 42 respectively.

$$\begin{aligned}
\dot{q} &\cong \dot{q}_0 + F_{q,\beta_{1c}} \Delta\beta_{1c} + \left(F_{q,q} - F_{q,\beta_{1c}} F^{-1}_{\beta_{1c},\beta_{1c}} F_{\beta_{1c},q}\right) \Delta q + \left(H_q - F_{q,\beta_{1c}} F^{-1}_{\beta_{1c},\beta_{1c}} H_{\beta_{1c}}\right) \Delta\theta_{1s} \\
&\cong \dot{q}_0 + 0 \cdot \Delta\beta_{1c} + \left(0 - -K_{\text{lon}} \cdot -\frac{\tau_\beta}{\Omega} \cdot \frac{16}{\gamma\tau_\beta}\right) \Delta q + \left(\alpha_{G_q} K_{\text{lon}} - -K_{\text{lon}} \cdot -\frac{\tau_\beta}{\Omega} \cdot -\frac{\Omega}{\tau_\beta}\right) \Delta\theta_{1s} \\
&\cong \dot{q}_0 - \frac{16}{\gamma\Omega} K_{\text{lon}} \Delta q + (1 + \alpha_{G_q}) K_{\text{lon}} \Delta\theta_{1s}
\end{aligned} \tag{41}$$

$$\begin{aligned}
\dot{q} &\cong \dot{q}_0 + F_{q,\beta_{1c}} \Delta\beta_{1c} + F_{q,q} \Delta q + H_q \Delta\theta_{1s} \\
&\cong \dot{q}_0 - K_{\text{lon}} \Delta\beta_{1c} + \alpha_{G_q} K_{\text{lon}} \Delta\theta_{1s}
\end{aligned} \tag{42}$$

Current pitch rate derivative and longitudinal cyclic control input are indicated by $\dot{q}_0$ and $\theta_{1s,0}$ respectively. Moreover, Δq, $\Delta\beta_{1c}$ and $\Delta\theta_{1s}$ are the incremental change in pitch rate, cyclic flapping angle and control input respectively. The first-order *Taylor* can neglect state-depended terms by assuming TSS [1, 15–17], for which the necessary condition is

$$\text{TSS condition for idealised Taylor series}: \quad (1 + \alpha_{G_q}) K_{\text{lon}} \Delta\theta_{1s} >> -\frac{16}{\gamma\Omega} K_{\text{lon}} \Delta q, \tag{43}$$

$$\text{TSS condition for actual Taylor series}: \quad \alpha_{G_q} K_{\text{lon}} \Delta\theta_{1s} >> -K_{\text{lon}} \Delta\beta_{1c}, \tag{44}$$

which is equivalent by assuming instantaneous control action given that sampling rate f_s is sufficiently high [15]. When Eq. 43 and Eq. 44 hold, then it will be robust to uncertainties in system dynamics. It can be observed that the TSS condition for the *idealised Taylor* series will hold, since $\gamma\Omega >> 16$. On the other hand, the TSS condition for the *actual Taylor* series will be violated as $\alpha_{G_q} << 1$. The following stabilising control law shall be used

$$\theta_{1s} = \theta_{1s,0} + \hat{G}_q^{-1} \left[-\dot{q}_0 + \dot{q}_{\text{ref}} - c_q z_q\right]. \tag{45}$$

E. Flapping synchronisation filter for synchronising actuator and angular rate derivative measurements

The Flapping synchronisation shall first be introduced in the time-domain, there after in the *Laplace*-domain. The expression for the synchronised control input and flapping angle are given in Eq. 46 and Eq. 47 respectively.

$$\left.\begin{aligned}
\dot{q} &= \hat{G}_q \theta_{1s,\text{sync}} \\
\dot{q} &= F_{q,\beta_{1c}} \beta_{1c,\text{sync}} + H_q \theta_{1s,\text{meas}}
\end{aligned}\right\} \quad \theta_{1s,\text{sync}} = \hat{G}_q^{-1} F_{q,\beta_{1c}} \beta_{1c,\text{sync}} + \hat{G}_q^{-1} H_q \theta_{1s,\text{meas}} \tag{46}$$

$$\dot{\beta}_{1c,\text{sync}} = F_{\beta_{1c},\beta_{1c}} \beta_{1c,\text{sync}} + H_{\beta_{1c}} \theta_{1s,\text{meas}} \tag{47}$$

The synchronisation filter can be written into the following state-space system

$$\begin{bmatrix} \dot{\beta}_{1c,\text{sync}} \\ \theta_{1s,\text{sync}} \end{bmatrix} = \begin{bmatrix} -\frac{\Omega}{\tau_\beta} \\ \gamma_q (K_{\text{lon}} + \alpha_{G_q} K_{\text{lon}})^{-1} \cdot -K_{\text{lon}} \end{bmatrix} \beta_{1c,\text{sync}} + \begin{bmatrix} -\frac{\Omega}{\tau_\beta} \\ \gamma_q (K_{\text{lon}} + \alpha_{G_q} K_{\text{lon}})^{-1} \cdot \alpha_{G_q} K_{\text{lon}} \end{bmatrix} \theta_{1s,\text{meas}}, \tag{48}$$

wherein $\theta_{1s,\text{meas}}$ and $\beta_{1c,\text{sync}}$ are the measured control input (fed through a second-order washout filter) and synchronised flapping angle respectively. Moreover, Eq. 48 does not depend on K_β, which confirms that the difference between *idealised* and *actual* models is not due to K_β. The transfer function for the flapping synchronisation filter is provided in Eq. 49 and Eq. 50 for $\alpha_{G_q} \neq 0$ and $\alpha_{G_q} = 0$ respectively.

$$H_{\text{sync}}(s) = \frac{\theta_{1s,\text{sync}}(s)}{\theta_{1s,\text{meas}}(s)} = \gamma_q^{-1}\left(1+\alpha_{G_q}\right)\frac{\left(1+\frac{\alpha_{G_q}\tau_\beta}{\Omega}\left(1+\alpha_{G_q}\right)^{-1}s\right)}{\left(\frac{\tau_\beta}{\Omega}s+1\right)} \tag{49}$$

$$H_{\text{sync}}(s) = \frac{\theta_{1s,\text{sync}}(s)}{\theta_{1s,\text{meas}}(s)} = \left(\gamma_q^{-1}\right)\frac{1}{\left(\frac{\tau_\beta}{\Omega}s+1\right)} \tag{50}$$

Of great interest are the effects of changes in γ_q, τ_β and α_{G_q} on synchronisation filter frequency response. In Fig. 7 the results are provided for different variations in α_{G_q}, γ_q and τ_β.

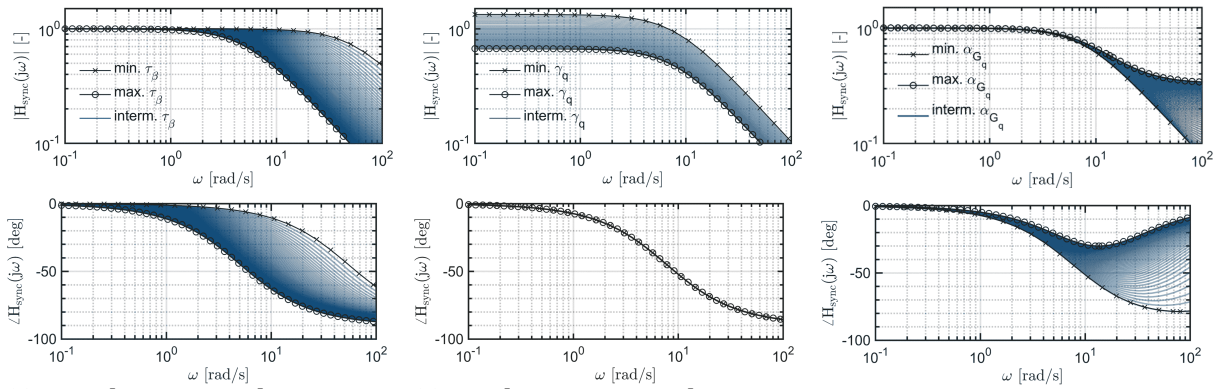

(a) $\tau_\beta \in [0.5, 0.6, ..., 5.5]$, $\gamma_q = 1$ **and** $\alpha_{G_q} = 0$. **(b)** $\gamma_q \in [0.75, 0.76, ..., 1.25]$, $\tau_\beta = 3$ **and** $\alpha_{G_q} = 0$. **(c)** $\alpha_{G_q} \in [0.0, 0.025, ..., 0.5]$, $\tau_\beta = 3$ **and** $\gamma_q = 1$.

Fig. 7 Frequency response of flapping synchronisation filter of τ_β-based rotorcraft model for varying τ_β, γ_q and α_{G_q}. Synchronisation filters from Eq. 49 and Eq. 50 are incorporated for assessing these changes.

Based on the results of the rotor synchronisation frequency analysis the following can be stated

- increasing τ_β will decrease rotor synchronisation filter bandwidth such that $\theta_{1s,\text{meas}}$ will be slowed down more. This shows that when the difference between the *idealised* and *actual* model increases, the feedback of the actuator measurement must be slowed down more to match the feedback of the angular acceleration measurement.
- γ_q^{-1} does act as a pure gain and will therefore affect magnitude response. Control effectiveness under- or overestimation will be associated with magnified and diminished control inputs respectively.
- greater α_{G_q} will be associated with greater magnitude at higher frequencies, which implies that $\theta_{1s,\text{meas}}$ will be less delayed. This is because $\dot{q}$ will be increasingly more directly governed by θ_{1s}, while the indirect channel ($\theta_{1s} \rightarrow \beta_{1c} \rightarrow \dot{q}$) remains the same.

F. Longitudinal ADS-33E-PRF tracking task for varying τ_β

Previously, the design of the controller was already touched upon, therefore the next step is to assess controller robustness. The necessity of incorporating an enhanced control effectiveness and adequate synchronisation of actuator and angular acceleration measurement will be of prime concern. In order to assess the above mentioned, it will be necessary to determine IBS controller performance with and without rotor synchronisation filter. A longitudinal tracking task will be executed in accordance with the regulations stipulated by the ADS-33E-PRF for aggressive agility [22]. This means that the rotorcraft shall reach a pitch rate of $\pm 30^\circ/s$. For all cases the following will hold: $\tau_\beta \in [0.5, 1.0, ..., 5.5]$ and $\alpha_{G_q} = 0$. The cases of interest are:

- **case 1**: without flapping synchronisation filter, $\hat{G}_q$ based on *method of residualised dynamics* with $y_q = 1$ and $c_q = 2.5$. This is equivalent to the Reduced inverse of control effectiveness matrix INDI (RINDI) method introduced in [24].
- **case 2**: with flapping synchronisation filter, $\hat{G}_q$ based on *method of residualised dynamics* with $y_q = 1$ for $\hat{G}_q$ of IBS control law and synchronisation filter and $c_q = 15$.
- **case 3**: with flapping synchronisation filter, $\hat{G}_q$ based on *method of residualised dynamics*, $y_q = 0.75$ for $\hat{G}_q$ of synchronisation filter, $\gamma_q = 1$ for $\hat{G}_q$ of IBS control law and $c_q = 10$.

In Fig. 8 the results of case 1 are provided, from which it can be observed that the increments in system dynamics $(F_{q,q} - F_{q,\beta_{1c}} F^{-1}_{\beta_{1c},\beta_{1c}} F_{\beta_{1c},q})\Delta q$ are less than the control-depended increments $(H_q - F_{q,\beta_{1c}} F^{-1}_{\beta_{1c},\beta_{1c}} H_{\beta_{1c}})\Delta\theta_{1s}$. However, tracking response is not desirable since it is quiet erratic. Moreover, $RMSE_q$ increases when τ_β increases.

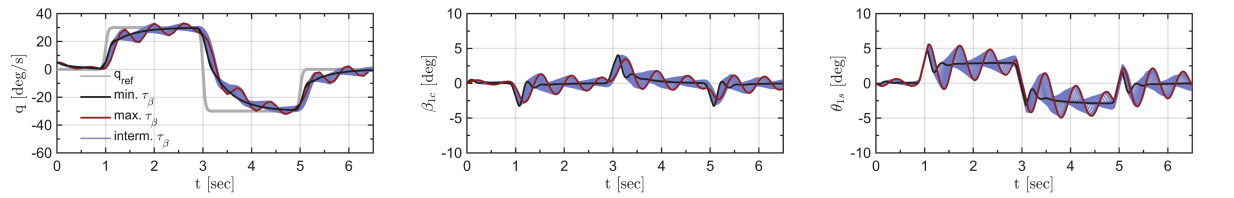

(a) Rotorcraft states q and β_{1c} along with cyclic control input θ_{1s}.

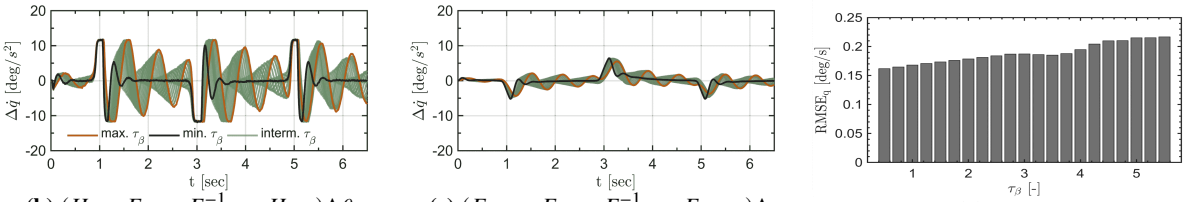

(b) $(H_q - F_{q,\beta_{1c}} F^{-1}_{\beta_{1c},\beta_{1c}} H_{\beta_{1c}})\Delta\theta_{1s}$ **(c)** $(F_{q,q} - F_{q,\beta_{1c}} F^{-1}_{\beta_{1c},\beta_{1c}} F_{\beta_{1c},q})\Delta q$ **(d)** $RMSE_q$

Fig. 8 Results of longitudinal tracking task of case 1. Effects of τ_β on tracking performance is being analysed for $\alpha_{G_q} = 0$, $\tau_\beta \in [0.5, 1.0, ..., 5.5]$, $c_q = 2.5$ and $\gamma_q = 1$ for $\hat{G}_q$ of IBS control law

The previous IBS controller did not yield the desired performance even though TSS condition was not violated. The problem lies therein that $\dot{q}_0$ was not well-synchronised with $\theta_{1s,0}$, which can be accounted for by means of the flapping synchronisation filter. From Fig. 9 it can be observed that for case 2 controller performance is significantly better, TSS condition is not violated and response is not erratic. Lastly, based on the difference in synchronised and unsynchronised actuator measurement, it can be stated that for increasing τ_β there will be more synchronisation effort required.

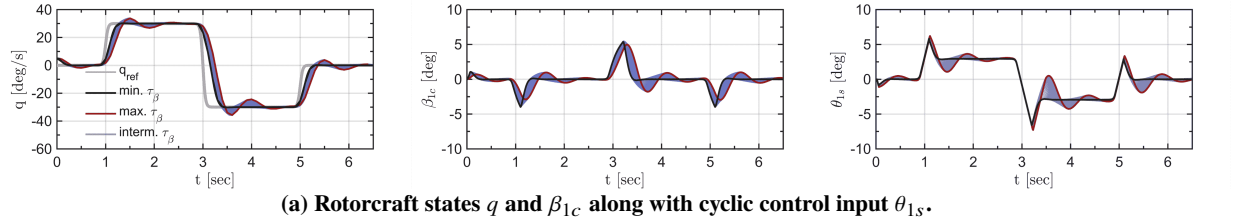

(a) Rotorcraft states q and β_{1c} along with cyclic control input θ_{1s}.

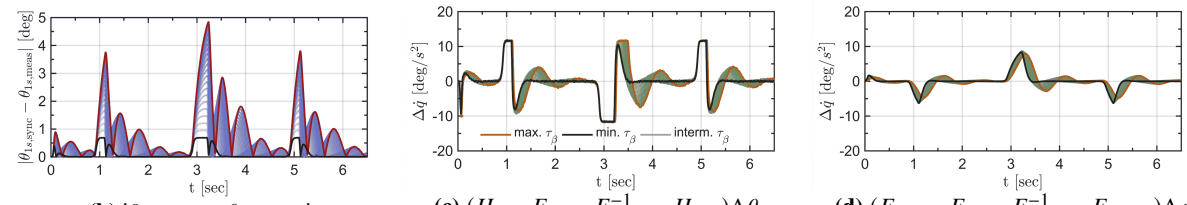

(b) $|\theta_{1s,\mathbf{sync}} - \theta_{1s,\mathbf{meas}}|$ **(c)** $(H_q - F_{q,\beta_{1c}} F^{-1}_{\beta_{1c},\beta_{1c}} H_{\beta_{1c}})\Delta\theta_{1s}$ **(d)** $(F_{q,q} - F_{q,\beta_{1c}} F^{-1}_{\beta_{1c},\beta_{1c}} F_{\beta_{1c},q})\Delta q$

Fig. 9 Results of longitudinal tracking task of case 2. Effect of τ_β on tracking performance is analysed for $\tau_\beta \in [0.5, 1.0, ..., 5.5]$, $c_q = 15$, $\alpha_{G_q} = 0$ and $\gamma_q = 1$ for $\hat{G}_q$ of IBS control law and synchronisation filter

A control effectiveness mismatch of $\gamma_q = 0.75$ is considered for the control effectiveness in the rotor synchronisation filter, while $\gamma_q = 1$ will be considered for the control effectiveness of the IBS control law. In Fig. 10 the results are provided for case 3, from which it can be observed that controller performance is severely affected as tracking response has become more erratic. Moreover, q has an offset with respect to q_{ref} as a result of inadequate signal synchronisation. It can be observed from Fig. 11 that $RMSE_q$ significantly increases when there exists control effectiveness mismatch for $\hat{G}_q$ in the synchronisation filter. The controller is therefore not robust to uncertainties in $\hat{G}_q$ of the synchronisation filter.

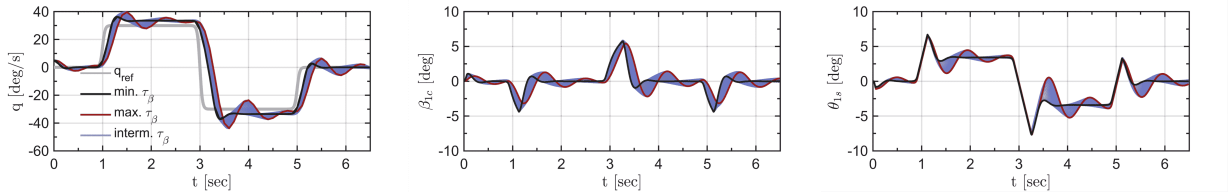

(a) Rotorcraft states q and β_{1c} along with cyclic control input θ_{1s}.

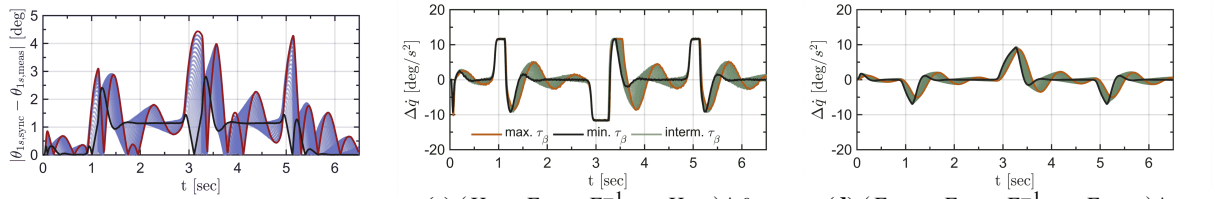

(b) $|\theta_{1s,\text{sync}} - \theta_{1s,\text{meas}}|$ **(c) $(H_q - F_{q,\beta_{1c}} F^{-1}_{\beta_{1c},\beta_{1c}} H_{\beta_{1c}})\Delta\theta_{1s}$** **(d) $(F_{q,q} - F_{q,\beta_{1c}} F^{-1}_{\beta_{1c},\beta_{1c}} F_{\beta_{1c},q})\Delta q$**

Fig. 10 Results of longitudinal tracking task of case 3. Effect of τ_β on tracking performance is analysed for $\tau_\beta \in [0.5, 1.0, ..., 5.0]$, $c_q = 10$, $\alpha_{G_q} = 0$, $\gamma_q = 0.75$ for $\hat{G}_q$ in synchronisation filter and $\gamma_q = 1.0$ for $\hat{G}_q$ in IBS control law.

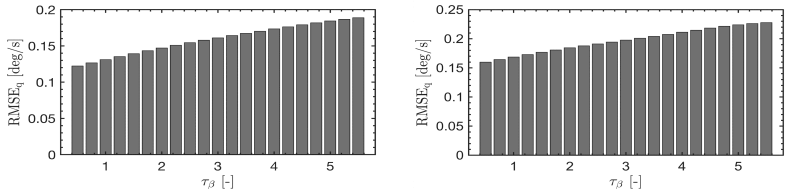

(a) Case 2. **(b) Case 3.**

Fig. 11 $RMSE_q$ of longitudinal tracking task for case 2 and case 3.

The following conclusions can be drawn:

- incorporating the *method of residualised dynamics* for enhancing control-dependency and diminishing state-dependency (see Eq. 41) did not violate the TSS condition from Eq. 44. However, it did not account for the difference in *actual* and *idealised* rotorcraft model, yielding inadequate synchronisation of actuator and state-derivative measurement. This resulted in erratic behaviour of the controlled and uncontrolled states.
- synchronisation of actuator and angular acceleration measurement by means of a flapping synchronisation filter can be regarded a requisite for BF models with significant difference in *actual* and *idealised* rotorcraft model. This especially holds for BF models with large, because synchronisation effort ($|\theta_{1s,\text{sync}} - \theta_{1s,\text{meas}}|$) is significant.
- control effectiveness mismatch for $\hat{G}_q$ in the rotor synchronisation filter can severely affect controller performance as vehicle response is associated with steady-state error. It is therefore not robust to uncertainties in $\hat{G}_q$.
- actuator limits do pose a problem regarding the TSS condition, as $(H_{q,q} - F_{q,\beta_{1c}} F^{-1}_{\beta_{1c},\beta_{1c}} H_{\beta_{1c}})\Delta\theta_{1s}$ can only reach maximum depending on actuator limits.

G. Closed-loop frequency response for IBS controller with or without rotor synchronisation filter

Next, it will be necessary to consider a closed-loop frequency analysis. It will be shown that a flapping synchronisation filter is necessary to assure adequate closed-loop frequency response and to proof that the controller is not robust to control effectiveness mismatch in the flapping synchronisation filter. The main parameters of interest for the analysis are: γ_q and τ_β. Below a set of cases will be outlined which are all considered with or without rotor synchronisation filter, $c_q \in [3, 9]$ and $\alpha_{G_q} = 0$. Next to this, the maximum region of overreaction (with 1% margin) of closed-loop

response is indicated. For the IBS controller with and without rotor synchronisation this is indicated in dark and light grey respectively. The following cases will be considered:

- **case 1**: variation in τ_β with $\gamma_q = 1$ ($\hat{G}_q = K_{\text{lon}}$) for IBS control law and synchronisation filter, $\alpha_{G_q} = 0$ and $\tau_\beta \in [0.5, 0.575, ..., 4]$.
- **case 2**: variation in γ_q ($\hat{G}_q = \gamma_q K_{\text{lon}}$) given that $\gamma_q \in [1.0, 1.05, ..., 3]$ for $\hat{G}_q$ in rotor synchronisation filter, $\gamma_q = 1$ for $\hat{G}_q$ of IBS control law, $\alpha_{G_q} = 0$ and $\tau_\beta = 3$.
- **case 3**: variation in γ_q ($\hat{G}_q = \gamma_q K_{\text{lon}}$) given that $\gamma_q \in [0.75, 0.775, .., 1.0]$ for $\hat{G}_q$ in rotor synchronisation filter, $\gamma_q = 1$ for $\hat{G}_q$ in IBS control law, $\alpha_{G_q} = 0$ and $\tau_\beta = 3$.

In Fig. 12 the results of the three above cases are provided.

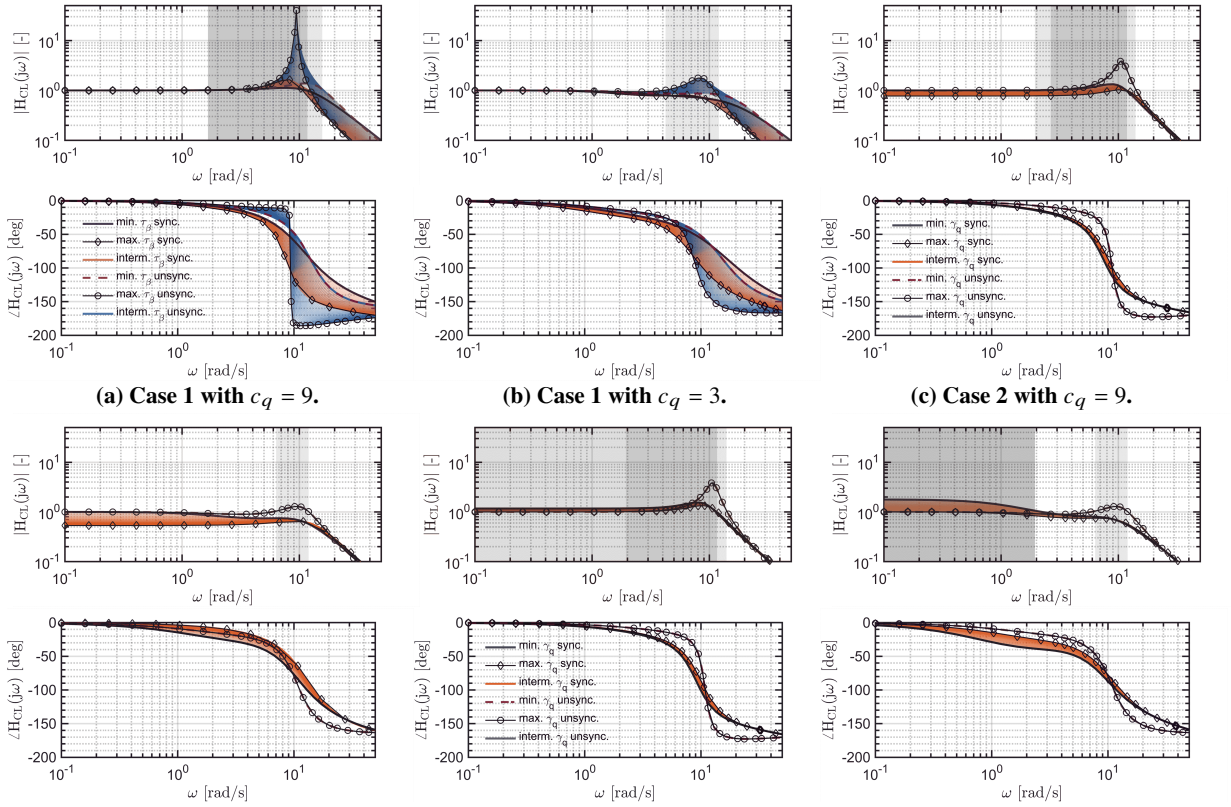

(a) Case 1 with $c_q = 9$. **(b) Case 1 with $c_q = 3$.** **(c) Case 2 with $c_q = 9$.**

(d) Case 2 with $c_q = 3$. **(e) Case 3 with $c_q = 3$.** **(f) Case 3 with $c_q = 9$.**

Fig. 12 Closed-loop frequency response for case 1-3.

Based on the closed-loop frequency analysis the following can be concluded:

- a flapping synchronisation filter is necessary to reduce the resonance peak in the closed-loop frequency response. When such a filter is not included, closed-loop response will be erratic and characterised with significant overestimation of the reference signal. This especially holds for large c_q and/or large τ_β.
- increasing τ_β yields a greater resonance peak, which is due to having a greater difference in *idealised* and *actual* rotorcraft model, which translates into a significant delay between actuator and angular acceleration measurement. The former is based on the *idealised* BF model, whereas the latter comes from the *actual* BF model. Since $\dot{q}_0$ is used in a negative feedback loop, there will be magnified control inputs when delayed with respect to $\theta_{1s,0}$.
- the IBS controller is not robust to uncertainties in $\hat{G}_q$ in the synchronisation filter. It can be observed that the closed-loop frequency response is not desirable for control effectiveness mismatch. For $\gamma_q > 1$ and $\gamma_q < 1$, there will be a significant region of under- and overestimation respectively. This shows that signal synchronisation can be affected when there are uncertainties in $\hat{G}_q$ of the synchronisation filter. In other words, the desired reference signal cannot be tracked well, when there exists control effectiveness mismatch for $\hat{G}_q$ in the synchronisation filter.

H. Closed-loop stability analysed using Routh-Hurwitz stability criterion

Next, the analytical closed-loop stability shall be determined using the *Routh-Hurwitz* stability criterion. The analysis shall be considered for the closed-loop system with and without flapping synchronisation filter, $c_q = 15$, $\tau_\beta \in [0.5, 1.0, \ldots, 5.0]$, $K_\beta \in [10, 15, \ldots, 150]$ kNm/rad and $\alpha_{G_q} = 0$. Full and accurate knowledge of system dynamics is assumed when constructing the filters, with the exception of $\hat{G}_q$. The objective is to show that without flapping synchronisation filter, closed-loop stability will be affected for high c_q and to proof that the controller is not robust to control effectiveness mismatch for $\hat{G}_q$ in the flapping synchronisation filter. The cases of interest are:

- **case 1**: without flapping synchronisation filter and $\gamma_q \in [0.5, 1, 3]$ for $\hat{G}_q$ in IBS control law.
- **case 2**: with flapping synchronisation filter given that $\gamma_q = 1$ for $\hat{G}_q$ in flapping synchronisation filter and $\gamma_q \in [0.5, 1, 3]$ for $\hat{G}_q$ in IBS control law.
- **case 3**: with flapping synchronisation filter given that $\gamma_q \in [0.5, 1, 3]$ for $\hat{G}_q$ in flapping synchronisation filter and $\gamma_q = 1$ for $\hat{G}_q$ in IBS control law.

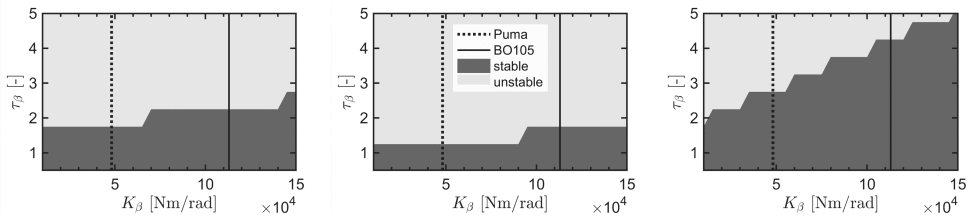

(a) Case 1 with $\gamma_q = 1$, $\gamma_q = 0.5$ and $\gamma_q = 3$ for $\hat{G}_q$ in IBS control law from left to right respectively.

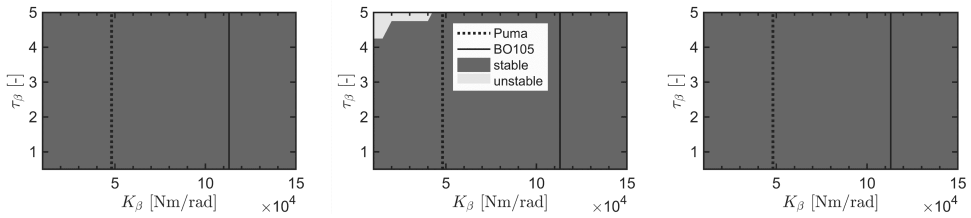

(b) Case 2 with $\gamma_q = 1$, $\gamma_q = 0.5$ and $\gamma_q = 3$ for $\hat{G}_q$ in IBS control law from left to right respectively.

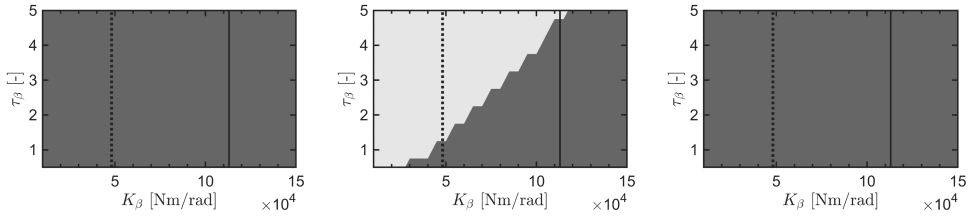

(c) Case 3 with $\gamma_q = 1$, $\gamma_q = 0.5$ and $\gamma_q = 3$ for $\hat{G}_q$ in IBS control law and synchronisation filter from left to right respectively.

Fig. 13 Results closed-loop stability analysis for case 1-3.

Based on the closed-loop stability analysis the following can be stated:

- without flapping synchronisation, $\dot{q}_0$ will be lagging behind $\theta_{1s,\text{meas}}$. Since $\dot{q}_0$ is used in a negative feedback loop (see Eq. 45) control inputs will be magnified, yielding quicker instability of the closed-loop system.
- decreasing γ_q for $\hat{G}_q$ in IBS control law, will also yield quicker system instability, because the incremental change in control input increases (see Eq. 45), which subsequently will yield magnified control inputs.
- for larger τ_β, there will be a greater time-delay between $\dot{q}_0$ and $\theta_{1s,\text{meas}}$, yielding quicker system instability.
- without synchronisation filter, system stability can be improved by increasing $\hat{G}_q$ (see top-right of Fig. 13).
- for control effectiveness mismatch of $\hat{G}_q$ in synchronisation filter, it can be stated that $\gamma_q < 1$ is most concerning, because it yields magnified control inputs (see Fig. 12 case 3), therefore quicker closed-loop system instability.
- stability can be assured for a greater range of τ_β for the hingeless MBB Bo 105 ($K_\beta = 113330$ Nm/rad from [9]) than for the articulated Aérospatiale SA 330 Puma ($K_\beta = 48149$ Nm/rad from [9]).

VI. Analysing the effects of lead-lag dynamics on IBS using first-order BF(L) models

In this section the effects of lead-lag dynamics on IBS shall be considered. The BF(L) models introduced in Section II shall be used and are described by Eq. 3 - 5. The analysis shall be conducted for the hingeless MBB Bo 105 and articulated Aérospatiale SA 330 Puma rotorcraft for which data is provided in the Appendix. First, the stabilising control law, control effectiveness and TSS condition shall be provided. Next, the difference in frequency response between the *actual* and *idealised* model will be considered. There after, synchronisation filter frequency response will be touched upon. Lastly, tracking performance and closed-loop frequency response shall be considered.

A. Stabilising control law for roll rate

The *Taylor* series can be established using the *actual* BFL model or the *idealised* BFL model, wherein the latter is based upon flap or flap-lag residualisation. The following first-order *idealised Taylor* series could be used

$$\begin{aligned}\text{Flap-lag residualisation}: \quad \dot{p} \cong \dot{p}_0 &+ \left(F_{p,p} - \begin{bmatrix}\boldsymbol{F}_{p,\beta} & \boldsymbol{F}_{p,\zeta}\end{bmatrix}\begin{bmatrix}\boldsymbol{F}_{\beta,\beta} & \boldsymbol{F}_{\beta,\zeta}\\ \boldsymbol{F}_{\zeta,\beta} & \boldsymbol{F}_{\zeta,\zeta}\end{bmatrix}^{-1}\begin{bmatrix}\boldsymbol{F}_{\beta,p}\\ \boldsymbol{F}_{\zeta,p}\end{bmatrix}\right)\Delta p + \\ &\left(H_p - \begin{bmatrix}\boldsymbol{F}_{p,\beta} & \boldsymbol{F}_{p,\zeta}\end{bmatrix}\begin{bmatrix}\boldsymbol{F}_{\beta,\beta} & \boldsymbol{F}_{\beta,\zeta}\\ \boldsymbol{F}_{\zeta,\beta} & \boldsymbol{F}_{\zeta,\zeta}\end{bmatrix}^{-1}\begin{bmatrix}\boldsymbol{H}_{\beta}\\ \boldsymbol{H}_{\zeta}\end{bmatrix}\right)\Delta\theta_{1c}\end{aligned} \tag{51}$$

$$\begin{aligned}\text{Flap residualisation}: \quad \dot{p} \cong \dot{p}_0 &+ \left(\boldsymbol{F}_{p,\zeta} - \boldsymbol{F}_{p,\beta}\boldsymbol{F}_{\beta,\beta}^{-1}\boldsymbol{F}_{\beta,\zeta}\right)\Delta\zeta + \left(\boldsymbol{F}_{p,p} - \boldsymbol{F}_{p,\beta}\boldsymbol{F}_{\beta,\beta}^{-1}\boldsymbol{F}_{\beta,p}\right)\Delta p + \\ &\left(H_p - \boldsymbol{F}_{p,\beta}\boldsymbol{F}_{\beta,\beta}^{-1}\boldsymbol{H}_{\beta}\right)\Delta\theta_{1c}\end{aligned} \tag{52}$$

wherein $\dot{p}_0$ is the current measured roll rate acceleration. Moreover Δp, $\Delta\beta$, $\Delta\zeta$ and $\Delta\theta_{1c}$ are the incremental change in roll rate, cyclic flapping angle, lead-lag angle and control input respectively. Moreover, G_p can be identified from the previous first-order *Taylor* series, which is the collection of terms in front of $\Delta\theta_{1c}$. Control effectiveness mismatch shall be considered for G_p, which is indicated by mismatch factor γ_p ($\hat{G}_p = \gamma_p G_p$). The previous first-order *Taylor* series can be simplified by neglecting system dynamics by assuming TSS [3, 15, 18]. The TSS conditions are:

$$\begin{aligned}\text{TSS condition for flap-lag residualisation}: \quad &\left(H_p - \begin{bmatrix}\boldsymbol{F}_{p,\beta} & \boldsymbol{F}_{p,\zeta}\end{bmatrix}\begin{bmatrix}\boldsymbol{F}_{\beta,\beta} & \boldsymbol{F}_{\beta,\zeta}\\ \boldsymbol{F}_{\zeta,\beta} & \boldsymbol{F}_{\zeta,\zeta}\end{bmatrix}^{-1}\begin{bmatrix}\boldsymbol{H}_{\beta}\\ \boldsymbol{H}_{\zeta}\end{bmatrix}\right)\Delta\theta_{1c} >> \\ &\left(F_{p,p} - \begin{bmatrix}\boldsymbol{F}_{p,\beta} & \boldsymbol{F}_{p,\zeta}\end{bmatrix}\begin{bmatrix}\boldsymbol{F}_{\beta,\beta} & \boldsymbol{F}_{\beta,\zeta}\\ \boldsymbol{F}_{\zeta,\beta} & \boldsymbol{F}_{\zeta,\zeta}\end{bmatrix}^{-1}\begin{bmatrix}\boldsymbol{F}_{\beta,p}\\ \boldsymbol{F}_{\zeta,p}\end{bmatrix}\right)\Delta p\end{aligned} \tag{53}$$

$$\begin{aligned}\text{TSS condition for flap residualisation}: \quad &\left(H_p - \boldsymbol{F}_{p,\beta}\boldsymbol{F}_{\beta,\beta}^{-1}\boldsymbol{H}_{\beta}\right)\Delta\theta_{1c} >> \\ &\left(\boldsymbol{F}_{p,\zeta} - \boldsymbol{F}_{p,\beta}\boldsymbol{F}_{\beta,\beta}^{-1}\boldsymbol{F}_{\beta,\zeta}\right)\Delta\zeta + \left(\boldsymbol{F}_{p,p} - \boldsymbol{F}_{p,\beta}\boldsymbol{F}_{\beta,\beta}^{-1}\boldsymbol{F}_{\beta,p}\right)\Delta p\end{aligned} \tag{54}$$

This is equivalent by assuming instantaneous control action given that sampling rate f_s is sufficiently high [15]. When Eq. 53 and Eq. 54 hold, then the controller can be regarded robust to uncertainties in system dynamics. When Eq. 54 is being violated, flap-lag residualisation must be considered in order to enhance control-dependency and diminish state-dependency of $\dot{p}$. This is of prime concern when conducting the analysis as it will reveal whether inclusion of lead-lag dynamics to rotor synchronisation will be necessary. The following control law shall be considered:

$$\theta_{1c} = \theta_{1c,0} + \hat{G}_p^{-1}\left[-\dot{p}_0 + \dot{p}_{\text{ref}} - c_p z_p\right], \tag{55}$$

wherein $\theta_{1c,0}$, c_p and z_p are the actuator measurement, IBS control gain and tracking error respectively.

B. Actual and idealised modes of motion of BF(L) rotorcraft models

First, the modes of motion shall be considered for varying lead-lag damping coefficient C_ζ. In Fig. 14 and Fig. 15 the *actual* modes of motion of models I-IV are provided for a hingeless and articulated rotor configuration respectively. It can be observed that the *actual* modes of motion do not differ significantly among the four models for the hingeless and articulated rotorcraft. In Fig. 14 and Fig. 15 the *idealised* modes of motion based upon residualised flap-lag and flap dynamics are provided as well for the hingeless and articulated rotor configuration respectively. Only models I,III and IV are considered for flap-lag residualisation, as model II does not include lead-lag dynamics. The decoupled flap-lag and flap modes of motion are provided as well for the flap-lag and flap residualised models respectively. These decoupled modes of motion shall be used for the synchronisation filter.

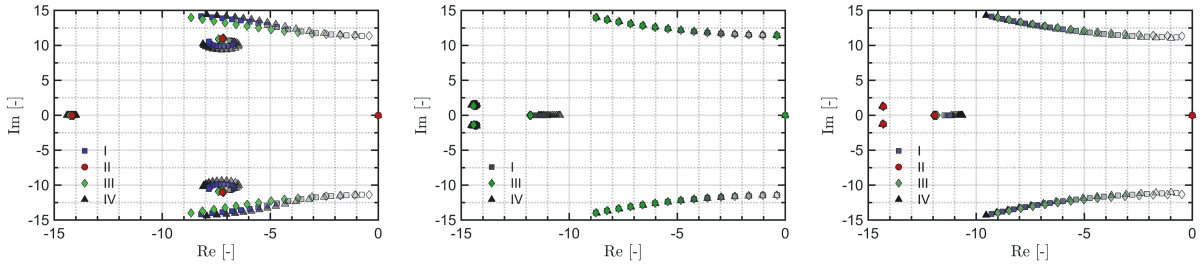

(a) Actual **(b) *Idealised* flap-lag residualised.** **(c) *Idealised* flap residualised.**

Fig. 14 Modes of motion of *idealised* and *actual* MBB Bo 105 BF(L) models I-IV for $C_\zeta \in [0.02, 0.06, ..., 0.58]$.

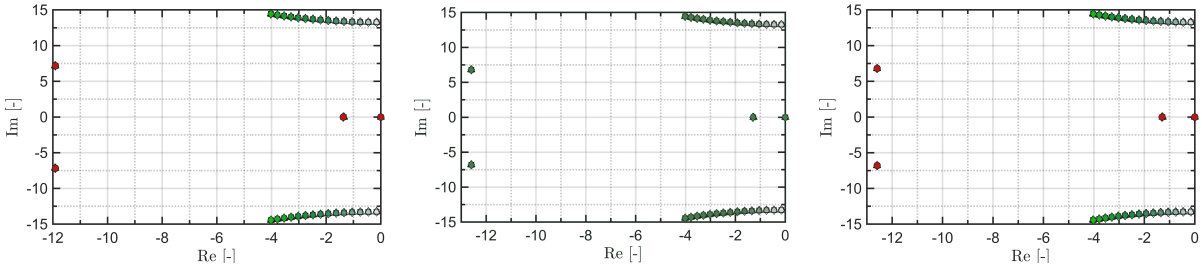

(a) *Actual*. **(b) *Idealised* flap-lag residualised.** **(c) *Idealised* flap residualised.**

Fig. 15 Modes of motion of *idealised* and *actual* Aérospatiale SA 330 Puma BF(L) models I-IV for $C_\zeta \in [0.02, 0.06, ..., 0.58]$.

Based on the modes of motion the following can be concluded:

- the difference in *idealised* modes of motion for flap or flap-lag residualised dynamics is not significant for both rotorcraft, thus the largest discrepancy between *idealised* and *actual* modes of motion is due to flapping dynamics.
- the difference in *idealised* and *actual* modes of motion is greater for the hingeless rotorcraft than for the articulated rotorcraft. This is because the flap and body (roll) modes of motion of the *actual* articulated BF(L) model were already well-separated (loosely coupled). This yields a small difference in coupled and uncoupled (*idealised*) modes of motion. The hingeless rotorcraft is associated with stronger coupling between flap and body (roll) mode. Decoupling these modes will therefore yield a greater difference with respect to the *actual* modes of motion.

C. Frequency response of roll rate to lateral cyclic control input

Next, it is necessary to determine the *actual* and *idealised* angular body frequency response for the four established BF(L) models. The main objective is to determine the difference in frequency response for the *idealised* models based upon flap (F) or flap-lag (FL) residualisation. The transfer function for the *idealised* BFL models based upon residualisation of flap-lag and flap dynamics are provided in Eq. 56 and Eq. 57 respectively. The transfer function for the *actual* BFL and BF model are given in Eq. 58 and Eq. 59 respectively (Roll angle was not considered in the state-space system)

$$H_p(s) = \left(s - \left(F_{p,p} - [\boldsymbol{F}_{p,\beta} \quad \boldsymbol{F}_{p,\zeta}] \begin{bmatrix} \boldsymbol{F}_{\beta,\beta} & \boldsymbol{F}_{\beta,\zeta} \\ \boldsymbol{F}_{\zeta,\beta} & \boldsymbol{F}_{\zeta,\zeta} \end{bmatrix}^{-1} \begin{bmatrix} \boldsymbol{F}_{p,\beta} \\ \boldsymbol{F}_{p,\zeta} \end{bmatrix}\right)\right)^{-1} \left(H_p - [\boldsymbol{F}_{p,\beta} \quad \boldsymbol{F}_{p,\zeta}] \begin{bmatrix} \boldsymbol{F}_{\beta,\beta} & \boldsymbol{F}_{\beta,\zeta} \\ \boldsymbol{F}_{\zeta,\beta} & \boldsymbol{F}_{\zeta,\zeta} \end{bmatrix}^{-1} \begin{bmatrix} \boldsymbol{H}_\beta \\ \boldsymbol{H}_\zeta \end{bmatrix}\right) \tag{56}$$

$$H_p(s) = [0 \quad 0 \quad 1] \left(s\boldsymbol{I}_{3x3} - \begin{bmatrix} \boldsymbol{F}_{\zeta,\zeta} - \boldsymbol{F}_{\zeta,\beta}\boldsymbol{F}_{\beta,\beta}^{-1}\boldsymbol{F}_{\beta,\zeta} & F_{\zeta,p} - \boldsymbol{F}_{\zeta,\beta}\boldsymbol{F}_{\beta,\beta}^{-1}\boldsymbol{F}_{\beta,p} \\ \boldsymbol{F}_{p,\zeta} - \boldsymbol{F}_{p,\beta}\boldsymbol{F}_{\beta,\beta}^{-1}\boldsymbol{F}_{\beta,\zeta} & F_{p,p} - \boldsymbol{F}_{p,\beta}\boldsymbol{F}_{\beta,\beta}^{-1}\boldsymbol{F}_{\beta,p} \end{bmatrix}\right)^{-1} \begin{bmatrix} H_\zeta - \boldsymbol{F}_{\zeta,\beta}\boldsymbol{F}_{\beta,\beta}^{-1}\boldsymbol{H}_\beta \\ H_p - \boldsymbol{F}_{p,\beta}\boldsymbol{F}_{\beta,\beta}^{-1}\boldsymbol{H}_\beta \end{bmatrix} \tag{57}$$

$$H_p(s) = \begin{bmatrix} 0 & 0 & 0 & 0 & 1 \end{bmatrix} \left(s\boldsymbol{I}_{5x5} - \begin{bmatrix} \boldsymbol{F}_{\beta,\beta} & \boldsymbol{F}_{\beta,\zeta} & F_{\beta,p} \\ \boldsymbol{F}_{\zeta,\beta} & \boldsymbol{F}_{\zeta,\zeta} & F_{\zeta,p} \\ \boldsymbol{F}_{p,\beta} & \boldsymbol{F}_{p,\zeta} & F_{p,p} \end{bmatrix}\right)^{-1} \begin{bmatrix} \boldsymbol{H}_\beta \\ \boldsymbol{H}_\zeta \\ H_p \end{bmatrix} \tag{58}$$

$$H_p(s) = \begin{bmatrix} 0 & 0 & 1 \end{bmatrix} \left(s\boldsymbol{I}_{3x3} - \begin{bmatrix} \boldsymbol{F}_{\beta,\beta} & F_{\beta,p} \\ \boldsymbol{F}_{p,\beta} & F_{p,p} \end{bmatrix}\right)^{-1} \begin{bmatrix} \boldsymbol{H}_\beta \\ H_p \end{bmatrix} \tag{59}$$

In Fig. 16 and Fig. 17 the *Bode* frequency response of the *actual* and *idealised* rotorcraft model is provided for the hingeless MBB Bo 105 and articulated Aérospatiale SA 330 Puma rotorcraft respectively.

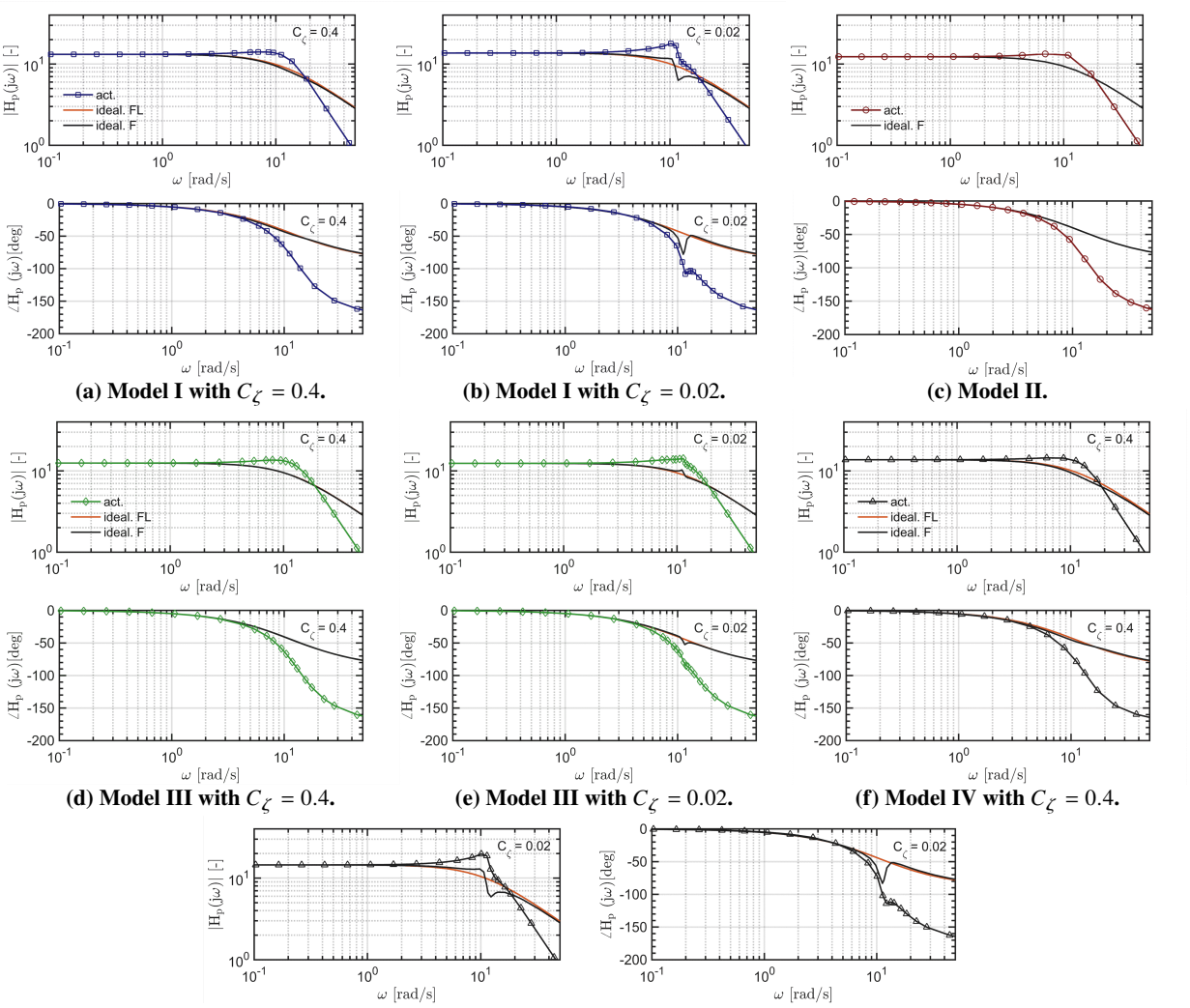

(a) Model I with $C_\zeta = 0.4$. **(b) Model I with $C_\zeta = 0.02$.** **(c) Model II.**

(d) Model III with $C_\zeta = 0.4$. **(e) Model III with $C_\zeta = 0.02$.** **(f) Model IV with $C_\zeta = 0.4$.**

(g) Model IV with $C_\zeta = 0.02$.

Fig. 16 Frequency response of *actual* and *idealised* MBB Bo 105 BF(L) models I-IV for $C_\zeta \in [0.02, 0.4]$.

The following conclusions can be drawn from the open-loop frequency response analysis:

- based on the frequency response of model I with $C_\zeta = 0.02$, it can be stated that the implementation of the body-lag coupling, as discussed in Section II, is correct [11, 12].
- the difference in open-loop frequency response for the articulated rotorcraft using flap or flap-lag residualisation is minor for models I-IV. This shows that lead-lag dynamics does have little effect on the open-loop frequency response. Flap synchronisation would suffice for synchronising actuator and state derivative measurement.
- for the hingeless rotorcraft it can be observed that, for model III there is little difference in flap or flap-lag residualised BFL model, therefore flap synchronisation would suffice. However, for models I and IV there exists difference in *idealised* model based upon flap-lag or flap residualisation when $C_\zeta = 0.02$. This subsequently implies that the flap-lag and flap synchronisation filters will differ from each other. This can be best understood by realising that if $H_{\text{actual}}(s)$ and $H_{\text{ideal}}(s)$ are the *actual* and *idealised* open-loop frequency response of the BF(L) models, then $H_{\text{sync}}(s)H_{\text{ideal}}(s)$ must equal to $H_{\text{actual}}(s)$.

Based on the above mentioned it was decided to continue the analysis with the hingeless MBB Bo 105 rotorcraft, because of the greater difference in *idealised* and *actual* BF(L) models. On top of this, only model I shall be considered for further research, because the difference with respect to model IV is not significant.

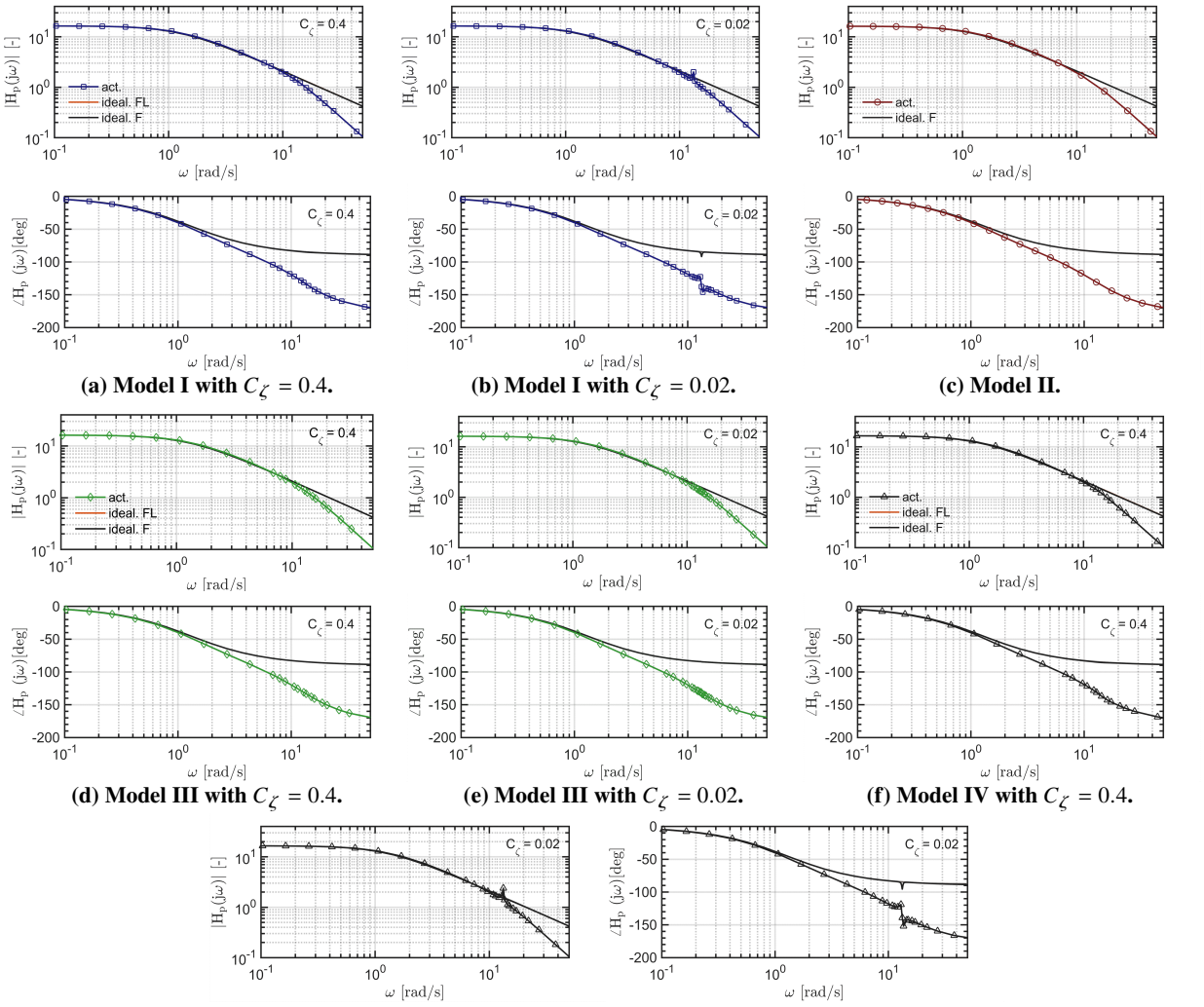

(a) Model I with $C_\zeta = 0.4$. **(b) Model I with $C_\zeta = 0.02$.** **(c) Model II.**

(d) Model III with $C_\zeta = 0.4$. **(e) Model III with $C_\zeta = 0.02$.** **(f) Model IV with $C_\zeta = 0.4$.**

(g) Model IV with $C_\zeta = 0.02$.

Fig. 17 Frequency response of *actual* and *idealised* BF(L) models for $C_\zeta \in [0.02, 0.4]$ for Aérospatiale SA 330 Puma.

D. Rotor synchronisation filter

Two rotor synchronisation filters shall be introduced and analysed in which one synchronisation filter accounts for the time-delay introduced by flapping dynamics, whereas the other one accounts for the cumulative delay introduced by flap-lag dynamics. First, a flap-lag synchronisation shall be established based upon flap-lag residualisation. The expression for the synchronised control input and rotor states are given in Eq. 60 and Eq. 61 respectively.

$$\left.\begin{aligned} \dot{p} &= \hat{G}_p \theta_{1c,\text{sync}} \\ \dot{p} &= \begin{bmatrix} \boldsymbol{F}_{p,\beta} & \boldsymbol{F}_{p,\zeta} \end{bmatrix} \begin{bmatrix} \boldsymbol{\beta}_{\text{sync}} \\ \boldsymbol{\zeta}_{\text{sync}} \end{bmatrix} + H_p \theta_{1c,\text{meas}} \end{aligned}\right\} \quad \theta_{1c,\text{sync}} = \hat{G}_p^{-1} \begin{bmatrix} \boldsymbol{F}_{p,\beta} & \boldsymbol{F}_{p,\zeta} \end{bmatrix} \begin{bmatrix} \boldsymbol{\beta}_{\text{sync}} \\ \boldsymbol{\zeta}_{\text{sync}} \end{bmatrix} + \hat{G}_p^{-1} H_p \theta_{1c,\text{meas}} \tag{60}$$

$$\begin{bmatrix} \dot{\boldsymbol{\beta}}_{\text{sync}} \\ \dot{\boldsymbol{\zeta}}_{\text{sync}} \end{bmatrix} = \begin{bmatrix} \boldsymbol{F}_{\beta,\beta} & \boldsymbol{F}_{\beta,\zeta} \\ \boldsymbol{F}_{\zeta,\beta} & \boldsymbol{F}_{\zeta,\zeta} \end{bmatrix} \begin{bmatrix} \boldsymbol{\beta}_{\text{sync}} \\ \boldsymbol{\zeta}_{\text{sync}} \end{bmatrix} + \begin{bmatrix} \boldsymbol{H}_\beta \\ \boldsymbol{H}_\zeta \end{bmatrix} \theta_{1c,\text{meas}} \tag{61}$$

The above can be rewritten into the following state-space system

$$\begin{bmatrix} \boldsymbol{\theta}_{1c,\text{sync}} \\ \dot{\boldsymbol{\beta}}_{\text{sync}} \\ \dot{\boldsymbol{\zeta}}_{\text{sync}} \end{bmatrix} = \begin{bmatrix} \hat{G}_p^{-1} \boldsymbol{F}_{p,\beta} & \hat{G}_p^{-1} \boldsymbol{F}_{p,\zeta} \\ \boldsymbol{F}_{\beta,\beta} & \boldsymbol{F}_{\beta,\zeta} \\ \boldsymbol{F}_{\zeta,\beta} & \boldsymbol{F}_{\zeta,\zeta} \end{bmatrix} \begin{bmatrix} \boldsymbol{\beta}_{\text{sync}} \\ \boldsymbol{\zeta}_{\text{sync}} \end{bmatrix} + \begin{bmatrix} \hat{G}_p^{-1} H_p \\ \boldsymbol{H}_\beta \\ \boldsymbol{H}_\zeta \end{bmatrix} \theta_{1c,\text{meas}}. \tag{62}$$

From Eq. 62 the state-space system for flap synchronisation can be identified, which is namely equal to

$$\begin{bmatrix} \boldsymbol{\theta}_{1c,\text{sync}} \\ \dot{\boldsymbol{\beta}}_{\text{sync}} \end{bmatrix} = \begin{bmatrix} \hat{G}_p^{-1} \boldsymbol{F}_{p,\beta} \\ \boldsymbol{F}_{\beta,\beta} \end{bmatrix} \left[\boldsymbol{\beta}_{\text{sync}} \right] + \begin{bmatrix} \hat{G}_p^{-1} H_p \\ \boldsymbol{H}_{\beta} \end{bmatrix} \theta_{1c,\text{meas}}. \tag{63}$$

It should be noted that $\theta_{1c,\text{meas}}$, $\boldsymbol{\beta}_{\text{sync}}$ and $\boldsymbol{\zeta}_{\text{sync}}$ are the measured control input (after the second-order washout filter), synchronised flapping angles and synchronised lead-lag angles respectively. Moreover, both filters do only have $\theta_{1c,\text{meas}}$ as input. The flap and flap-lag synchronisation filter in the *Laplace*-domain are respectively equal to

$$\boldsymbol{H}_{\text{sync}}(s) = \hat{G}_p^{-1} \left[\boldsymbol{F}_{p,\beta} \right] \left(s\boldsymbol{I}_{2x2} - \left[\boldsymbol{F}_{\beta,\beta} \right] \right)^{-1} \left[\boldsymbol{H}_{\beta} \right] + \hat{G}_p^{-1} \left[H_p \right], \tag{64}$$

$$\boldsymbol{H}_{\text{sync}}(s) = \hat{G}_p^{-1} \begin{bmatrix} \boldsymbol{F}_{p,\beta} & \boldsymbol{F}_{p,\zeta} \end{bmatrix} \left(s\boldsymbol{I}_{4x4} - \begin{bmatrix} \boldsymbol{F}_{\beta,\beta} & \boldsymbol{F}_{\beta,\zeta} \\ \boldsymbol{F}_{\zeta,\beta} & \boldsymbol{F}_{\zeta,\zeta} \end{bmatrix} \right)^{-1} \begin{bmatrix} \boldsymbol{H}_{\beta} \\ \boldsymbol{H}_{\zeta} \end{bmatrix} + \hat{G}_p^{-1} \left[H_p \right]. \tag{65}$$

It should be noted that $\hat{G}_p$ in Eq. 64 and Eq. 65 is based upon flap and flap-lag residualisation respectively. It can be observed from Eq. 65 that the flap-lag synchronisation filter requires more model knowledge.

Next, the objective is to determine whether lead-lag dynamics changes the frequency response of the rotor synchronisation filter. It shall only be considered for the MBB Bo 105 model I, because of reasons given earlier. Full and accurate knowledge of system dynamics is assumed for the flap and flap-lag synchronisation filter, with the exception of $\hat{G}_p$, which may contains a mismatch. The following cases shall be considered

- **case 1**: $\gamma_p = 1$ for $\hat{G}_p$ and $C_\zeta \in [0.02, 0.4]$.
- **case 2**: $\gamma_p \in [0.5, 3]$ for $\hat{G}_p$ and $C_\zeta = 0.4$

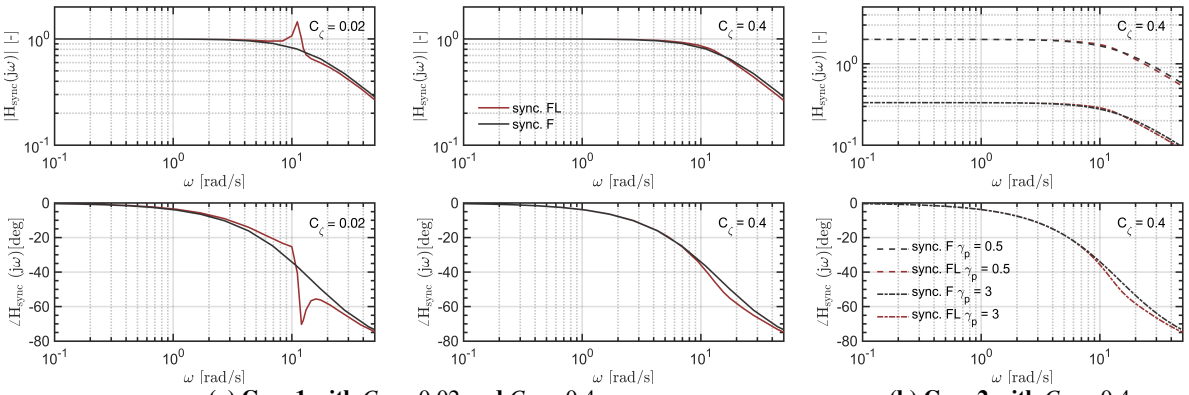

(a) Case 1 with $C_\zeta = 0.02$ and $C_\zeta = 0.4$. **(b) Case 2 with $C_\zeta = 0.4$.**

Fig. 18 Frequency response of rotor synchronisation filters for case 1 and case 2.

Next, it is necessary to summarise findings so far. It is namely found that:

- frequency response of flap and flap-lag synchronisation filters do not significantly differ for large C_ζ. This is in line with results from Fig. 16 as there was minor difference in frequency response between both *idealised* models.
- when there is difference in frequency response between the *idealised* flap and flap-lag residualised model (e.g. MBB Bo 105 model I with $C_\zeta = 0.02$ given in Fig. 16), then there will also be a difference in frequency response for the flap and flap-lag synchronisation filter. In this particular case the discrepancy is due to $\boldsymbol{F}_{p,\zeta}$ and $\boldsymbol{H}_{\zeta}$. Even though the frequency response may differ, both filters can still be considered suitable as long as the *actual* frequency response can be reconstructed from the synchronisation filter and the *idealised* frequency response. The TSS condition could for example determine which of the two filters would be needed.
- when $\gamma_p \neq 1$ then magnitude response of the synchronisation does alter. It is being observed that $\gamma_p < 1$ and $\gamma_p > 1$ are associated with upward and downward translation of magnitude response respectively. In other words γ_p^{-1} does act as a pure gain. This shows that inadequate signal synchronisation can occur when $\gamma_p \neq 1$ for $\hat{G}_p$ in the synchronisation filter, because control inputs will either be too large or too small.

E. Lateral ADS-33E-PRF tracking task for aggressive agility

Next, it is necessary to consider a lateral tracking task. The rotorcraft shall track a predefined roll rate doublet of $\pm 50^\circ/s$, which is in accordance with regulations stipulated by the ADS-33E-PRF for aggressive agility in hover condition. The objective is to determine whether the IBS controller with control effectiveness based upon flap-lag residualisation will yield an increase in controller performance. Accounting for lead-lag dynamics might be necessary when Eq. 53 could be considered more favourable over Eq. 54. A set of cases will be considered for which it will be assumed that there is full and accurate knowledge of system dynamics for establishing the synchronisation filters, with the exception of $\hat{G}_p$ in the syncrhonisaiton filter. The following cases shall be considered:

I **case 1**: $\gamma_p = 1$ for $\hat{G}_p$ in IBS control law and synchronisation filter, using flap or flap-lag residualisation, $c_p = 30$ and $C_\zeta = 0.02$.

II **case 2**: $\gamma_p = 0.75$ for $\hat{G}_p$ in synchronisation filter, $\gamma_p = 1$ for $\hat{G}_p$in IBS control law, using flap or flap-lag residualisation, $c_p = 30$ and $C_\zeta = 0.02$.

Important to note is that when $\hat{G}_p$ is established based upon a flap or flap-lag residualised model, it will be complemented by means of a flap and flap-lag synchronisation filter respectively. Results provided in Fig. 19 and Fig. 20 also include the increments due system dynamics and control-depended increments without actuator limits to compare it with the real case, wherein actuator limits are used.

From Fig. 19 it can be observed that low C_ζ has little effect on tracking response, apart from flapping and lead-lag dynamics, which are oscillatory. Moreover, there is significant synchronisation effort required and synchronisation is done in a different manner for both filters. Next to this, residualisation of lead-lag dynamics does not significantly reduce the increments due to system dynamics nor does it increase the control-depended increments. Flapping residualisation is therefore of prime concern when establishing $\hat{G}_p$ and the synchronisation filter.

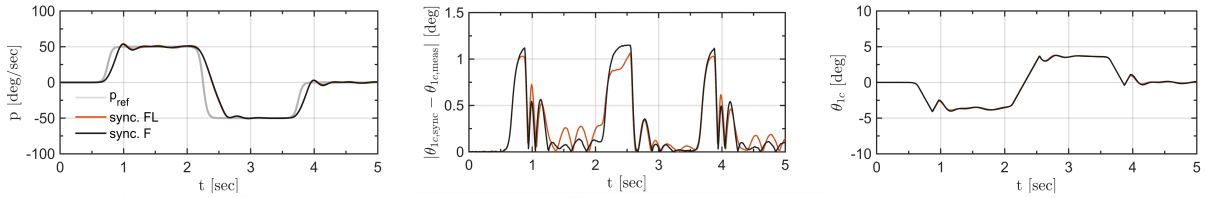

(a) Rotorcraft body state p, synchronisation effort $|\theta_{1c,\text{sync}} - \theta_{1c,\text{meas}}|$ and cyclic control inputs θ_{1c}.

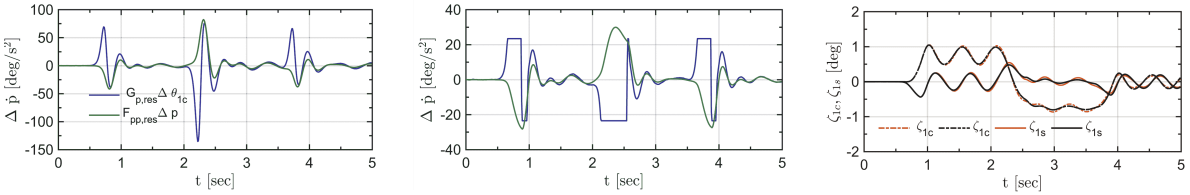

(b) Increments in system dynamics ($F_{p,p}\Delta p$) and control-depended increments ($\hat{G}_p \Delta\theta_{1c}$) for flap-lag residualised model with/without actuator limits.

(c) Lead-lag states ζ_{1c} and ζ_{1s}.

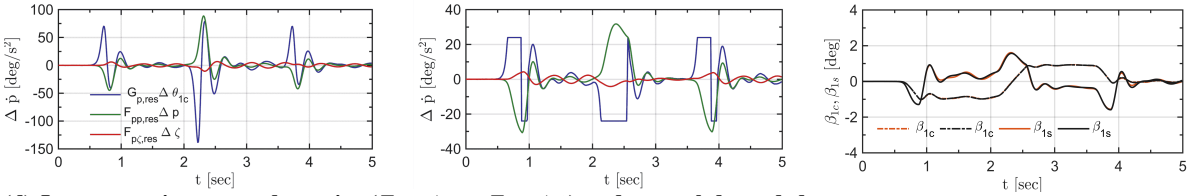

(d) Increments in system dynamics ($F_{p,p}\Delta p + F_{p,\zeta}\Delta\zeta$) and control-depended increments ($\hat{G}_p \Delta\theta_{1c}$) for flap residualised model with/without actuator limits.

(e) Flapping states β_{1c} and β_{1s}.

Fig. 19 Tracking response for case 1.

Next, the effect of control effectiveness mismatch in synchronisation filter shall be discussed. From Fig. 20 it can be observed that control effectiveness underestimation does yield inadequate controller performance. Synchronised control inputs will be magnified for $\gamma_p < 1$, yielding too large control inputs and therefore overestimation of p_{ref}. Moreover, there will be a steady-state error ($z_p \neq 0$) when $p_{\text{ref}} \neq 0$. This shows that the IBS controller is not robust to uncertainties in $\hat{G}_p$ of the synchronisation filter.

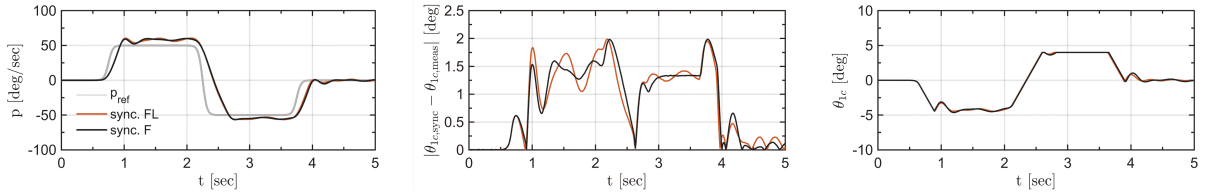

(a) Rotorcraft body state p, synchronisation effort $|\theta_{1c,\text{sync}} - \theta_{1c,\text{meas}}|$ and cyclic control inputs θ_{1c}.

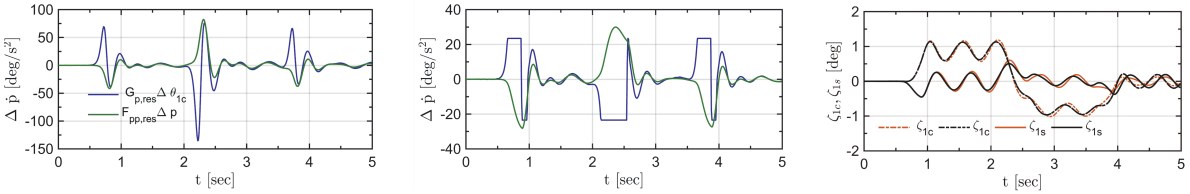

(b) Increments in system dynamics ($F_{p,p}\Delta p$) and control-depended increments ($\hat{G}_p\Delta\theta_{1c}$) for flap-lag residualised model with/without actuator limits.

(c) Lead-lag states ζ_{1c} and ζ_{1s}.

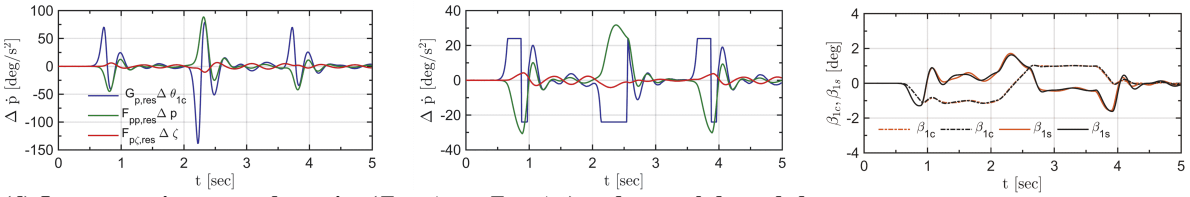

(d) Increments in system dynamics ($F_{p,p}\Delta p + F_{p,\zeta}\Delta\zeta$) and control-depended increments ($\hat{G}_p\Delta\theta_{1c}$) for flap residualised model with/without actuator limits.

(e) Flapping states β_{1c} and β_{1s}.

Fig. 20 Tracking response for case 2.

Based on the results of the lateral ADS-33E-PRF tracking task, the following conclusions can be drawn:

- the difference in $\hat{G}_p$ based upon flap or flap-lag residualisation was minor (-146.74 and -149.88 for flap and flap-lag residualisation respectively). Most importantly, flap-lag residualisation did not improve the ratio of the control-depended increments to the increments due to system dynamics. Moreover, the improvement in performance was minor, since $RMSE_p$ was found to be equal to 0.241 deg/s and 0.240 deg/s for flap and flap-lag residualisation respectively. The IBS controller is therefore robust enough to uncertainties in lead-lag dynamics, because it does not significantly improve controller performance.
- for model I it can be stated that it is not robust to uncertainties in control effectiveness in the synchronisation filter. Control effectiveness mismatch for the rotor synchronisation filter did severely affect controller performance, because $RMSE_p$ changed to 0.287 deg/s and 0.283 deg/s for flap and flap-lag residualisation respectively.

F. Closed-loop frequency analysis for IBS controller with synchronisation filter

Next, a closed-loop frequency analysis will be considered. The main objective is to show that adequate closed-loop frequency response can be assured without accounting for lead-lag dynamics in the synchronisation filter and to proof that the controller is not robust to uncertainties in control effectiveness mismatch for $\hat{G}_p$ in the rotor synchronisation filter. The former is equivalent to stating that residualisation of lead-lag dynamics is redundant for improving the ratio of control-depended increments to increments due to system dynamics. The analysis shall be conducted for model I with flap or flap-lag synchronisation filter, $C_\zeta \in [0.02\ 0.4]$ and with or without control effectiveness mismatch. The cases of interest are:

- **case 1**: $\gamma_p = 1$ for $\hat{G}_p$ in IBS control law and synchronisation filter and $c_p \in [20, 40]$.
- **case 2**: $\gamma_p = 0.75$ for $\hat{G}_p$ in synchronisation filter, $\gamma_p = 1$ for $\hat{G}_p$ in IBS control law and $c_p = 40$.

In Fig. 21 the results of the closed-loop frequencies analysis are provided.

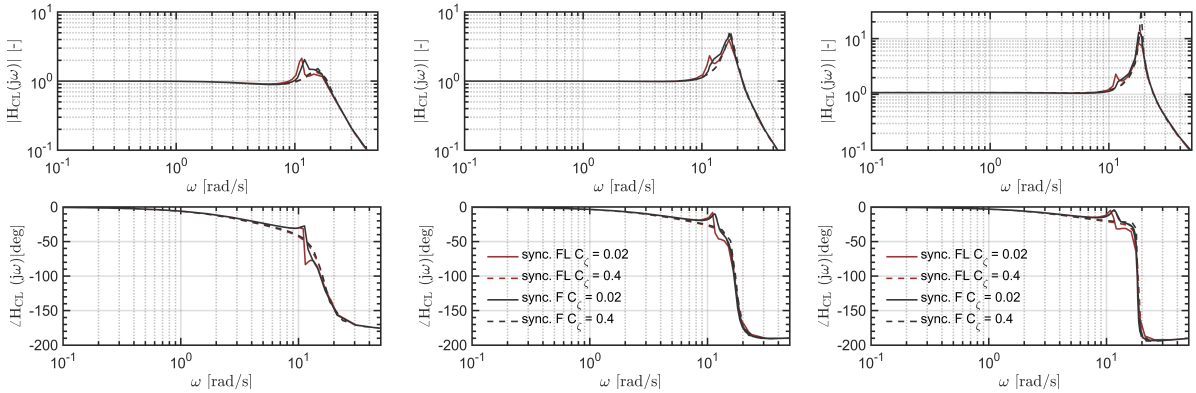

(a) Case 1 with $c_p = 20$ (left) and $c_p = 40$ (right). **(b) Case 2 with $c_p = 40$.**

Fig. 21 Results of closed-loop frequency analysis for cases 1 and 2.

Based on the closed-loop frequency analysis the following can be concluded:

- increasing c_p does increase both bandwidth as well as the resonance peak. This shows that quicker controller response does come at cost of overreaction of the closed-loop system.
- closed-loop frequency response has not significantly improved when accounting for lead-lag dynamics in establishing the control effectiveness. The significant amount of additional model knowledge does outweigh the benefits of using a control effectiveness based upon flap-lag residualisation, therefore the IBS controller is robust to uncertainties in lead-lag dynamics. Modification of control effectiveness and synchronisation filter is therefore not required when lead-lag dynamics is being added to a rotorcraft model.
- the IBS controller is not robust to control effectiveness mismatch in the synchronisation filter. For $\gamma_p < 1$ it was found that p_{ref} was being overestimated and therefore a steady-state error was present in the tracking response. It should be noted that for case 2 given in Fig. 21, $|H_{CL}(j\omega)| > 1$ for 0.1 rad/s to 23 rad/s, which implies a significant region of overestimation. This is because the synchronisation filter magnifies measured control inputs.

G. Closed-loop stability analysed using Routh-Hurwitz stability criterion

Next, it will be necessary to consider the analytical closed-loop stability using the *Routh-Hurwitz* stability criterion. The analysis shall be considered for a closed-loop system using model I, with IBS controller and flap or flap-lag synchronisation filter, $C_\zeta \in [0.01, 0.015, ..., 0.03]$ and $c_p \in [0, 2, ..., 50]$. Full and accurate knowledge of system dynamics is assumed when constructing the filters, with the exception of $\hat{G}_p$. The objective is to determine closed-loop system stability for BFL model I under specified conditions. The following cases shall be considered:

- **case 1**: $\gamma_p = 1$ for $\hat{G}_p$ in flap or flap-lag synchronisation filter and $\gamma_p \in [1, 0.5, 3]$ for $\hat{G}_p$ in IBS control law.
- **case 2**: $\gamma_p = 1$ for $\hat{G}_p$ in IBS control law and $\gamma_p \in [1, 0.5, 3]$ for $\hat{G}_p$ in flap or flap-lag synchronisation filter.

The main variables that shall be changed during the analysis are: γ_p, c_p and C_ζ. In Fig. 22 and Fig. 23 the results of the closed-loop stability analysis are provided for case 1 and 2 respectively. Moreover, a constant line of $C_\zeta = 0.02$ is provided, which represents the low structural damping of a hingeless MBB Bo 105 rotor (taken from [25]). Based on obtained results the following can be stated:

- for case 1, $\gamma_p < 1$ does pose the most stringent restrictions on allowable c_p, because it will magnify the incremental control part from Eq. 55, yielding magnified control inputs. Moreover, there is little difference in stability region for the flap and flap-lag synchronisation filter. This shows that flap-lag synchronisation, or equivalently flap-lag residualisation, does not yield a significant improvement in closed-loop stability.
- for case 2 and $\gamma_p > 1$ for $\hat{G}_p$ in synchronisation filter there is little difference in closed-loop stability with respect to the previous case. For $\gamma_p < 1$ there is a decrease in stability region, because the synchronisation filter provides magnified control inputs, resulting in quicker system instability. There is also a difference in closed-loop stability for the flap and flap-lag synchronisation filter. The region of stability for the flap-lag synchronisation filter appears to be less. This is because the flap-lag synchronisation filter would be associated with a larger peak at the regressive lead-lag frequency, which becomes greater for decreasing C_ζ (see Fig. 18). This subsequently would

yield magnified control inputs at this frequency and therefore a greater likelihood of closed-loop system instability.

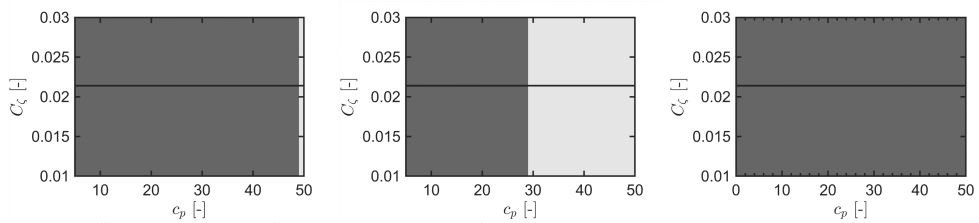

(a) IBS controller with flap synchronisation filter and $\gamma_p = 1$, $\gamma_p = 0.5$ and $\gamma_p = 3$ respectively.

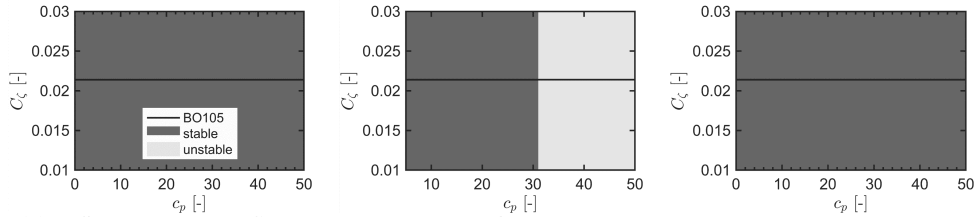

(b) IBS controller with flap-lag synchronisation filter and $\gamma_p = 1$, $\gamma_p = 0.5$ and $\gamma_p = 3$ respectively.

Fig. 22 Results of closed-loop stability analysis for case 1.

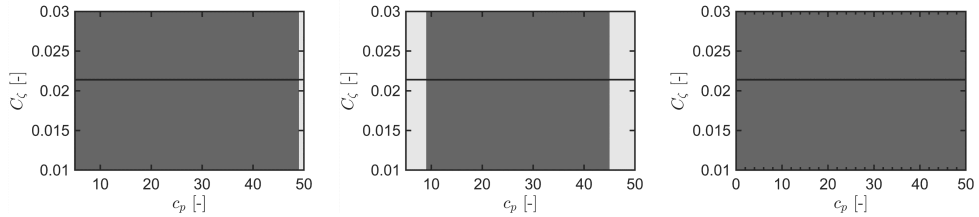

(a) IBS controller with flap synchronisation filter and $\gamma_p = 1$, $\gamma_p = 0.5$ and $\gamma_p = 3$ respectively.

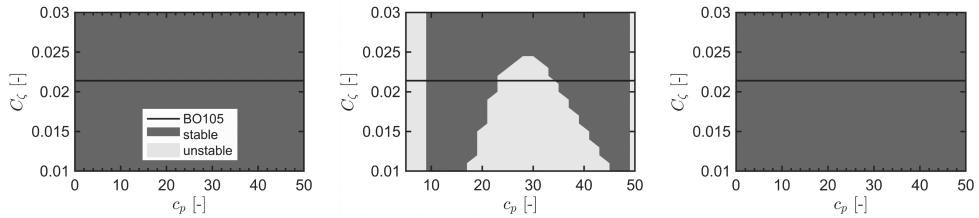

(b) IBS controller with flap-lag synchronisation filter and $\gamma_p = 1$, $\gamma_p = 0.5$ and $\gamma_p = 3$ respectively.

Fig. 23 Results of closed-loop stability analysis for case 2.

VII. Analysis on CFIBS controller using main MBB Bo 105 simulation model

In this section, robustness of the CFIBS controller with rotor synchronisation filter shall be considered for the main MBB Bo 105 simulation model. It will be shown that, accounting for lead-lag dynamics when establishing $\boldsymbol{G}_\omega$ using the *method of residualised dynamics* is redundant, since $\boldsymbol{F}_{\omega,\zeta}$ and $\boldsymbol{F}_{\omega,\dot{\zeta}}$ are not present in the current model. Moreover, it will be proven that establishing $\boldsymbol{G}_\omega$ by means of first-order flap residualisation will suffice for a model associated with second-order flapping dynamics. On top of this, inadequate synchronisation will be related to control effectiveness mismatch in the rotor synchronisation filter. First, simulation conditions and tracking task for the angular rate control mode will be provided. There after, *actual* and *idealised* modes of motion will be provided along with synchronisation filter frequency response. Lastly, tracking response is given.

A. Simulation conditions and tracking task for angular rate control mode

The analysis will involve a tracking task in accordance with regulations stipulated by the ADS-33E-PRF for aggressive agility [22]. The main objective is to reach level 1 rate response for p and q, which implies that rates of $\pm 50^\circ/s$ and $\pm 30^\circ/s$ must be reached respectively. On the other hand, yaw rate will be considered $0^\circ/s$. On top of this, the tracking task shall be executed from a trim condition of 1000 m altitude, 10 m/s forward flight and fixed main rotor

collective. Most importantly, C_ζ was set equal to 0.02, which represents the low structural damping of a hingeless MBB Bo 105 rotor [25]. General conditions under which the simulations are being conducted, are provided in Section IV. The CFIBS controller from Section III shall be used along with the magnitude and rate limitations from Table 8 given in the Appendix. Control effectiveness and synchronisation filter design shall be considered in this section. The above mentioned tracking task shall be considered for a set of cases. All cases will incorporate rotor synchronisation filters that are established using the second-order flap(-lag) model from the main simulation model, except for the filter used in the last case. Moreover, full and accurate model knowledge is assumed for the synchronisation filters, with the except of $\hat{\boldsymbol{G}}_\omega$, which may not be considered fully known. The following cases shall be analysed:

- **case 1**: $\boldsymbol{\Gamma}_\omega = \boldsymbol{I}_{3x3}$ for $\hat{\boldsymbol{G}}_\omega$ in CFIBS control law and synchronisation filter and $\hat{\boldsymbol{G}}_\omega$ is established based upon flap residualisation, therefore a flap synchronisation filter shall be used.
- **case 2**: $\boldsymbol{\Gamma}_\omega = \boldsymbol{I}_{3x3}$ for $\hat{\boldsymbol{G}}_\omega$ in CFIBS control law and synchronisation filter and $\hat{\boldsymbol{G}}_\omega$ is established based upon flap-lag residualisation, therefore a flap-lag synchronisation filter shall be used.
- **case 3**: $\boldsymbol{\Gamma}_\omega = 0.75 \cdot \boldsymbol{I}_{3x3}$ for $\hat{\boldsymbol{G}}_\omega$ used in synchronisation filter, $\boldsymbol{\Gamma}_\omega = \boldsymbol{I}_{3x3}$ for $\hat{\boldsymbol{G}}_\omega$ used in the CFIBS control law and $\hat{\boldsymbol{G}}_\omega$ is established based upon flap residualisation, therefore a flap synchronisation filter shall be used.
- **case 4**: $\boldsymbol{\Gamma}_\omega = \boldsymbol{I}_{3x3}$ for $\hat{\boldsymbol{G}}_\omega$ in CFIBS control law and synchronisation filter and $\hat{\boldsymbol{G}}_\omega$ is established based upon flap residualisation, therefore a flap synchronisation filter shall be used. However, both $\hat{\boldsymbol{G}}_\omega$ and synchronisation filter are based upon first-order flap dynamics.

The control effectiveness based upon flap residualisation given a first-order flapping model is provided in Eq. 66. The first-order flapping model could be obtained from the second-order flapping model of the main MBB Bo 105 rotorcraft model by neglecting second-order derivatives and rewriting the equation. In Eq. 67 and Eq. 68. $\hat{\boldsymbol{G}}_{\omega,R}$ is provided for flap or flap-lag residualisation given second-order flap and flap-lag dynamics respectively.

$$\hat{\boldsymbol{G}}_{\omega,R} = \boldsymbol{H}_\omega - \boldsymbol{F}_{\omega,\beta}\boldsymbol{F}_{\beta,\beta}^{-1}\boldsymbol{H}_\beta \tag{66}$$

$$\hat{\boldsymbol{G}}_{\omega,R} = \boldsymbol{H}_\omega - \boldsymbol{F}_{\omega,\beta}\boldsymbol{F}_{\dot{\beta},\beta}^{-1}\boldsymbol{H}_{\dot{\beta}} \tag{67}$$

$$\hat{\boldsymbol{G}}_{\omega,R} = \boldsymbol{H}_\omega - \begin{bmatrix}\boldsymbol{F}_{\omega,\beta} & \boldsymbol{F}_{\omega,\zeta}\end{bmatrix}\begin{bmatrix}\boldsymbol{F}_{\dot{\beta},\beta} & \boldsymbol{F}_{\dot{\beta},\zeta} \\ \boldsymbol{F}_{\dot{\zeta},\beta} & \boldsymbol{F}_{\dot{\zeta},\zeta}\end{bmatrix}^{-1}\begin{bmatrix}\boldsymbol{H}_{\dot{\beta}} \\ \boldsymbol{H}_{\dot{\zeta}}\end{bmatrix} \tag{68}$$

Case 1 and case 3 use $\hat{\boldsymbol{G}}_{\omega,R}$ from Eq. 67, case 2 incorporates $\hat{\boldsymbol{G}}_{\omega,R}$ from Eq. 68 and case 4 uses $\hat{\boldsymbol{G}}_{\omega,R}$ from Eq. 66. The synchronised control inputs for flap and flap-lag residualisation are provided in Eq. 69 and Eq. 70 respectively. All cases incorporate Eq. 69 for obtaining synchronised control inputs, with the exception of case 2, which uses Eq. 70.

$$\boldsymbol{U}_{\text{sync}} = \hat{\boldsymbol{G}}_{\omega,R}^{-1}\left[\boldsymbol{F}_{\omega,\beta}\boldsymbol{\beta}_{\text{sync}} + \boldsymbol{H}_\omega\boldsymbol{U}_{\text{meas}}\right], \tag{69}$$

$$\boldsymbol{U}_{\text{sync}} = \hat{\boldsymbol{G}}_{\omega,R}^{-1}\left[\begin{bmatrix}\boldsymbol{F}_{\omega,\beta} & \boldsymbol{F}_{\omega,\zeta}\end{bmatrix}\begin{bmatrix}\boldsymbol{\beta}_{\text{sync}} \\ \boldsymbol{\zeta}_{\text{sync}}\end{bmatrix} + \boldsymbol{H}_\omega\boldsymbol{U}_{\text{meas}}\right]. \tag{70}$$

The measured control inputs, after being fed through the second-order washout filter, are required to obtain the synchronised control inputs given Eq. 69 and Eq. 70. The synchronised flapping angles for the *idealised* model based upon first-order flap residualisation (case 4) can be obtained from Eq. 71. The synchronised flapping angles for the flapping synchronisation filter based upon second-order flap residualisation (case 1 and 3) can be determined using Eq. 72. The synchronised flapping and lead-lag angles for the flap-lag synchronisation filter based upon second-order flap-lag residualisation (case 2) can be determined using Eq. 73.

$$\dot{\boldsymbol{\beta}} = \boldsymbol{F}_{\beta,\beta}\boldsymbol{\beta}_{\text{sync}} + \boldsymbol{H}_\beta\boldsymbol{U}_{\text{meas}} \tag{71}$$

$$\begin{bmatrix}\dot{\boldsymbol{\beta}}_{\text{sync}} \\ \ddot{\boldsymbol{\beta}}_{\text{sync}}\end{bmatrix} = \begin{bmatrix}\boldsymbol{F}_{\beta,\beta} & \boldsymbol{F}_{\beta,\dot{\beta}} \\ \boldsymbol{F}_{\dot{\beta},\beta} & \boldsymbol{F}_{\dot{\beta},\dot{\beta}}\end{bmatrix}\begin{bmatrix}\boldsymbol{\beta}_{\text{sync}} \\ \dot{\boldsymbol{\beta}}_{\text{sync}}\end{bmatrix} + \begin{bmatrix}\boldsymbol{H}_\beta \\ \boldsymbol{H}_{\dot{\beta}}\end{bmatrix}\boldsymbol{U}_{\text{meas}} \tag{72}$$

$$\begin{bmatrix}\dot{\boldsymbol{\beta}}_{\text{sync}} \\ \ddot{\boldsymbol{\beta}}_{\text{sync}} \\ \dot{\boldsymbol{\zeta}}_{\text{sync}} \\ \ddot{\boldsymbol{\zeta}}_{\text{sync}}\end{bmatrix} = \begin{bmatrix}\boldsymbol{F}_{\beta,\beta} & \boldsymbol{F}_{\beta,\dot{\beta}} & \boldsymbol{F}_{\beta,\zeta} & \boldsymbol{F}_{\beta,\dot{\zeta}} \\ \boldsymbol{F}_{\dot{\beta},\beta} & \boldsymbol{F}_{\dot{\beta},\dot{\beta}} & \boldsymbol{F}_{\dot{\beta},\zeta} & \boldsymbol{F}_{\dot{\beta},\dot{\zeta}} \\ \boldsymbol{F}_{\zeta,\beta} & \boldsymbol{F}_{\zeta,\dot{\beta}} & \boldsymbol{F}_{\zeta,\zeta} & \boldsymbol{F}_{\zeta,\dot{\zeta}} \\ \boldsymbol{F}_{\dot{\zeta},\beta} & \boldsymbol{F}_{\dot{\zeta},\dot{\beta}} & \boldsymbol{F}_{\dot{\zeta},\zeta} & \boldsymbol{F}_{\dot{\zeta},\dot{\zeta}}\end{bmatrix}\begin{bmatrix}\boldsymbol{\beta}_{\text{sync}} \\ \dot{\boldsymbol{\beta}}_{\text{sync}} \\ \boldsymbol{\zeta}_{\text{sync}} \\ \dot{\boldsymbol{\zeta}}_{\text{sync}}\end{bmatrix} + \begin{bmatrix}\boldsymbol{H}_\beta \\ \boldsymbol{H}_{\dot{\beta}} \\ \boldsymbol{H}_\zeta \\ \boldsymbol{H}_{\dot{\zeta}}\end{bmatrix}\boldsymbol{U}_{\text{meas}} \tag{73}$$

B. Actual and idealised modes of motion

First, the *actual* (full model described by Eq. 10) and *idealised* modes of motion shall be considered, which are provided in Fig. 24. The modes of motion were obtained from the simulation model during the execution of the tracking task at a sampling rate of 0.2 sec between $t = 0$ sec and $t = 7$ sec. The *idealised* modes of motion for case 1,3 and 4 are decoupled from flapping dynamics, whereas the *idealised* modes of motion for case 2 are decoupled from flap-lag dynamics. The *idealised* and *actual* modes of motion differ for all cases analysed, however there is little difference among the four cases. The difference in *idealised* modes of motion using flap or flap-lag residualisation is not significant, which implies that the largest discrepancy between *idealised* and *actual* modes of motion is due to flapping dynamics.

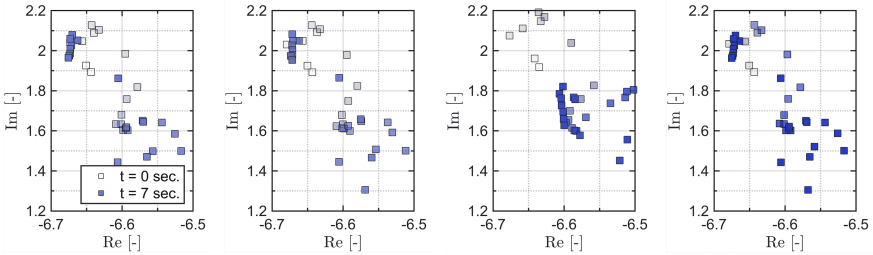

(a) Actual coupled pitch mode of motion for case 1 - 4 from left to right respectively.

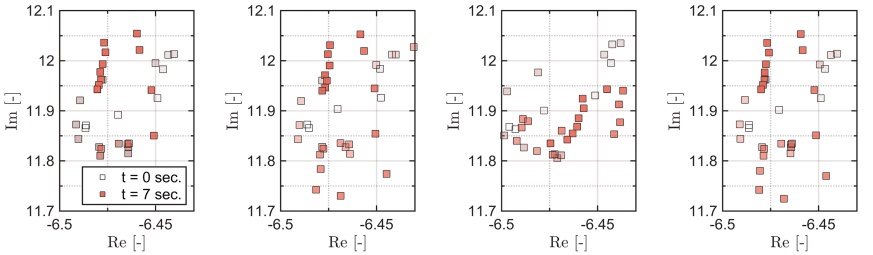

(b) Actual coupled roll mode of motion for case 1 - 4 from left to right respectively.

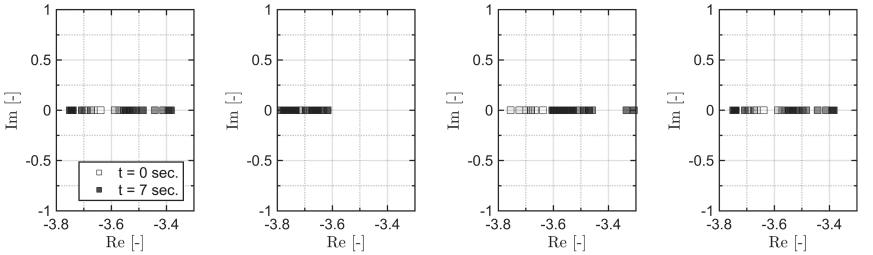

(c) idealised (decoupled) pitch mode of motion for case 1 - 4 from left to right respectively.

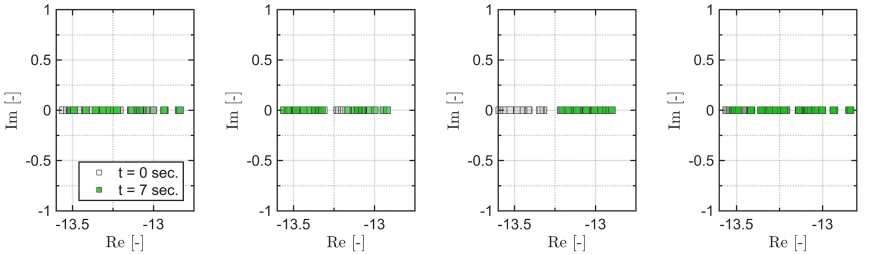

(d) idealised (decoupled) roll mode of motion for case 1 - 4 from left to right respectively.

Fig. 24 Actual and idealised modes of motion of open-loop system without controller during execution of tracking task.

C. Rotor synchronisation filter frequency response

Next, frequency response of the rotor synchronisation filters will be discussed. In Fig. 25 the frequency response of the flap and flap-lag synchronisation filter is provided for case 1 and 2. It can be observed that there is little difference in frequency response, with the exception at the regressive and advancing lead-lag frequencies. Lead-lag dynamics did not significantly alter rotor synchronisation filter response, which is due to $\boldsymbol{F}_{\omega,\zeta}$ and $\boldsymbol{F}_{\omega,\dot{\zeta}}$ being absent in the current model. In Fig. 26 the frequency response of the rotor synchronisation filter for case 3 is provided. It can be observed

that for $\mathbf{\Gamma}_\omega < I_{3x3}$, magnitude shifts upwards. This means that $\mathbf{\Gamma}_\omega^{-1}$ acts as a pure gain, yielding magnified actuator measurements. In Fig. 27 the frequency response for the rotor synchronisation filter from case 1 and 4 are provided. It can be observed that the difference between both filters is neglectable, with the exception at higher frequencies.

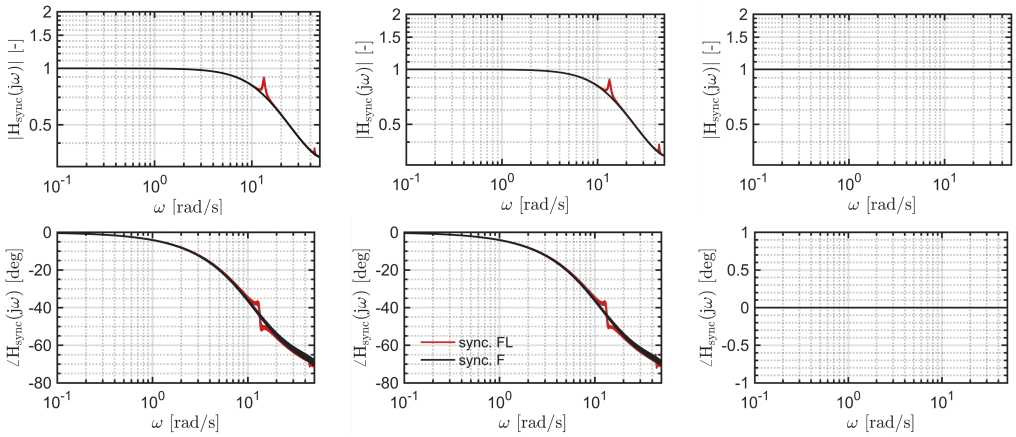

Fig. 25 Frequency response of flap (F) and flap-lag (FL) synchronisation filter for case 1 and case 2 respectively.

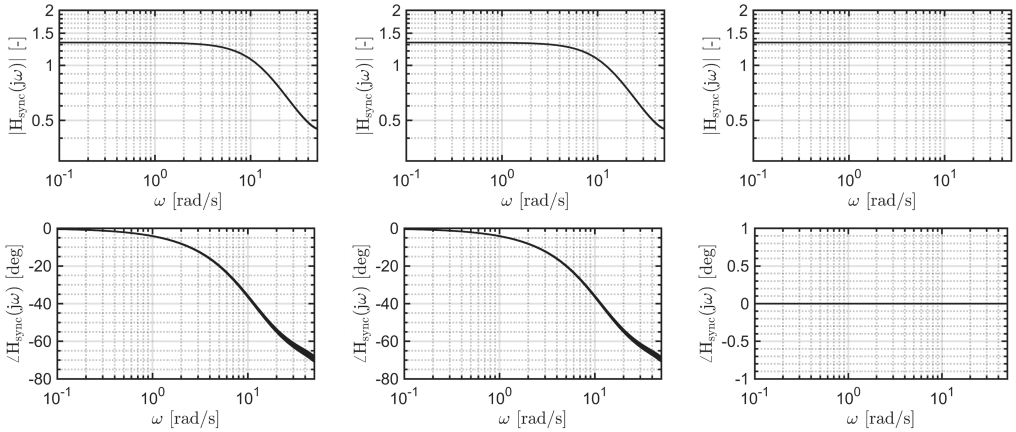

Fig. 26 Frequency response of flapping synchronisation filter for case 3.

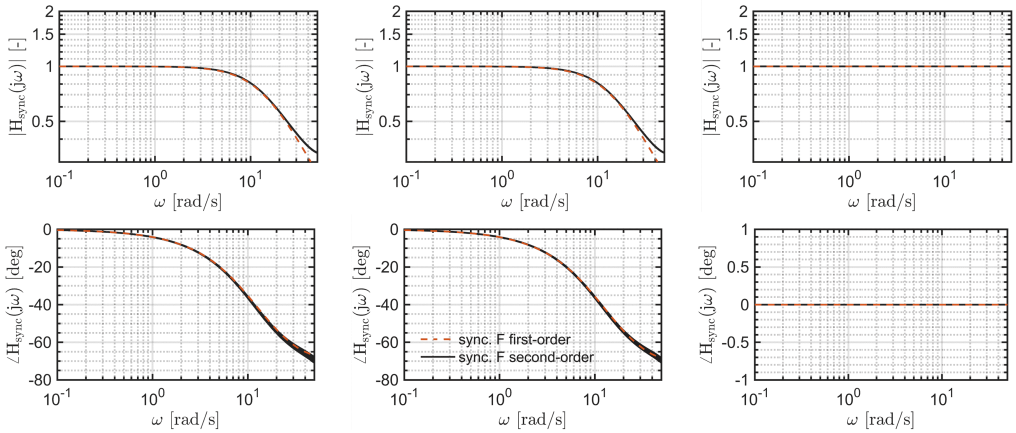

Fig. 27 Frequency response of flapping synchronisation filter for case 4.

D. Tracking response of combined lateral and longitudinal tracking task

Next, results of the tracking task shall be discussed. In Fig. 28 - 31 the results are provided for case 1 to 4 respectively. It should be noted that gains were chosen empirically and set equal to diag([15,14,10]) for all cases. First,

the difference in tracking response for case 1 and case 2 will be considered. Based on results provided in Fig. 29, it can be stated that accounting for lead-lag dynamics in rotor synchronisation is undesirable as it leads to oscillatory tracking response. Synchronised actuator measurements are slightly erratic, which is most likely due to the small peak in the synchronisation filter frequency response (see Fig. 25). Based on the results for case 1 given in Fig. 28, it can be stated that adequate response can be achieved by residualisation of (second-order) flapping dynamics only. This is based on the fact that control effectiveness based upon flap residualisation does not differ from the control effectiveness based upon flap-lag residualisation. This shows that controller is robust to uncertainties in lead-lag dynamics.

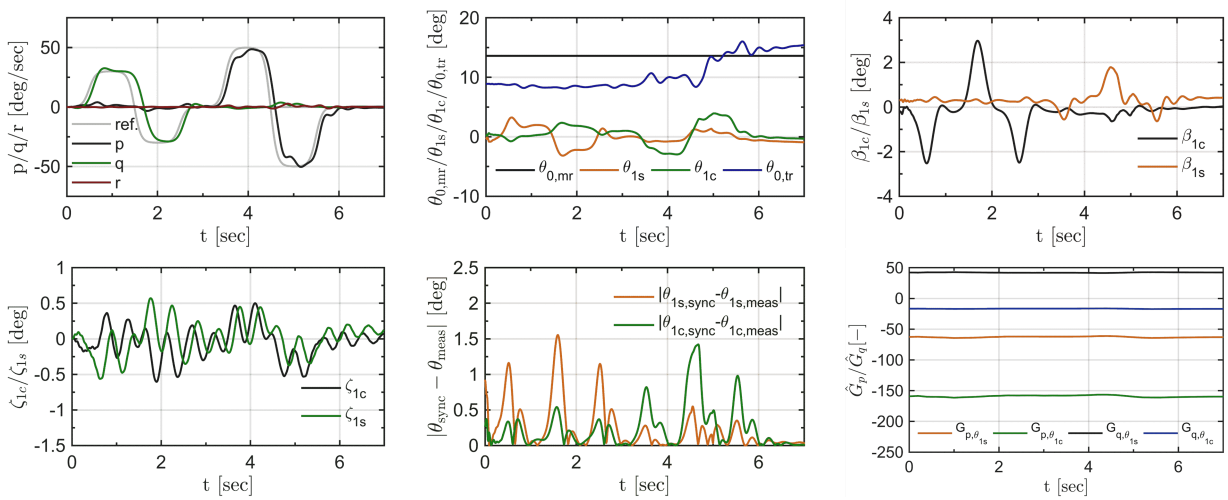

Fig. 28 Results of tracking task for case 1, showing rotorcraft state variables, control inputs, absolute difference in synchronised and unsynchronised actuator measurement and control effectiveness for IBS control law.

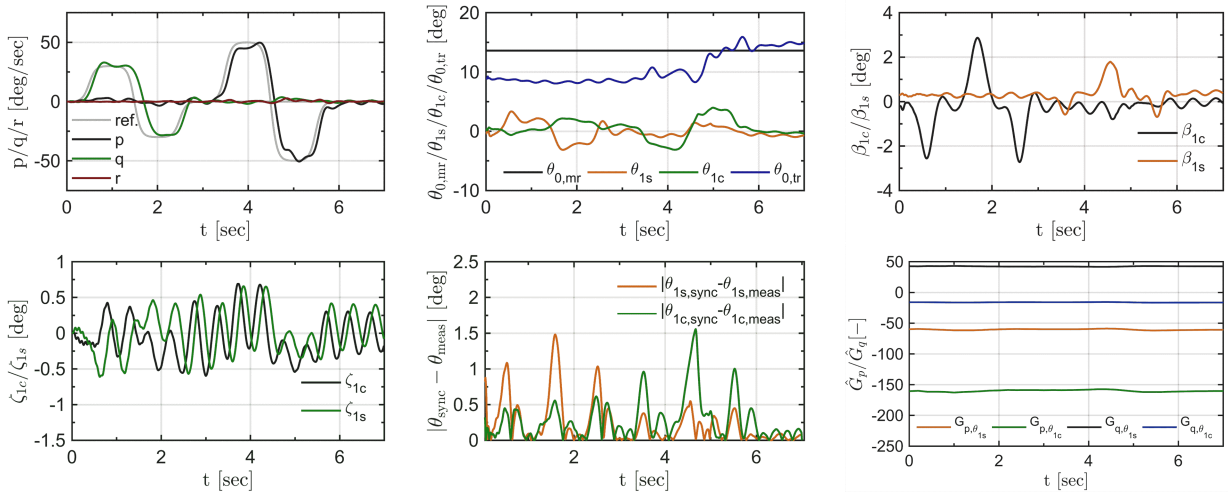

Fig. 29 Results of tracking task for case 2, showing rotorcraft state variables, control inputs, absolute difference in synchronised and unsynchronised actuator measurement and control effectiveness for IBS control law.

It can be observed from Fig. 30 that tracking response is significantly affected when there is mismatch of the control effectiveness in the flapping synchronisation filter. This is based upon the fact that the flapping synchronisation filter does magnify the measured actuator measurements. This can be observed from the absolute difference in synchronised and unsynchronised actuator measurement. This means that ω_{ref} will always be overestimated, therefore there does exist a steady-state error. The controller is therefore not robust to uncertainties in control effectiveness of the rotor synchronisation filter. The difference in tracking response between case 1 from Fig. 28 and case 4 from Fig. 31 is neglectable. This shows that the rotor synchronisation filter can be established using first-order flapping dynamics only. This was also expected as the rotor synchronisation filters for both cases were almost identical. Moreover, the control effectiveness is also similar for case 1 and case 4. This is an important result, because the control effectiveness

can therefore be established by means of residualisation of first-order flapping dynamics, which requires less model knowledge. Likewise, the synchronisation filter can also be established by only considering first-order flapping dynamics.

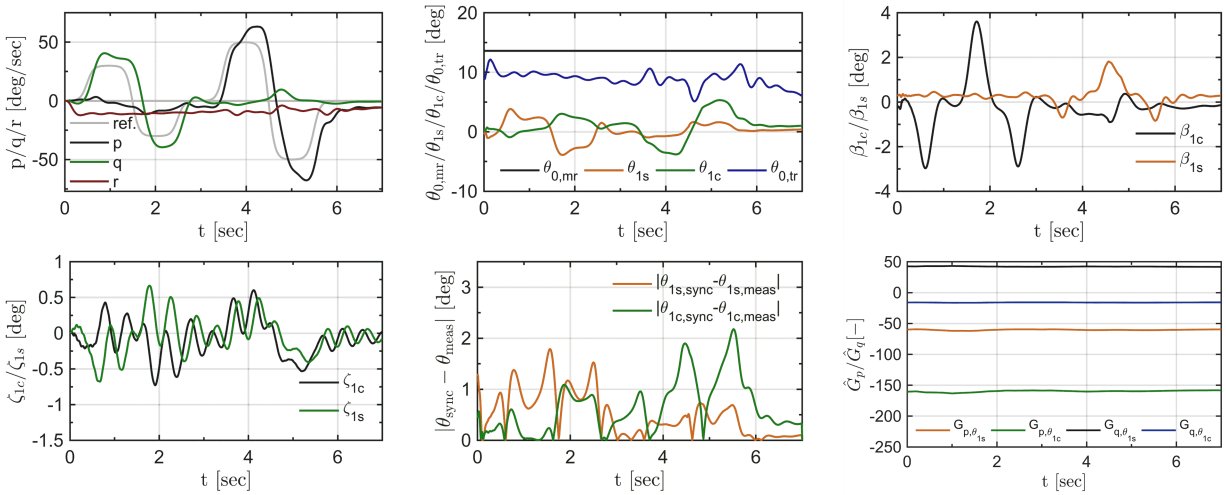

Fig. 30 Results of tracking task for case 3, showing rotorcraft state variables, control inputs, absolute difference in synchronised and unsynchronised actuator measurement and control effectiveness for IBS control law.

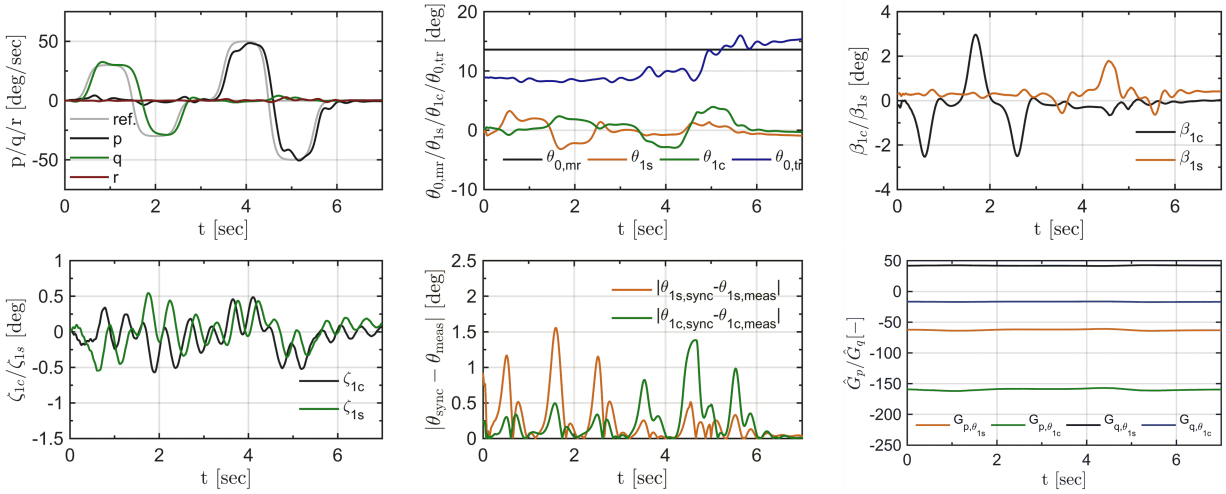

Fig. 31 Results of tracking task for case 4, showing rotorcraft state variables, control inputs, absolute difference in synchronised and unsynchronised actuator measurement and control effectiveness for IBS control law.

Table 1 Tracking RMSE for different cases.

Robustness case	$RMSE_p$ [deg/sec]	$RMSE_q$ [deg/sec]	$RMSE_r$ [deg/sec]
case 1	0.1193	0.1215	0.0109
case 2	0.1134	0.1202	0.011
case 3	0.2220	0.1533	0.1443
case 4	0.1186	0.1212	0.011

Based on previous results, it would suffice to establish control effectiveness by means of residualisation of first-order flapping dynamics only. This does obviate the need of having full and accurate knowledge of the second-order flapping model. This is in contrast by which the CFIBS controller with synchronisation filter was established in [3]. This shows that with less model knowledge the control effectiveness, and hence the synchronisation filter, can be established. On the other hand, control effectiveness must be well-known, otherwise control inputs can be magnified or diminished. In Table 1 the RMSE is provided for the different cases, which confirms previous findings.

Another important aspect when considering IBS is the validity of the TSS condition. It will therefore be of great

interest to assess the assumption of neglecting increments in system dynamics. The expression of the first-order *Taylor* series expansion of the angular rate derivative around its current solution is provided in Eq. 74. Neglecting increments due to system dynamics and higher-order terms will yield the expression provided in Eq. 75.

$$\dot{\boldsymbol{\omega}} = \dot{\boldsymbol{\omega}}_0 + \boldsymbol{F}_{\omega,0}\Delta\boldsymbol{X} + \boldsymbol{H}_{\omega,0}\Delta\boldsymbol{U} + \boldsymbol{O}(\Delta\boldsymbol{X}^2, \Delta\boldsymbol{U}^2) \tag{74}$$

$$\dot{\boldsymbol{\omega}} \cong \dot{\boldsymbol{\omega}}_0 + \boldsymbol{H}_{\omega,0}\Delta\boldsymbol{U} \tag{75}$$

In Fig. 32 increments in system dynamics and control-depended increments are provided for the four cases, wherein $\boldsymbol{O}(\Delta\boldsymbol{X}^2, \Delta\boldsymbol{U}^2)$ was not considered. It can be observed that increments due to system dynamics are not significantly smaller than the control-depended increments. This shows that the TSS assumption is not completely valid. The tracking error of the angular rates can be identified from the significant non-zero increments of the system dynamics. Moreover, it does also suggest that residualisation of other internal dynamics such as inflow dynamics could diminish the increments due to system dynamics and increase the control-depended increments. However, this would require additional model knowledge, which is not desirable. Another solution would be by reducing the delay of the incremental control loop, which can be achieved by means of faster actuator dynamics, smaller step size of the incremental-based controller, smaller acceleration measurement delay and more [6].

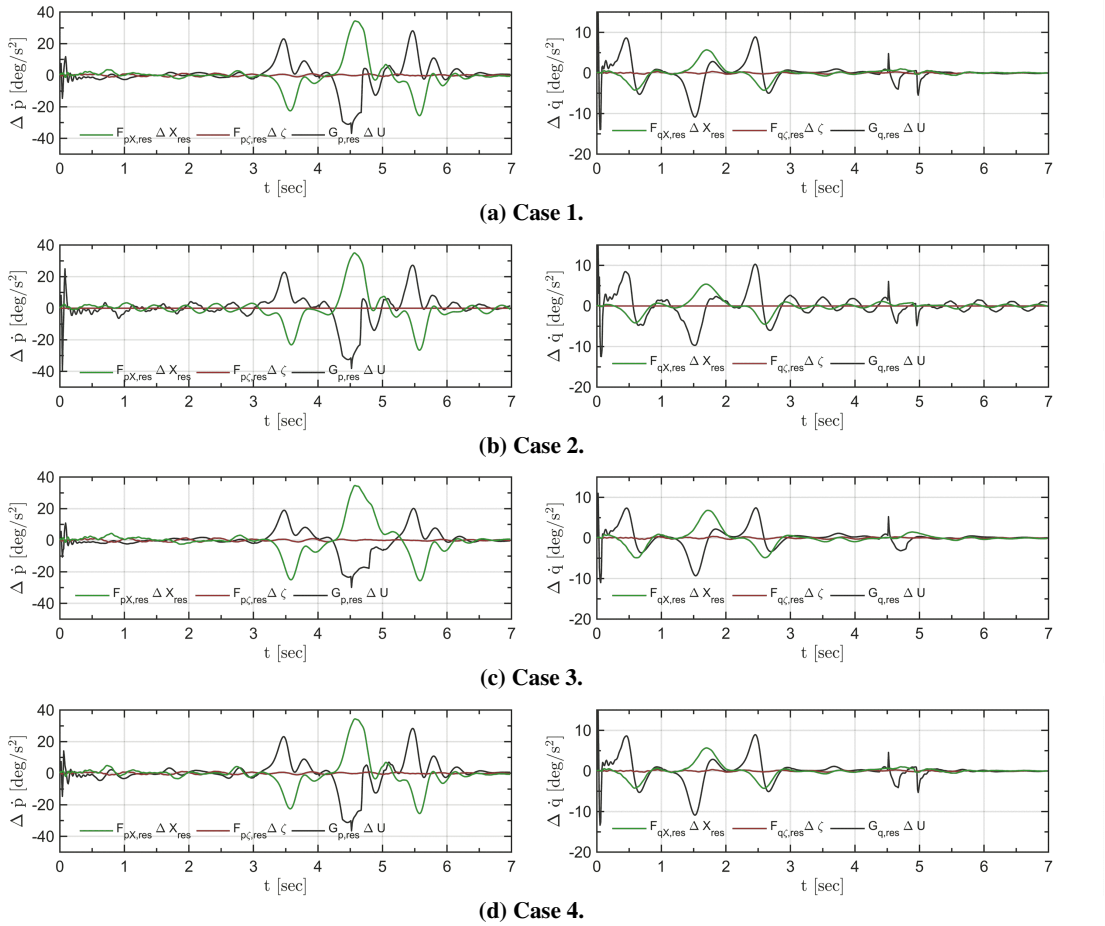

(a) Case 1.

(b) Case 2.

(c) Case 3.

(d) Case 4.

Fig. 32 Increments in system dynamics and control-depended increments for flap-lag residualised case II and flap residualised cases I,III and IV. It should be noted that X_{res} can be identified as the residualised state vector.

VIII. Conclusion

In this particular research the effects of flapping and lead-lag dynamics on IBS control design, performance and robustness were considered. For BFL models it was found that residualisation of flapping dynamics was sufficient to

establish an *idealised* rotorcraft model for which control-dependency was greater than state-dependency in the first-order *Taylor* series. In other words, when executing a control task, it was found that increments in system dynamics were already sufficiently diminished and control-depended increments were greatly enhanced. Residualisation of flapping dynamics did therefore yield a sufficient modified control effectiveness matrix, which could be used in an IBS control law. On the other hand, residualisation of flap-lag dynamics did not yield an *idealised* rotorcraft model that differed from the *idealised* rotorcraft model based upon flap residualisation. This shows that, the IBS controller is robust enough to uncertainties in lead-lag dynamics and adequate controller performance can be achieved by considering flap residualisation only.

An *idealised* rotorcraft model based upon flap residualisation, would yield a flap synchronisation that requires knowledge of the flapping dynamics. This can be regarded as one of the drawbacks when establishing an IBS controller based upon an *idealised* rotorcraft model. When the control effectiveness matrix in the synchronisation filter is associated with a control effectiveness mismatch, a steady-error would be apparent in the tracking response. This shows that the synchronisation filter is not robust to uncertainties in the control effectiveness matrix. All in all, it can be stated that sufficient model knowledge is required when incorporating an IBS controller with synchronisation filter. This is highly undesirable, because even though IBS is being considered for establishing the stabilising control law, one does still rely upon model knowledge to assure adequate controller performance.

Appendix

Helicopter data

This appendix provides helicopter data of the MBB Bo 105 used for simulations. Rotorcraft data was obtained from [1, 3, 26–29]. Actuator magnitude and rate limits were taken from [1]. Moreover, helicopter data for the Aérospatiale SA 330 Puma are also provided. Actuator limits for this rotorcraft were set equal to the ones provided for the MBB Bo 105.

Table 2 Parameters of the MBB Bo 105.

description of parameter	symbol	value	unit
Normalised flapping frequency	$\lambda_\beta = 1 + \frac{3}{2}\frac{\epsilon_\beta}{1-\epsilon_\beta}$	1.12	-
Normalised lagging frequency	$\lambda_\zeta^2 = \frac{3}{2}\frac{\epsilon_\zeta}{1-\epsilon_\zeta}$	0.49	-
Lag center-spring stiffness	$K_\zeta = \lambda_\zeta^2 I_{\mathrm{bl}}\Omega^2$	224	$\mathrm{kNm \cdot rad^{-1}}$
Flap center-spring stiffness	$K_\beta = (\lambda_\beta^2 - 1) I_\beta \Omega^2$	113	$\mathrm{kNm \cdot rad^{-1}}$
Main rotor Lock number	$\gamma = \frac{\rho C_{\mathrm{L}_\alpha} c_{\mathrm{e}} R^4}{I_\beta}$	5.0692	$\mathrm{rad^{-1}}$
Main rotor solidity	$\sigma = \frac{N c_{\mathrm{e}}}{\pi R}$	0.007	-
Tail rotor solidity	$\sigma_{\mathrm{tr}} = \frac{N_{\mathrm{tr}} c_{\mathrm{e_{tr}}}}{\pi R_{\mathrm{tr}}}$	0.1206	-

Table 3 Parameters main rotor of MBB Bo 105.

description of parameter	symbol	value	unit
Rotational speed	Ω	44.4	rad/s
Rotor radius	R	4.91	m
Steady-state coning angle	$\beta_{ss} = \beta_0$	2.5	deg
Number of blades	b/N	4	-
Equivalent blade chord	c_e	0.27	m
Zero lift profile drag coefficient	C_{D_0}	0.011	-
Profile drag coefficient $C_{D,1}$	C_{D_1}	0.4	-
Non-dimensional inflow velocity hover	λ_i	0.0495	-
Static blade moment (approximated)	m_s	50	mkg
Blade lift curve slope	C_{L_α}	6.11	$\mathrm{rad^{-1}}$
Linear blade twist	θ_{tw}	-0.1396	rad
Blade mass	m_{bl}	27.3	kg
Blade moment of inertia about its flapping hinge	I_{bl}	231.7	$\mathrm{kgm^2}$
Equivalent hinge offset ratio	ϵ_β	0.14	-
Rotor shaft tilt angle	γ_s	0.0524	rad
Lateral position with respect to the helicopter c.g.	l_1	0.02995	m
Longitudinal position with respect to the helicopter c.g.	l	-0.00761	m
Vertical position with respect to the helicopter c.g.	h	0.94468	m

Table 4 Tail rotor parameters of MBB Bo 105.

description of parameter	symbol	value	unit
Rotational speed	Ω_{tr}	233.1	rad/s
Rotor radius	R_{tr}	0.95	m
Number of blades	N_{tr}	2	-
Equivalent blade chord	$c_{e_{tr}}$	0.18	m
Blade lift curve slope	$C_{L_{\alpha,\text{tr}}}$	5.70	rad^{-1}
Main rotor downwash factor at the tail rotor	K_{tr}	1	-
Longitudinal position with respect to the helicopter c.g.	l_{tr}	6.00965	m
Vertical position with respect to the helicopter c.g.	h_{tr}	1.05418	m

Table 5 Fuselage parameters of MBB Bo 105.

description of parameter	symbol	value	unit
Parasite drag area	F_0	1.3	m^2
Eq. volume in the horizontal plane with only circular sections	V_{fus_M}	6.126	m^3
Eq. volume in the lateral plane with only circular sections	V_{fus_N}	25.525	m^3
Incidence angle for zero pitch moment	$\alpha_{\text{fus},M=0}$	0	rad
Correction coefficient for moment calculation	K_{fus}	0.83	-

Table 6 Horizontal tail parameters of the MBB Bo 105.

description of parameter	symbol	value	unit
Surface area	S_{ht}	0.803	m^2
Surface lift curve slope	$C_{L_\alpha,\text{ht}}$	4.0	rad^{-1}
Built-in surface incidence	α_{hto}	0.0698	rad
Correction coefficient in the pitch moment	K_{ht}	1.5	-
Longitudinal position with respect to the helicopter c.g.	l_{ht}	4.548	m

Table 7 Vertical tail parameters of the MBB Bo 105.

description of parameter	symbol	value	unit
Surface area	S_{vt}	0.805	m^2
Surface lift curve slope	$C_{L_\alpha,\text{vt}}$	4.0	rad^{-1}
Built-in surface incidence	β_{vto}	-0.0812	rad
Longitudinal position with respect to the helicopter c.g.	l_{vt}	5.416	m
Vertical position with respect to the helicopter c.g.	h_{vt}	0.970	m

Table 8 Actuator limitations of the MBB Bo 105.

description of parameter	symbol	Min. saturation limit [deg]	Max. saturation limit [deg]	Rate limit [deg/sec]
Collective pitch main rotor	θ_0	-0.2	20.0	16.0
Longitudinal cyclic	$\theta_{1\text{s}}$	-6.0	11.0	28.8
Lateral cyclic	$\theta_{1\text{c}}$	-5.7	4.2	16.0
Collective pitch tail rotor	$\theta_{0,\text{tr}}$	-8.0	20.0	32.0

Table 9 Mass and inertia properties of the MBB Bo 105.

description of parameter	symbol	value	unit
Total mass	M	2200	kg
Total weight	W	21574	N
Inertia tensor	J	$\begin{bmatrix} 1433 & 0 & -660 \\ 0 & 4973 & 0 \\ -660 & 0 & 4099 \end{bmatrix}$	$\text{kg}\cdot\text{m}^2$

Table 10 Parameters of Aérospatiale SA 330 Puma [9, 13].

description of parameter	symbol	value	unit
Rotational speed	Ω	28.3	rad/s
Rotor radius	R	7.5	m
Steady-state coning angle	$\beta_{ss} = \beta_0$	0.74	deg
Number of blades	b/N	4	-
Equivalent blade chord	c_e	0.3	m
Zero lift profile drag coefficient $C_{D,0}$ in ($C_D = C_{D,0} + C_{D,1}\alpha^2$)	C_{D_0}	0.011	-
Profile drag coefficient $C_{D,1}$ in ($C_D = C_{D,0} + C_{D,1}\alpha^2$)	C_{D_1}	0.4	-
Non-dimensional inflow velocity in hover	λ_i	0.0565	-
Static blade moment (approximated)	m_s	200	mkg
Blade mass	m_{bl}	68	kg
Blade moment of inertia about its flapping hinge	I_{bl}	1280	kgm^2
Equivalent hinge offset ratio	ϵ_β	0.3	-
Total mass	M	5805	kg
Total weight	W	56947	N
height main hub above centre of gravity	h	1.875	m
Normalised flapping frequency	$\lambda_\beta = 1 + \frac{3}{2}\frac{\epsilon_\beta}{1-\epsilon_\beta}$	1.02	-
Normalised lagging frequency	$\lambda_\zeta^2 = \frac{3}{2}\frac{\epsilon_\zeta}{1-\epsilon_\zeta}$	0.0625	-
Main rotor Lock number	$\gamma = \frac{\rho C_{L_\alpha} c_e R^4}{I_{bl}}$	9.374	rad^{-1}
Flap center-spring stiffness	$K_\beta = (\lambda_\beta^2 - 1) I_{bl}\Omega^2$	48	$kNm \cdot rad^{-1}$
helicopter moment of inertia about roll axis	I_{xx}	9638	$kg \cdot m^2$
helicopter moment of inertia about pitch axis	I_{yy}	33240	$kg \cdot m^2$

References

[1] Simplicio, P., "Helicopter nonlinear flight control: An acceleration measurements-based approach using incremental nonlinear dynamic inversion," 2011.

[2] Simplício, P., Pavel, M., Van Kampen, E., and Chu, Q., "An acceleration measurements-based approach for helicopter nonlinear flight control using incremental nonlinear dynamic inversion," *Control Engineering Practice*, Vol. 21, No. 8, 2013, pp. 1065–1077.

[3] Van Goot, R., "Helicopter Control using Incremental Adaptive Backstepping," 2017.

[4] Howitt, J., "Application of non-linear dynamic inversion to rotorcraft flight control," *ANNUAL FORUM PROCEEDINGS-AMERICAN HELICOPTER SOCIETY*, Vol. 61, AMERICAN HELICOPTER SOCIETY, INC, 2005, p. 1160.

[5] Skogestad, S., and Postlethwaite, I., *Multivariable feedback control: analysis and design*, Vol. 2, Wiley New York, 2007.

[6] van Ekeren, W., "Incremental Nonlinear Flight Control for Fixed-Wing Aircraft," 2016.

[7] Keijzer, T., "Design and Flight Testing of Incremental Control Laws using Angular Accelerometer Feedback on a CS-25 Aircraft," Ph.D. thesis, Delft University of Technology, 2018.

[8] van't Veld, R., "Incremental Nonlinear Dynamic Inversion Flight Control: Stability and Robustness Analysis and Improvements," 2016.

[9] Pavel, M., "Modeling Lead-Lag Dynamics for Rotorcraft-Pilot-Couplings Investigation," *American Helicopter Society 66th Annual Forum, Phoenix Arizona*, 2010.

[10] Tod, G., Pavel, M. D., Malburet, F., Gomand, J., and Barre, P.-J., "Understanding pilot biodynamical feedthrough coupling in helicopter adverse roll axis instability via lateral cyclic feedback control," *Aerospace Science and Technology*, Vol. 59, 2016, pp. 18–31.

[11] Fragnière, B., and Wartmann, J., "Local polynomial method frequency-response calculation for rotorcraft applications," *AHS 71st Annual Forum*, 2015.

[12] Fu, K.-H., and Kaletka, J., "Frequency-Domain Identification of BO 105 Derivative Models with Rotor Degrees of Freedom," *Journal of the American Helicopter Society*, Vol. 38, No. 1, 1993, pp. 73–83.

[13] Nguyen, A., "The Development of a Body-Flap-Lag Model for Rotorcraft-Pilot Couplings Investigation," 2008.

[14] Padfield, G. D., *Helicopter flight dynamics*, Wiley Online Library, 2008.

[15] Van Gils, P., "Adaptive Incremental Backstepping Flight Control," 2015.

[16] Sieberling, S., Chu, Q., and Mulder, J., "Robust flight control using incremental nonlinear dynamic inversion and angular acceleration prediction," *Journal of guidance, control, and dynamics*, Vol. 33, No. 6, 2010, pp. 1732–1742.

[17] Acquatella, B., "Robust Nonlinear Spacecraft Attitude Control: An Incremental Backstepping Approach," 2011.

[18] Booms, J. T., "Improving Helicopter Handling Qualities with Constrained Incremental Backstepping," 2017.

[19] Johnson, W., *Helicopter theory*, Courier Corporation, 2012.

[20] Hall Jr, W., and Bryson Jr, A., "Inclusion of rotor dynamics in controller design for helicopters," *Journal of Aircraft*, Vol. 10, No. 4, 1973, pp. 200–206.

[21] Sonneveldt, L., "Adaptive Backstepping Flight Control for Modern Fighter Aircraft," 2010.

[22] Aviation, U. A., and Command, M., "Aeronautical design standard performance specification handling qualities requirement for military rotorcraft. Redstone Arsenal, AL," *Redstone Arsenal, AL*, 2000.

[23] Ogata, K., and Yang, Y., *Modern control engineering*, Vol. 5, Prentice hall Upper Saddle River, NJ, 2010.

[24] Pavel, M., Shanthakumaran, P., Stroosma, O., et al., "Development of advanced flight control laws for the AH-64 apache helicopter-sketches from the work of TU Delft-Boeing project in SIMONA simulator," *Proceedings of the American Helicopter Society 72th Annual Forum*, 2016.

[25] Kaletka, J., Tischler, M. B., Fletcher, J. W., et al., "Time and Frequency-Domain Identification and Verification of BO 105 Dynamic Models," *Journal of the American Helicopter Society*, Vol. 36, No. 4, 1991, pp. 25–38.

[26] Prouty, R. W., and Curtiss, H., "Helicopter control systems: A history," *Journal of Guidance, Control, and Dynamics*, Vol. 26, No. 1, 2003, pp. 12–18.

[27] Prouty, R. W., *Helicopter performance, stability, and control*, 1995.

[28] Pavel, M. D., "On the necessary degrees of freedom for helicopter and wind turbine low-frequency mode modeling," 2001.

[29] Padfield, G. D., McCallum, A., Haverdings, H., Dequin, A.-M., Haddon, D., Kampa, K., Basset, P.-M., and Von Gruenhagen, W., "Predicting rotorcraft flying qualities through simulation modelling. A review of key results from Garteur AG06," *European Rotorcraft Forum*, Vol. 22, ASSOCIAZIONE ITALIANA DI AERONAUTICA ED ASTRONAUTICA, 1996, pp. 71–1.

Part II
Main Report

2
Rotorcraft Simulation Models

In this chapter the main BO-105 rotorcraft simulation model is introduced along with a set of simplified BF(L) rotorcraft models. The original BO-105 model originates from [46] and has been extended with a first-order *Pitt-Peters* inflow model and second-order flapping model from [38] by van der Goot [55]. The main simulation model has been extended by means of lead-lag dynamics from [34]. In Section 2.1 the coupled body-rotor equations of motion are provided using the CSER model. In Section 2.2 the coupled nature between flap and lag dynamics is provided. The coupled flap-lag EOM from [34] are provided in Section 2.3. The first-order *Pitt-Peters* inflow model is introduced in Section 2.4. The forces and moments generated by the rotorcraft are touched upon in Section 2.5. Body dynamics will be considered in Section 2.6. Numerical integration of the EOM will be considered in Section 2.7. In Section 2.8 simplified rotorcraft models are provided.

2.1. Coupled Body-Rotor Equations of Motion

The main objective of this section is provide background information about the rotor model of the main simulation model. The current rotorcraft model does incorporate a quasi-steady second-order flapping model from Padfield [37] modelled up to the first harmonic of the rotor speed. Below the derivation of the CSER flapping model from Padfield [37] is provided. The reference frames used to derive the coupled body-rotor EOM can be found in Appendix A.

2.1.1. Second-order flapping dynamics model defined using CSER model

In order to obtain the flapping EOM, it is first necessary to determine the moments around the center of rotation of each *i*th blade. This is analogous to taking moments about the centre hinge spring, because of the spring being situated at the the center of rotation with spring stiffness K_β. The moment can be written as

$$\int_0^R r_{bl}\left(f_z(r_{bl}) + m_{bl}a_{zb}\right)dr_b + K_\beta\beta_i = 0, \tag{2.1}$$

wherein $f_z(r_{bl})$ is the aerodynamic normal force acting on the blade element, a_{zb} the acceleration of a blade element with mass m and K_β the centre-spring stiffness acting over radial distance β [37]. Blade weight force was not taken into account, because the acceleration and mean lift forces are approximately one or two orders of magnitude greater. The aerodynamic normal force is given in Eq. 2.2 [37].

$$f_z = -\cos(\phi)l - d\sin(\phi) \approx -\cos(\phi)l - d\phi. \tag{2.2}$$

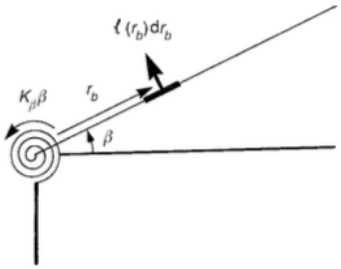

Figure 2.1: CSER model with model parameters [37].

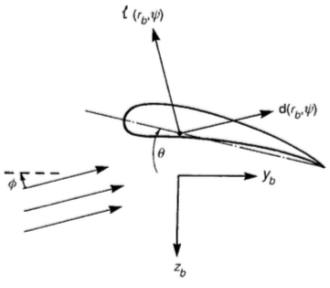

Figure 2.2: Blade element with decomposed forces [37].

It can be observed that l and d are the decomposed components of $f_z(r_b)$. The magnitude of l and d depend upon ϕ, being the incidence angle between rotor inflow and the plane normal to the rotor shaft. The blade element acceleration a_{zb} does include the component of gyroscopic effect, which is due to the fuselage and hub rotation. The approximate expression for a_{zb} is given in Eq. 2.3 [37].

$$a_{zbl} \approx r_{bl}\left(2\Omega\left(p_{hw}\cos\left(\psi_i^{bw}\right) - q_{hw}\sin\left(\psi_i^{bw}\right)\right) + \left(\dot{q}_{hw}\cos\left(\psi_i^{bw}\right) + \dot{p}_{hw}\sin\left(\psi_i^{bw}\right)\right) - \Omega^2\beta_i - \ddot{\beta}_i\right) \tag{2.3}$$

Angular accelerations and velocities have been defined with respect to the hub-wind (hw) reference frame. This reference frame is analogous to the hub reference frame, but the x_{hw}-axis aligned with the hub velocity in the hub plane. The hub-wind frame of reference is found suitable for the derivation of the BF EOM. However, later on the BF EOM needs to be transformed to the hub frame of reference to determine forces and moments. The analytical expressions for lift $l(\psi_i^{bw}, r_{bl})$ and drag $d(\psi_i^{bw}, r_{bl})$ are respectively

$$l\left(\psi_i^{bw}, r_{bl}\right) = \frac{1}{2}\rho c a_0\left(\theta + \frac{U_T}{U_P}\right)\left(U_T^2 + U_P^2\right), \tag{2.4}$$

$$d\left(\psi_i^{bw}, r_{bl}\right) = \frac{1}{2}\rho c\delta\left(U_T^2 + U_P^2\right), \tag{2.5}$$

wherein U_T and U_p are the in-plane and normal velocity components, ρ the air density, a_0 the lift curve slop, c the chord length, θ the blade pitch angle and δ the profile drag coefficient is written as a function of a mean value and a thrust-depended term [37]. This is due to blade incidence alterations. The profile drag coefficient is a linear combination of the constant coefficients δ_0 and $\delta_2 C_T^2$ thus $\delta_0 + \delta_2 C_T^2$ [37]. As mentioned previously, $l\left(\psi_i^{bw}, r_{bl}\right)$ and $d\left(\psi_i^{bw}, r_{bl}\right)$ do depend on U_T and U_P, which can be expressed in normalised form as

$$\bar{U}_T\left(\psi_i^{bw}, r_{bl}\right) = \frac{U_T}{\Omega R} = \bar{r}_{bl}\left(1 + \bar{\omega}_x\beta_i\right) + \mu\sin\left(\psi_i^{bw}\right), \tag{2.6}$$

$$\bar{U}_P\left(\psi_i^{bw}, r_{bl}\right) = \frac{U_T}{\Omega R} = \left(\mu_z - \lambda_0 - \beta_i\mu\cos\left(\psi_i^{bw}\right)\right) + \bar{r}_{bl}\left(\bar{\omega}_y - \frac{\dot{\beta}_i}{\Omega} - \lambda_1\right), \tag{2.7}$$

wherein $\bar{U}_T\left(\psi_i^{bw}, r_{bl}\right)$ and $\bar{U}_P\left(\psi_i^{bw}, r_{bl}\right)$ depend on the non-dimensional advance ratios μ and μ_z respectively [37]. These depend on local velocities in the hub-wind reference frame at a given azimuth angle ψ_i^{bw}. The normalised velocity components do also depend on the non-dimensional angular velocity components $\bar{\omega}_x$ and $\bar{\omega}_y$ respectively. $\bar{U}_T\left(\psi_i^{bw}, r_{bl}\right)$ does not explicitly depend on the inflow dynamics, on the contrary $\bar{U}_P\left(\psi_i^{bw}, r_{bl}\right)$ does depend on λ_0 and λ_1, being a constant inflow component and an inflow component varying with ψ_i^{bw} and $\bar{r}_{bl}$ respectively. The advance ratios μ and μ_z are provided in Eq. 2.8 [37].

$$\mu = \frac{u_{hw}}{\Omega R} = \left(\frac{u_h^2 + v_h^2}{(\Omega R)^2}\right)^{1/2}, \quad \mu_z = \frac{w_{hw}}{\Omega R}. \tag{2.8}$$

The advance ratios depend on hub velocities in the hub-wind reference frame. The non-dimensional angular velocity components about the x_{hw}- and y_{hw}-axis of the fuselage are given in Eq. 2.9 and Eq. 2.10 [37].

$$\bar{\omega}_x = \bar{p}_{hw}\cos\left(\psi_i^{bw}\right) - \bar{q}_{hw}\sin\left(\psi_i^{bw}\right) \tag{2.9}$$

$$\bar{\omega}_y = \bar{p}_{hw}\sin\left(\psi_i^{bw}\right) + \bar{q}_{hw}\cos\left(\psi_i^{bw}\right) \tag{2.10}$$

Both $\bar{\omega}_x$ and $\bar{\omega}_y$ show dependency on the non-dimensional downwash velocity . The non-dimensional downwash velocity normal to the disc plane is a linearly varying with ψ and r_{bl}. Additionally it also depends on a constant inflow component, namely λ_0. The expression for $\lambda(\psi_i^{hw})$ is given in Eq. 2.11 [37].

$$\lambda(\psi_i^{hw}) = \frac{v_i}{\Omega R} = \lambda_0 + \lambda_1(\psi_i^{hw})\bar{r}_{bl} \tag{2.11}$$

The moment equation for each i^{th} rotor blade around the center spring hinge from Eq. 2.1 can be rewritten by using Eq. 2.3-2.9. The second-order differential equation of the flapping motion for each rotor blade is given in the next equation [37].

$$\beta_i'' + \lambda_\beta^2 \beta_i = 2\left(\left(\bar{p}_{hw} + \frac{\bar{q}_{hw}'}{2}\right)\cos\psi_i - \left(\bar{q}_{hw} + \frac{\bar{p}_{hw}'}{2}\right)\sin\psi_i\right) + \frac{\gamma}{2}\int_0^1 \left(\bar{U}_T^2\theta + \bar{U}_T\bar{U}_P\right)_i \bar{r}_b \mathrm{d}\bar{r}_b \tag{2.12}$$

The equation can be expanded into another form, which depends on λ_β, γ and I_β. The expanded form also does require the rotor blade pitch angle θ to be rewritten as the summation of the local twist linear with radial position $\bar{r}_b\theta_{tr}$ and the applied twist θ_p, thus θ is $\theta_p + \bar{r}_{bl}\theta_{tw}$ with $\bar{r}_{bl}$ equal to $dr_{bl}/d\theta_{tw}$ [37]. The second-order differential equation of the flapping motion can be expanded into the form given in Eq. 2.13 [37].

$$\begin{aligned}\beta_i'' + f_{\beta'}\gamma\beta_i' + \left(\lambda_\beta^2 + \gamma\mu\cos\psi_i f_\beta\right)\beta_i = 2\left(\left(\bar{p}_w + \tfrac{\bar{q}_w'}{2}\right)\cos\psi_i - \left(\bar{q}_w - \tfrac{\bar{p}_w'}{2}\right)\sin\psi_i\right) \\ +\gamma\left[f_{\theta p}\theta_p + f_{\theta tw}\theta_{tw} + f_\lambda\left(\mu_z - \lambda_0\right) + f_\omega\left(\bar{\omega}_y - \lambda_1\right)\right]\end{aligned} \tag{2.13}$$

The Aerodynamic coefficients in Eq. 2.13 have been expanded up to $O(\mu^2)$, therefore higher order terms are neglected. This affects flapping response for $\mu \leq 0.35$. The aerodynamic coefficients are given in Eq. 2.14 [37].

$$\boldsymbol{f}\begin{cases} f_{\beta'} = \dfrac{1 + \frac{4}{3}\mu\sin\psi_i}{8} \\ f_\beta = f_\lambda = \dfrac{\frac{4}{3} + 2\mu\sin\psi_i}{8} \\ f_\omega = \dfrac{1 + \frac{4}{3}\mu\sin\psi_i}{8} \\ f_{\theta p} = \dfrac{1 + \frac{8}{3}\mu\sin\psi_i + 2\mu^2\sin^2\psi_i}{8} \\ f_{\theta tw} = \dfrac{\frac{4}{5} + 2\mu\sin\psi_i + \frac{4}{3}\mu^2\sin^2\psi_i}{8} \end{cases} \tag{2.14}$$

The second-order differential equation of the flapping motion for each i^{th} rotor blade defined in Eq. 2.13, can be written into the following general form

$$\boldsymbol{\beta}_I'' + \boldsymbol{C}_I(\psi^{hw})\boldsymbol{\beta}_I' + \boldsymbol{D}_I(\psi^{hw})\boldsymbol{\beta}_I = \boldsymbol{H}_I(\psi^{hw}), \tag{2.15}$$

which is defined in the rotating hub-wind reference frame [37]. The individual blade coordinates (IBCs) shall be converted to multi-blade coordinates (MBCs), which can be achieved by the following transformation

$$\boldsymbol{\beta}_I = \boldsymbol{L}_\beta\boldsymbol{\beta}_M, \text{ with } \begin{cases} \beta_0 = \dfrac{1}{N_b}\sum_{i=1}^{N_b}\beta_i \\ \beta_{0d} = \dfrac{1}{N_b}\sum_{i=1}^{N_b}\beta_i\left[-1\right]^i \\ \beta_{jc} = \dfrac{2}{N_b}\sum_{i=1}^{N_b}\beta_i\cos(j\psi_i^{hw}) \\ \beta_{js} = \dfrac{2}{N_b}\sum_{i=1}^{N_b}\beta_i\sin(j\psi_i^{hw}) \end{cases} \text{ and } \boldsymbol{\beta}_I = [\beta_1,\ \beta_2,\ \beta_3,\ \beta_4]^T, \tag{2.16}$$

wherein the *MBCs* can be obtained by considering the inverse transformation, thus $\boldsymbol{L}_\beta^{-1}\boldsymbol{\beta}_I$ [37]. Additionally it should be noted that the individual blade azimuth angles are related with each other in accordance with

$$\psi_i^{hw} = \psi^{hw} - \frac{\pi}{2}(i-1), \quad \text{for} \quad i = 1, 2..n. \tag{2.17}$$

The transformation from Eq. 2.16 can be written in matrix form, which is given in Eq. 2.18 [37]. The transformation to *MBCs* is associated with the inverse of $\boldsymbol{L}_\beta(\psi^{hw})$, which is provided in Eq. 2.19 [37].

$$\mathbf{L}_\beta(\psi^{hw}) = \begin{bmatrix} 1 & -1 & \cos(\psi^{hw}) & \sin(\psi^{hw}) \\ 1 & 1 & \sin(\psi^{hw}) & -\cos(\psi^{hw}) \\ 1 & -1 & -\cos(\psi^{hw}) & -\sin(\psi^{hw}) \\ 1 & 1 & -\sin(\psi^{hw}) & \cos(\psi^{hw} \end{bmatrix} \tag{2.18}$$

$$\mathbf{L}_{\beta}^{-1}(\psi^{hw}) = \frac{1}{4}\begin{bmatrix} 1 & 1 & 1 & 1 \\ -1 & 1 & -1 & 1 \\ 2\cos(\psi^{hw}) & 2\sin(\psi^{hw}) & -2\cos(\psi^{hw}) & -2\sin(\psi^{hw}) \\ 2\sin(\psi^{hw}) & -2\cos(\psi^{hw}) & -2\sin(\psi^{hw}) & 2\cos(\psi^{hw}) \end{bmatrix} \tag{2.19}$$

The transformation matrix $\mathbf{L}_{\beta}(\psi^{hw})$ enables to perform the transformation from rotating to the non-rating hub-frame of reference. This also requires Eq. 2.15 to be rewritten in the non-rotating frame of reference

$$\boldsymbol{\beta}_M'' + \boldsymbol{C}_M(\psi^{hw})\boldsymbol{\beta}_M' + \boldsymbol{D}_M(\psi^{hw})\boldsymbol{\beta}_M = \boldsymbol{M}_M(\psi^{hw}), \tag{2.20}$$

wherein $\boldsymbol{\beta}_M$ does consist of the vector with the MBC coordinates β_0, β_{1c}, β_{1s} and $\beta_{N/2}$ [37]. In order to establish the *MBC* transformation it is deemed necessary to consider it with respect to the hub reference frame. Transforming the IBCs in the rotating hub-wind reference frame to MBCs in the non-rotating frame of reference is problematic, because the hub-wind reference frame is non-inertial around hover state. It is therefore a natural choice to obtain MBCs from the IBCs using the hub reference frame. This can be achieved by observing the following relation between the transformation matrices

$$\boldsymbol{L}_{\beta}(\psi^{hw}) = \boldsymbol{L}_{\beta}(\psi^{h} + \psi^{w}) = \boldsymbol{L}_{\beta}(\psi^{h})\boldsymbol{T}_{w}(\psi^{w}), \quad \text{thus} \quad \boldsymbol{L}_{\beta}(\psi^{hw}) = \boldsymbol{L}_{\beta}(\psi^{hw})T_{w}^{-1}(\psi^{hw}), \tag{2.21}$$

wherein $\boldsymbol{T}_w$ is of course the transformation from the hub to the hub-wind reference frame [37]. In order to define Eq. 2.15 by means of Eq. 2.21, it is also necessary to have its first and second order derive with respect to ψ^{hw}. In order to establish this, the derivative equivalence provided below must be considered [37].

$$\frac{d\boldsymbol{L}_{\beta}(\psi^{hw})}{d\psi^{hw}} = \frac{d\boldsymbol{L}_{\beta}(\psi^{h}+\psi_{w})}{d(\psi^{h}+\psi_{w})} = \frac{d\boldsymbol{L}_{\beta}(\psi^{h}+\psi_{w})}{d(\psi^{h}+\psi_{w})} = \frac{d\boldsymbol{L}_{\beta}(d\psi^{b}}{d\psi^{h}} = \frac{d\boldsymbol{L}_{\beta}(d\psi^{hw})}{d\psi^{h}}. \tag{2.22}$$

The transformation from Eq. 2.21 and derivative equivalence from Eq. 2.22 enables to define the first and second order derivatives of Eq. 2.15 in the hub frame of reference with respect to ψ^{h}.

$$\begin{aligned} \boldsymbol{\beta}_I &= \boldsymbol{L}_{\beta}(\psi^{hw})\boldsymbol{T}_{w}^{-1}(\psi^{w})\boldsymbol{\beta}_M \\ \boldsymbol{\beta}_I' &= \boldsymbol{L}_{\beta}'(\psi^{hw})\boldsymbol{T}_{w}^{-1}(\psi^{w})\boldsymbol{\beta}_M + \boldsymbol{L}_{\beta}(\psi^{hw})\boldsymbol{T}_{w}^{-1}(\psi^{w})\boldsymbol{\beta}_M' \\ \boldsymbol{\beta}_I'' &= \boldsymbol{L}_{\beta}''(\psi^{hw})\boldsymbol{T}_{w}^{-1}(\psi^{w})\boldsymbol{\beta}_M + 2\boldsymbol{L}_{\beta}'(\psi^{hw})\boldsymbol{T}_{w}^{-1}(\psi^{w})\boldsymbol{\beta}_M' + \boldsymbol{L}_{\beta}(\psi^{hw})\boldsymbol{T}_{w}^{-1}(\psi^{w})\boldsymbol{\beta}_M'' \end{aligned} \tag{2.23}$$

Substituting the derivatives into 2.20 and isolating the terms associated with the *inertia, damping, stiffness* and *excitation* of the system yields the following set of matrices

$$\begin{aligned} \boldsymbol{C}_{NR} &= \boldsymbol{T}_w\boldsymbol{L}_{\beta}^{-1}(\psi^{hw})\Big(2\boldsymbol{L}_{\beta}'\boldsymbol{T}_{w}^{-1} + \boldsymbol{C}_I\boldsymbol{L}_{\beta}(\psi^{hw})\boldsymbol{T}_{w}^{-1}\Big), \\ \boldsymbol{D}_{NR} &= \boldsymbol{T}_w\boldsymbol{L}_{\beta}^{-1}(\psi^{hw})\Big(\boldsymbol{L}_{\beta}''(\psi^{hw})\boldsymbol{T}_{w}^{-1} + \boldsymbol{C}_I\boldsymbol{L}_{\beta}'(\psi^{hw})\boldsymbol{T}_{w}^{-1} + \boldsymbol{D}_I L_{\beta}(\psi^{bw})\boldsymbol{T}_{w}^{-1}\Big), \\ \boldsymbol{H}_{NR} &= \boldsymbol{T}_w\boldsymbol{L}(\psi^{hw})^{-1}\boldsymbol{H}_I. \end{aligned} \tag{2.24}$$

The second-order differential equation for flapping dynamics with respect to time can be defined as

$$\boldsymbol{M}_{NR}\ddot{\boldsymbol{\beta}}_{NR} + \Omega\boldsymbol{C}_{NR}\dot{\boldsymbol{\beta}} + \Omega^2\boldsymbol{D}_{NR}\beta = \Omega^2\boldsymbol{F}_{NR}. \tag{2.25}$$

The matrices associated with this differential equation are provided in Eq. 2.26 [37].

$$\mathbf{M}_{NR} = I_{n\times n}, \quad \mathbf{C}_{NR} = \frac{\gamma}{8}\begin{bmatrix} 1 & 0 & 0 & \frac{2}{3}\mu \\ 0 & 1 & 0 & 0 \\ 0 & 0 & 1 & \frac{16}{\gamma} \\ \frac{4}{3}\mu & 0 & -\frac{16}{\gamma} & 1 \end{bmatrix}, \quad \mathbf{D}_{NR} = \frac{\gamma}{8}\begin{bmatrix} \frac{8\lambda_\beta^2}{\gamma} & 0 & 0 & 0 \\ \frac{\gamma}{0} & \frac{8\lambda_\beta^2}{\gamma} & 0 & 0 \\ \frac{4}{3}\mu & 0 & \frac{8\left(\lambda_\beta^2-1\right)}{\gamma} & 1+\frac{\mu^2}{2} \\ 0 & 0 & -\left(1-\frac{\mu^2}{2}\right) & \frac{8\left(\alpha_\beta^2-1\right)}{\gamma} \end{bmatrix} \text{ and}$$

$$\mathbf{F}_{NR} = \begin{bmatrix} \theta_0\left(1+\mu^2\right)+\frac{4}{3}\lambda+4\theta_{tw}(\frac{1}{5}+\frac{\mu^2}{6})+\frac{2}{3} \\ \frac{8}{3}\mu\theta_0+2\mu\lambda+2\mu\lambda+2\mu\theta_{tw}+\bar{p}-\frac{16}{\gamma}q+\left(1+\frac{3}{2}\mu^2\right)\theta_{1s}-\lambda_{1s} \\ 0 \\ \left(1+\frac{\mu^2}{2}\right)\theta_{1c}+\frac{16}{\gamma}\bar{p}+\bar{q}-\lambda_{1c}+\left(\frac{8}{\gamma}K\lambda_0\right) \end{bmatrix} \tag{2.26}$$

2.2. Coupled nature of flapping and lead-lag dynamics

With flapping dynamics being defined, it is necessary to introduce lead-lag dynamics. It is of great interest to understand the coupled nature of the out-of-plane and in-plane motion of the rotor blade. The coupled flap-lag motion in simplified form from Padfield [37] can be written as

$$\boldsymbol{\beta}'' + \lambda_\beta^2\beta - 2\boldsymbol{\beta}\dot{\boldsymbol{\zeta}} = \boldsymbol{M}_\beta, \tag{2.27}$$

$$\boldsymbol{\zeta}'' + C_\zeta\dot{\boldsymbol{\zeta}} + \lambda_\zeta^2\boldsymbol{\zeta} + 2\beta\dot{\boldsymbol{\beta}} = \boldsymbol{M}_\zeta, \tag{2.28}$$

wherein $\boldsymbol{M}_F$ and $\boldsymbol{M}_L$ are the generalised flapping and lead-lag moments. From Eq. 2.27 and Eq. 2.28 it can be observed that there is mutual influence between the flapping and lagging motion. Lead-lag and flapping motion are coupled as a result of the *Coriolis* and aerodynamic forces [31]. The *Coriolis* effect can be regarded as an additional inertial force, which was first described by *Gustave-Gaspard Coriolis* in 1835. When there is radial lengthening or shortening of the rotor blade about the rotational axis, there will be Coriolis force. The dominant coupling terms for the flapping and lagging motion are therefore $-2\beta\dot{\zeta}$ and $2\beta\dot{\beta}$ respectively. Due to the low damping characteristics, the *Coriolis* effect will affect lead-lag motion more than flapping motion [37, 40]. The lag dynamics can be described by means of a mass-spring system being excited by means of in-plane aerodynamic forces (profile and induced drag) and *Coriolis* force due to blade flapping. The aerodynamic forces do damping the lag motion, but less effectively than the out-of-plane motion. It is important to note that all lag moments are small compared to the flap moments, thus the Coriolis force due to the flapping velocity is an important factor in the lag dynamics. For hingeless rotors the structural damping of the rotor blades should be included. Structural damping is low, but it can be considered important to lag dynamics because of the in-plane forces being small.

2.3. Lagrange method for defining coupled flap-lag EOM

Rotorcraft model fidelity can be enhanced by including the in-plane motion of the rotor. Implementation of flap dynamics could be achieved without taking lead-lag dynamics into account, because its effect on flapping dynamics is minor when comparing the effect of flapping dynamics on lead-lag dynamics. The aforementioned thus also implies that implementation of lead-lag dynamics also requires flapping dynamics to be defined. The main objective is therefore to provide the coupled flap-lag model based upon Lagrange's method, which was introduced in [34]. A full derivation of the BFL model shall not be given, but a short version will be considered here. The first step towards deriving the coupled flap-lag EOM is by defining a set of reference frames as given in Appendix A and a set of assumptions as given in Appendix B. It is first deemed necessary to determine the velocity vector of the shaft axis origin written in the body axis system, which is provided in Eq. 2.29 [34].

$$\vec{\boldsymbol{V}}_s = \vec{\boldsymbol{V}} + \vec{\boldsymbol{\omega}} \times \vec{\boldsymbol{r}} = (u,v,w)\left\{\vec{E}_b\right\} + h(0,0,-1)[\omega]_x\left\{\vec{E}_b\right\} \qquad \text{with} \quad [\omega]_x = \begin{bmatrix} 0 & r & -q \\ -r & 0 & p \\ q & -p & 0 \end{bmatrix} \tag{2.29}$$

The angular velocity of the rotor blade is the sum of the angular velocity of the centre of gravity of the helicopter, the anticlockwise rotor speed and the angular motion of the blade due to flapping. The expression for the total angular velocity of the rotor blade is provided in Eq. 2.30 [34].

$$\vec{\omega}_{bl} = (p,q,r)\left\{\vec{E}_s\right\} + \Omega(0,0,-1)\left\{\vec{E}_s\right\} + \dot{\zeta}(0,0,-1)\left\{\vec{E}_\zeta\right\} + \dot{\beta}(0,-1,0)\left\{\vec{E}_{bl}\right\}. \tag{2.30}$$

The blade angular velocity expressed in blade plane of reference can be written as given in Eq. 2.31 [34].

$$\left\{\vec{\omega}_{bl}\right\} = \left\{\begin{array}{c} p_{bl} \\ q_{bl} \\ r_{bl} \end{array}\right\}\left\{\vec{E}_{bl}\right\}, \quad \text{thus} \quad \left\{\begin{array}{c} p_{bl} \\ q_{bl} \\ r_{bl} \end{array}\right\} = \left\{\vec{E}_{bl}\right\}^{-1}\left\{\vec{\omega}_{bl}\right\} \tag{2.31}$$

The individual components p_{bl}, q_{bl} and r_{bl} can be expressed respectively as

$$p_{bl} = -p\cos\beta\cos\zeta\cos\psi + q\sin\psi\cos\zeta\cos\beta - p\sin\psi\cos\beta\sin\zeta - q\cos\psi\cos\beta\sin\zeta - \dot{\zeta}\sin\beta + \Omega\sin\beta \ , \tag{2.32}$$

$$q_{bl} = p\sin\zeta\cos\psi - q\sin\psi\sin\zeta\cos\beta + \dot{\beta} - p\sin\psi\cos\zeta - q\cos\psi\cos\zeta \ , \tag{2.33}$$

$$r_{bl} = -p\sin\beta\cos\zeta\cos\psi + q\sin\psi\cos\zeta\sin\beta - p\sin\psi\sin\beta\sin\zeta - q\cos\psi\sin\beta\sin\zeta + \dot{\zeta}\cos\beta - \Omega\cos\beta \ . \tag{2.34}$$

An arbitrary point on the blade situated at a distance $\boldsymbol{r}$ from the hub has a velocity $\vec{\boldsymbol{V}}_\omega$, with respect to the blade system of reference, for which the expression is provided in Eq. 2.35 [34].

$$\vec{V}_\omega = \vec{\omega}_{bl} \times \vec{r}_{bl} = r_{bl}(-1,0,0)\,[\omega_{bl}]_x\left\{\vec{E}_{bl}\right\}, \quad \text{with } [\omega_{bl}]_x = \left[\begin{array}{ccc} 0 & r_{bl} & -q_{bl} \\ -r_{bl} & 0 & p_{bl} \\ q_{bl} & -p_{bl} & 0 \end{array}\right]. \tag{2.35}$$

An arbitrary point on the rotor blade does have total velocity $\vec{\boldsymbol{V}}_{bl}$ consisting of the velocity of the shaft origin $\vec{\boldsymbol{V}}_{O_s}$ and the velocity with respect to this given origin $\vec{\boldsymbol{V}}_\omega$. Blade velocity $\left\{\vec{\boldsymbol{E}}_s\right\}$ is given in Eq. 2.36 [34].

$$\vec{V}_{bl} = (u - hq, v + hp, w)\left\{\vec{E}_s\right\} + r_{bl}(-1,0,0)\,[\beta]\,[\zeta]\,[\psi]\,[\omega_{bl}]_x\left\{\vec{E}_s\right\} \tag{2.36}$$

Transforming the blade velocity to the blade axis system yields Eq. 2.37 [34].

$$\vec{V}_{bl} = (u - hq, v + hp, w)\,[\psi]^T\,[\zeta]^T\,[\beta]^T\left\{\vec{E}_{bl}\right\} + r_{bl}(-1,0,0)\,[\omega_{bl}]_x\left\{\vec{E}_{bl}\right\} \tag{2.37}$$

The expression for the tangential and perpendicular velocity components of a blade element are provided in Eq. 2.38 and Eq. 2.39 respectively, wherein v_0 is the local inflow velocity [34].

$$\begin{aligned} U_T = {} & ((\sin\zeta)\cos\psi\sin\beta - \cos\zeta\sin\psi\sin\beta)q + (\sin\zeta\sin\psi\sin\beta + \cos\zeta\cos\psi\sin\beta)p - r\cos\beta - \\ & \cos\beta\left(\dot{\zeta}\right) + \cos\beta\omega\big)\,r_\beta + (\cos\psi\cos\beta + \sin\psi\sin\zeta)hp + (\sin\psi\cos\zeta - \cos\psi\sin\zeta)u + \\ & (-\sin(\psi)\cos\zeta - \cos\psi\sin\zeta)qh + (\cos\psi\cos\zeta + \sin\psi\sin\zeta)v \end{aligned} \tag{2.38}$$

$$\begin{aligned} U_P = {} & ((-\sin\psi\cos\zeta + \cos\psi\sin\zeta))p + (-\cos\psi\cos\zeta - \sin\psi\sin\zeta)q + \dot{\beta}\big)\,r_{\mathrm{bl}} + (\sin\zeta\cos\psi\sin\beta \\ & - \cos\zeta\sin\psi\sin\beta)hp + (\sin\zeta\sin\psi\sin\beta)hp + (-\sin\zeta\sin\psi\sin\beta + \cos\zeta\cos\psi\sin\beta)u - \\ & \cos\zeta\cos\psi\sin\beta - \cos\zeta\cos\psi\sin\beta)qh + v_o + (\sin\zeta\cos\psi\sin\beta - \cos\zeta\sin\psi\sin\beta)v - w\cos\beta \end{aligned} \tag{2.39}$$

The *Lagrangian* equations for β and ζ are given in Eq. 2.40 and 2.41 respectively, wherein the total energy consists of kinetic T and potential V energy [34]. Furthermore Q_β and Q_ζ are the generalised moments applied to the system in β- and z-direction respectively. *Rayleigh* damping is taken into account for lagging motion.

$$\frac{d}{dt}\frac{\partial\left(\frac{1}{2}I_{bl}\left(q_{bl}^2 + r_{bl}^2\right)\right)}{\partial\dot{\beta}} - \frac{\partial\left(\frac{1}{2}I_{bl}\left(q_{bl}^2 + r_{bl}^2\right)\right)}{\partial\beta} + \frac{\partial\left(\frac{1}{2}K_\beta\beta^2 + \frac{1}{2}K_\zeta\zeta^2\right)}{\partial\beta} = \int_0^R \left(dL\cos\varphi + dD\sin\varphi\right)r_{bl} \tag{2.40}$$

$$\frac{d}{dt}\frac{\partial\left(\frac{1}{2}I_{bl}\left(q_{bl}^2 + r_{bl}^2\right)\right)}{\partial\dot{\zeta}} - \frac{\partial\left(\frac{1}{2}I_{bl}\left(q_{bl}^2 + r_{bl}^2\right)\right)}{\partial\zeta} + \frac{\partial\left(\frac{1}{2}K_\beta\beta^2 + \frac{1}{2}K_\zeta\zeta^2\right)}{\partial\zeta} + \frac{\frac{1}{2}C_\zeta\dot{\zeta}^2}{\partial\dot{\zeta}} = \int_0^R (dL\sin\varphi + dD\cos\varphi)\,r_{bl} \tag{2.41}$$

The generalised moments in β-and-z directions are due to the aerodynamic moments around the flapping and lagging hinges respectively. Moreover, the moment due to gravity force being neglected . The expression for Q_β and Q_ξ are provided in Eq. 2.42 and Eq. 2.43 respectively [34].

$$Q_\beta = \int_0^R (dL\cos\varphi + dD\sin\varphi) r_{bl} \approx \int_0^R \frac{\rho}{2}\big(cdr_{bl}\big)U_T^2 Cl_\alpha\Big(\alpha + \theta_{tw}\frac{r_{bl}}{R}\Big)r_{bl} \tag{2.42}$$

$$Q_\xi = \int_0^R (dL\sin\varphi + dD\cos\varphi) r_{bl} \approx \int_0^R (\frac{\rho}{2}\big(cdr_{bl}\big)U_T^2 Cl_\alpha\Big(\alpha + \theta_{tw}\frac{r_{bl}}{R}\Big)\varphi + \frac{\rho}{2}\big(cdr_{bl}\big)U_T^2 Cd_0 + Cd_2\alpha^2) r_{bl} \tag{2.43}$$

It should be noted that dL and dD are the incremental lift and drag force on a blade element respectively. Furthermore φ is the the local inflow angle of a blade element, which is approximately equal to U_P/U_T when using small angle assumption [34]. The generalised moment equation Q_β can be simplified by realising that $\cos(\varphi) > \sin(\varphi)$ and $dL > dD$, the expression for Q_β can be simplified by neglecting $dD\sin(\varphi)$. Herein, the small angle assumption was adopted. With the nonlinear coupled BFL EOM being defined in the rotating frame of reference, a linearisation procedure is required before transforming the EOM to the non-rotating frame of reference. The linearisation procedure from Appendix C is incorporated. Such a linearisation procedure is justified when the small angle assumption does hold, thus when the flapping and lead-lag angles are small. Linearisation of the nonlinear system of EOM can be achieved by incorporating a first-order *Taylor* series approximation about the steady state condition. The first-order *Taylor* series shall be taken around the trim (tr) condition of the rotorcraft. The small angle assumption shall be applied after linearising the coupled flap-lag equations of motion. This will assure that important terms will be retained, as being stressed in [34]. Applying small angle approximation principle before conducting the linearisation procedure will yield a loss in first order terms of the coupled nonlinear flap-lag EOM [34]. Therefore it is a natural choice of first conducting the first order *Taylor* series expansion before incorporating the small angle approximation principle. The linearised EOM for the lead-lag and flapping direction in the non-rotating frame of reference are provided in Eq. 2.44 and Eq. 2.45 respectively [34].

$$\begin{aligned}
&I_{bl}\Omega^2\zeta'' + C_\zeta\Omega\zeta' + ((-2r\Omega+2\Omega^2)\beta_{tr}I_{bl} + (-2p\zeta_{tr}\Omega+2q\omega)I_{bl}\sin(\psi) + (-2q\zeta_{tr}\Omega-2p\Omega)I_{bl}\cos(\psi))\beta' + \\
&((-pr\zeta_{tr}+qr)\beta_{tr}I_{bl}\sin(\psi) + ((-2pq\sin(2\psi)+p^2\cos(2\psi)-q^2\cos(2\psi))\zeta_{tr}^2 + 2pq\sin(2\psi) + \\
&(2q^2\sin(2\psi)-4pq\cos(2\psi)-2p^2\sin(2\psi))\zeta_{tr} + q^2\cos(2\psi)-p^2\cos(2\psi))I_{bl} + (-qr\zeta_{tr}-pr)\beta_{tr}I_{bl}\cos(\psi) \\
&+K_\zeta)\zeta + ((qr\zeta_{tr}+(-qr\zeta_{tr}-pr)\beta_{tr}^2+pr)I_{bl}\sin(\psi) + (-p^2\sin(2\psi)+q^2\sin(2\psi)+(2p^2\cos(2\psi)- \\
&2q^2\cos(2\psi)-4pq\sin(2\psi))\zeta_{tr}-2pq\cos(2\psi))\beta_{tr}I_{bl} + (-pr\zeta_{tr}+(pr\zeta_{tr}-qr)\beta_{tr}^2+qr)I_{bl}/\cos(\psi))\beta = \\
&(-qr\zeta_{tr}-pr)\beta_{tr}I_{bl}\sin(\psi) + (pr\zeta_{tr}-qr)\beta_{tr}I_{bl}\cos(\psi) + (-pq\cos(2\psi) + (-2pq\sin(2\psi)+p^2\cos(2\psi) \\
&-q^2\cos(2\psi))\zeta_{tr} - \frac{1}{2}p^2\sin(2\psi) + \frac{1}{2}q^2\sin(2\psi)I_{bl} - K_\zeta\zeta_{tr} + Q_\zeta
\end{aligned} \tag{2.44}$$

$$\begin{aligned}
&I_{bl}\Omega^2\beta'' + ((2r\Omega-2\Omega^2)\beta_{tr}I_{bl} + (2p\zeta_{tr}\Omega-2q\Omega)I_{bl}\sin(\psi) + (2q\zeta_{tr}\Omega+2p\Omega)I_{bl}\cos(\psi))\zeta' + ((pr-2p\Omega+ \\
&(qr-2q\Omega)\zeta_{tr})I_{bl}\sin(\psi) + (qr-2q\Omega+(-pr+2p\Omega)\zeta_{tr})I_{bl}\cos(\psi) + ((p^2\sin(2\psi)+2pq\cos(2\psi)- \\
&q^2\sin(2\psi))\zeta_{tr}^2 + q^2\sin(2\psi) - 2pq\cos(2\psi) + (2p^2\cos(2\psi)-2q^2\cos(2\psi)-4pq\sin(2\psi))\zeta_{tr} - \\
&p^2\sin(2\psi))\beta_{tr}I_{bl})\zeta + ((4qr-4q\Omega+(-4pr+4p\Omega)\zeta_{tr})\beta_{tr}I_{bl}\sin(\psi) + (-4pr+4p\Omega+(-4qr+ \\
&4q\Omega)\zeta_{tr})\beta_{tr}I_{bl}\cos(\psi) + ((p^2\sin(2\psi)+2pq\cos(2\psi)-q^2\sin(2\psi))\zeta_{tr} + 2r\Omega-\Omega^2-r^2 + (-\frac{1}{2}\cos(2\psi)+ \\
&\frac{1}{2})q^2 + (\frac{1}{2}\cos(2\psi)+\frac{1}{2})p^2 - pq\sin(2\psi))\beta_{tr}^2 + (\frac{1}{2}\cos(2\psi)-\frac{1}{2})q^2 + (q^2\sin(2\psi)-p^2\sin(2\psi)-2pq \\
&\cos(2\psi))\zeta_{tr} + r^2 + \Omega^2 - 2r\Omega + (-\frac{1}{2}-\frac{1}{2}\cos(2\psi))p^2 + pq\sin(2\psi))I_{bl} + K_\beta)\beta = (qr-2q\Omega+(-pr+ \\
&2p\Omega)\zeta_{tr})I_{bl}\sin(\psi) + (-pr+2p\Omega+(-qr+2q\Omega)\zeta_{tr})I_{bl}\cos(\psi) + ((p^2\sin(2\psi)+2pq\cos(2\psi)- \\
&q^2\sin(2\psi))\zeta_{tr} + 2r\Omega-\Omega^2-r^2 + (-\frac{1}{2}\cos(2\psi)+\frac{1}{2})q^2 + (\frac{1}{2}\cos(2\psi)+\frac{1}{2})p^2 - pq\sin(2\psi))\beta_{tr}I_{bl} - \\
&\beta_{tr}K_\beta + Q_\beta
\end{aligned} \tag{2.45}$$

There after the IBC to MBC transformation must be incorporated. Below this transformation is provided and it taken from [39]. For a four-bladed rotorcraft $N = 4$, thus the transformation matrix $[L_{NR}]$ can be written as

$$[\boldsymbol{L}_{NR}]_{N=4} = \begin{bmatrix} \frac{1}{4} & \frac{1}{4} & \frac{1}{4} & \frac{1}{4} \\ 2\cos(\psi_1) & 2\cos(\psi_2) & 2\cos(\psi_3) & 2\cos(\psi_4) \\ 2\sin(\psi_1) & 2\sin(\psi_2) & 2\sin(\psi_3) & 2\sin(\psi_4) \\ -\frac{1}{4} & \frac{1}{4} & -\frac{1}{4} & \frac{1}{4} \end{bmatrix}. \tag{2.46}$$

It is a natural choice to convert the EOM from the rotating frame of reference to the non-rotating frame of reference by means of such a general system. Thus the system of differential equations shall be presented in the following matrix form

$$[\boldsymbol{M}_R]\{\boldsymbol{\chi}_R\}'' + [\boldsymbol{C}_R]\{\boldsymbol{\chi}_R\}' + [\boldsymbol{K}_R]\{\boldsymbol{\chi}_R\} = [\boldsymbol{F}_R], \tag{2.47}$$

wherein $[M_R]$, $[C_R]$ and $[K_R]$ are the mass, damping and spring stiffness matrix respectively [39]. In addition to this F_R is the externally applied force. In order to transform this general system from the rotating to the non-rotating system, it is necessary to determine first and second order derivatives of $\vec{\chi}$, which are respectively equal to

$$\{\boldsymbol{\chi}_R\}' = \left([\boldsymbol{L}_R]\{\boldsymbol{\chi}_{NR}\}]\right)' = [\boldsymbol{L}_R]\{\boldsymbol{\chi}_{NR}\}' + [\boldsymbol{L}_R]\{\boldsymbol{\chi}_{NR}\}' \tag{2.48}$$

$$\{\boldsymbol{\chi}_R\}'' = \left([\boldsymbol{L}_R]\{\boldsymbol{\chi}_{NR}\}' + [\boldsymbol{L}_R]\{\boldsymbol{\chi}_{NR}\}'\right)' = [\boldsymbol{L}_R]\{\boldsymbol{\chi}_{NR}\}'' + 2[\boldsymbol{L}_R]'\{\boldsymbol{\chi}_{NR}\}' + [\boldsymbol{L}_R]''\{\boldsymbol{\chi}_{NR}\} \tag{2.49}$$

Substituting these derivatives into the general form of the vibrating systems, does yield Eq. 2.50 [39].

$$\begin{gathered}[\boldsymbol{L}_R]''\{\boldsymbol{\chi}_{NR}\} + 2[\boldsymbol{L}_R]'\{\boldsymbol{\chi}_{NR}\}' + [\boldsymbol{L}_R]\{\boldsymbol{\chi}_{NR}\}'' + [\boldsymbol{M}_R^{-1}\boldsymbol{C}_R][\boldsymbol{L}_R]'\{\boldsymbol{\chi}_{NR}\} + [\boldsymbol{M}_R^{-1}\boldsymbol{C}_R][\boldsymbol{L}_R]\{\boldsymbol{\chi}_{NR}\}' + \\ [\boldsymbol{K}_R][\boldsymbol{L}_R]\{\boldsymbol{\chi}_{NR}\} = \{\boldsymbol{F}_R\}\end{gathered} \tag{2.50}$$

Multiplying Eq. 2.50 with $[L_R]^{-1}$ and rewriting it as a function of $\{\chi_{NR}\}''$, does yield the following:

$$\begin{gathered}\{\boldsymbol{\chi}_{NR}\}'' + \underbrace{[\boldsymbol{L}_{nr}]\left[2[\boldsymbol{L}_R]' + [\boldsymbol{M}_R^{-1}\boldsymbol{C}_R\boldsymbol{L}_R]\right]}_{\boldsymbol{C}_{NR}}\{\boldsymbol{\chi}_{NR}\}' + \underbrace{[\boldsymbol{L}_{NR}]\left[[\boldsymbol{L}_R]'' + [\boldsymbol{M}_R^{-1}\boldsymbol{K}_R\boldsymbol{L}_R + [\boldsymbol{M}_R^{-1}\boldsymbol{C}_R\boldsymbol{L}_R']\right]}_{\boldsymbol{K}_{NR}}\{\boldsymbol{\chi}_{NR}\} \\ = \underbrace{[\boldsymbol{L}_{NR}\boldsymbol{M}_R^{-1}]\{\boldsymbol{F}_R\}}_{\boldsymbol{F}_{NR}},\end{gathered} \tag{2.51}$$

from which it must be observed that $[L_R]^{-1}$ was replaced by $[L_{NR}]$ [39]. From the previous expression the damping $[C_{NR}]$, spring $[K_{NR}]$ and external force $[F_{NR}]$ matrices can be identified in the non-rotating frame of reference [39]. The transformation matrix $[L_{NR}]_{N=4}$ for the four-bladed BO-105 rotorcraft was previously defined in Eq. 2.46. The matrices C_{NR}, K_{NR} and F_{NR} can be identified from the coupled body-flap-lag EOM. These matrices can thus be isolated from the linearised lead-lag or flapping EOM as being defined in Eq. 2.44 and 2.45 respectively.

2.4. Inflow model

With the coupled body-flap-lag EOM being defined, it is a natural choice to incorporate a compatible inflow model. The original BF model did incorporate a first-order *Pitt-Peters* inflow model [37]. On the other hand the BFL model from [34] did incorporate a quasi-dynamic inflow model. The former shall be touched upon here. Information about how the quasi-dynamic inflow model is established can be found in [46]. Information regarding reference frames can be found in Appendix A.

2.4.1. First-order Pitt-Peters inflow model

The first-order Pitt-Peters inflow model from Padfield [37] shall be incorporated. The inflow dynamics is governed by the set of first-order differential equations given in Eq. 2.52 [37].

$$\boldsymbol{M}\begin{bmatrix}\dot{\lambda}_0\\ \dot{\lambda}_{1sw}\\ \dot{\lambda}_{1cw}\end{bmatrix}+\boldsymbol{L}^{-1}\begin{bmatrix}\lambda_0\\ \lambda_{1sw}\\ \lambda_{1cw}\end{bmatrix}=\begin{bmatrix}C_{Tdw}\\ C_{Ldw}\\ C_{Mdw}\end{bmatrix},$$
$$\text{with}\quad \boldsymbol{M}=\begin{bmatrix}\frac{128}{75\pi} & 0 & 0\\ 0 & \frac{16}{45\pi} & 0\\ 0 & 0 & \frac{16}{45\pi}\end{bmatrix}\quad\text{and}\quad \boldsymbol{L}=\frac{1}{\tilde{v}}\begin{bmatrix}\frac{1}{2} & 0 & \frac{15\pi}{64}\sqrt{\frac{1-\sin(\alpha_{rot})}{1+\sin(\alpha_{rot})}}\\ 0 & \frac{-4}{1+\sin(\alpha_{rot})} & 0\\ \frac{15\pi}{64}\sqrt{\frac{1-\sin(\alpha_{rot})}{1+\sin(\alpha_{rot})}} & 0 & \frac{-4\sin(\alpha_{rot})}{1+\sin(\alpha_{rot})}\end{bmatrix}. \tag{2.52}$$

The inflow model is defined in the disc-wind frame of reference. The azimuthal direction of this reference frame is aligned with the wind vector allowing for coupling between the inflow states appearing in $\boldsymbol{L}$. The aforementioned can only occur by means of rotational asymmetry, which is characteristic for the wind vector. The incidence angle at the rotor α_{rot} and the mass flow parameter $\tilde{v}$ are given in Eq. 2.53 [37].

$$\alpha_{rot}=\tan^{-1}\left(\frac{\lambda_0-\mu_{zdw}}{\mu_{dw}}\right)\quad\text{and}\quad \tilde{v}=\frac{\mu_{dw}^2+\left(\lambda_0-\mu_{zdw}\right)\left(2\lambda_0-\mu_{zdw}\right)}{\sqrt{\mu_{dw}^2+\left(\lambda_0-\mu_{zdw}\right)^2}} \tag{2.53}$$

The main implication of the *Pitt-Peters* inflow model being defined in the disc-wind reference frame is that it can be considered a non-inertial reference system as it is governed by the wind vector. In (near) hover condition the wind vector will continuously alter direction, thus rendering the disc-wind reference system non-inertial [37]. This discrepancy was also encountered when defining the coupled body-rotor EOM. The *Pitt-Peters* inflow model from Eq. 2.52 can be defined in the inertial North-East-Down (NED) reference frame, such that the above mentioned problem can be circumvented. The *Pitt-Peters* inflow model defined in the disc-north reference system is given in Eq. 2.54 [37].

$$\lambda\left(\psi^{dn},\bar{r}_b\right)=L_\lambda\left(\psi^{dn},\bar{r}_b\right)\begin{bmatrix}\lambda_0\\ \lambda_{1sn}\\ \lambda_{1cn}\end{bmatrix}\quad\text{with}\quad \dot{\lambda}\left(\psi^{dn},\bar{r}_b\right)=L_\lambda\left(\psi^{dn},\bar{r}_b\right)\begin{bmatrix}\dot{\lambda}_0\\ \dot{\lambda}_{1sn}\\ \dot{\lambda}_{1cn}\end{bmatrix} \tag{2.54}$$

The transformation matrix matrix $\boldsymbol{L}_\lambda(\psi)$, given be defined as follows

$$L_\lambda(\psi)=[1\sin(\psi)\cos(\psi)]. \tag{2.55}$$

Azimuth angles in the disc-wind and disc-north reference frame are related via $\psi^{dw}=\psi^{dn}-\psi_{dw}^{dw}$, which is equivalent to $\psi^{dw}=\psi^{dn}-\psi_b-\psi_w$. Furthermore this relation is associated with $\psi^{dw}=-r^{dp}-\dot{\psi}_w^{dp}$ as its derivative, wherein ψ^{dn} is zero since the disc-north reference frame is inertial. Furthermore ψ_b and ψ_w are the azimuth angles of the body with respect to the north and the wind vector azimuth angle with respect to the body. The time derivative of the harmonic inflow components defined in the disc-wind can be written as provided in Eq. 2.56 [37].

$$\begin{aligned}\dot{\lambda}\left(\psi^{dw},\bar{r}_b\right)&=\frac{d}{dt}\left[L_\lambda\left(\psi^{dw},\bar{r}_b\right)\right]\begin{bmatrix}\lambda_0\\ \lambda_{1sw}\\ \lambda_{1sw}\end{bmatrix}+L_\lambda\left(\psi^{dw},\bar{r}_b\right)\begin{bmatrix}\dot{\lambda}_0\\ \dot{\lambda}_{1sw}\\ \dot{\lambda}_{1cw}\end{bmatrix}\\ &=\frac{dL_\lambda\left(\psi^{dw},\bar{r}_b\right)d\psi^{dw}}{dt}\begin{bmatrix}\lambda_0\\ \lambda_{1sw}\\ \lambda_{1cw}\end{bmatrix}+L_\lambda\left(\psi^{dw},\bar{r}_b\right)\begin{bmatrix}\lambda_{1sw}\\ \dot{\lambda}_{1cw}\end{bmatrix}\\ &=-\frac{dL_\lambda\left(\psi^{dw},\bar{r}_b\right)}{d\psi^{dw}}\left(r^{dp}+\dot{\psi}_w\right)\begin{bmatrix}\lambda_{1sw}\\ \lambda_{1cw}\end{bmatrix}+L_\lambda\left(\psi^{dw},\bar{r}_b\right)\begin{bmatrix}\dot{\lambda}_{1sw}\\ \dot{\lambda}_{1cw}\end{bmatrix}\end{aligned} \tag{2.56}$$

The harmonic transformation matrices defined in the disc-north and disc-wind reference frames are related by means of the expression given in Eq. 2.57 [37].

$$L_\lambda\left(\psi^{dw}\right)=L_\lambda\left(\psi^{dn}-\psi_b-\psi_w\right)=L_\lambda\left(\psi^{dn}\right)T_{\Delta\psi}\left(-\psi_b-\psi_w\right), \tag{2.57}$$

wherein the azimuthal rotation matrix $\boldsymbol{T}_{\Delta_\psi}(\Delta\psi)$ for a given rotation angle $\Delta\psi$ can be defined as follows

$$T_{\Delta\psi}(\Delta\psi) = \begin{bmatrix} 1 & 0 & 0 \\ 0 & \cos(\Delta\psi) & \sin(\Delta\psi) \\ 0 & -\sin(\Delta\psi) & \cos(\Delta\psi) \end{bmatrix}. \tag{2.58}$$

The relation between the inflow harmonics in the disc-north and disc-wind reference is given in Eq. 2.59 [37].

$$\begin{bmatrix} \dot{\lambda}_0 \\ \dot{\lambda}_{1sn} \\ \dot{\lambda}_{1cn} \end{bmatrix} = T_{\Delta\psi}\left(-\psi_b - \psi_w\right) \begin{bmatrix} \dot{\lambda}_0 \\ \dot{\lambda}_{1sw} \\ \dot{\lambda}_{1cw} \end{bmatrix} \tag{2.59}$$

Rewriting Eq. 2.52 by taking the transformation from Eq. 2.59 into consideration does yield the following

$$MT_{\Delta\psi}\left(\psi_b + \psi_b\right) \begin{bmatrix} \dot{\lambda}_0 \\ \dot{\lambda}_{1sn} \\ \dot{\lambda}_{1cn} \end{bmatrix} + L^{-1} T_{\Delta\psi}\left(\psi_b + \psi_b\right) \begin{bmatrix} \lambda_0 \\ \lambda_{1sn} \\ \lambda_{1cn} \end{bmatrix} = \begin{bmatrix} C_{Tdw} \\ C_{Ldw} \\ C_{Mdw} \end{bmatrix}, \tag{2.60}$$

from which the explicit expression of the inflow time derivatives can be defined, namely

$$\begin{bmatrix} \dot{\lambda}_0 \\ \dot{\lambda}_{1sn} \\ \dot{\lambda}_{1cn} \end{bmatrix} = T_{\Delta\psi}\left(-\psi_b - \psi_b\right) M^{-1} \left(\begin{bmatrix} C_{Tdw} \\ C_{Ldw} \\ C_{Mdw} \end{bmatrix} - L^{-1} T_{\Delta\psi}\left(\psi_b + \psi_b\right) \begin{bmatrix} \lambda_0 \\ \lambda_{1sn} \\ \lambda_{1cn} \end{bmatrix} \right). \tag{2.61}$$

This will eventually yield the first-order *Pitt-Peters* inflow model given in Eq. 2.62 [37].

$$\begin{bmatrix} \dot{\lambda}_0 \\ \dot{\lambda}_{1s} \\ \dot{\lambda}_{1c} \end{bmatrix}_{dp} = T_w^{-1} M^{-1} \left(T_w \begin{bmatrix} -C_{z_{dp}} \\ C_{Ld_p} \\ C_{M_{dp}} \end{bmatrix} - L^{-1} T_w \begin{bmatrix} \lambda_0 \\ \lambda_{1s} \\ \lambda_{1c} \end{bmatrix}_{dp} \right) \tag{2.62}$$

2.5. Forces and moments

With the complex rotor dynamics being considered, it is necessary to focus on the forces and moments that act on the rotorcraft. The contribution of lead-lag dynamics to forces and moments was not yet considered. First the in-plane and out-of-plane forces generated by the main rotor will be considered. There after the moments generated by the main rotor will be touched upon. Lastly, the forces and moments generated by the fuselage, tail rotor and empennage will be touched upon. The procedure from Padfield [38] was incorporated for calculating the forces and moments.

2.5.1. In-plane and out-of-plane forces generated by the main rotor

The aerodynamic forces impinging on each ith rotor blade do consist of a perpendicular force component $\boldsymbol{F}^p$ and in-plane force component $\boldsymbol{F}^t$. The aforementioned force components do, which accounts for lift and drag respectively, wherein the latter can be broken down into induced and profile drag. The expression for $\boldsymbol{F}^p$ and $\boldsymbol{F}^t$ defined in the hub-wind reference frame are given in Eq. 2.63 and Eq. 2.64 respectively [37].

$$F^p\left(\psi_i^{bw}\right) = -\int_0^1 \left(\bar{U}_T^2 \theta_i + \bar{U}^P \bar{U}_T\right) d\bar{r}_{bl} \tag{2.63}$$

$$F^t\left(\psi_i^{bw}\right) = -\int_0^1 \left(\bar{U}_P \bar{U}_T \theta_i + \bar{U}_P^2 - \frac{\delta_i \bar{U}_T^2}{a_0}\right) d\bar{r}_{bl} \tag{2.64}$$

Below the force coefficients in the hub-wind frame are provided [37].

$$C_{xw} = \frac{X_{hw}}{\rho\Omega^2\pi R^4} = \frac{a_0 s}{2N_b} \sum_{i=1}^{N_b} F^p\left(\psi_i^{bw}\right) \beta_i \cos\left(\psi_i^{bw}\right) + F^t\left(\psi_i^{bw}\right) \sin\left(\psi_i^{bw}\right), \tag{2.65}$$

$$C_{yw} = \frac{Y_{hw}}{\rho\Omega^2\pi R^4} = \frac{a_0 s}{2N_b} \sum_{i=1}^{N_b} -F^p\left(\psi_i^{bw}\right) \beta_i \sin\left(\psi_i^{bw}\right) + F^t\left(\psi_i^{bw}\right) \cos\left(\psi_i^{bw}\right), \tag{2.66}$$

$$C_{zw} = \frac{Z_{hw}}{\rho\Omega^2\pi R^4} = \frac{a_0 s}{2N_b}\sum_{i=1}^{N_b} -F^p\left(\psi_i^{bw}\right). \tag{2.67}$$

Force components $\vec{\boldsymbol{F}}^p$ and $\vec{\boldsymbol{F}}^t$ can be expanded by substituting Eq. 2.6 and Eq. 2.7 into Eq. 2.63 and Eq. 2.64. The aforementioned does yield the following expressions for $\boldsymbol{F}^p$ and $\boldsymbol{F}^t$ respectively [37].

$$\begin{aligned} F^p\left(\psi^{bw}\right) = &\left(\frac{1}{3} + \mu\sin\left(\psi^{bw}\right) + \mu^2\sin^2\left(\psi^{bw}\right)\right)\theta_p + \left(\frac{1}{4} + \frac{2}{3}\mu\sin\left(\psi^{bw}\right) + \frac{1}{2}\mu^2\sin^2\left(\psi^{bw}\right)\right)\theta_{tw} \\ &+ \left(\frac{1}{3} + \frac{\mu\sin\left(\psi^{bw}\right)}{2}\right)\left(\bar{\omega}_y - \lambda_1 - \beta'\right) + \left(\frac{1}{2} + \mu\sin\left(\psi^{bw}\right)\right)\left(\mu_z - \lambda_0 - \beta\mu\cos\left(\psi^{bw}\right)\right), \end{aligned} \tag{2.68}$$

$$\begin{aligned} F^t\left(\psi^{bw}\right) = &\left(\left(\frac{1}{3} + \frac{1}{2}\mu\sin\left(\psi^{bw}\right)\right)\left(\bar{\omega}_y - \lambda_1 - \beta'\right) + \left(\frac{1}{2} + \mu\sin\left(\psi^{bw}\right)\right)\left(\mu_z - \lambda_0 - \beta\mu\cos\left(\psi^{bw}\right)\right)\right)\theta_p \\ &+ \left(\left(\frac{1}{4} + \frac{\mu\sin\left(\psi^{bw}\right)}{3}\right)\left(\bar{\omega}_y - \lambda_1 - \beta'\right) + \left(\frac{1}{3} + \frac{\mu\sin\left(\psi^{bw}\right)}{2}\right)\left(\mu_z - \lambda_0 - \beta^{bw}\right)\right)\theta_{tw} \\ &+ \left(\mu_z - \lambda_0 - \beta\mu\cos\left(\psi^{bw}\right)\right)^2 + \left(\mu_z - \lambda_0 - \beta\mu\cos\left(\psi^{bw}\right)\right)\left(\bar{\omega}_y - \lambda_1 - \beta'\right) + \frac{\left(\bar{\omega}_y - \lambda_1 - \beta'\right)^2}{3} \\ &- \frac{\delta}{a_0}\left(\frac{1}{3} + \mu\sin\left(\psi^{bw}\right) + \mu^2\sin^2\left(\psi^{bw}\right)\right). \end{aligned} \tag{2.69}$$

The normal and in-plane forces will provide quasi-steady loads and harmonic loads at the hub [37]. The quasi-steady components can be considered of prime interest, which can be obtained by expanding the loads in the rotating system of equations up to the second harmonic [37].

$$F^p\left(\psi^{bw}\right) = F_0^p + F_{1c}^p\cos\left(\psi^{bw}\right) + F_{1s}^p\sin\left(\psi^{bw}\right) + F_{2c}^p\cos\left(2\psi^{bw}\right) + F_{2s}^p\sin\left(2\psi^{bw}\right) \tag{2.70}$$

$$F^t\left(\psi^{bw}\right) = F_0^t + F_{1c}^t\cos\left(\psi^{bw}\right) + F_{1s}^t\sin\left(\psi^{bw}\right) + F_{2c}^t\cos\left(2\psi^{bw}\right) + F_{2s}^t\sin\left(2\psi^{bw}\right) \tag{2.71}$$

The hub force coefficients C_{xw}, C_{yw} and C_{zw} from Eq. 2.65, 2.66 and 2.67 respectively can be rewritten into

$$C_{xw} = a_0 s\left(\left(\frac{F_0^p}{4} + \frac{F_{2c}^p}{8}\right)\beta_{1cw} + \frac{F_{1c}^p}{4}\beta_0 + \frac{F_{2s}^p}{8}\beta_{1sw} + \frac{F_{1s}^t}{4}\right) \tag{2.72}$$

$$C_{yw} = a_0 s\left(\left(-\frac{F_0^p}{4} + \frac{F_{2c}^p}{8}\right)\beta_{1sw} - \frac{F_{1s}^p}{4}\beta_0 - \frac{F_{2s}^p}{8}\beta_{1cw} + \frac{F_{1c}^t}{4}\right) \tag{2.73}$$

$$C_{zw} = -\frac{a_0 s}{2}F_0^p \tag{2.74}$$

The hub force coefficients from Eq. 2.72, 2.73 and 2.74 depend on the harmonic coefficients given below [37].

$$F_0^p = \theta_0\left(\frac{1}{3} + \frac{\mu^2}{2}\right) + \frac{\mu}{2}\left(\theta_{1sw} + \frac{\bar{p}_{hw}}{2}\right) + \frac{\mu_z - \lambda_0}{2} + \frac{1}{4}\left(1 + \mu^2\right)\theta_{tw} \tag{2.75}$$

$$F_{1s}^p = \frac{\alpha_{1sw}}{3} + \mu\left(\theta_0 + \mu_z - \lambda_0 + \frac{2}{3}\theta_{tw}\right) \tag{2.76}$$

$$F_{1c}^p = \frac{\alpha_{1cw}}{3} - \mu\frac{\beta_0}{2} \tag{2.77}$$

$$F_{2s}^p = \frac{\mu}{2}\left(\frac{\alpha_{1cw}}{2} + \frac{\theta_{1cw} - \beta_{1sw} - \mu\beta_0}{2}\right) \tag{2.78}$$

$$F_{2c}^p = -\frac{\mu}{2}\left(\frac{\alpha_{1sw}}{2} + \frac{\theta_{1sw} + \beta_{1cw}}{2} + \mu\left(\theta_0 + \frac{\theta_{tw}}{2}\right)\right) \tag{2.79}$$

$$\begin{aligned} F_{1s}^t = &\frac{\mu^2}{2}\beta_0\beta_{1sw} + \left(\mu_z - \lambda_0 - \frac{\mu}{4}\beta_{1cw}\right)\left(\alpha_{1sw} - \theta_{1sw}\right) - \frac{\mu}{4}\beta_{1sw}\left(\alpha_{1cw} - \theta_{1cw}\right) + \theta_0\left(\frac{\alpha_{1sw} - \theta_{1sw}}{3} + \right. \\ &\mu\left(\mu_z - \lambda_0\right) - \frac{\mu^2}{4}\beta_{1cw}\Big) + \theta_{tw}\left(\frac{\alpha_{1sw} - \theta_{1sw}}{4} + \frac{\mu}{2}\left(\mu_z - \lambda_0 - \frac{\beta_{1cw}\mu}{4}\right)\right) + \theta_{1sw}\left(\frac{\mu_z - \lambda_0}{2} + \right. \\ &\left.\mu\left(\frac{3}{8}\left(\bar{p}_{hw} - \lambda_{1sw}\right) + \frac{\beta_{1cw}}{4}\right)\right) + \frac{\mu}{4}\theta_{1cw}\left(\frac{\bar{q}_{hw} - \lambda_{1cw}}{2} - \beta_{1sw} - \mu\beta_0\right) - \frac{\delta\mu}{a_0} \end{aligned} \tag{2.80}$$

$$F_{1c}^{t} = (\alpha_{1cw} - \theta_{1cw} - 2\beta_0\mu)\left(\mu_z - \lambda_0 - \frac{3}{4}\mu\beta_{1cw}\right) - \frac{\mu}{4}\beta_{1sw}(\alpha_{1sw} - \theta_{1sw}) + \theta_0\left(\frac{\alpha_{1cw} - \theta_{1cw}}{3} - \frac{\mu}{2}\left(\beta_0 + \frac{\mu}{2}\beta_{1sw}\right)\right) + \theta_{tw}\left(\frac{\alpha_{1cw} - \theta_{1cw}}{4} - \mu\left(\frac{\beta_0}{3} + \frac{\beta_{1sw}\mu}{8}\right)\right) + \theta_{1cw}\left(\frac{\mu_z - \lambda_0}{2} - \frac{\mu}{4}\left(\frac{\bar{p}_{hw} - \lambda_{1sw}}{2} - \beta_{1cw}\right)\right) + \frac{\mu}{4}\theta_{1sw}\left(\frac{\bar{q}_{hw} - \lambda_{1cw}}{2} - \beta_{1sw} - \mu\beta_0\right) \tag{2.81}$$

The coefficients show an explicit dependency on the effective blade incidence angles α_{1sw} and α_{1cw}, which are given in Eq. 2.82 and Eq. 2.83 respectively [37].

$$\alpha_{1sw} = \bar{p}_{hw} - \lambda_{1sw} + \beta_{1cw} + \theta_{1sw}, \tag{2.82}$$

$$\alpha_{1cw} = \bar{q}_{hw} - \lambda_{1cw} - \beta_{1sw} + \theta_{1cw}. \tag{2.83}$$

The rotor forces are being defined in the non-rotating hub-wind axes system, therefore the transformation $\boldsymbol{T}_{hw}^{h}$ is required for transforming the forces $\boldsymbol{F}_h$ to the non-rotating hub axes system [37].

$$\boldsymbol{F}_h = \boldsymbol{T}_{hw}^{h}\boldsymbol{F}_{hw} = \rho\Omega^2\pi R^4\boldsymbol{T}_{hw}^{h}\boldsymbol{C}_{hw}, \quad \text{with} \quad \boldsymbol{F_h} = [F_x \; F_y \; F_z]^T \text{ and } \boldsymbol{C_{hw}} = [C_{xw} \; C_{yw} \; C_{zw}]^T. \tag{2.84}$$

2.5.2. Moments generated by main rotor

A hingeless rotor can be idealised as a centrally hinged rigid blade with a spring restraint [37], wherein the hub moments L_h and M_h can be respectively defined as

$$L_h = -\frac{N_b}{2}K_\beta\beta_{1s}, \tag{2.85}$$

$$M_h = -\frac{N_b}{2}K_\beta\beta_{1c}. \tag{2.86}$$

The moments generated by the main rotor are primarily governed by the cyclic flapping angles MBCs defined with respect to the shaft plane. Aside from this Eq. 2.85 and 2.86 depend on hub stiffness K_β, which subsequently depends on the equivalent hinge spring offset e_β. The yawing moment, given in Eq. 2.87, can be approximated by integrating the in-plane forces about the shaft axis [37].

$$N_h = \sum_{i=1}^{N_b}\int_0^R r_{bl}\left(f_y - ma_{yb}\right)_i dr_{bl}, \tag{2.87}$$

It should be noted that $f_y - ma_{yb}$ is the force per unit blade element. Integration of the complete rotor blade for all rotor blades yields the complete contribution to N_h. Eq. 2.87 can be reduced by neglecting all inertia terms except for the torque acceleration, which is due to the angular acceleration of the rotor. This yields

$$N_h = \sum_{i=1}^{N_b}\int_0^R r_{bl}(d - l\phi)dr_\omega + I_R\dot{\Omega}. \tag{2.88}$$

The last term from Eq. 2.88 accounts for the inertia of the hub about the shaft axis and rotor blades. Normalisation of N_h is given in Eq 2.88 [37].

$$N_h = \frac{1}{2}\rho(\Omega R)^2\pi R^3 s a_0\left(\frac{2C_Q}{a_0 s} + \frac{2}{\gamma}\left(\frac{I_R}{N_b I_\beta}\right)\frac{\dot{\Omega}}{\Omega^2}\right). \tag{2.89}$$

The expression for N_h from Eq. 2.89 shows dependency on the aerodynamic torque coefficient C_Q, which is provided in Eq. 2.90 [37]. The first expression in Eq. 2.90 can be rewritten into the second expression by approximating r/R with $\bar{U}_T - \mu\sin(\psi)$. Expanding the second expression does yield the last expression.

$$\begin{aligned} C_Q &= -\frac{a_0 s}{2}\int_0^R r_{bl}\left(\bar{U}_P\bar{U}_T\theta + \bar{U}_P^2 - \frac{\delta}{a_0}\bar{U}_T^2\right)dr_{bl} \\ &= -\frac{a_0 s}{2}\left(\int_0^R\left(\bar{U}_T - \mu sin(\psi)\right)\frac{\bar{U}_p}{\bar{U}_T}\left(\bar{U}_T^2\theta + \bar{U}_p\bar{U}_T\right)r_{bl}dr_{bl} + \int_0^R\frac{\delta}{a_0}\bar{U}_T^2 r_{bl}dr_{bl}\right) \\ &= -\frac{a_0 s}{2}\left(-\int_0^R\left(\bar{U}_p\bar{U}_T^2 + \bar{U}_p^2\bar{U}_T\right)dr_{bl} + \mu sin(\psi)\int_0^R\left(\bar{U}_P\bar{U}_T\theta + \bar{U}_p^2\right)dr_{bl} + \int_0^R\frac{\delta}{a_0}\bar{U}_T^2 r_{bl}dr_{bl}\right) \end{aligned} \tag{2.90}$$

The aerodynamic rotor torque coefficient C_Q from Eq 2.90 can be simplified by neglecting small terms, which does yield the simplified form for C_Q given in Eq. 2.91 [37].

$$C_Q = -\left(\mu_z - \lambda_0\right) C_{zw} + \mu C_{xw} + \frac{\delta s}{8}\left(1 + 3\mu^2\right). \tag{2.91}$$

The yaw moment N_h in Eq. 2.89 can thus be solved using Eq. 2.91. The torque moment N_h does also contribute to L_h and M_h, but are of significant less order than the center spring induced moments. The aforementioned contributions are due to the plane normal to shaft axis being tilted with respect to the rotor disc. The rotor also produces a torque moment about the shaft axis. The contribution of C_Q to L_h and M_h is given in Eq. 2.92 and Eq. 2.93 respectively [37].

$$L_{hQ} = -\frac{\rho\Omega^2 R^5 \pi C_Q}{2}\beta_{1c} \tag{2.92}$$

$$M_{hQ} = \frac{\rho\Omega^2 R^5 \pi C_Q}{2}\beta_{1s} \tag{2.93}$$

2.5.3. Forces and moments generated by tail rotor

Rotorcraft fidelity can be improved by including the effects of the tail rotor. The tail rotor is characterised with no cyclic pitch variation, thus only collective changes. Furthermore the untwisted rotor blades do not show any flapping motion. The tail rotor does produce a small torque force, which can be neglected. The tail rotor does only produce a lateral force Y_{tr} at an offset from the body cg. Since the tail rotor is located at a vertical and longitudinal offset from the body cg, there will also be a yawing and rolling moment. The ratio between the free-stream fluid speed to the tail rotor tip speed must first be defined and is given in Eq. 2.94 [37].

$$\mu_{x_{tr}} = \frac{\sqrt{u^2 + \left(w + K_{tr}\Omega R\lambda_0 + q l_{tr}\right)^2}}{\Omega_{tr} R_{tr}}, \tag{2.94}$$

It should be noted that K_{tr} can be identified as the rotor downwash factor. Furthermore the inflow ratio λ_{tr} is given in Eq. 2.95

$$\lambda_{tr} = -\frac{v - r l_{tr} + p h_{tr}}{\Omega R_{tr}} - \lambda_{0tr}, \tag{2.95}$$

wherein $\lambda_{0,tr}$ is the tail rotor induced inflow factor [37]. From Eq. 2.94 and Eq. 2.95 it can be observed that these depend on a combination of body velocities and tail rotor specific properties. In Eq. 2.96 the thrust coefficient $C_{T_{tr}}$ of the tail rotor is provided [37].

$$C_{T_{tr}} = \frac{\sigma_{tr} C_{L_{\alpha,tr}}}{2}\left[\left(\frac{1}{3} + \frac{\mu_{x_{tr}}^2}{2}\right)\theta_{0_{tr}} + \frac{\lambda_{tr}}{2}\right] \tag{2.96}$$

The tail rotor thrust coefficient was based upon blade element theory. The longitudinal and vertical offset of the tail rotor with respect to the body c.g. are indicated by the arms l_{tr} and h_{tr} respectively. The thrust force T_{tr} generated by the tail rotor can be used to determine the lateral side force Y_{tr}. The expression for Y_{tr} defined in the body frame of reference is

$$Y_{\text{tr}} = \underbrace{C_{T_{\text{tr}}}\rho\pi\Omega_{\text{tr}}^2 R_{\text{tr}}^4}_{=T_{tr}}\left[1 - \frac{3S_{vt}}{4\pi R_{tr}^2}\right], \tag{2.97}$$

wherein the explicit dependency on T_{tr} does appear [37]. The effect of tail rotor wake blockage by the vertical stabiliser was also taken into account. With the tail rotor force established its global contribution can be established. The tail rotor force defined in he body-fixed reference frame can be defined as

$$\boldsymbol{F}_{tr} = [0 \ \boldsymbol{Y}_{tr} \ 0]^T. \tag{2.98}$$

Since $\boldsymbol{Y}_{tr}$ is located at an offset, there will also be moments about the cg. In the body-fixed reference frame the moments due to the tail rotor can be expressed as follows

$$\boldsymbol{M}_{tr} = [h_{tr}\boldsymbol{Y}_{tr}\ 0\ -l_{tr}\boldsymbol{Y}_{tr}]^T, \tag{2.99}$$

wherein h_{tr} and l_{tr} are the vertical and horizontal offset of the tail rotor center of rotation and body cg. The tail rotor is associated with an uniform *Pitt-Peters* inflow model, which does depend on $C_{T_{tr}}$, $\mu_{x_{tr}}$ and $\lambda_{0_{tr}}$. The differential equation for the non-dimensional inflow ratio is provide in Eq. 2.100 [37].

$$\dot{\lambda}_{0tr} = \frac{75\pi}{128}\left[C_{T_{tr}} - 2\sqrt{\mu_{x_{tr}}^2 + \lambda_{0tr}^2}\right] \tag{2.100}$$

2.5.4. Forces and moments introduced by fuselage

Model fidelity can be further enhancement by taking into account aerodynamic drag of the fuselage body. The aerodynamic drag force is opposing the direction of the velocity vector and can be expressed as follows

$$D_{\text{fus,b}} = \frac{1}{2}\rho V^2 S_{\text{eq}}, \tag{2.101}$$

wherein S_{eq} is the equivalent flat plate drag area of the fuselage [37]. Since the rotorcraft is capable of flying in any direction, S_{eq} would actually vary with the direction of V. It was decided to set S_{eq} fixed to simplify the contribution of D_{fus}. Since D_{fus} is aligned with V, a transformation is necessary to transform D_{fus} to the body reference frame. Since the application point of the aerodynamic drag force does have an offset with respect to the body cg, moments will also be introduced. The pitch and yaw moment coefficient are respectively

$$C_{M_{fus}} = \left(\frac{V}{\Omega R}\right)^2\left[\frac{K_{\text{fus}}V_{\text{fus}_M}}{\pi R^3}\left(\alpha_{fus} - \alpha_{\text{fus}_{M=0}}\right)\right], \tag{2.102}$$

$$C_{N_{fus}} = \left(\frac{V}{\Omega R}\right)^2\left[\frac{K_{\text{fus}}V_{\text{fus}_N}}{\pi R^3}\beta_{\text{fus}}\right], \tag{2.103}$$

wherein K_{fus} is a shape-dependent correction factor [37]. Furthermore V_{fus_M} is the volume of a body rotationally symmetric around the longitudinal axis with the same projection in the horizontal plane. In other words the volume is equivalent, but the shape is idealised as a circular rod. Likewise, V_{fus_N} is analogues to V_{fus_M}, but now the volume of the body that is rotationally symmetric around the vertical axis with the same projection in the vertical fore-aft plane [37]. Next to this α_{fus} and β_{fus} are the fuselage incidence angle and are equal to $-\arctan(w/u)$ and $\arctan(v/V)$ respectively. With the forces and moments due to fuselage drag being determined, its global contribution can be determined. The fuselage force defined in the body-fixed reference frame requires two successive rotations and is provided below [37].

$$\boldsymbol{F}_{\text{fus}} = \boldsymbol{R}_y(\alpha_{\text{fus}})\boldsymbol{R}_z(-\beta_{\text{fus}})[-R_{\text{fus}}\ 0\ 0]^T. \tag{2.104}$$

The contribution of the fuselage moments needs to be expressed in the body-fixed reference frame and can be expressed in accordance with Eq. 2.105 [37].

$$\boldsymbol{M}_{\text{fus}} = \rho\left(\pi R^2\right)(\pi R)^2 R[0\ C_{M_{\text{fus}}}\ C_{N_{\text{fus}}}]^T \tag{2.105}$$

2.5.5. Forces and moments introduced by vertical and horizontal stabiliser

The rotorcraft is equipped with a horizontal tail, which does as a wing in forward flight. Drag due to horizontal stabiliser can be neglected, as its overall contribution to rotorcraft drag is neglectable [46] . On the other hand the horizontal stabiliser does contribute to the lift force and is given in Eq. 2.106 [37].

$$L_{ht} = \frac{1}{2}\rho\underbrace{\left\{u^2 + \left(w + ql_{ht}\right)^2\right\}}_{=V_{ht}^2}S_{ht}C_{L_{\alpha,ht}}\underbrace{\left\{\arctan\left(\frac{w + ql_{ht}}{u}\right) + \alpha_{ht_0}\right\}}_{=\alpha_{ht}} \tag{2.106}$$

From Eq. 2.106 it can be observed that there is dependency on V_{ht} and α_{ht}, which are the local relative air velocity and angle of attack of the horizontal stabiliser. Additionally L_{ht} depends on horizontal stabiliser surface area S_{ht} and lift curve slope α_{ht}. There is also a vertical velocity component introduced by ql_{ht}, wherein L_{ht} is the longitudinal distance between body cg and point on the horizontal stabiliser where L_{ht}

acts. The moment introduced by L_{ht} is then $-l_{ht}L_{ht}$. The vertical stabiliser does also introduce a lift force L_{vt} when there exist an angle of sideslip β_{vt}. The expression for L_{vt} is given in Eq. 2.107 [46].

$$L_{vt} = \frac{1}{2}\rho \underbrace{\left\{u^2 + \left(v + ph_{vt} - rl_{vt}\right)^2\right\}}_{=V_{vt}^2} S_{vt} C_{L_{\alpha,vt}} \underbrace{\left\{\arcsin\left(\frac{v + ph_{vt} - rl_{vt}}{u}\right) + \beta_{vt_0}\right\}}_{=\beta_{vt}}. \tag{2.107}$$

From Eq. 2.107 it can be observed that L_{vt} does depend on the relative air velocity V_{vt} at the vertical stabiliser and the lift curve slope $C_{L_{\alpha,vt}}$. Lateral velocity components ph_{vt} and rl_{vt} are also being introduced, which are due to the vertical stabiliser being at an longitudinal and vertical offset with respect to the body cg.

2.6. Body dynamics

In the previous sections the main rotorcraft model has been established. The novelty introduced in the new rotorcraft model is the inclusion of lead-lag dynamics. However, lead-lag dynamics was not considered for the forces and moments. This implies that there will not be a body-lag coupling. Inclusion of lead-lag dynamics to the hingeless rotorcraft model has introduced six additional states, which means that the total state vector of the rotorcraft has become

$$\boldsymbol{X}^T = [\underbrace{u\ v\ w}_{\boldsymbol{V}}\ \underbrace{x\ y\ z}_{\boldsymbol{P}}\ \underbrace{p\ q\ r}_{\boldsymbol{\omega}}\ \underbrace{\phi\ \theta\ \psi}_{\boldsymbol{\theta}}\ \underbrace{\lambda_{0,\mathrm{mr}}\ \lambda_{1\mathrm{s}}\ \lambda_{1\mathrm{c}}\ \lambda_{0,\mathrm{tr}}}_{\boldsymbol{\lambda}}\ \underbrace{\beta_0\ \beta_{1\mathrm{s}}\ \beta_{1\mathrm{c}}}_{\boldsymbol{\beta}}\ \underbrace{\dot{\beta}_0\ \dot{\beta}_{1\mathrm{s}}\ \dot{\beta}_{1\mathrm{c}}}_{\dot{\boldsymbol{\beta}}}\ \underbrace{\zeta_0\ \zeta_{1\mathrm{c}}\ \zeta_{1\mathrm{s}}}_{\boldsymbol{\zeta}}\ \underbrace{\dot{\zeta}_0\ \dot{\zeta}_{1\mathrm{c}}\ \dot{\zeta}_{1\mathrm{s}}}_{\dot{\boldsymbol{\zeta}}}]^T, \tag{2.108}$$

wherein the complete state vector can be divided into smaller parts. The body-fixed linear velocity and the position of the rotorcraft in the NED reference frame are indicated by means of $\boldsymbol{V}$ and $\boldsymbol{P}$ respectively. Furthermore the body angular rates and attitude angles are provided by $\boldsymbol{\omega}$ and $\boldsymbol{\theta}$ respectively. Next to this $\boldsymbol{\lambda}$ is the vector containing the non-dimensional inflow components. It should be noted that the BF model depends on all of the four inflow states, whereas lead-lag states $\boldsymbol{\zeta}$ and $\dot{\boldsymbol{\zeta}}$ only depend on λ_0. Previously it has already been outlined that the BFL model [34] did incorporate a simple quasi-steady inflow model, which could not be modified. The vectors $\boldsymbol{\beta}$ and $\dot{\boldsymbol{\beta}}$ contain the flapping angles and derivatives respectively, which are defined with respect to the shaft plane of reference. The six last states, $\boldsymbol{\zeta}$ and $\dot{\boldsymbol{\zeta}}$ have been added to the original model from [55]. The inclusion of these in-plane rotor states can be considered the novelty of the introduced rotorcraft model. The total force and moment of the rotorcraft defined in the body frame of reference are given in Eq. 2.109 and 2.110 respectively.

$$\boldsymbol{F}_{\mathrm{B,tot}} = \boldsymbol{F}_{\mathrm{B,mr}} + \boldsymbol{F}_{\mathrm{B,tr}} + \boldsymbol{F}_{\mathrm{B,fus}} + \boldsymbol{F}_{\mathrm{B,vt}} + \boldsymbol{F}_{\mathrm{B,ht}} \tag{2.109}$$

$$\boldsymbol{M}_{\mathrm{B,tot}} = \boldsymbol{M}_{\mathrm{B,mr}} + \boldsymbol{M}_{\mathrm{B,tr}} + \boldsymbol{M}_{\mathrm{B,fus}} + \boldsymbol{M}_{\mathrm{B,vt}} + \boldsymbol{M}_{\mathrm{B,ht}} \tag{2.110}$$

Having defined the expressions for the total force and moment of the rotorcraft, it is necessary to consider the rotational and translational dynamics and kinematics of the vehicle. In addition to this the assumptions introduced in [46] should also be considered, namely that the rotorcraft can be considered a rigid body with both constant inertia and mass. This can be considered valid since simulations shall be conducted for a short amount time. Moreover, Earth can be considered flat and non-rotating, wherein the gravitational field can be considered homogeneous, which subsequently implies that the center of mass and center of gravity do coincidence with each other. In Eq. 2.111. the dynamics of the rotorcraft translational motion is provided

$$\dot{\mathbf{V}} = m^{-1}\mathbf{F}_{\mathrm{B,tot}} + \boldsymbol{T}_{\mathrm{B}}^{\mathrm{O}}\vec{g} - \boldsymbol{\Omega}\times\mathbf{V} = m^{-1}\mathbf{F}_{\mathrm{B,tot}} + \begin{bmatrix} -\sin(\theta) \\ \sin(\phi)\cos(\theta) \\ \cos(\phi)\cos(\theta) \end{bmatrix} g - \begin{bmatrix} qw - rv \\ ru - pw \\ pv - qu \end{bmatrix}. \tag{2.111}$$

The expression describing the translational kinematics is given in Eq. 2.112.

$$\dot{\boldsymbol{p}} = \boldsymbol{T}_{\mathrm{O}}^{\mathrm{B}}\boldsymbol{V} \tag{2.112}$$

In Eq. 2.113 the expression for the rotational dynamics is being provided, wherein the angular accelerations are governed by the applied hub moments and gyroscopic precession. The resistance in control action of the rotorcraft is indicated by means of $\boldsymbol{J}$, being the moment of inertia tensor.

$$\dot{\boldsymbol{\omega}} = \boldsymbol{J}^{-1}\left(\boldsymbol{M}_{\mathrm{B,tot}} - \boldsymbol{\omega}\times\boldsymbol{J}\boldsymbol{\omega}\right), \tag{2.113}$$

In Eq. 2.114 the kinematics of the rotational motion is provided.

$$\dot{\boldsymbol{\theta}} = \begin{bmatrix} 1 & \frac{\sin(\phi)\sin(\theta)}{\cos(\theta)} & \frac{\cos(\phi)\sin(\theta)}{\cos(\theta)} \\ 0 & \cos(\phi) & -\sin(\phi) \\ 0 & \frac{\sin\phi}{\cos(\theta)} & \frac{\cos(\phi)}{\cos(\theta)} \end{bmatrix} \boldsymbol{\omega} \tag{2.114}$$

2.7. Numerical integration

The coupled body-flap-lag model proposed in previous sections and the forces and moments it comes with needs to be integrated such that it simulates the rotorcraft model. In the previous model the *classical Runge-Kutta* (RK4) integration method was introduced and shall also be considered for the extended BFL model. The integration method under consideration is an explicit method as it calculates the state of a system at a later time instance based on the current system state. In [55] it has been outlined the poles of the system fall with in ROC of the integration method. The inclusion of lead-lag dynamics has led to a set of additional poles near the imaginary axis and will therefore not be problematic for the integration method under consideration. The advantage of using this numerical integration method is that only function evaluations are required, thus wherein not equations have to be solved. The idea is to solve the initial value problem given in Eq. 2.115 [19].

$$\dot{\boldsymbol{y}} = \boldsymbol{f}(t, \boldsymbol{t}), \quad \text{with } \boldsymbol{y}(t_0) = \boldsymbol{y}_0 \tag{2.115}$$

The idea of the algorithm proposed is that it does find an approximate value for $\boldsymbol{y}$ at a given instance t. Important to note is that the *Runge-Kutta* integration method can only solve first order differential equations. However, the previous proposed BFL is second-order, thus this had to be accounted for. The estimated value $\boldsymbol{y}_{i+1}$ can be determined by solving

$$\boldsymbol{y}_{i+1} = \boldsymbol{y}_n + \frac{1}{6}(\boldsymbol{k}_1 + 2\boldsymbol{k}_2 + 2\boldsymbol{k}_3 + \boldsymbol{k}_4) \begin{cases} \boldsymbol{K}_1 = h\boldsymbol{f}\left(t_i, \boldsymbol{y}_i\right) \\ \boldsymbol{K}_2 = h\boldsymbol{f}\left(t_i + \frac{h}{2}, t_i + \frac{h}{2}\right) \\ \boldsymbol{K}_3 = h\boldsymbol{f}\left(t_i + \frac{h}{2}, t_i + \frac{h}{2}\right) \\ \boldsymbol{K}_4 = h\boldsymbol{f}\left(t_i + h, t_i + h\right) \end{cases} \tag{2.116}$$

wherein the individual coefficients $\boldsymbol{K}_1$, $\boldsymbol{K}_2$, $\boldsymbol{K}_3$ and $\boldsymbol{K}_4$ can be identified, which are the function evaluations at a given time instant multiplied with step size h [19]. In [19] it was outlined that the *classical Runge-Kutta* integration method can be considered absolutely convergent when the eigenvalues of the rotorcraft adhere to the condition stipulated in Eq. 2.117.

$$\left|1 + \Delta t\lambda + \frac{(\Delta t\lambda)^2}{2!} + \frac{(\Delta t\lambda)^3}{3!} + \frac{(\Delta t\lambda)^4}{4!}\right| \leq 1 \tag{2.117}$$

Numerical divergence of the system can be considered unlikely as the eigenvalues fall within the ROC of RK4. The ROC does scale with the time step of the integration [55]. Thus a smaller time step will yield a larger ROC, therefore numerical stability can be assured even more.

2.8. Coupled body-rotor models for hover condition

To assess the effects of rotor dynamics on *Lyapunov*-based control design and performance, it will be necessary to consider a set of simplified models. The models proposed here were derived in [41] and represent the first few instants during the transition from hover to forward flight without building up horizontal speed. Three models shall be introduced in total. The first model to be considered is a **longitudinal steady-state body-flap model**. The flapping model is provided in Eq. 2.118, from it can be observed that it depends on pitch rate q and longitudinal cyclic input θ_{1s}.

$$\beta_{1c} = \frac{16}{\gamma\Omega} q - \theta_{1s} \tag{2.118}$$

Moreover, the angular body dynamics is provided in Eq. 2.119. It can be observed that it depends on the hub moment per unit flapping angle M_β, which is a function of flap centre-spring rotor stiffness K_β, moment of inertia about pitch axis I_{yy}, number of blades N and height h of rotorcraft hub above center of gravity.

$$\dot{q} = -\frac{\frac{N}{2}K_\beta + Th}{I_{yy}}\beta_{1c} \tag{2.119}$$

The next model to be considered is a longitudinal body-flap model with flapping dynamics. It is a so-called **longitudinal τ_β-based rotorcraft** model, wherein τ_β ($=\frac{16}{\gamma}$) is a dimensionless parameter that indicates disc-tilt quickness. A large value for τ_β is associated with slow disc-tilt motion. In Eq. 2.120 the first-order flapping model is provided. The longitudinal body dynamics is represented by means of Eq. 2.119.

$$\dot{\beta}_{1c} = -\frac{\Omega}{\tau_\beta}\beta_{1c} + \frac{16q}{\gamma\tau_\beta} - \frac{\Omega}{\tau_\beta}\theta_{1s} \tag{2.120}$$

The last model to be considered incorporates two flapping states (β_{1c} and β_{1s}), two lead-lag states (ζ_{1s},ζ_{1c}) and lateral body dynamics (p and ϕ). Moreover, it also includes four corrective terms, because the BFL model in [40] does not account for body-lag coupling, whereas this is deemed necessary to conduct a particular analysis later on. It was therefore decided to include the body-lag coupling terms from [52]. The exact expressions shall not be given, but can be found in the aforementioned paper. Moreover, the control-depended terms for lead-lag are also taken from [52] as these account for more main rotor and individual blade parameters. This model shall be designated as the **lateral body-flap-lag model** for which the general expression for the flap-lag EOM are provided in Eq. 2.121 and the corresponding matrices in Eq. 2.122. After solving Eq. 2.121 the corrective terms need to be added to the EOM. In other words $F_{p,\zeta_{1c}}$, $F_{p,\zeta_{1s}}$, $H_{\zeta_{1c}}$ and $H_{\zeta_{1s}}$ obtained from [52] shall be replace the original values for these coupling and control-depended terms, because of reasons given earlier. It should be noted that the above mentioned coupling terms are a function of Number of blades N, rotor radius R, blade root eccentricity e_{bl}, lock number γ, rotor angular velocity Ω, coning angle β_0 ($=\beta_{ss}$), static moments m_s, rotor blade inertia I_{bl}, rotor blade mass, lag damper stiffness K_ζ, lag damper damping C^*_ζ, roll inertia I_{yy}, vehicle mass M and height h of rotorcraft hub above center of gravity. Moreover, the matrices from Eq. 2.122 also depend on non-dimensional lagging frequency λ_ζ, non-dimensional flapping frequency λ_β, non-dimensional inflow velocity in hover condition λ_i and drag coefficient C_{D1} (from $C_d = C_{d_0} + C_{d1}\alpha^2$).

$$\boldsymbol{C}_{NR}\begin{bmatrix}\dot{\boldsymbol{\beta}}\\ \dot{\boldsymbol{\zeta}}\end{bmatrix} = \Omega\boldsymbol{K}_{NR}\begin{bmatrix}\boldsymbol{\beta}\\ \boldsymbol{\zeta}\end{bmatrix} + \Omega\boldsymbol{F}_{NR}, \quad \text{with } \boldsymbol{\beta} = [\beta_{1c},\ \beta_{1s}]^T \text{ and } \boldsymbol{\zeta} = [\zeta_{1c},\ \zeta_{1s}]^T. \tag{2.121}$$

$$\mathbf{C}_{NR} = \begin{bmatrix} -2 & \gamma/8 & 0 & -2\beta_{ss} \\ \gamma/8 & 2 & -2\beta_{ss} & 0 \\ 0 & 2\beta_{ss} & -2 & C^*_\zeta \\ 2\beta_{ss} & 0 & C^*_\zeta & 2 \end{bmatrix}, \quad \mathbf{K}_{NR} = \begin{bmatrix} \gamma/8 & 1-\lambda^2_\beta & -2\beta_{ss} & 0 \\ 1-\lambda^2_\beta & -\gamma/8 & 0 & 2\beta_{ss} \\ 2\beta_{ss} & 0 & C^*_\zeta & 1-\lambda^2_\zeta \\ 0 & -2\beta_{ss} & 1-\lambda^2_\zeta & -C^*_\zeta \end{bmatrix} \text{ and}$$
$$\mathbf{F}_{NR} = \begin{bmatrix} \frac{\gamma}{8}\bar{p} - 2\bar{q} + \frac{\gamma}{8}\theta_{1s} \\ 2\bar{p} + \frac{\gamma}{8}\bar{q} + \frac{\gamma}{8}\theta_{1c} \\ \frac{\gamma}{6}\lambda_i(1-2C_{D1})\theta_{1s} \\ \frac{\gamma}{6}\lambda_i(1-2C_{D1})\theta_{1c} \end{bmatrix} \tag{2.122}$$

Having considered the flap-lag dynamics of the **lateral body-flap-lag model** it will be deemed necessary to provide information about the lateral body dynamics of the vehicle. Only roll rate (and roll angle) shall be considered in this model for which the expression is provided in Eq. 2.123. Roll angle can be obtained using integration of roll rate.

$$\dot{p} = -\frac{\frac{N}{2}K_\beta + Th}{I_{xx}}\beta_{1s} \tag{2.123}$$

3
Advanced Non-linear Flight Control

In this chapter the main focus will be on non-linear flight control and in particular *Lyapunov*-based flight control. Various *Lyapunov*-based controllers exists, however the main focus in this thesis will be on four types, namely recursive backstepping (BS), incremental backstepping (IBS), command-filtered backstepping (CFBS) and command-filtered incremental backstepping (CFIBS). First in Section 3.1 the derivation of BS shall be provided. There after in Section 3.2 the same shall be considered for incremental backstepping. Lastly, in Sections 3.3 and 3.4 the derivation of CFBS and CFIBS shall be provided respectively.

3.1. Recursive Backstepping Controller

Fundamental theory related to recursive BS has been provided in [25, 26, 29]. In addition to this, extensive research about recursive BS has been carried out by Sonneveldt [49] from which information about the derivation of conventional BS controller has been retrieved. Additional information regarding BS was retrieved from [1, 8, 27, 33, 53–55]. Due to the recursive nature of BS, it is deemed necessary to start at the subsystem with the highest amount of integrations removed from the physical control input [8]. It can therefore be stated main concept of BS is to design a controller in a recursive manner in which some of the state variables of the system must be considered as virtual controls for which intermediate control laws are being designed for, starting at the scalar equation separated by the largest number of integrations from the direct control input [49, 54, 56]. The procedure does end when reaching the actual control input. In general strict-feedback systems will be considered. These are the type of system were the state variables are fed back. In order to limit the scope of the analysis it is deemed necessary to only consider strict-feedback systems. Additional material related to more general types of systems, such as feed-forward systems, pure-feedback systems or block-strict-feedback systems when should consult the work from Krstic [30].

3.1.1. Recursive backstepping main advantages and disadvantages

Before providing detailed information it is of great importance to consider the main advantages and disadvantages of this controller. The aforementioned will be of great importance when selecting a particular type of *Lyapunov*-based controller. Below the main advantages and disadvantages of the controller are provided.

I It is a flexible control technique, which is capable of either including or excluding non-linearities based on required properties of the systems [50]. Some non-linearities may exhibit stabilising properties and can therefore be regarded as desirable and should therefore not be excluded [14]. On the other hand, NDI is a feedback linearisation type of technique which removes all non-linearities, hence also the ones that may have a stabilising effect on the system.

II It is based on *Lyapunov* stability, and therefore It guarantees stability of the system, or more accurately, it guarantees of global asymptotic stabilisation and tracking [13, 54].

III Design is of recursive nature, in which each subsystem is stabilised by following the same procedure, except for the first and last subsystem [8, 50]. Due to the nature of the structure, one can focus on each subsystem individually.

IV BS control allows for coupling between the inner and outer loops, unlike NDI control ,which requires time-scale separation between inner and outer loops [54, 55].

Having considered the main advantages of recursive BS, it is also necessary to consider it disadvantages, which have been briefly summarised below.

I Asymptotic stability can be achieved, but this does not imply that the transient behaviour of the system can be regarded as adequate [8, 27].

II Tuning of backstepping gains can be regarded as a nontrivial assignment as adequately tuning gains can improve the system response [8, 50]. It is very common to select backstepping by means of trial and error. On the other hand there are also nonlinear optimisation techniques which can determine the optimal backstepping gain values [6, 22]

III BS control is a model based control technique, which implies that small model error may can destabilise the system [50]. The aforementioned is especially of great concern for complex systems which exhibit unknown dynamics. Accurate model knowledge should then be obtained by means of adequate system identification techniques [8, 27].

IV Application of BS is limited to systems being of lower triangular form and affine-in-control [50, 55].

3.1.2. Derivation of recursive Backstepping

With the advantages and disadvantages of recursive BS being defined, the derivation shall be touched upon. The derivation provided by Gils [54] shall be considered. The main procedure for recursive BS was obtained from Sonneveldt [49], which can be divided into three parts:

I Introducing a virtual control input, state error and current state equation rewritten in terms of these

II Adequately choosing a CLF for the (sub-)system and treating it as a final stage

III Choosing a stabilising feedback function for the virtual control such that the CLF is stabilised.

In order to provide the derivation of recursive BS it is deemed necessary to make use of a strict-feedback system of lower triangular form, which can be defined as follows [50]:

$$\dot{\boldsymbol{x}}_j = \boldsymbol{f}_j(\bar{\boldsymbol{x}}_j) + \boldsymbol{g}_j(\bar{\boldsymbol{x}}_j)x_{j+1}, \qquad \text{for } j = 1,..,n-1 \tag{3.1}$$

$$\dot{\boldsymbol{x}}_n = \boldsymbol{f}_n(\boldsymbol{x}) + \boldsymbol{g}_n(\boldsymbol{x})\boldsymbol{u}, \tag{3.2}$$

wherein $\bar{\boldsymbol{x}}_j$ and $\boldsymbol{x}$ are state vectors $[\boldsymbol{x}_1, \boldsymbol{x}_2, .., \boldsymbol{x}_j]^{\mathrm{T}}$ and $[\boldsymbol{x}_1, \boldsymbol{x}_2, .., \boldsymbol{x}_n]^{\mathrm{T}}$ respectively with $\boldsymbol{x}_j \in \mathbb{R}^n$ [54]. Furthermore $\boldsymbol{u} \in \mathbb{R}^m$ is the control vector of the system. Furthermore $\boldsymbol{f}_j(\bar{\boldsymbol{x}}_j)$ and $\boldsymbol{g}_j(\bar{\boldsymbol{x}}_j)$ are assumed to be fully known and do have $n-j$ continuous derivatives, thus wherein $\boldsymbol{f}_j(\bar{\boldsymbol{x}}_j)$ and $\boldsymbol{g}_j(\bar{\boldsymbol{x}}_j) \in C^{n-j}$ for $j = 1,..,n-1$. The control objective considered for the derivations consists of tracking a smooth reference signal $\boldsymbol{x}_{1,\mathrm{ref}}$ for which the n^{th}-order time derivatives are known and bounded [51, 56]. States $\boldsymbol{x}_j$ for $j = 1,..,n$ must remain bounded when executing the tracking task [49, 56]. The complete system can be divided into three parts: the subsystem furthest away from the physical control input u, intermediate subsystems and the subsystem governed by physical control input u [50]. Below the derivation of recursive BS is provided.

Subsystem j=1 (furthest away from the physical control input)
For the derivation it is deemed necessary to start with the subsystem furthest away from the physical control input. The differential equation describing this subsystem can written as

$$\dot{\boldsymbol{x}}_1 = \boldsymbol{f}_1(\boldsymbol{x}_1) + \boldsymbol{g}_1(\boldsymbol{x}_1)\boldsymbol{x}_2, \tag{3.3}$$

wherein $\boldsymbol{x}_2$ can be regarded as the control input to this subsystem [54]. Since $\boldsymbol{x}_2$ is a system state, it must be regarded as a *"virtual"* control input. Furthermore the tracking error for the first subsystem and for the subsystem being hierarchical one higher can be respectively defined as

$$\boldsymbol{z}_1 = \boldsymbol{x}_1 - \boldsymbol{x}_{1,\mathrm{ref}}, \tag{3.4}$$

$$\boldsymbol{z}_2 = \boldsymbol{x}_2 - \boldsymbol{\alpha}_1, \tag{3.5}$$

with $\boldsymbol{\alpha}_1$ (=$\boldsymbol{x}_{2,\text{ref}}$) being the stabilising function for the first subsystem [54]. The derivative of $\boldsymbol{z}_1$ must be defined when taking the first order time derivative of the CLF. The expression for $\dot{\boldsymbol{z}}_1$ shall be obtained in terms of the system dynamics from Eq. 3.3 and can be defined as follows

$$\begin{aligned}\dot{\boldsymbol{z}}_1 &= \dot{\boldsymbol{x}}_1 - \dot{\boldsymbol{x}}_{1,\text{ref}} \\ &= \boldsymbol{f}_1(\boldsymbol{x}_1) + \boldsymbol{g}_1(\boldsymbol{x}_1)\boldsymbol{x}_2 - \dot{\boldsymbol{x}}_{1,\text{ref}} \\ &= \boldsymbol{f}_1(\boldsymbol{x}_1) + \boldsymbol{g}_1(\boldsymbol{x}_1)(\boldsymbol{z}_2 + \boldsymbol{\alpha}_1) - \dot{\boldsymbol{x}}_{1,\text{ref}},\end{aligned} \tag{3.6}$$

wherein the last expression $\boldsymbol{x}_2$ was replaced by the expression given in Eq. 3.5 [54]. To proceed further it is deemed necessary to define a CLF. A quadratic CLF is being incorporated, which is favourable because of its sign check capabilities. The quadratic CLF and its derivative are given in Eq. 3.7 and Eq. 3.8 respectively [54].

$$\mathcal{V}_1(\boldsymbol{z}_1) = 0.5\boldsymbol{z}_1^T\boldsymbol{z}_1 \tag{3.7}$$

$$\dot{\mathcal{V}}_1 = \boldsymbol{z}_1^T\dot{\boldsymbol{z}}_1 \tag{3.8}$$

Substituting the expression of $\dot{\boldsymbol{z}}_1$ from Eq. 3.6 into $\dot{\mathcal{V}}_1$, will enable to determine the stabilising control law for the first subsystem. The aforementioned will yield the following expression for $\dot{\mathcal{V}}_1$

$$\dot{\mathcal{V}}_1 = \boldsymbol{z}_1^T\left[\boldsymbol{f}_1(\boldsymbol{x}_1) + \boldsymbol{g}_1(\boldsymbol{x}_1)(\boldsymbol{z}_2 + \boldsymbol{\alpha}_1) - \dot{\boldsymbol{x}}_{1,\text{ref}}\right] \tag{3.9}$$

The stabilising control law can be determined by making $\dot{\boldsymbol{\mathcal{V}}}_1$ negative definite, thus $\boldsymbol{\alpha}_1$ must be equal to

$$\boldsymbol{\alpha}_1 = \boldsymbol{g}_1(\boldsymbol{x}_1)^{-1}\left[-\boldsymbol{f}_1(\boldsymbol{x}_1) + \dot{\boldsymbol{x}}_{1,\text{ref}} - \boldsymbol{c}_1\boldsymbol{z}_1\right] \quad \text{with } \boldsymbol{c}_1 > 0. \tag{3.10}$$

With $\boldsymbol{\alpha}_1$ being obtained, the final expression for $\dot{\mathcal{V}}_1$ can be obtained. Substituting the stabilising function from Eq. 3.10 into the derivative expression of the CLF yields:

$$\dot{\mathcal{V}}_1 = \boldsymbol{z}_1^T\boldsymbol{g}_1(\boldsymbol{x}_1)\boldsymbol{z}_2 - \boldsymbol{z}_1^T\boldsymbol{c}_1\boldsymbol{z}_1 \quad \text{with } \boldsymbol{c}_1 > 0. \tag{3.11}$$

From the previous expression it can be observed that $\dot{\mathcal{V}}_1$ is not negative definite, due to the cross term $\boldsymbol{z}_1^T\boldsymbol{g}_1(\boldsymbol{x}_1)\boldsymbol{z}_2$. For certain combinations of $\boldsymbol{z}_1$ and $\boldsymbol{z}_2$ the expression might not be negative definite [54]. The cross-term shall therefore be removed in the next steps. All of the natural dynamics have been removed. Additional non-linear dynamics can still be retained when it provides adequate stabilisation [15].

Subsystem j with j = 2, ... , n - 1 (intermediate subsystems)
The intermediate subsystem do consist of all subsystems between the subsystem furthest away from the physical control input **u** and the subsystem governed by **u** [54]. The derivation for the intermediate subsystem will be presented below. The dynamics of the intermediate subsystems can be written as follows

$$\dot{\boldsymbol{x}}_j = \boldsymbol{f}_j(\bar{\boldsymbol{x}}_j) + \boldsymbol{g}_j(\bar{\boldsymbol{x}}_j)x_{j+1}, \quad \text{with } j = 2,...,n-1, \tag{3.12}$$

wherein $\boldsymbol{x}_{j+1}$ can be regarded the virtual control input for subsystem j [54]. Tracking error for subsystem j can be defined as follows

$$\boldsymbol{z}_j = \boldsymbol{x}_j - \boldsymbol{\alpha}_{j-1}, \quad \text{with } j = 3,...,n, \tag{3.13}$$

with $\boldsymbol{\alpha}_{j-1}$(=$\boldsymbol{x}_{j,\text{ref}}$) being the stabilising function for subsystem j [54]. The derivative of $\boldsymbol{z}_j$ is equal to the following

$$\begin{aligned}\dot{\boldsymbol{z}}_j &= \boldsymbol{f}_j(\bar{\boldsymbol{x}}_j) + \boldsymbol{g}_j(\bar{\boldsymbol{x}}_j)\boldsymbol{x}_{j+1} - \dot{\boldsymbol{\alpha}}_{j-1}, \quad \text{with } j = 2,...,n-1, \\ &= \boldsymbol{f}_j(\bar{\boldsymbol{x}}_{\boldsymbol{j}}) + \boldsymbol{g}_j(\bar{\boldsymbol{x}}_j)(\boldsymbol{z}_{j+1} + \boldsymbol{\alpha}_j) - \dot{\boldsymbol{\alpha}}_{j-1},\end{aligned} \tag{3.14}$$

in which $\boldsymbol{x}_{j+1}$ has been replaced with the expression given in Eq. 3.13. For all intermediate subsystem a quadratic CLF is chosen, due to its attractive properties and because of staying consistent with the other subsystems. The CLF of subsystem $j-1$ will be augmented with the CLF from subsystem j, which yields the expression given in Eq. 3.15 [54].

$$\mathcal{V}_j(\bar{\boldsymbol{z}}_j) = \mathcal{V}_1(\boldsymbol{z}_1) + \sum_{k=2}^{j} 0.5\boldsymbol{z}_k^T\boldsymbol{z}_k \qquad \text{with } j = 2,...,n-1. \tag{3.15}$$

In order to obtain an expression for the stabilising control function, it is first necessary to take the derivative of $\mathcal{V}_j(\boldsymbol{z}_j)$ along the trajectories of $\dot{\boldsymbol{z}}_j$ and $\dot{\boldsymbol{z}}_1$. In Eq. 3.16 the expression for $\dot{\mathcal{V}}_j$ has been provided [54]. Substituting the derivative for tracking error $\boldsymbol{z}_j$ into this equation expression does yield the second expression.

$$\begin{aligned}\dot{\mathcal{V}}_j &= \dot{\mathcal{V}}_1 + \sum_{k=2}^{j} \boldsymbol{z}_k^T\dot{\boldsymbol{z}}_k, \qquad \text{with } j = 2,...,n-1. \\ &= \boldsymbol{z}_1^T\boldsymbol{g}_1(\boldsymbol{x}_1)\boldsymbol{z}_2 - \boldsymbol{z}_1^T\boldsymbol{c}_1\boldsymbol{z}_1 + \sum_{k=2}^{j} \boldsymbol{z}_k^T\big[\boldsymbol{f}_k(\bar{\boldsymbol{x}}_k) + \boldsymbol{g}_k(\bar{\boldsymbol{x}}_k)(\boldsymbol{z}_{k+1} + \boldsymbol{\alpha}_k) - \dot{\boldsymbol{\alpha}}_{k-1}\big].\end{aligned} \tag{3.16}$$

The stabilising control function can be obtained by making $\dot{\mathcal{V}}_j$ negative definite. In order to achieve the aforementioned, the stabilising function must be equal to the one given in Eq. 3.17 [54].

$$\boldsymbol{\alpha}_k = \boldsymbol{g}_k(\bar{\boldsymbol{x}}_k)^{-1}\big[-\boldsymbol{f}_k(\bar{\boldsymbol{x}}_k) + \dot{\boldsymbol{\alpha}}_{k-1} - \boldsymbol{c}_k\boldsymbol{z}_k - \boldsymbol{g}_{k-1}(\bar{\boldsymbol{x}}_{k-1})\boldsymbol{z}_{k-1}\big] \qquad \text{with } \boldsymbol{c}_k > 0 \qquad \text{with } k = 2,...,j. \tag{3.17}$$

Based on the expression for the stabilising function, one does obtain the following CLF

$$\dot{\mathcal{V}}_j = \sum_{k=1}^{j} \boldsymbol{z}_j^T\boldsymbol{g}_j(\bar{\boldsymbol{x}}_j)\boldsymbol{z}_{j+1} - \boldsymbol{z}_k^T\boldsymbol{c}_k\boldsymbol{z}_k \qquad \text{with } j = 2,...,n-1. \tag{3.18}$$

Based on the obtained stabilising function $\boldsymbol{a}_k$, one can state that the CLF for a given j^{th} subsystem is not negative definite for all values of $\boldsymbol{z}_{j+1}$ and $\boldsymbol{z}_j$, given a $\boldsymbol{g}_j(\bar{\boldsymbol{x}}_j)$ [54]. The cross-term $\boldsymbol{z}_j^T\boldsymbol{g}_j(\bar{\boldsymbol{x}}_j)\boldsymbol{z}_{j+1}$ shall be removed in the last step of the recursive BS procedure. Likewise, for the first subsystem, all of the natural dynamics has been removed. Additional non-linear dynamics can be retained when it provides adequate stabilisation [15].

Subsystem j=n (subsystems with physical control input u)

To complete the derivation of conventional recursive BS, it is necessary to end with the subsystem, which is governed by the physical control input u. The recursive BS procedure will be similar as for the previous subsystems except for the fact that all cross-terms will be removed. The system dynamics of the last subsystem can be written into the following form

$$\dot{\boldsymbol{x}}_n = \boldsymbol{f}_n(\boldsymbol{x}) + \boldsymbol{g}_n(\boldsymbol{x})\boldsymbol{u}, \tag{3.19}$$

wherein $\boldsymbol{u}$ can be regarded as the physical control input for subsystem n [54]. Tracking error for subsystem n is given in Eq. 3.20 [54].

$$\boldsymbol{z}_n = \boldsymbol{x}_n - \boldsymbol{\alpha}_{n-1}. \tag{3.20}$$

For establishing $\dot{\mathcal{V}}_n$, the derivative of $\boldsymbol{z}_n$ from Eq. 3.20 is necessary, which is found to be equal to the following

$$\begin{aligned}\dot{\boldsymbol{z}}_n &= \dot{\boldsymbol{x}}_n - \dot{\boldsymbol{\alpha}}_{n-1} \\ &= \boldsymbol{f}_n(\boldsymbol{x}) + \boldsymbol{g}_n(\boldsymbol{x})\boldsymbol{u} - \dot{\boldsymbol{\alpha}}_{n-1},\end{aligned} \tag{3.21}$$

from which it can be observed that the error dynamics was written in terms of system dynamics from Eq. 3.19. The CLF's of the previous subsystems will be augmented with the CLF from subsystem n, which yields the expression provided in Eq. 3.22 [54].

$$\begin{aligned}\mathcal{V}_n(\boldsymbol{z}_n) &= \sum_{k=1}^{n} 0.5\boldsymbol{z}_k^T\boldsymbol{z}_k \\ &= \mathcal{V}_{n-1}(\bar{\boldsymbol{z}}_{n-1}) + 0.5\boldsymbol{z}_n^T\boldsymbol{z}_n.\end{aligned} \tag{3.22}$$

Taking the derivative of the augmented CLF along the trajectories of the error dynamics does yield

$$\begin{aligned}\dot{\mathcal{V}}_n &= \dot{\mathcal{V}}_{n-1} + \boldsymbol{z}_n\dot{\boldsymbol{z}}_n \\ &= \sum_{k=1}^{n-1} -\boldsymbol{z}_k^T\boldsymbol{c}_k\boldsymbol{z}_k + \boldsymbol{z}_{n-1}^T\boldsymbol{g}_{n-1}(\bar{\boldsymbol{x}}_{n-1})\boldsymbol{z}_{n-1} + \boldsymbol{z}_n^T\big[\boldsymbol{f}_n(\boldsymbol{x}) + \boldsymbol{g}_n(\boldsymbol{x})\boldsymbol{u} - \dot{\boldsymbol{\alpha}}_{n-1}\big].\end{aligned} \tag{3.23}$$

To render the CLF derivative from Eq. 3.23 negative definite, the following control law u must be selected

$$\boldsymbol{u} = \boldsymbol{g}_n(\boldsymbol{x})^{-1}\big[-\boldsymbol{f}_n(\boldsymbol{x}) + \dot{\boldsymbol{\alpha}}_{n-1} - \boldsymbol{c}_n\boldsymbol{z}_n - \boldsymbol{g}_{n-1}(\bar{\boldsymbol{x}}_{n-1})\boldsymbol{z}_{n-1}\big], \tag{3.24}$$

from which it can be observed that $\boldsymbol{u}$ depends on the analytical derivative of $\boldsymbol{\alpha}_{n-1}$, which can be rather tedious to obtain [54]. Based on the expression for $\boldsymbol{u}$, the CLF derivative $\dot{\mathcal{V}}_n$ can be rewritten into

$$\dot{\mathcal{V}}_n = \sum_{k=1}^{n} -\boldsymbol{z}_k^T\boldsymbol{c}_k\boldsymbol{z}_k. \tag{3.25}$$

In accordance with the theorem of LaSalle-Yoshizawa $\boldsymbol{z}$ can be regarded as uniformly asymptotically stable when given that $\boldsymbol{c}_k > 0$ for all $k = 1,..,n$ [54]. The aforementioned subsequently means that the desired reference signals as defined earlier can be tracked by the *Lyapunov*-based controller. To put this into a more mathematical form, the following would hold

$$\lim_{t\to\infty}\big[\boldsymbol{x}_1 - \boldsymbol{x}_{1,\text{ref}}\big] = \boldsymbol{0}. \tag{3.26}$$

Recursive backstepping is suitable for defining stabilising control laws for which the system dynamics is well-known (e.g. kinematic relation). Considering the fact that *Lyapunov*-based control design will also be exposed to uncertainties, it is deemed necessary to consider other *Lyapunov*-based control techniques which enable to cope with these uncertainties. Of prime concern is the analytical derivative for $\boldsymbol{\alpha}$ which is required for establishing $\boldsymbol{u}$, which is difficult to obtain analytically. In the next section incremental backstepping will be considered, which can deal with uncertainties to some extent.

3.2. Incremental Backstepping

The next *Lyapunov*-based controller that will be considered is incremental backstepping. IBS is an effective control design methodology for which stability can be guaranteed given a set of assumptions [27]. With IBS a sensor-based approach is pursued, in which less model knowledge is required as complex system dynamics can be linearised by means of a first-order *Taylor* series [23, 27, 54]. Conventional BS however, is a model-based control strategy, hence sensitive to model uncertainties [27, 54]. IBS has been used in various types of applications in which there is unknown dynamics in one or more loops of the controller [8, 13, 54]. This deficiency must be circumvented in order to assure fault tolerant BS control, which can be realised by means of IBS as it reduces model dependency, thus improving model robustness [27, 54]. The design procedure for IBS using a strict feedback system is similar to BS, except for a first-order *Taylor* Series being used for approximating complex system dynamics [8, 54]. Recursive BS is limited to systems which are affine in control, which is in contrast to IBS, for which systems do not necessarily need to be affine in control [27, 55].

With IBS the system states and its derivative must be measured to obtain model information, rather than using model knowledge. In [27] it is explained that this approach is desirable as it reduces the effect of model mismatch. In case of model mismatch, performance is likely to degrade performance of the system and stability cannot be guaranteed [55]. The effectiveness of incorporating an IBS design in terms of system robustness was already proven in [1]. IBS also overcome the need for model identification or conservatism [13]. This is desirable for certifiability for aerospace vehicles [27]. In general controllers can be modelled by means of slow outer loop kinematic and fast inner loop dynamic equations [8]. The former equations can be regarded well-known and can be adequately modelled [8]. The inner loop dynamics do consists of less well-known functions difficult to model, which means that there are uncertainties present in this loop [8, 55]. The kinematic outer loop and inner loop must be controlled by means of BS and IBS respectively [8].

3.2.1. Incremental backstepping main advantages and disadvantages

In order to compare various types of *Lyapunov*-based controllers it is deemed necessary to consider both the advantages and disadvantages of IBS. The main advantages of IBS are:

I IBS was found to be robust against mismatches in control effectiveness as it enables adequate controller performance even when the control effectiveness mismatch is 50% [8, 27, 53]. This holds when the controller update rate is sufficiently high [27, 55]. High update rates increase the allowed control effectiveness mismatch, thus underlining the importance of time-scale separation [8],

II The restriction of affine-in-control system requirement is not deemed necessary as a first-order *Taylor* series is incorporated for representing the system dynamics [49, 55].

Furthermore the main disadvantage of IBS are:

I It is assumed that there is complete and accurate knowledge of the system states and sufficiently high sampling rate, hence instantaneous control actions [1, 54]. This requires adequate and complete information of state derivatives from the system, such as angular accelerations for which there in general no sensors for which can adequately measure this as only prototypes exist. The drawback is that angular accelerations shall therefore be estimated based on angular rate measurements, which contain noise.

II IBS requires control deflections, which cannot always be provided, hence therefore must be estimated on the basis of high-fidelity model of the actuator dynamics [1, 54]. The latter implies the negligence of *Taylor* series terms. In terms of robustness this can also be considered of importance because when this assumption holds, the IBS control law can be considered robust to system uncertainties [50].

3.2.2. Assumptions incremental backstepping

For providing the derivation of IBS it is deemed necessary to consider the following set of assumptions.

I There must be *accurate, reliable and complete knowledge of the system states and their derivatives* [1, 8, 54]. Former is obtained by means of system measurements. The IBS controller must be robust against measurement biases and noise for sufficiently high update rate of the controller.

II There is *time-scale separation* between the controlled states (slow time-scale) and the states on which control action has direct effect (fast time-scale) [1, 8, 54]. For small time increments and quick actuators, large control inputs will cause the controlled states too change slower than the direct affected states.

III *Instantaneous control action* will be assumed, wherein system response is instantaneous to commanded signals [1, 54]. It does not account for actuator dynamics and additional internal system delays.

IV *Fast evaluation rate* is considered, wherein the controller does send continuous input commands to the system [1, 54]. Due to the digital nature of the controller, this is unlikely, thus a high update rate is assumed.

3.2.3. Derivation of incremental backstepping for two-cascaded system

The derivation of IBS from [54] shall be used. In order to provide a derivation of IBS, it is first necessary to define the dynamics of the system. In this particular case a cascaded system with two subsystems is being considered in which one subsystem contains the kinematic equations of motion and the other subsystem the unknown or uncertain dynamics [55]. The aforementioned represents the natural division of the rotational dynamics of the rotorcraft into attitude kinematics and angular rates. Herein, the former can be regarded as slow and known, whereas the latter is fast and partially known (unknown). Based on this, the cascaded system can be described with the following equations

$$\dot{\boldsymbol{x}}_1 = \boldsymbol{f}_{\mathrm{k}}(\boldsymbol{x}_1) + \boldsymbol{g}_{\mathrm{k}}(\boldsymbol{x}_1)\boldsymbol{x}_2 \tag{3.27}$$

$$\dot{\boldsymbol{x}}_2 = \boldsymbol{f}_{\mathrm{d}}(\boldsymbol{x}_1, \boldsymbol{x}_2) + \boldsymbol{g}_{d}(\boldsymbol{x}_1, \boldsymbol{x}_2)\boldsymbol{u}, \tag{3.28}$$

wherein subscript *"k"* and *"d"* are referring to the kinematics and dynamics of the system [54, 55]. Furthermore x_1 and x_2 can be as the state vectors, hence $\boldsymbol{x}_1 \in \mathbb{R}^n$ and $\boldsymbol{x}_2 \in \mathbb{R}^n$ [54]. Furthermore $\boldsymbol{u} \in \mathbb{R}^m$ is the physical control input of the two-cascaded system. In the derivation below use is made of the time-scale separation principle.

Subsystem j=1 (furthest away from the physical control input)

For the derivation it is deemed necessary to start with the subsystem furthest away from the physical control input $\boldsymbol{u}$ [54]. The dynamics of the first subsystem is provided in Eq. 3.27, wherein $\boldsymbol{x}_2$ is a state of the system and shall therefore be regarded as a virtual control input to this subsystem. Tracking error for the first subsystem and one hierarchical higher can be expressed respectively as

$$\boldsymbol{z}_1 = \boldsymbol{x}_1 - \boldsymbol{x}_{1,\text{ref}} \tag{3.29}$$

$$\boldsymbol{z}_2 = \boldsymbol{x}_2 - \boldsymbol{x}_{2,\text{ref}}, \tag{3.30}$$

with $\boldsymbol{\alpha}_1$ (=$\boldsymbol{\alpha}_1$) being the stabilising function for the first subsystem [54]. The derivative of $\boldsymbol{z}_1$ will be needed when computing the derivative of the CLF. The next step is to determine $\dot{\boldsymbol{z}}_1$, which is found to be equal to

$$\begin{aligned} \dot{\boldsymbol{z}}_1 = \dot{\boldsymbol{x}}_1 - \dot{\boldsymbol{x}}_{1,\text{ref}} &= \boldsymbol{f}_k(\boldsymbol{x}_1) + \boldsymbol{g}_k(\boldsymbol{x}_1)\boldsymbol{x}_2 - \dot{\boldsymbol{x}}_{1,\text{ref}} \\ &= \boldsymbol{f}_k(\boldsymbol{x}_1) + \boldsymbol{g}_k(\boldsymbol{x}_1)(\boldsymbol{z}_2 + \boldsymbol{\alpha}_1) - \dot{\boldsymbol{x}}_{1,\text{ref}}, \end{aligned} \tag{3.31}$$

wherein x_2 has been replaced by the expression given in Eq. 3.30. A quadratic CLF is incorporated, which is favourable because of its sign check definiteness. The quadratic CLF and its time derivative are given in Eq. 3.32 and Eq. 3.33 respectively [54].

$$\mathcal{V}_1(\boldsymbol{z}_1) = 0.5\boldsymbol{z}_1^T\boldsymbol{z} \tag{3.32}$$

$$\dot{\mathcal{V}}_1(\boldsymbol{z}_1) = \boldsymbol{z}_1^T\dot{\boldsymbol{z}}_1 \tag{3.33}$$

Substituting the derivative of $\boldsymbol{z}_1$ into the first order time derivative expression for the CLF does yield

$$\dot{\mathcal{V}}_1 = \boldsymbol{z}_1^T\left[\boldsymbol{f}_k(\boldsymbol{x}_1) + \boldsymbol{g}_k(\boldsymbol{x}_1)(\boldsymbol{z}_2 + \boldsymbol{\alpha}_1) - \dot{\boldsymbol{x}}_{1,\text{ref}}\right] \tag{3.34}$$

In order to make CLF derivative negative definite, the stabilising function must be equal to the following

$$\boldsymbol{\alpha}_1 = \boldsymbol{g}_k(\boldsymbol{x}_1)^{-1}\left[-f_k(\boldsymbol{x}_1) + \dot{\boldsymbol{x}}_{1,\text{ref}} - \boldsymbol{c}_1\boldsymbol{z}_1\right], \qquad \text{with } \boldsymbol{c}_1 > 0 \tag{3.35}$$

Substituting the stabilising function into the derivative expression of the CLF yields:

$$\dot{\boldsymbol{\mathcal{V}}}_1(\boldsymbol{z}_1) = \boldsymbol{z}_1^T\boldsymbol{g}_\text{k}(\boldsymbol{x}_1)\boldsymbol{z}_2 - \boldsymbol{z}_1^T\boldsymbol{c}_1\boldsymbol{z}_1, \qquad \text{with } \boldsymbol{c}_1 > 0 \tag{3.36}$$

From the previous expression it can be observed that $\dot{\mathcal{V}}_1(\boldsymbol{z}_1)$ is not negative definite for all $\boldsymbol{c}_1$, which is due to the cross term $\boldsymbol{z}_1^T\boldsymbol{g}(\boldsymbol{x}_1)\boldsymbol{z}_2$. For certain combinations of $\boldsymbol{z}_1$ and $\boldsymbol{z}_2$ the expression might not be negative definite, and shall therefore be removed when constructing the incremental-based control law for the last subsystem [54]. In addition to this all natural dynamics has been removed when defining the stabilising control law for the first subsystem. Additional non-linear dynamics can be retained when it provides adequate stabilisation [15]. The stabilising control law of the first subsystem was established by means of recursive BS, as there are no uncertainties present in the differential equation given in Eq. 3.27.

Subsystem j=n=2 (subsystems with physical control input u)
Since a two-cascaded system is being considered, there will be no intermediate subsystems considered for the derivation. The last subsystem is governed by the physical control input $\boldsymbol{u}$. The main objective is derive a control law in terms of u. The dynamics of the last subsystem was provided in Eq. 3.28. For deriving an IBS control law, Eq. 3.28 could also be written in non-affine form. In the proceeding analysis the affine form will be considered. This subsystem is characterised with (partially) unknown dynamics, hence the first-order *Taylor* series expansion shall be considered around the current solution $(\boldsymbol{x}_0, \boldsymbol{u}_0)$. at t_0. of Eq. 3.28 [54, 55]. The first order *Taylor* series expansion about the current solution is can be written as

$$\dot{\boldsymbol{x}}_2 \approx \underbrace{\boldsymbol{f}_d(\boldsymbol{x}_0) + \boldsymbol{g}_d(\boldsymbol{x}_0\boldsymbol{u}_0)}_{\dot{\boldsymbol{x}}_{2,0}} + \underbrace{\frac{\partial}{\partial \boldsymbol{x}}\left[\boldsymbol{f}_d(\boldsymbol{x}) + \boldsymbol{g}_d(\boldsymbol{x})\right]\Big|_{\substack{\boldsymbol{x}=\boldsymbol{x}_0\\ \boldsymbol{u}=\boldsymbol{u}_0}}}_{\boldsymbol{f}_{d(\boldsymbol{x})}} \underbrace{\left(\boldsymbol{x}-\boldsymbol{x}_0\right)}_{\Delta\boldsymbol{x}} + \underbrace{\frac{\partial}{\partial \boldsymbol{u}}\left[\boldsymbol{f}_d(\boldsymbol{x}) + \boldsymbol{g}_d(\boldsymbol{x})\right]\Big|_{\substack{\boldsymbol{x}=\boldsymbol{x}_0\\ \boldsymbol{u}=\boldsymbol{u}_0}}}_{\boldsymbol{g}_d(\boldsymbol{x})} \underbrace{\left(\boldsymbol{u}-\boldsymbol{u}_0\right)}_{\Delta\boldsymbol{u}}, \tag{3.37}$$

wherein $\Delta\boldsymbol{x}$ and $\Delta\boldsymbol{u}$ are the incremental state and control vector respectively [54, 55]. Higher-order terms are neglected as these do not contribute significantly to the dynamics for small t_s. The error of the first-order *Taylor* series approximation is approximately $\mathcal{O}(t_s)$, which is acceptable for small t_s [8, 46]. The first-order *Taylor* series shall be further simplified by considering the time-scale separation principle. This means that $\Delta\boldsymbol{u}$ and $\Delta\dot{\boldsymbol{x}}$ are significantly greater than $\Delta\boldsymbol{x}$, therefore the latter can be neglected [1, 8, 45, 46, 54]. The incremental change in state vector ($\Delta\boldsymbol{x}$) can therefore be regarded small, and thus neglected. The system dynamics from Eq. 3.28 is written in simplified form in Eq. 3.38.

$$\dot{\boldsymbol{x}}_\mathbf{2} \approx \dot{\boldsymbol{x}}_{2,0} + \boldsymbol{g}_\text{d}(\boldsymbol{x}_0)\Delta\boldsymbol{u}. \tag{3.38}$$

The rewritten system dynamics can subsequently be used for defining an adequate control law without having knowledge of the state dynamics of this subsystem. On the other hand, the control-depended dynamics is still required for defining the control law [54]. The derivative of the tracking error in Eq. 3.30 is equal to

$$\begin{aligned}\dot{\boldsymbol{z}}_2 &= \dot{\boldsymbol{x}}_2 - \dot{\boldsymbol{x}}_{2,\text{ref}} \\ &= \dot{\boldsymbol{x}}_{2,0} + \boldsymbol{g}_d(\boldsymbol{x}_0)\Delta\boldsymbol{u} - \dot{\boldsymbol{x}}_{2,\text{ref}}\end{aligned} \tag{3.39}$$

The CLF of the previous subsystem will be augmented with the CLF for this subsystem, such that The CLF and its first-order derivative are provided in Eq. 3.40 and 3.41 respectively [54].

$$\mathcal{V}_2(\boldsymbol{z}_1, \boldsymbol{z}_2) = \mathcal{V}_1(\boldsymbol{z}_1) + 0.5\boldsymbol{z}_2^T\boldsymbol{z}_2 \tag{3.40}$$

$$\dot{\mathcal{V}}_2 = \dot{\mathcal{V}}_1 + \boldsymbol{z}_2^T\dot{\boldsymbol{z}}_2 \tag{3.41}$$

Furthermore the derivative of this augmented CLF for subsystem j is. Substituting the derivative for tracking error z_1 into the derivative expression for the CLF, yields

$$\begin{aligned}\dot{\mathcal{V}}_2 &= \dot{\mathcal{V}}_1 + \boldsymbol{z}_2^T\left[\dot{\boldsymbol{x}}_{2,0} + \boldsymbol{g}_\text{d}(\boldsymbol{x}_0)\Delta\boldsymbol{u} - \dot{\boldsymbol{x}}_{2,\text{ref}}\right] \\ &= \boldsymbol{z}_1^T g_2(\boldsymbol{x}_1)\boldsymbol{z}_2 - \boldsymbol{z}_1^T\boldsymbol{c}_1\boldsymbol{z}_1^2 + \boldsymbol{z}_2^T\left[\dot{\boldsymbol{x}}_{2,0} + \boldsymbol{g}_d(x_0)\Delta\boldsymbol{u} - \dot{\boldsymbol{x}}_{2,\text{ref}}\right]\end{aligned} \tag{3.42}$$

In order to make $\dot{\mathcal{V}}_2$ negative definite, the incremental control law $\Delta\boldsymbol{u}$ and total control law u must be:

$$\Delta\boldsymbol{u} = \boldsymbol{g}_\text{d}^{-1}(\boldsymbol{x}_0)\left[-\dot{\boldsymbol{x}}_{2,0} + \dot{\boldsymbol{x}}_{2,\text{ref}} - \boldsymbol{z}_1\boldsymbol{g}_1 - \boldsymbol{c}_2\boldsymbol{z}_2\right], \qquad \text{with } \boldsymbol{c}_2 > 0 \tag{3.43}$$

$$u = u_0 + \Delta u \tag{3.44}$$

Based on the expression for the stabilising function, one does obtain the following CLF

$$\dot{\mathcal{V}}_2 = -\boldsymbol{z}_1^T\boldsymbol{c}_1\boldsymbol{z}_1 - \boldsymbol{z}_2^T\boldsymbol{c}_2\boldsymbol{z}_2, \quad \text{with } c_1 > 0 \text{ and } \boldsymbol{c}_2 > 0 \tag{3.45}$$

It can be observed that the cross-term from the first subsystem has been cancelled. In addition to this $\dot{\mathcal{V}}_2(z_2)$ is negative definite when both c_1 and c_2 are strictly greater than zero. In the derivation of the incremental-based control law a two-cascaded system was considered, which resembles the angular kinematics and dynamics of a rotorcraft [55].

3.3. Command-Filtered Backstepping

In this section command-filter backstepping (CFBS) will be considered. In accordance with previous studies CFBS can be regarded as an attractive extension with respect to conventional recursive BS [49]. It is also very common that the CFBS approach is referred to as dynamic surface control [49, 54]. CFBS incorporates command-filters which enable to impose bandwidth, magnitude and rate limitations of the virtual controls [54]. In addition to this, it also obviates the need to have the systems dynamics in lower triangular form, which means that a broader ranch of system dynamics can be considered by constructing a *Lyapunov*-based control law [50, 54]. Next to this, it also does not require the analytical determination of the virtual control derivatives, which can be regarded as beneficial when considered large cascaded systems [50, 54]. The aforementioned is especially the case when considering adaptive BS. Below the main advantages of CFBS, as mentioned by van Gils [54], have been summarised:

I Imposing bandwidth, magnitude and rate limitations on the raw reference signal.

II Nonlinear systems do not have to be of lower triangular form.

III Analytical determination of the virtual control derivatives is not required.

3.3.1. Derivation Command-Filtered Backstepping

In contrast to recursive backstepping, command-filtered backstepping enables to derive a stabilising control law for a non-triangular system. This system shall therefore be considered for the derivation. The derivation from [54] was used. For the derivation of command-filtered backstepping a non-triangular feedback passive system, which can be described as follows

$$\dot{\boldsymbol{x}}_j = \boldsymbol{f}_j(\boldsymbol{x}) + \boldsymbol{g}_j(\boldsymbol{x})\boldsymbol{x}_{j+1}, \qquad \text{with } j = 1,2,3,...,n-1 \tag{3.46}$$

$$\dot{\boldsymbol{x}}_n = \boldsymbol{f}_n(\boldsymbol{x}) + g_n(\boldsymbol{x})\boldsymbol{u}, \tag{3.47}$$

wherein $\boldsymbol{x} \in \mathbb{R}^n$ and $\boldsymbol{x}_j \in \mathbb{R}^j$ for $1 \leq j \leq n-1$ and can be considered the state vectors of the (sub)-system [54]. Furthermore $\boldsymbol{u} \in \mathbb{R}^m$ is the control vector of the system. The main control objective is to let $\boldsymbol{x}_1$ track a smooth reference signal $\boldsymbol{x}_{1,\text{ref}}$ for which its derivative is both known and bounded [54]. The other system states x_j (for $2 \leq j \leq n-1$), which are the virtual control signals, are bounded as well [54]. Next to this $f_j(x)$ and $g_j(x)$ shall be regarded as smooth vector fields being a function of *all system state variables.* The latter is in contrast with the "*traditional*" lower triangular form. In addition to this $f_i(x) \in C^1$ and $g_i(x) \in C^1$, implying that the first order derivatives of these vector fields are continuous.

Subsystem j=1 (furthest away from the physical control input)
For the derivation it is deemed necessary to start with the subsystem furthest away from the physical control input $\boldsymbol{u}$. This subsystem is associated with the following differential equation

$$\dot{\boldsymbol{x}}_1 = \boldsymbol{f}_1(\boldsymbol{x}) + \boldsymbol{g}_1(\boldsymbol{x})\boldsymbol{x}_2, \tag{3.48}$$

wherein $\boldsymbol{x}_2$ is the control input to this subsystem [54]. Since $\boldsymbol{x}_2$ is a state of the system, it must be a virtual control input. The tracking for this subsystem and one hierarchical higher can be respectively defined as

$$\boldsymbol{z}_1 = \boldsymbol{x}_1 - \boldsymbol{x}_{1,\text{ref}} \tag{3.49}$$

$$\boldsymbol{z}_2 = \boldsymbol{x}_2 - \boldsymbol{\alpha}_1, \tag{3.50}$$

with $\boldsymbol{\alpha}_1 (= \boldsymbol{x}_{2,\text{ref}})$ being the stabilising function for the first subsystem [54]. Next to this, it is necessary to determine the derivative of $\boldsymbol{z}_1$, as this will be used in the CLF derivative. The following expression for $\dot{\boldsymbol{z}}_1$ can be derived, in which the virtual control input $\boldsymbol{x}_2$ has been replaced by the tracking error $\boldsymbol{z}_2$ and stabilising function $\boldsymbol{\alpha}_1$.

$$\begin{aligned} \dot{\boldsymbol{z}}_1 &= \dot{\boldsymbol{x}}_1 - \dot{\boldsymbol{x}}_{1,\text{ref}} \\ &= \boldsymbol{f}_1(x) + \boldsymbol{g}_1(\boldsymbol{x})\boldsymbol{x}_2 - \dot{\boldsymbol{x}}_{1,\text{ref}} \\ &= \boldsymbol{f}_1(\boldsymbol{x}) + \boldsymbol{g}_1(\boldsymbol{x})(\boldsymbol{z}_2 + \boldsymbol{\alpha}_1) - \dot{\boldsymbol{x}}_{1,\text{ref}} \end{aligned} \tag{3.51}$$

A quadratic CLF is being incorporated for the first subsystem. As mentioned in previous derivation, the quadratic CLF is chosen because of its ease in determining sign definiteness. In order to obtain the expression for the stabilising function $\boldsymbol{\alpha_1}$, it is necessary to take the first time derivative of the CLF along the trajectories of the error dynamics. The quadratic CLF and its first order time derivative are provided below [54].

$$\mathcal{V}_1(\boldsymbol{z}_1) = 0.5\boldsymbol{z}_1^T\boldsymbol{z}_1 \tag{3.52}$$

$$\dot{\mathcal{V}}_1 = \boldsymbol{z}_1^T\dot{\boldsymbol{z}}_1 = \boldsymbol{z}_1^T\left\{\boldsymbol{f}_1(\boldsymbol{x}) + \boldsymbol{g}_1(\boldsymbol{x})(\boldsymbol{z}_2 + \boldsymbol{\alpha}_1) - \dot{\boldsymbol{x}}_{1,\text{ref}}\right\} \tag{3.53}$$

In order to make the derivative of the CLF negative definite, the stabilising function shall be defined as

$$\boldsymbol{\alpha}_1 = \boldsymbol{g}_1^{-1}(\boldsymbol{x})\left\{-\boldsymbol{f}_1(\boldsymbol{x}) + \dot{\boldsymbol{x}}_{1,\text{ref}} - \boldsymbol{c}_1\boldsymbol{z}_1\right\}, \qquad \text{for } \boldsymbol{c}_1 > 0 \tag{3.54}$$

The previous steps are in accordance with the standard BS procedure. Here a command filtering approach is being considered, thus $\boldsymbol{\alpha}_1$ shall not be used directly, but used to define a new raw reference signal, namely

$$\boldsymbol{x}_{2,\text{ref}}^0 = \boldsymbol{\alpha}_1 - \boldsymbol{\chi}_2. \tag{3.55}$$

which shall be led through a command filter, yielding corresponding reference signals $\boldsymbol{x}_{2,\text{ref}}$ and $\dot{\boldsymbol{x}}_{2,\text{ref}}$ [54]. A stable linear filter shall be used to estimate the effect that the command filter has on the tracking error $\boldsymbol{z}_1$. The stable linear filter is defined below [54].

$$\dot{\boldsymbol{\chi}}_1 = \boldsymbol{g}_1(\boldsymbol{x})\left[\boldsymbol{x}_{2,\text{ref}} - \boldsymbol{x}^0_{2,\text{ref}}\right] - \boldsymbol{c}_1\chi_1, \quad \text{with } \boldsymbol{\chi}_1(0) = 0 \tag{3.56}$$

Magnitude, rate and bandwidth constraints can be imposed on this filter, thus making intermediate control laws not unbounded. Next, it is necessary to introduce the compensated tracking error for this subsystem and one hierarchical higher. The compensated tracking errors are given below [54].

$$\bar{\boldsymbol{z}}_1 = \boldsymbol{z}_1 - \boldsymbol{\chi}_1 \tag{3.57}$$

$$\bar{\boldsymbol{z}}_2 = \boldsymbol{z}_2 - \boldsymbol{\chi}_2 \tag{3.58}$$

In order to proceed further it is necessary to take the first order time derivative of $\bar{\boldsymbol{z}}_1$, which is equal to

$$\dot{\bar{\boldsymbol{z}}}_1 = \dot{\boldsymbol{z}}_1 - \dot{\boldsymbol{\chi}}_1 = \boldsymbol{f}_1(\boldsymbol{x}) + \boldsymbol{g}_1(\boldsymbol{x})(\boldsymbol{x}_{2,\text{ref}} + \boldsymbol{z}_2) - \dot{\boldsymbol{x}}_{1,\text{ref}} + \boldsymbol{c}_1\boldsymbol{\chi}_1 - \boldsymbol{g}_1(\boldsymbol{x})(\boldsymbol{x}_{2,\text{ref}} - \boldsymbol{x}^0_{2,\text{ref}}) \tag{3.59}$$

The quadratic CLF for $\bar{\boldsymbol{z}}_1$ and its associated derivative are provided below [50].

$$\mathcal{V}_1(\bar{\boldsymbol{z}}_1) = 0.5\bar{\boldsymbol{z}}_1^T\bar{\boldsymbol{z}}_1 \tag{3.60}$$

$$\dot{\mathcal{V}}_1 = \bar{\boldsymbol{z}}_1^T\dot{\bar{\boldsymbol{z}}}_1 \tag{3.61}$$

In order to obtain the expression for the stabilising function $\boldsymbol{\alpha}_1$, it is necessary to take the first order time derivative of the CLF $\mathcal{V}_1(\bar{\boldsymbol{z}}_1)$ along the trajectories of the compensated error dynamics [50, 54]. The first expression in Eq. 3.62 can be simply obtained by substituting Eq. 3.59 into Eq. 3.61. The second expression is rewritten in such a way that $\boldsymbol{g}_1(\boldsymbol{x})\boldsymbol{x}^0_{2,\text{ref}}$ is both added and subtracted from $\dot{\mathcal{V}}_1$. The third expression alters $+\boldsymbol{g}_1(\boldsymbol{x})\boldsymbol{x}^0_{2,\text{ref}}$, by substituting the equation for $\boldsymbol{x}^0_{2,\text{ref}}$, as given in Eq. 3.55, into it. This yields the cancellation of the following terms: $\boldsymbol{g}_1(\boldsymbol{x})\boldsymbol{x}^0_{2,\text{ref}}$ and $\boldsymbol{g}_1(\boldsymbol{x})\boldsymbol{\alpha}_1$ (=$\boldsymbol{g}_1(\boldsymbol{x})\boldsymbol{x}_{2,\text{ref}}$). In the fourth expression the cancellation of the aforementioned terms was taken into account. Next to this the stabilising control law $\boldsymbol{\alpha}_1$ from Eq. 3.54 is being substituted, where after terms are being cancelled out as well. In particular the following terms did cancel out: $\boldsymbol{f}_1(\boldsymbol{x})$ and $\dot{\boldsymbol{x}}_{1,\text{ref}}$. In the fifth expression terms are being grouped with each other, such that the compensated tracking errors, as defined in Eq. 3.57 and Eq. 3.58, can be substituted.

$$\begin{aligned}
\dot{\mathcal{V}}_1 &= \bar{\boldsymbol{z}}_1^T\left[\boldsymbol{f}_1(\boldsymbol{x}) + \boldsymbol{g}_1(\boldsymbol{x})(\boldsymbol{x}_{2,\text{ref}} + \boldsymbol{z}_2) - \dot{\boldsymbol{x}}_{1,\text{ref}} + \boldsymbol{c}_1\boldsymbol{\chi}_1 - \boldsymbol{g}_1(\boldsymbol{x})(\boldsymbol{x}_{2,\text{ref}} - \boldsymbol{x}^0_{2,\text{ref}})\right] \\
&= \bar{\boldsymbol{z}}_1^T\left[\boldsymbol{f}_1(\boldsymbol{x}) + \boldsymbol{g}_1(\boldsymbol{x})(\boldsymbol{x}_{2,\text{ref}} + \boldsymbol{z}_2) - \dot{\boldsymbol{x}}_{1,\text{ref}} + \boldsymbol{c}_1\boldsymbol{\chi}_1 - \boldsymbol{g}_1(\boldsymbol{x})(\boldsymbol{x}_{2,\text{ref}} - \boldsymbol{x}^0_{2,\text{ref}}) + \boldsymbol{g}_1(\boldsymbol{x})\boldsymbol{x}^0_{2,\text{ref}} - \boldsymbol{g}_1(\boldsymbol{x})\boldsymbol{x}^0_{2,\text{ref}}\right] \\
&= \bar{\boldsymbol{z}}_1^T\left[\boldsymbol{f}_1(\boldsymbol{x}) + \boldsymbol{g}_1(\boldsymbol{x})(\boldsymbol{x}_{2,\text{ref}} + \boldsymbol{z}_2) - \dot{\boldsymbol{x}}_{1,\text{ref}} + \boldsymbol{c}_1\boldsymbol{\chi}_1 - \boldsymbol{g}_1(\boldsymbol{x})(\boldsymbol{x}_{2,\text{ref}} - \boldsymbol{x}^0_{2,\text{ref}}) + \boldsymbol{g}_1(\boldsymbol{x})(\boldsymbol{\alpha}_1 - \boldsymbol{\chi}_2) - \boldsymbol{g}_1(\boldsymbol{x})\boldsymbol{x}^0_{2,\text{ref}}\right] \\
&= \bar{\boldsymbol{z}}_1^T\left[\boldsymbol{g}_1(\boldsymbol{x})(\boldsymbol{x}_{2,\text{ref}} + \boldsymbol{z}_2) + \boldsymbol{c}_1\chi_1 - \boldsymbol{g}_1(\boldsymbol{x})(\boldsymbol{x}_{2,\text{ref}} - \boldsymbol{x}^0_{2,\text{ref}}) - \boldsymbol{g}_1(\boldsymbol{x})\boldsymbol{\chi}_2 - \boldsymbol{c}_1\boldsymbol{z}_1 - \boldsymbol{g}_1(\boldsymbol{x})\boldsymbol{x}^0_{2,\text{ref}}\right] \\
&= \bar{\boldsymbol{z}}_1^T\left[-\boldsymbol{c}_1\left(\boldsymbol{z}_1 - \boldsymbol{\chi}_1\right) + \boldsymbol{g}_1(\boldsymbol{x})\left(\boldsymbol{z}_2 - \boldsymbol{\chi}_2\right)\right] \\
&= -\bar{\boldsymbol{z}}_1^T\boldsymbol{c}_1\bar{\boldsymbol{z}}_1 + \bar{\boldsymbol{z}}_1^T\boldsymbol{g}_1(\boldsymbol{x})\bar{\boldsymbol{z}}_2, \qquad \text{with } \boldsymbol{c}_1 > 0
\end{aligned} \tag{3.62}$$

In the last expression the cross-term $\bar{\boldsymbol{z}}_1^T\boldsymbol{g}_1(\boldsymbol{x})\bar{\boldsymbol{z}}_2$ is observed, which implies that $\dot{\mathcal{V}}_1(\bar{\boldsymbol{z}}_1)$ is not negative definite for all combinations $\bar{\boldsymbol{z}}_1$ and $\bar{\boldsymbol{z}}_2$. The cross-term which will be removed when constructing a stabilising control law for the subsystem being heroically one higher [54]. The first term is negative definite only when $\boldsymbol{c}_1 > 0$.

Subsystem j = 2, ... ,n - 1 (intermediate subsystems)
For the intermediate subsystems a similar procedure will be followed as for the first subsystem. The intermediate subsystems can be written into the following general form

$$\dot{\boldsymbol{x}}_j = \boldsymbol{f}_j(\boldsymbol{x}) + \boldsymbol{g}_j(\boldsymbol{x})\boldsymbol{x}_{j+1}, \quad \text{with } j = 2, ..., n-1, \tag{3.63}$$

wherein $\boldsymbol{x}_{j+1}$ can be regarded as the virtual control input for subsystem j [54]. Furthermore the tracking error $\boldsymbol{z}_j$ for subsystem j can be defined as follows

$$\boldsymbol{z}_j = \boldsymbol{x}_j - \boldsymbol{\alpha}_{j-1}, \quad \text{with } j = 3, .., n, \tag{3.64}$$

with $\boldsymbol{\alpha}_{j-1}$ (= $\boldsymbol{x}_{j,\text{ref}}$) being the stabilising function for subsystem j [54]. The derivative of $\boldsymbol{z}_j$ is equal to

$$\begin{aligned}\dot{\boldsymbol{z}}_\text{j} = \dot{\boldsymbol{x}}_j - \dot{\boldsymbol{x}}_{j,\text{ref}} &= \boldsymbol{f}_\text{j}(\boldsymbol{x}) + \boldsymbol{g}_\text{j}(\boldsymbol{x})\boldsymbol{x}_{j+1} - \dot{\boldsymbol{x}}_{j,\text{ref}}, \quad \text{with } j = 3,..,n \\ &= \boldsymbol{f}_j(\boldsymbol{x}) + \boldsymbol{g}_j(\boldsymbol{x})(\boldsymbol{z}_{j+1} + \boldsymbol{\alpha}_j) - \dot{\boldsymbol{x}}_{j,\text{ref}},\end{aligned} \tag{3.65}$$

A command-filtered BS control strategy is being pursued, which requires the use of a new raw reference signal, namely $\boldsymbol{x}^0_{j+1,\text{ref}}$, which is defined in Eq. 3.66 [54].

$$\boldsymbol{x}^0_{j+1,\text{ref}} = \boldsymbol{\alpha}_{j-1} - \boldsymbol{\chi}_j, \quad \text{with } j = 3,...,n. \tag{3.66}$$

This signal shall be led through a command filter, which will provide the corresponding reference signals $\boldsymbol{x}_{j+1,\text{ref}}$ and the associated derivative $\dot{\boldsymbol{x}}_{j+1,\text{ref}}$ [54] . A stable linear filter shall be used to estimate the effect that the command filter has on the tracking error $\boldsymbol{z}_j$. The stable linear filter is provided in Eq. 3.67 [54].

$$\dot{\boldsymbol{\chi}}_j = \boldsymbol{g}_j(\boldsymbol{x})\left[\boldsymbol{x}_{j+1,\text{ref}} - \boldsymbol{x}^0_{j+1,\text{ref}}\right] - \boldsymbol{c}_j\boldsymbol{\chi}_j, \quad \text{with } j = 2,...,n-1 \tag{3.67}$$

The compensated tracking error $\bar{\boldsymbol{z}}_j$ is the difference between $\boldsymbol{z}_j$ and $\boldsymbol{\chi}_j$ and is given in Eq. 3.68 [54].

$$\bar{\boldsymbol{z}}_j = \boldsymbol{z}_j - \boldsymbol{\chi}_j, \quad \text{with } j = 3,...,n \tag{3.68}$$

The derivative of $\bar{\boldsymbol{z}}_j$ is given below in which $\dot{\boldsymbol{z}}_j$ and $\dot{\boldsymbol{\chi}}_j$ from Eq. 3.65 and Eq. 3.67 have been used.

$$\begin{aligned}\dot{\bar{\boldsymbol{z}}}_j &= \dot{\boldsymbol{z}}_j - \dot{\boldsymbol{\chi}}_j, \quad \text{with } j = 2,..,n-1 \\ &= \boldsymbol{f}_\text{j}(\boldsymbol{x}) + \boldsymbol{g}_j(\boldsymbol{x})\left(\boldsymbol{x}_{j+1,\text{ref}} + \boldsymbol{z}_{j+1}\right) - \dot{\boldsymbol{x}}_{j,\text{ref}} + \boldsymbol{c}_j\boldsymbol{\chi}_j - \boldsymbol{g}_j(x)\left(\boldsymbol{x}_{j+1,\text{ref}} - \boldsymbol{x}^0_{j+1,\text{ref}}\right)\end{aligned} \tag{3.69}$$

The CLF from subsystem j will be augmented with the quadratic CLF from subsystem $j-1$, yielding the expression provided below [54] .

$$\mathcal{V}_j(\boldsymbol{z}_1, \bar{\boldsymbol{z}}_j) = \mathcal{V}_1(\bar{\boldsymbol{z}}_1) + \sum_{k=1}^{j} 0.5\bar{\boldsymbol{z}}_k^T\bar{\boldsymbol{z}}_k, \qquad \text{with } j = 2,...,n-1. \tag{3.70}$$

Next to this, it is deemed necessary to determine CLF derivative, which was found to be equal to the following

$$\dot{\mathcal{V}}_j = \dot{\mathcal{V}}_1 + \sum_{k=1}^{j} \dot{\bar{\boldsymbol{z}}}_k^T\dot{\bar{\boldsymbol{z}}}_k, \qquad \text{with } j = 2,...,n-1. \tag{3.71}$$

In order to obtain the expression for the stabilising function $\boldsymbol{\alpha}_j$, it is necessary to take the first order derivative of the CLF $\mathcal{V}_j(\bar{\boldsymbol{z}}_j)$ along the trajectories of the compensated tracking errors of subsystem j given in Eq. 3.69. The expression for the CLF derivative $\dot{\mathcal{V}}_j$ is provided in Eq. 3.72 [54].

$$\begin{aligned}\dot{\mathcal{V}}_j = \mathcal{V}_1(\bar{\boldsymbol{z}}_1) + \sum_{\text{k=2}}^{\text{j}} \bar{\boldsymbol{z}}_k\Big[\boldsymbol{f}_k(\boldsymbol{x}) + \boldsymbol{g}_k(\boldsymbol{x})(x_{k+1,\text{ref}} + \boldsymbol{z}_{k+1}) - \dot{\boldsymbol{x}}_{k,\text{ref}} + \boldsymbol{c}_k\boldsymbol{\chi}_k - \boldsymbol{g}_k(\boldsymbol{x})(\boldsymbol{x})(\boldsymbol{x}_{k+1,\text{ref}} - \boldsymbol{x}^0_{k+1,\text{ref}})\Big] \\ \text{with } j = 2,..,n-1\end{aligned} \tag{3.72}$$

The expression from Eq. 3.72 shall be extended in such a way that $\boldsymbol{g}_k(\boldsymbol{x})\boldsymbol{x}^0_{k+1,\text{ref}}$ is both added and subtracted from it, which is provided in Eq. 3.73. The second expression from Eq. 3.73 alters $+\boldsymbol{g}_k(\boldsymbol{x})\boldsymbol{x}^0_{k+1,\text{ref}}$, by substituting the equation for $\boldsymbol{x}^0_{k+1,\text{ref}}$, as given in Eq. 3.66, into it. This yields cancellation of $\boldsymbol{g}_k(\boldsymbol{x})x^0_{k+1,\text{ref}}$ and $\boldsymbol{g}_k(\boldsymbol{x})\boldsymbol{\alpha}_k$ (=$\boldsymbol{g}_k(\boldsymbol{x})_{\text{k+1,ref}}$), which can be observed in the fourth expression. The stabilising control law can be identified from the fifth expression

$$\begin{aligned}\dot{\mathcal{V}}_j &= \mathcal{V}_1(\bar{\boldsymbol{z}}_1) + \sum_{k=2}^{j} \bar{\boldsymbol{z}}_k \Big[\boldsymbol{f}_k(\boldsymbol{x}) + \boldsymbol{g}_{\mathrm{k}}(\boldsymbol{x})(\boldsymbol{x}_{k+1,\mathrm{ref}} + \boldsymbol{z}_{k+1}) - \dot{\boldsymbol{x}}_{k,\mathrm{ref}} + \boldsymbol{c}_k \boldsymbol{\chi}_k - \boldsymbol{g}_k(\boldsymbol{x})(\boldsymbol{x}_{k+1,\mathrm{ref}} - \boldsymbol{x}^0_{k+1,\mathrm{ref}}) \\ &\qquad + \boldsymbol{g}_{\mathrm{k}}(\boldsymbol{x})\boldsymbol{x}^0_{k+1,\mathrm{ref}} - \boldsymbol{g}_k(\boldsymbol{x})\boldsymbol{x}^0_{k+1,\mathrm{ref}} \Big] \\ &= \mathcal{V}_1(\bar{\boldsymbol{z}}_1) + \sum_{k=2}^{j} \bar{\boldsymbol{z}}_k \Big[\boldsymbol{f}_k(\boldsymbol{x}) + \boldsymbol{g}_k(\boldsymbol{x})(\boldsymbol{x}_{k+1,\mathrm{ref}} + \boldsymbol{z}_{k+1}) - \dot{\boldsymbol{x}}_{k,\mathrm{ref}} + \boldsymbol{c}_k \boldsymbol{\chi}_k - \boldsymbol{g}_k(\boldsymbol{x})(\boldsymbol{x}_{k+1,\mathrm{ref}} - \boldsymbol{x}^0_{k+1,\mathrm{ref}}) \\ &\qquad + \boldsymbol{g}_k(\boldsymbol{x})(\boldsymbol{\alpha}_k - \boldsymbol{\chi}_{k+1}) - \boldsymbol{g}_k \boldsymbol{x}^0_{k+1,\mathrm{ref}} \Big] \\ &= \mathcal{V}_1(\bar{\boldsymbol{z}}_1) + \sum_{k=2}^{j} \bar{\boldsymbol{z}}_k \Big[\boldsymbol{f}_k(\boldsymbol{x}) + \boldsymbol{g}_k(\boldsymbol{x})(\boldsymbol{x}_{k+1,\mathrm{ref}} + \boldsymbol{z}_{k+1}) - \dot{\boldsymbol{x}}_{k,\mathrm{ref}} + \boldsymbol{c}_k \boldsymbol{\chi}_k - \boldsymbol{g}_k(\boldsymbol{x})\boldsymbol{\chi}_{k+1} \Big], \quad \text{with } j = 2,..,n-1\end{aligned} \tag{3.73}$$

In order to render Eq. 3.73 negative definite along the compensated error dynamics the following stabilising control law $\boldsymbol{\alpha}_j$ needs to be incorporated

$$\boldsymbol{\alpha}_j = \boldsymbol{g}_j^{-1}(\boldsymbol{x}) \big[-\boldsymbol{f}_j(\boldsymbol{x}) + \dot{\boldsymbol{x}}_{j,\mathrm{ref}} - \boldsymbol{c}_j \boldsymbol{z}_j - \bar{\boldsymbol{z}}^T_{j-1} \boldsymbol{g}_{j-1} \big], \quad \text{for } \boldsymbol{c}_{\mathrm{j}} > 0 \text{ with } j = 2,...,n-1. \tag{3.74}$$

Substitution of Eq. 3.74 into the last expression of Eq. 3.73 does yield the first expression of Eq. 3.75 [54]. Inclusion of the stabilising control law does cancel out $\boldsymbol{f}_k(\boldsymbol{x})$ and $\dot{\boldsymbol{x}}_{k,\mathrm{ref}}$, which can be observed from the second expression of Eq. 3.75. In the second expression terms are also being grouped with each other, such that the compensated tracking errors, as defined in Eq. 3.68 can be substituted. In the third expression, substitution of the compensated tracking errors is shown. From the last expression it can be seen that $\dot{\bar{\mathcal{V}}}_j$ includes a cross-term, namely $\bar{\boldsymbol{z}}^T_{n-1} \boldsymbol{g}_{n-1}(\boldsymbol{x}) \bar{\boldsymbol{z}}_{n-1}$, therefore $\dot{V}_j$ is not negative definite for all values of $\bar{z}_{\mathrm{k}}$ and $\bar{z}_{\text{k-1}}$ [54] .

$$\begin{aligned}\dot{\mathcal{V}}_j &= \mathcal{V}_1(\bar{\boldsymbol{z}}_1) + \sum_{k=2}^{j} \bar{\boldsymbol{z}}_k \Big[\boldsymbol{f}_k(\boldsymbol{x}) + \boldsymbol{g}_k(\boldsymbol{x})(\boldsymbol{g}_k^{-1}(\boldsymbol{x}) \big[-\boldsymbol{f}_k(\boldsymbol{x}) + \dot{\boldsymbol{x}}_{k,\mathrm{ref}} - \boldsymbol{c}_k \boldsymbol{z}_k - \bar{\boldsymbol{z}}_{k-1} \boldsymbol{g}_{k-1}(\boldsymbol{x}) \big] + \boldsymbol{z}_{k+1}) \\ &\qquad - \dot{\boldsymbol{x}}_{k,\mathrm{ref}} + \boldsymbol{c}_k \boldsymbol{\chi}_k - \boldsymbol{g}_k(\boldsymbol{x})\boldsymbol{\chi}_{k+1} \Big] \\ &= \mathcal{V}_1(\bar{\boldsymbol{z}}_1) + \sum_{k=2}^{j} \bar{\boldsymbol{z}}_k \Big[\boldsymbol{g}_k(\boldsymbol{x})(\boldsymbol{z}_{k+1} - \boldsymbol{\chi}_{k+1}) - \boldsymbol{c}_k(\boldsymbol{z}_k - \boldsymbol{\chi}_k) - \bar{\boldsymbol{z}}_{k-1} \boldsymbol{g}_{k-1} \Big] \\ &= \mathcal{V}_1(\bar{\boldsymbol{z}}_1) + \sum_{k=2}^{j} \bar{\boldsymbol{z}}_k \Big[\boldsymbol{g}_k(\boldsymbol{x}) \bar{\boldsymbol{z}}_{k+1} - \boldsymbol{c}_k \bar{\boldsymbol{z}}_k - \bar{\boldsymbol{z}}_{k-1} \boldsymbol{g}_{k-1} \Big] \\ &= \sum_{k=1}^{j} -\boldsymbol{c}_k \bar{\boldsymbol{z}}_k^2 - \bar{\boldsymbol{z}}_k g_{k-1} \bar{\boldsymbol{z}}_{k+1}, \quad \text{with } j = 2,..,n-1\end{aligned} \tag{3.75}$$

The cross-term $\bar{\boldsymbol{z}}^T_{n-1} \boldsymbol{g}_{n-1}(\boldsymbol{x}) \bar{\boldsymbol{z}}_{n-1}$ shall be removed during the derivation of the last stabilising control law. Derivation of the final stabilising control law shall be considered here after.

Subsystem j = n (last subsystems)
To complete the derivation of CFBS it is deemed necessary to end with the subsystem which is governed by the physical control input **u**. For the last subsystems a similar procedure will be followed as for the previous subsystem. The last subsystem can be written as

$$\dot{\boldsymbol{x}}_{\mathrm{n}} = \boldsymbol{f}_n(\boldsymbol{x}) + \boldsymbol{g}_n(\boldsymbol{x}) \boldsymbol{u}, \tag{3.76}$$

where $\boldsymbol{u}$ can be regarded as the physical control input [54] . The tracking error for this subsystem is equal to

$$\boldsymbol{z}_{\mathrm{n}} = \boldsymbol{x}_{\mathrm{n}} - \boldsymbol{x}_{n,\mathrm{ref}}, \tag{3.77}$$

with $\boldsymbol{x}_{n,\mathrm{ref}}$ being the reference signal [54]. The tracking error derivative $\boldsymbol{z}_n$ has been defined in Eq. 3.78.

$$\begin{aligned}\dot{\boldsymbol{z}}_n &= \dot{\boldsymbol{x}}_n - \dot{\boldsymbol{x}}_{n,\mathrm{ref}} \\ &= \boldsymbol{f}_n(\boldsymbol{x}) + \boldsymbol{g}_n(\boldsymbol{x}) \boldsymbol{u} - \dot{\boldsymbol{x}}_{n,\mathrm{ref}}\end{aligned} \tag{3.78}$$

A command-filtered BS control strategy is being pursued, which requires the use of a new raw reference signal, namely $\boldsymbol{u}^0$, which is defined in Eq. 3.79 [54].

$$\boldsymbol{u}^0 = \boldsymbol{u} - \boldsymbol{\chi}_n. \tag{3.79}$$

This signal shall be led through a command filter, which will provide the corresponding reference signals $\boldsymbol{u}$ and the associated derivative $\dot{\boldsymbol{u}}$. A stable linear filter shall be used to estimate the effect that the command filter has on the tracking error $\boldsymbol{z}_n$. The stable linear is given below [54].

$$\dot{\boldsymbol{\chi}}_n = \boldsymbol{g}_n(\boldsymbol{x})\big[\boldsymbol{u} - \boldsymbol{u}^0\big] - \boldsymbol{c}_n\boldsymbol{\chi}_n \tag{3.80}$$

In addition to this the compensated tracking error $\bar{\boldsymbol{z}}_n$ can be defined as

$$\bar{\boldsymbol{z}}_n = \boldsymbol{z}_n - \boldsymbol{\chi}_n. \tag{3.81}$$

The derivative of $\bar{\boldsymbol{z}}_n$ is given below in which $\dot{\boldsymbol{z}}_n$ and $\dot{\boldsymbol{\chi}}_n$ from Eq. 3.78 and 3.81 respectively have been used.

$$\begin{aligned}\dot{\bar{\boldsymbol{z}}}_n &= \dot{\boldsymbol{z}}_n - \dot{\boldsymbol{\chi}}_n \\ &= \boldsymbol{f}_n(\boldsymbol{x}) + \boldsymbol{g}_n(\boldsymbol{x})\boldsymbol{u} - \dot{\boldsymbol{x}}_{n,\mathrm{ref}} + \boldsymbol{c}_n\boldsymbol{\chi}_n - \boldsymbol{g}_n(\boldsymbol{x})\big(\boldsymbol{u} - \boldsymbol{u}^0\big)\end{aligned} \tag{3.82}$$

The CLF from subsystems $n-1$ will be augmented with the quadratic CLF from subsystem n, yielding Eq. 3.83 [54].

$$\bar{\mathcal{V}}_n(\boldsymbol{z}) = \sum_{k=1}^{n} 0.5\bar{\boldsymbol{z}}_k^T\bar{\boldsymbol{z}}_k = \mathcal{V}_{n-1}(\bar{\boldsymbol{z}}_{n-1}) + 0.5\bar{\boldsymbol{z}}_n^T\bar{\boldsymbol{z}}_n \tag{3.83}$$

Next to this it is deemed necessary to determine CLF derivative, which was found to be equal to the expression given below.

$$\dot{\mathcal{V}}_n = \dot{\mathcal{V}}_{n-1} + \bar{\boldsymbol{z}}_n^T\dot{\bar{\boldsymbol{z}}}_n \tag{3.84}$$

Substituting the derivative for tracking error $\boldsymbol{z}_n$ into the derivative expression for the CLF does yield the first expression from Eq. 3.85. The second expression was obtained by cancelling out the $\boldsymbol{u}$-term.

$$\begin{aligned}\dot{\mathcal{V}}_n &= \sum_{k=1}^{n-1} -\bar{\boldsymbol{z}}_k^T\boldsymbol{c}_k\bar{\boldsymbol{z}}_k + \bar{\boldsymbol{z}}_{n-1}^T\bar{\boldsymbol{g}}_{n-1}(\boldsymbol{x})\bar{\boldsymbol{z}}_n + \bar{\boldsymbol{z}}_n^T\big[\boldsymbol{f}_n(\boldsymbol{x}) + \boldsymbol{g}_n(\boldsymbol{x})\boldsymbol{u} - \dot{\boldsymbol{x}}_{n,\mathrm{ref}} + \boldsymbol{c}_n\boldsymbol{\chi}_n - \boldsymbol{g}_n(\boldsymbol{x})\big(\boldsymbol{u} - \boldsymbol{u}^0\big)\big] \\ &= \sum_{k=1}^{n-1} -\bar{\boldsymbol{z}}_k^T\boldsymbol{c}_k\bar{\boldsymbol{z}}_k + \bar{\boldsymbol{z}}_{n-1}^T\bar{\boldsymbol{g}}_{n-1}(\boldsymbol{x})\bar{\boldsymbol{z}}_n + \bar{\boldsymbol{z}}_n^T\big[\boldsymbol{f}_n(\boldsymbol{x}) + \boldsymbol{g}_n(\boldsymbol{x})\boldsymbol{u}^0 - \dot{\boldsymbol{x}}_{n,\mathrm{ref}} + \boldsymbol{c}_n\boldsymbol{\chi}_n\big]\end{aligned} \tag{3.85}$$

In order to render the CLF derivative of negative definite from Eq. 3.85, the stabilising control law must be equal to the expression in Eq. 3.86 [54].

$$\boldsymbol{u}^0 = \boldsymbol{g}_n^{-1}(\boldsymbol{x})\left[\dot{\boldsymbol{x}}_{n,\mathrm{ref}} - \boldsymbol{c}_n\boldsymbol{z}_n - \boldsymbol{f}_n(\boldsymbol{x}) - \boldsymbol{g}_{n-1}(\boldsymbol{x})\bar{\boldsymbol{z}}_{n-1}\right] \tag{3.86}$$

Substitution of the stabilising control law from Eq. 3.86 into the CLF derivative from Eq. 3.85 does yield the first expression in Eq. 3.87. The second expression is obtained by cancellation of $\bar{\boldsymbol{z}}_{n-1}^T\bar{\boldsymbol{g}}_{n-1}(\boldsymbol{x})\bar{\boldsymbol{z}}_n$. The last expression is obtained by realising that $\bar{\boldsymbol{z}}_n$ from Eq. 3.81 explicitly appears in it.

$$\begin{aligned}\dot{\mathcal{V}}_n &= \sum_{k=1}^{n-1} -\bar{\boldsymbol{z}}_k^T\boldsymbol{c}_k\bar{\boldsymbol{z}}_k + \bar{\boldsymbol{z}}_{n-1}^T\bar{\boldsymbol{g}}_{n-1}(\boldsymbol{x})\bar{\boldsymbol{z}}_n + \bar{\boldsymbol{z}}_n^T\big[-\boldsymbol{c}_n\boldsymbol{z}_n + \boldsymbol{c}_n\boldsymbol{\chi}_n - \boldsymbol{g}_{n-1}(\boldsymbol{x})\bar{\boldsymbol{z}}_{n-1}\big] \\ &= \sum_{k=1}^{n-1} -\bar{\boldsymbol{z}}_k^T\boldsymbol{c}_k\bar{\boldsymbol{z}}_k + \bar{\boldsymbol{z}}_n^T\big[-\boldsymbol{c}_n\boldsymbol{z}_n + \boldsymbol{c}_n\boldsymbol{\chi}_n\big] \\ &= \sum_{k=1}^{n} -\bar{\boldsymbol{z}}_k^T\boldsymbol{c}_k\bar{\boldsymbol{z}}_k\end{aligned} \tag{3.87}$$

In accordance with the theorem of LaSalle-Yoshizawa the equilibrium $\bar{\boldsymbol{z}} = \boldsymbol{0}$ can be considered globally uniformly asymptotically stable [50, 54]. CFBS can assure desirable properties for $\bar{\boldsymbol{z}}$, but not for $\boldsymbol{z}$ [54]. In [54] it was addressed that convergence of $\boldsymbol{z}$ can still be assured in the absence of physical limitations, that is without limitations on the commanded states and control inputs. CF limits will come into effect when aggressive manoeuvres are being executed. Without command filters, CFBS is still an attractive control strategy because the analytical determination of virtual control derivatives is not required.

3.3.2. Command filters for imposing physical limitations

Augmenting recursive BS with command filters enables to put *bandwidth, magnitude* and *rate constrains* on *(virtual) control inputs* [54]. CFBS incorporates a transformation wherein the raw reference signal $\boldsymbol{x}^0_{j,\text{ref}}$ is transformed to $\boldsymbol{x}_{j,\text{ref}}$ and its time derivative $\dot{\boldsymbol{x}}_{j,\text{ref}}$ in which magnitude, rate and bandwidth limitations are taken into account [54]. Various types of filters can be used to impose the limitations on $\boldsymbol{x}^0_{j,\text{ref}}$. The most commonly used filters are first or second order. Information about other types of filters can be found in [15].

The first filter to be considered is the first-order low-pass filter. This particular type of filter is associated with bandwidth ω_n and unity low-frequency gain ζ_n. The filter is provided in Eq. 3.88 [54].

$$\dot{\boldsymbol{x}}_{j,\text{ref}} = \boldsymbol{S}_{\text{Rat}}\left(\left\{\boldsymbol{S}_{\text{Mag}}\left[\boldsymbol{x}^0_{j,\text{ref}}\right] - \boldsymbol{x}_{j,\text{ref}}\right\}\omega_{\text{n}}\right), \quad \text{with initial condition} \quad \boldsymbol{x}_{j,\text{ref}}(0) = \boldsymbol{\alpha}_1\left(z_{j-1}(0), \boldsymbol{x}_{j-1,\text{ref}}(0)\right). \tag{3.88}$$

The magnitude and rate limitations for the first order filter are defined in Eq. 3.89 [54].

$$\boldsymbol{S}_{\text{Mag}}\left[\boldsymbol{x}^0_{j,\text{ref}}\right] = \begin{cases} \boldsymbol{M} & \text{if} \quad \boldsymbol{x}^0_{j,\text{ref}} \geq \boldsymbol{M} \\ \boldsymbol{x}^0_{j,\text{ref}} & \text{if} \quad |\boldsymbol{x}^0_{j,\text{ref}}| < \boldsymbol{M} \\ -\boldsymbol{M} & \text{if} \quad \boldsymbol{x}^0_{j,\text{ref}} \leq \boldsymbol{M} \end{cases} \quad \text{and} \quad \boldsymbol{S}_{\text{Rat}}\left[\dot{\boldsymbol{x}}^0_{j,\text{ref}}\right] = \begin{cases} \boldsymbol{R} & \text{if} \quad \dot{\boldsymbol{x}}^0_{j,\text{ref}} \geq \boldsymbol{R} \\ \dot{\boldsymbol{x}}^0_{j,\text{ref}} & \text{if} \quad |\dot{\boldsymbol{x}}^0_{j,\text{ref}}| < \boldsymbol{R} \\ -\boldsymbol{R} & \text{if} \quad \dot{\boldsymbol{x}}^0_{j,\text{ref}} \leq \boldsymbol{R} \end{cases} \tag{3.89}$$

The first-order wash-out filter is desirable, because of its simplicity. Combining two first-order filters enables to create a second-order filter. A second-order filter does suppress the noise more than a first-order filter, however there will be an increase in time-delay between input and output of the command-filter [54]. The expression of the second-order filter is given in Eq. 3.90 [54].

$$\begin{aligned} &\begin{bmatrix} \dot{\boldsymbol{x}}_{j,\text{ref}} \\ \ddot{\boldsymbol{x}}_{j,\text{ref}} \end{bmatrix} = \begin{bmatrix} \dot{x}_{\text{j,ref}} \\ 2\zeta\omega_n\left(\boldsymbol{S}_{\text{Rat}}\left\{\frac{\omega_n^2}{2\zeta\omega_n}\left[\boldsymbol{S}_{\text{Mag}}\left(\boldsymbol{x}^0_{j,\text{ref}}\right) - \boldsymbol{x}_{j,\text{ref}}\right]\right\} - \dot{\boldsymbol{x}}_{j,\text{ref}}\right) \end{bmatrix}, \\ &\text{with initial conditions} \quad \begin{matrix} \boldsymbol{x}_{j,\text{ref}}(0) = \boldsymbol{\alpha}_j\left(\boldsymbol{z}_{j-1}(0), \boldsymbol{x}_{j-1,\text{ref}}(0)\right) \\ \dot{\boldsymbol{x}}_{j,\text{ref}}(0) = 0 \end{matrix} \end{aligned} \tag{3.90}$$

The second-order CF is illustrated in Fig. 3.1, wherein the magnitude, rate and bandwidth can be observed.

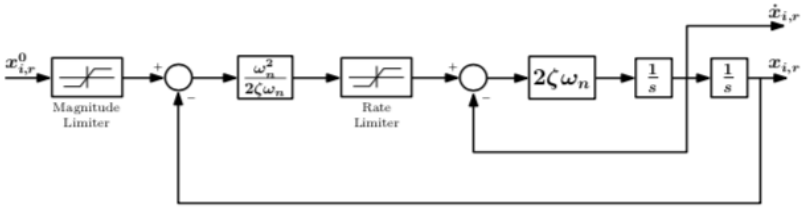

Figure 3.1: Second-order command filter capable of generating command signals $x_{\text{j,ref}}$ and $\dot{x}_{\text{j,ref}}$ while imposing bandwidth, magnitude and rate limitations on reference signal $x^0_{\text{j,ref}}$ [54].

Command filters can be incorporated without taking any magnitude or rate limitations into consideration, thus enabling computation of the command signal and its derivative only, which can be achieved by setting both S_{Mag} and S_{Rat} equal to one [54]. When it is desirable to have magnitude limitations, then ζ must be greater or equal to 1 in order to prevent $x_{j,\text{ref}}$ from overshooting the magnitude limitations ($\pm M$) [54]. The sampling rate t_{s} must be sufficiently large enough in order to capture the high frequency dynamics of a system [50, 54]. In other words t_s and ω_n need to be consistent with each other in order to avoid instability of the system [54]. When ω_{n} has been increased sufficiently large enough, then CFBS and BS will yield approximately similar results for the same tracking problem [15]. Command filters impose magnitude, rate and bandwidth limitations on the *commanded states* and not on the *actual states* of the system.

3.4. Command-Filtered incremental Backstepping

In this section IBS will be augmented by means of command-filters, thus making it command-filtered incremental backstepping (CFIBS). A sensor-based control approach will be pursued, wherein command-filters enable to provide magnitude, rate and bandwidth limitations on signals [54]. In addition to this, it also obviates the need to have the systems dynamics in lower triangular form. This means that a broader ranch of

system dynamics can be considered by constructing a *Lyapunov*-based control law [50, 54]. Next to this, it also does not require the analytical determination of the virtual control derivatives, which can be regarded as beneficial when considered large cascaded systems [54]. The cascaded system provided in Eq. 3.91 shall be considered for the derivation [55].

$$\dot{\boldsymbol{x}}_1 = \boldsymbol{f}_k(\boldsymbol{x}) + \boldsymbol{g}_k(\boldsymbol{x})\,\boldsymbol{x}_2 \tag{3.91}$$

$$\dot{\boldsymbol{x}}_2 = \boldsymbol{f}_d(\boldsymbol{x}) + \boldsymbol{g}_d(\boldsymbol{x})\,\boldsymbol{u}, \tag{3.92}$$

wherein $\boldsymbol{x}_{1,\text{ref}} \in \mathbb{R}^n$ and $\boldsymbol{x}_2 \in \mathbb{R}^n$ are the state vectors of the system and $\boldsymbol{u} \in \mathbb{R}^m$ the input vector [54].

Subsystem j=1 (furthest away from the physical control input)
For the derivation it is necessary to start at the subsystem furthest away from the physical control input $\boldsymbol{u}$. This subsystem is described with the differential equation from Eq. 3.91, wherein $\boldsymbol{x}_2$ is the virtual control input of this subsystem. The tracking of the first and second subsystem can be defined respectively as

$$\boldsymbol{z}_1 = \boldsymbol{x}_1 - \boldsymbol{x}_{1,\text{ref}} \tag{3.93}$$

$$\boldsymbol{z}_2 = \boldsymbol{x}_2 - \boldsymbol{\alpha}_1 \tag{3.94}$$

with $\boldsymbol{\alpha}_1$ ($= \boldsymbol{x}_{2,\text{ref}}$) being the stabilising function for the first subsystem [54]. The derivative of Eq. 3.93 can be written in terms of the system dynamics from Eq. 3.91 and the tracking error given in Eq. 3.94 the second subsystem. This does yield expression for $\dot{\boldsymbol{z}}_1$ given in Eq. 3.95 [54].

$$\begin{aligned}\dot{\boldsymbol{z}}_1 &= \dot{\boldsymbol{x}}_1 - \dot{\boldsymbol{x}}_{1,\text{ref}} \\ &= \boldsymbol{f}_k(\boldsymbol{x}) + \boldsymbol{g}_k(\boldsymbol{x})\left(\boldsymbol{z}_2 + \boldsymbol{\alpha}_1\right) - \dot{\boldsymbol{x}}_{1,\text{ref}}.\end{aligned} \tag{3.95}$$

The expression from Eq. 3.95 shall be used for the CLF derivative. A quadratic CLF shall be used because of its ease in determining sign definiteness. In order to obtain the expression for the stabilising control law $\boldsymbol{\alpha}_1$, it is necessary to take the first time derivative of the CLF along the trajectories of the error dynamics from Eq. 3.95. The quadratic CLF and its first order time derivative are given in Eq. 3.96 and Eq. 3.97 respectively [54].

$$\mathcal{V}_1(\boldsymbol{z}_1) = 0.5\boldsymbol{z}_1^T\boldsymbol{z}_1 \tag{3.96}$$

$$\dot{\mathcal{V}}_1 = \boldsymbol{z}_1^T\dot{\boldsymbol{z}}_1 = \boldsymbol{z}_1^T\left\{\boldsymbol{f}_k(\boldsymbol{x}) + g_k(\boldsymbol{x})\left(\boldsymbol{z}_2 + \boldsymbol{\alpha}_1\right) - \dot{\boldsymbol{x}}_{1,\text{ref}}\right\} \tag{3.97}$$

To make the derivative of the CLF from Eq. 3.97 negative definite, the stabilising function must be

$$\boldsymbol{\alpha}_1 = \boldsymbol{g}_k^{-1}(\boldsymbol{x})\left\{-\boldsymbol{f}_k(\boldsymbol{x}) + \dot{\boldsymbol{x}}_{1,\text{ ref}} - \boldsymbol{c}_1\boldsymbol{z}_1\right\}, \quad \text{for } \boldsymbol{c}_1 > 0 \tag{3.98}$$

The previous derivation is in accordance with the standard BS procedure. A command filtered approach is considered, wherein $\boldsymbol{\alpha}_1$ will not be used directly, but rather to define the following raw reference signal

$$\boldsymbol{x}^0_{2,\text{ ref}} = \boldsymbol{\alpha}_1 - \boldsymbol{\chi}_2, \tag{3.99}$$

which shall be led through a command filter, providing reference signals $\boldsymbol{x}_{2,\text{ref}}$ and $\dot{\boldsymbol{x}}_{2,\text{ref}}$ [54]. A stable linear filter shall be used to estimate the effect the command filter has on tracking error $\boldsymbol{z}_1$. The stable filter is defined in Eq. 3.100 [54].

$$\dot{\boldsymbol{\chi}}_1 = -\boldsymbol{c}_1\boldsymbol{\chi}_1 + \boldsymbol{g}_k(\boldsymbol{x})\left[\boldsymbol{x}_{2,\text{ref}} - \boldsymbol{x}^0_{2,\text{ref}}\right], \quad \text{with } \boldsymbol{\chi}_1(0) = 0. \tag{3.100}$$

Magnitude, rate and bandwidth constraints can be imposed on this filter, thus making intermediate control laws not unbounded [54]. It is necessary to introduce the compensated tracking error for the first and second subsystem, which are provided in Eq. 3.101 and Eq. 3.102 respectively [54].

$$\bar{\boldsymbol{z}}_1 = \boldsymbol{z}_1 - \boldsymbol{\chi}_1 \tag{3.101}$$

$$\bar{\boldsymbol{z}}_2 = \boldsymbol{z}_2 - \boldsymbol{\chi}_2 \tag{3.102}$$

In order to proceed further it is necessary to take the first order time derivative of $\bar{\boldsymbol{z}}_1$, which is defined below

$$\dot{\bar{\boldsymbol{z}}}_1 = \dot{\boldsymbol{z}}_1 - \dot{\boldsymbol{\chi}}_1 = \boldsymbol{f}_k(\boldsymbol{x}) + \boldsymbol{g}_k(\boldsymbol{x})\left(\boldsymbol{x}_{2,\text{ref}} + \boldsymbol{z}_2\right) - \dot{\boldsymbol{x}}_{1,\text{ref}} + \boldsymbol{c}_1\boldsymbol{\chi}_1 - \boldsymbol{g}_k(\boldsymbol{x})\left(\boldsymbol{x}_{2,\text{ref}} - \boldsymbol{x}^0_{2,\text{ref}}\right) \tag{3.103}$$

The quadratic CLF for $\bar{\boldsymbol{z}}_1$ and its associated derivative are given in Eq. 3.104 and Eq. 3.105 respectively [54].

$$\mathcal{V}_1(\bar{\boldsymbol{z}}_1) = \frac{1}{2}\bar{\boldsymbol{z}}_1^T\bar{\boldsymbol{z}}_1 \tag{3.104}$$

$$\mathcal{V}_1 = \bar{\boldsymbol{z}}_1^T\dot{\bar{\boldsymbol{z}}}_1 \tag{3.105}$$

In order to obtain the expression for the stabilising function $\boldsymbol{\alpha}_1$, it is necessary to take the first order time derivative of the CLF $\mathcal{V}_1(\bar{\boldsymbol{z}}_1)$ along the trajectories of the compensated error dynamics from Eq. 3.103. The first expression in Eq. 3.106 can be simply obtained by substituting Eq. 3.103 into Eq. 3.105. The second expression is rewritten in such a way that $\boldsymbol{g}_k(\boldsymbol{x})\boldsymbol{x}^0_{2,\text{ref}}$ is both added and subtracted from $\dot{\mathcal{V}}_1$. The third expression alters $+\boldsymbol{g}_k(\boldsymbol{x})\boldsymbol{x}^0_{2,\text{ref}}$, by substituting the equation for $\boldsymbol{x}^0_{2,\text{ref}}$, as given in Eq. 3.99, into it. This cancels out the following terms: $\boldsymbol{g}_k(\boldsymbol{x})\boldsymbol{x}^0_{2,\text{ref}}$ and $\boldsymbol{g}_k(\boldsymbol{x})\boldsymbol{\alpha}_1$ (=$\boldsymbol{g}_k(\boldsymbol{x})\boldsymbol{x}_{2,\text{ref}}$), which can be observed from the fourth expression. The stabilising control law $\boldsymbol{\alpha}_1$ from Eq. 3.98 is being substituted in the fifth expression where after terms cancel out as well, namely $\boldsymbol{f}_k(\boldsymbol{x})$ and $\dot{\boldsymbol{x}}_{1,\text{ref}}$. In the sixth expression terms are being grouped together such that the compensated tracking errors, as defined in Eq. 3.101 and Eq. 3.102, can be substituted into it, yielding the last expression [54].

$$\begin{aligned}
\dot{\mathcal{V}}_1 &= \bar{\boldsymbol{z}}_1^T\left[\boldsymbol{f}_k(\boldsymbol{x}) + \boldsymbol{g}_k(\boldsymbol{x})(\boldsymbol{x}_{2,\text{ref}} + \boldsymbol{z}_2) - \dot{\boldsymbol{x}}_{1,\text{ref}} + \boldsymbol{c}_1\boldsymbol{\chi}_1 - \boldsymbol{g}_k(\boldsymbol{x})(\boldsymbol{x}_{2,\text{ref}} - \boldsymbol{x}^0_{2,\text{ref}})\right] \\
&= \bar{\boldsymbol{z}}_1^T\left[\boldsymbol{f}_k(\boldsymbol{x}) + \boldsymbol{g}_k(\boldsymbol{x})(\boldsymbol{x}_{2,\text{ref}} + \boldsymbol{z}_2) - \dot{\boldsymbol{x}}_{1,\text{ref}} + \boldsymbol{c}_1\boldsymbol{\chi}_1 - \boldsymbol{g}_k(\boldsymbol{x})(\boldsymbol{x}_{2,\text{ref}} - \boldsymbol{x}^0_{2,\text{ref}}) + \boldsymbol{g}_k(\boldsymbol{x})\boldsymbol{x}^0_{2,\text{ref}} - \boldsymbol{g}_k(\boldsymbol{x})\boldsymbol{x}^0_{2,\text{ref}}\right] \\
&= \bar{\boldsymbol{z}}_1^T\left[\boldsymbol{f}_k(\boldsymbol{x}) + \boldsymbol{g}_k(\boldsymbol{x})(\boldsymbol{x}_{2,\text{ref}} + \boldsymbol{z}_2) - \dot{\boldsymbol{x}}_{1,\text{ref}} + \boldsymbol{c}_1\boldsymbol{\chi}_1 - \boldsymbol{g}_k(\boldsymbol{x})(\boldsymbol{x}_{2,\text{ref}} - \boldsymbol{x}^0_{2,\text{ref}}) + \boldsymbol{g}_k(\boldsymbol{x})(\boldsymbol{\alpha}_1 - \boldsymbol{\chi}_2) - \boldsymbol{g}_k(\boldsymbol{x})\boldsymbol{x}^0_{2,\text{ref}}\right] \\
&= \bar{\boldsymbol{z}}_1^T\left[\boldsymbol{f}_k(\boldsymbol{x}) + \boldsymbol{g}_k(\boldsymbol{x})(\boldsymbol{x}_{2,\text{ref}} + \boldsymbol{z}_2) - \dot{\boldsymbol{x}}_{1,\text{ref}} + \boldsymbol{c}_1\boldsymbol{\chi}_1 - \boldsymbol{g}_k(\boldsymbol{x})\boldsymbol{\chi}_2\right] \\
&= \bar{\boldsymbol{z}}_1^T\left[\boldsymbol{g}_k(\boldsymbol{x})(\boldsymbol{x}_{2,\text{ref}} + \boldsymbol{z}_2) + \boldsymbol{c}_1\chi_1 - \boldsymbol{g}_k(\boldsymbol{x})(\boldsymbol{x}_{2,\text{ref}} - \boldsymbol{x}^0_{2,\text{ref}}) - \boldsymbol{g}_k(\boldsymbol{x})\boldsymbol{\chi}_2 - \boldsymbol{c}_1\boldsymbol{z}_1 - \boldsymbol{g}_k(\boldsymbol{x})\boldsymbol{x}^0_{2,\text{ref}}\right] \\
&= \bar{\boldsymbol{z}}_1^T\left[-\boldsymbol{c}_1\big(\boldsymbol{z}_1 - \boldsymbol{\chi}_1\big) + \boldsymbol{g}_k(\boldsymbol{x})\big(\boldsymbol{z}_2 - \boldsymbol{\chi}_2\big)\right] \\
&= -\bar{\boldsymbol{z}}_1^T\boldsymbol{c}_1\bar{\boldsymbol{z}}_1 + \bar{\boldsymbol{z}}_1^T\boldsymbol{g}_k(\boldsymbol{x})\bar{\boldsymbol{z}}_2, \qquad \text{with } \boldsymbol{c}_1 > 0
\end{aligned} \tag{3.106}$$

In the last expression the cross-term $\bar{\boldsymbol{z}}_1^T\boldsymbol{g}_k(\boldsymbol{x})\bar{\boldsymbol{z}}_2$ is observed, which implies that $\dot{\mathcal{V}}_1(\bar{\boldsymbol{z}}_1)$ is not negative definite for all combinations $\bar{\boldsymbol{z}}_1$ and $\bar{\boldsymbol{z}}_2$. The cross-term which will be removed when constructing a stabilising control law for the subsystem being hierarchically one higher [54]. The first term is negative definite only when $\boldsymbol{c}_1 > 0$.

Subsystem j = n (last subsystems))

With the stabilising control law for the first subsystem being defined, it is deemed necessary to continue with the subsystem which is directly governed by the physical control input $\boldsymbol{u}$. This subsystem is described with the differential equation from Eq. 3.92. Furthermore the tracking error for the last subsystem was also provided in Eq. 3.94. This subsystem is characterised with (partially) unknown dynamics, hence the first-order *Taylor* series expansion shall be considered around the current solution $(\boldsymbol{x}_0, \boldsymbol{u}_0)$ at t_0 given below [55].

$$\dot{\boldsymbol{x}}_2 \approx \underbrace{\boldsymbol{f}_d(\boldsymbol{x}_0) + \boldsymbol{g}_d(\boldsymbol{x}_0\boldsymbol{u}_0)}_{\dot{\boldsymbol{x}}_{2,0}} + \underbrace{\frac{\partial}{\partial \boldsymbol{x}}\Big[\boldsymbol{f}_d(\boldsymbol{x}) + \boldsymbol{g}_d(\boldsymbol{x})\Big]\Big|_{\substack{\boldsymbol{x}=\boldsymbol{x}_0\\ \boldsymbol{u}=\boldsymbol{u}_0}}}_{\boldsymbol{f}_{d(\boldsymbol{x})}}\underbrace{\Big(\boldsymbol{x} - \boldsymbol{x}_0\Big)}_{\Delta\boldsymbol{x}} + \underbrace{\frac{\partial}{\partial \boldsymbol{u}}\Big[\boldsymbol{f}_d(\boldsymbol{x}) + \boldsymbol{g}_d(\boldsymbol{x})\Big]\Big|_{\substack{\boldsymbol{x}=\boldsymbol{x}_0\\ \boldsymbol{u}=\boldsymbol{u}_0}}}_{\boldsymbol{g}_d(\boldsymbol{x})}\underbrace{\Big(\boldsymbol{u} - \boldsymbol{u}_0\Big)}_{\Delta\boldsymbol{u}}, \tag{3.107}$$

wherein $\Delta\boldsymbol{x}$ and $\Delta\boldsymbol{u}$ are the incremental state and control vector respectively. Neglecting higher-order terms of the *Taylor* series expansion can be regarded as justified as these do not contribute significant to dynamics. This implies that the error of the first-order *Taylor* series approximation is in the order of $\mathcal{O}(t_s)$, which is acceptable for small time samples (t_s) [8, 47]. In order to make the control law less model-depended, the first-order *Taylor* series shall be further simplified by incorporating time-scale separation principle, which assumes that there is a natural time-scale separation between the controlled state and the state on which the control input has a direct effect [50, 54]. This implies that the increments $\Delta\boldsymbol{u}$ and $\Delta\dot{\boldsymbol{x}}$ are significantly greater than the state increment $\Delta\boldsymbol{x}$, therefore the latter can be neglected [1, 8, 45, 46, 54]. Based on this assumption, the incremental change in state vector $(\Delta\boldsymbol{x})$ can be regarded small, and can therefore be neglected. The system dynamics of the second subsystem can be rewritten into the expression given in Eq. 3.108 [54].

$$\dot{\boldsymbol{x}}_2 \cong \dot{\boldsymbol{x}}_{2,0} + \boldsymbol{g}_d(\boldsymbol{x}_0)\Delta\boldsymbol{u} \tag{3.108}$$

Next to this it is necessary to determine of derivative of $\boldsymbol{z}_2$, as this will be used in the CLF derivative. The expression for $\dot{\boldsymbol{z}}_2$ is equal to the following

$$\begin{aligned}\dot{\boldsymbol{z}}_2 &= \dot{\boldsymbol{x}}_2 - \dot{\boldsymbol{x}}_{2,\text{ref}} \\ &= \dot{\boldsymbol{x}}_{2,0} + \boldsymbol{g}_d(\boldsymbol{x}_0)\Delta\boldsymbol{u} - \dot{\boldsymbol{x}}_{2,\text{ref}}.\end{aligned} \tag{3.109}$$

A command-filtered BS control strategy is being pursued, which requires the use of a new raw reference signal, namely $\boldsymbol{u}^0$, which is defined in Eq. 3.110 [54].

$$\boldsymbol{u}^0 = \boldsymbol{u} - \boldsymbol{\chi}_2 \tag{3.110}$$

This signal shall be led through a command filter, which will provide the corresponding reference signals $\boldsymbol{u}$ and $\dot{\boldsymbol{u}}$. A stable linear filter shall be used to estimate the effect that the command filter has on the tracking error $\boldsymbol{z}_2$. This stable linear filter is defined in Eq. 3.111 [54].

$$\dot{\boldsymbol{\chi}}_2 = \boldsymbol{g}_d(\boldsymbol{x}_0)\left[\boldsymbol{u} - \boldsymbol{u}^0\right] - \boldsymbol{c}_2\boldsymbol{\chi}_2, \quad \text{with } \boldsymbol{\chi}_2(0) = 0. \tag{3.111}$$

Magnitude, rate and bandwidth constraints can be imposed on this filter, thus making intermediate control laws not unbounded [50]. The compensated tracking errors were previously defined in Eq. 3.101 and 3.102. Taking the first order time derivative of $\bar{\boldsymbol{z}}_2$ does yield

$$\dot{\bar{\boldsymbol{z}}}_2 = \dot{\boldsymbol{z}}_2 - \dot{\boldsymbol{\chi}}_2 = \dot{\boldsymbol{x}}_{2,0} + \boldsymbol{g}_d(\boldsymbol{x})_0\Delta\boldsymbol{u} - \dot{\boldsymbol{x}}_{2,\text{ref}} + \boldsymbol{c}_2\boldsymbol{\chi}_2 - \boldsymbol{g}_d(\boldsymbol{x})\left(\boldsymbol{u} - \boldsymbol{u}^0\right) \tag{3.112}$$

The quadratic CLF shall be augmented to penalise the error dynamics of the second subsystem. The expression for $\bar{\mathcal{V}}_2(\bar{\boldsymbol{z}}_1, \bar{\boldsymbol{z}}_2)$ and $\dot{\bar{\mathcal{V}}}_2$ are given in Eq. 3.113 and Eq. 3.114 respectively [54].

$$\bar{\mathcal{V}}_2(\bar{\boldsymbol{z}}_1, \bar{\boldsymbol{z}}_2) = \bar{\mathcal{V}}_1(\bar{\boldsymbol{z}}_1) + \frac{1}{2}\bar{\boldsymbol{z}}_1^T\bar{\boldsymbol{z}}_1 \tag{3.113}$$

$$\dot{\bar{\mathcal{V}}}_2 = \dot{\bar{\mathcal{V}}}_1 + \bar{\boldsymbol{z}}_2^T\dot{\bar{\boldsymbol{z}}}_2 \tag{3.114}$$

In order to obtain the expression for the stabilising function $\boldsymbol{u}$, it is necessary to take the first order derivative of the CLF $\bar{\mathcal{V}}_2$ along the trajectories of the compensated error dynamics from Eq. 3.112. The first expression in Eq. 3.115 can be simply obtained by substituting Eq. 3.112 into Eq. 3.114. The second expression is obtained by substituting $\boldsymbol{u} - \boldsymbol{u}_0$ for $\Delta\boldsymbol{u}$, which yields cancellation of $\boldsymbol{u}$.

$$\begin{aligned}\dot{\bar{\mathcal{V}}}_2 &= \dot{\bar{\mathcal{V}}}_1 + \bar{\boldsymbol{z}}_2^T\left[\dot{\boldsymbol{x}}_{2,0} + \boldsymbol{g}_d(\boldsymbol{x}_0)\Delta\boldsymbol{u} - \dot{\boldsymbol{x}}_{2,\text{ref}} + \boldsymbol{c}_2\boldsymbol{\chi}_2 - \boldsymbol{g}_d(\boldsymbol{x})\left(\boldsymbol{u} - \boldsymbol{u}^0\right)\right] \\ &= \dot{\bar{\mathcal{V}}}_1 + \bar{\boldsymbol{z}}_2^T\left[\dot{\boldsymbol{x}}_{2,0} + \boldsymbol{g}_d(\boldsymbol{x}_0)\left(\boldsymbol{u}^0 - \boldsymbol{u}_0\right) - \dot{\boldsymbol{x}}_{2,\text{ref}} + \boldsymbol{c}_2\boldsymbol{\chi}_2\right]\end{aligned} \tag{3.115}$$

In order to render Eq. 3.62 negative definite, the following stabilising control law needs to be selected

$$\boldsymbol{u}^0 = \boldsymbol{u}_0 + \boldsymbol{g}_d(\boldsymbol{x}_0)^{-1}\left[-\dot{\boldsymbol{x}}_{2,0} + \dot{\boldsymbol{x}}_{2,\text{ref}} - \boldsymbol{c}_2\boldsymbol{z}_2 - \boldsymbol{g}_k(\boldsymbol{x})\bar{\boldsymbol{z}}_1\right]. \tag{3.116}$$

Incorporating the stabilising control law form Eq. 3.116 does yield the first expression in Eq. 3.117, from which it can be observed that $\dot{\boldsymbol{x}}_{2,0}$ and $\dot{\boldsymbol{x}}_{2,\text{ref}}$ have cancelled out. From the second expression it can be observed that the cross-term $\bar{\boldsymbol{z}}_1^T\boldsymbol{g}_k(\boldsymbol{x})\bar{\boldsymbol{z}}_2$ has been cancelled out as well. In the third expression the grouped terms from the second expression were replaced by the compensated tracking error given in Eq. 3.102.

$$\begin{aligned}\dot{\bar{\mathcal{V}}}_2 &= -\bar{\boldsymbol{z}}_1^T\boldsymbol{c}_1\bar{\boldsymbol{z}}_1 + \bar{\boldsymbol{z}}_1^T\boldsymbol{g}_k(\boldsymbol{x})\bar{\boldsymbol{z}}_2 + \bar{\boldsymbol{z}}_1^T\left[-\boldsymbol{c}_2\left(\boldsymbol{z}_2 - \boldsymbol{\chi}_2\right) - \boldsymbol{g}_k(\boldsymbol{x})\bar{\boldsymbol{z}}_1\right] \\ &= -\bar{\boldsymbol{z}}_1^T\boldsymbol{c}_1\bar{\boldsymbol{z}}_1 + \bar{\boldsymbol{z}}_1^T\left[-\boldsymbol{c}_2\left(\boldsymbol{z}_2 - \boldsymbol{\chi}_1\right)\right] \\ &= -\bar{\boldsymbol{z}}_1^T\boldsymbol{c}_1\bar{\boldsymbol{z}}_1 - \bar{\boldsymbol{z}}_2^T\boldsymbol{c}_2\bar{\boldsymbol{z}}_2, \qquad \text{with } \boldsymbol{c}_1 > 0 \text{ and } \boldsymbol{c}_2 > 0.\end{aligned} \tag{3.117}$$

From Eq. 3.117 it can be observed that Eq. 3.116 does not depend on the analytical derivative of $\dot{\boldsymbol{\alpha}}_1$, but rather on $\boldsymbol{x}_{2,\text{ref}}$ and $\dot{\boldsymbol{x}}_{2,\text{ref}}$, which are the CF outputs. For sufficiently high update rate of the controller $\bar{\boldsymbol{z}}$ will go to $\mathbf{0}$ for sufficiently large amount of time [54]. Closed-loop stability can be assured without the inclusion of physical limitations, that is without constraints on intermediate signals, given that the controller update rate is sufficiently high enough [54]. The aforementioned even holds when there are uncertainties present in the control effectiveness matrix and/or system dynamics [54].

4

Control strategies for rotorcraft control

This chapter describes the various control strategies available for rotorcraft control with a main focus on the angular rate subsystem. This subsystem dictates to a large extent which control strategy should be used. In section 4.1 the main crux in control design of rotorcraft control will be outlined. There after, different control strategies will be considered, which could be used for establishing the stabilising control law for the angular rate subsystem. In section 4.2 the main discrepancies of the control strategies from section 4.1 will be considered. In section 4.3 a particular control strategy from section 4.1 will be considered in more detail.

4.1. Background information on rotorcraft control design

In this section background information is provided on rotorcraft control. The main focus will be on the angular rate subsystem, as it can be considered the main crux in control design for rotorcraft. It will be outlined that it is difficult to define a well-established IBS control law due to the violation of the IBS TSS condition. Moreover, information shall also be provided on the various control strategies that can be used for designing the angular rate subsystem.

4.1.1. Angular rate subsystem: crux in rotorcraft control design

The main crux in control design for rotorcraft control does find its roots in the angular rate subsystem. The angular rate dynamics of the rotorcraft does depend upon complex aerodynamics, therefore it is a natural choice to incorporate an IBS controller in which there is less model dependency required [8, 55]. This especially holds for the main rotor and therefore has primarily affect on the design of the stabilising control law for the cyclic control inputs. On the other hand, providing a stabilising control law for the yaw rate is less complicated, because the negligence of flapping and because it is mainly governed by tail rotor collective. When trying to establish an stabilising control law for the angular rate subsystem it is found that control-dependency is significantly less than state-dependency [55]. This can be considered a major problem when considering IBS (or INDI), because the TSS condition will be violated. In order to counteract this problem it would be deemed necessary to account for state-dependency, but that would make the IBS controller less robust to uncertainties in the model. The aforementioned specially holds for the main rotor, therefore establishing a stabilising control law for pitch rate, roll rate can be considered problematic. For example the expression for the angular accelerations $\dot{p}$ and $\dot{q}$ it is found that there is great dependency on the cyclic flapping angles (see Eq. 2.85, 2.86 and 2.113). Based on this it can be stated that flapping dynamics obstruct the design of an IBS controller, because of the TSS condition mentioned previously. On the other hand, when designing an attitude subsystem, the above mentioned issues will not occur. This because the expression from Eq. 2.114 could be used for establishing the attitude controller. Recursive BS could be sued for establishing the stabilising cantor law for the attitude subsystem. This shows that the main issue in control design is primarily due to the angular rate subsystem.

4.1.2. Advanced non-linear control methods for angular rate control

In order to design a *Lyapunov*-based controller for the rotorcraft under consideration, it is necessary to determine which control methods are available. This section does focus on various control methods and shortly touches upon the validity of these techniques. The methods discussed will primarily focus on the angular rate subsystem, which is of main concern for rotorcraft control design. Some of these control methods will

be elaborated on in sections here after. First, the *method of residualised dynamics* shall be considered, where after the *flapping angle equivalence* method will be touched upon. There after the *central finite difference method* will be introduced. Lastly, the *active flapping control method* will be outlined.

I The first method to be considered is the *method of residualised dynamics*, which was found to be a suitable method for establishing the stabilising control law for the angular rate subsystem [55]. The main objective using this control strategy is to establish an enhanced control effectiveness matrix for the angular rates p and q ($\boldsymbol{\omega}_{pq}$). The aforementioned angular rates shall be considered for the discussion. The method consists of setting the derivatives related to the fast modes equal to zero, which implies that these states are continuously at steady state [48]. This could be considered for all rotor dynamics, but for the sake of brevity only flapping dynamics shall be considered. When considering a BF rotorcraft model with second-order flapping dynamics defined with respect to the shaft plane (SP) (e.g. Eq. 2.26), this would mean that $\dot{\boldsymbol{\beta}}_{SP}$ and $\ddot{\boldsymbol{\beta}}_{SP}$ are set to $\mathbf{0}$, leaving only steady-state flapping $\boldsymbol{\beta}_{SP,ss}$. The second-order differential equation for flapping in matrix form can be written as

$$\ddot{\boldsymbol{\beta}}_{SP} = \boldsymbol{F}_{\dot{\beta}_{SP},X_{\text{res}}}\boldsymbol{X}_{\text{res}} + \boldsymbol{F}_{\dot{\beta}_{SP},\beta_{SP}}\boldsymbol{\beta}_{SP} + \boldsymbol{F}_{\dot{\beta}_{SP},\dot{\beta}_{SP}}\dot{\boldsymbol{\beta}}_{SP} + \boldsymbol{H}_{\dot{\beta}_{SP}}\boldsymbol{U}, \tag{4.1}$$

wherein $\boldsymbol{X}_{\text{res}} = \left[\boldsymbol{\omega}^T, ...\right]^T$ is the residualised state vector, which contains all states except for the flapping states. Setting $\ddot{\boldsymbol{\beta}}_{SP} = \dot{\boldsymbol{\beta}}_{SP} = 0$ and rewriting Eq. 4.1 yields

$$\boldsymbol{\beta}_{SP,ss} = -\boldsymbol{F}^{-1}_{\dot{\beta}_{SP},\beta_{SP}}\boldsymbol{F}_{\dot{\beta}_{SP},X_{\text{res}}}\boldsymbol{X}_{\text{res}} - \boldsymbol{F}^{-1}_{\dot{\beta}_{SP},\beta_{SP}}\boldsymbol{H}_{\dot{\beta}_{SP}}\boldsymbol{U}. \tag{4.2}$$

This means that the residualised dynamics using the previous expression can be written as follows

$$\dot{\boldsymbol{X}}_{\text{res}} = \underbrace{\left\{\boldsymbol{F}_{X_{\text{res}},X_{\text{res}}} - \boldsymbol{F}_{X_{\text{res}},\beta_{SP}}\boldsymbol{F}^{-1}_{\dot{\beta}_{SP},\beta_{SP}}\boldsymbol{F}_{\dot{\beta}_{SP},X_{\text{res}}}\right\}}_{\text{Adjusted system matrix}}\boldsymbol{X}_{\text{res}} + \underbrace{\left\{\boldsymbol{H}_{\text{X}_{\text{res}}} - \boldsymbol{F}_{\text{X}_{\text{res}},\beta_{SP}}\boldsymbol{F}^{-1}_{\dot{\beta}_{SP},\beta_{SP}}\boldsymbol{H}_{\dot{\beta}_{SP}}\right\}}_{=\boldsymbol{G}_R}\boldsymbol{U}. \tag{4.3}$$

Using the residualised rotorcraft dynamics from Eq. 4.3 it is possible to have an enhanced control effectiveness. This solves the problem of having a too large body-flag coupling and too small control-depended term for the angular rates ($\boldsymbol{F}_{\omega_{pq},\beta_{SP}} >> \boldsymbol{H}_{\omega_{pq}}$). The aforementioned would not allow for IBS as state-dependency was simply greater than control-dependency and thus violating the TSS condition [54]. The IBS TSS condition for the original and residualised model are provided in Eq. 4.4 and Eq. 4.5 respectively. The condition from Eq. 4.4 would be violated, whereas the condition from Eq. 4.5 would be less violated or not violated at all.

$$\boldsymbol{G}_{\omega_{pq}}\Delta\boldsymbol{U} >> \boldsymbol{F}_{\omega_{pq},\beta_{SP}}\Delta\boldsymbol{\beta}_{SP} + \boldsymbol{F}_{\omega_{pq},\omega_{pq}}\Delta\boldsymbol{\omega}_{pq} + ... \tag{4.4}$$

$$\boldsymbol{G}_{\omega_{pq,R}}\Delta\boldsymbol{U} >> 0\cdot\Delta\boldsymbol{\beta}_{SP} + \left(\boldsymbol{F}_{\omega_{pq},\omega_{pq}} - \boldsymbol{F}_{\omega_{pq},\beta_{SP}}\boldsymbol{F}^{-1}_{\dot{\beta}_{SP},\beta_{SP}}\boldsymbol{F}_{\dot{\beta}_{SP},X_{\text{res}}}\right)\Delta\boldsymbol{\omega}_{pq} + ... \tag{4.5}$$

It should be noted that $\boldsymbol{G}_{\omega_{pq,R}}$ can be identified as the residualised control effectiveness for pitch and roll rate only. The validity of the *method of residualised dynamics* greatly depends on whether the *idealised* rotorcraft model (= *residualised model*) and *actual* rotorcraft model are approximately the same. This can be assessed by considering the modes of motion or open-loop frequency response of both models. When the difference between the *idealised* and *actual* rotorcraft model is large then a countermeasure is required to compensate for this discrepancy. It is still possible to incorporate this method to rotorcraft models for which the *idealised* and *actual* rotorcraft model differ, but require adjustments to the feedback-loop of the actuator measurements. To be more specific a technique called *rotor synchronisation* must be considered to account for the fact that a steady-state flapping model has been used for establishing the stabilising control law, whereas the *actual* rotorcraft model is associated with non-instantaneous disc-tilt motion. This technique incorporates a lag filter to slow down the feedback loop of the actuator measurements. The aforementioned synchronisation technique shall be touched upon later. The main advantage of this approach is that it obviates the need for any state estimation technique for determining the flapping angles, making it more robust to such uncertainties.

II Next, the *flapping angle equivalence method* shall be considered, which can be regarded a novel method. This method does make use of a geometric transformation of the flapping angles from one plane of reference to another. To be more specific, the first-order *Taylor* series for the angular rates does consider the flapping angles with respect to the shaft plane first as inputs, where after a geometric transformation is being applied. This geometric transformation does transform the shaft plane flapping angles

into an equivalent form wherein the cyclic control inputs and flapping angles with respect to the control plane explicitly appear. This transformation shall be considered in more detail in section 4.3. The first-order *Taylor* series for $\dot{p}$ and $\dot{q}$ (denoted as $\dot{\boldsymbol{\omega}}_{pq} = [\dot{p},\ \dot{q}]^T$) can be written as follows

$$\begin{aligned}\dot{\boldsymbol{\omega}}_{pq} &= \dot{\boldsymbol{\omega}}_{pq,0} + \boldsymbol{F}_{\omega_{pq},\beta_{SP}} \Delta\boldsymbol{\beta}_{SP} \\ &= \dot{\boldsymbol{\omega}}_{pq,0} + \boldsymbol{F}_{\omega_{pq},\beta_{SP}} \Delta(\boldsymbol{\theta}_{C_F} + \boldsymbol{\beta}_{CP})\end{aligned} \quad \text{with } \boldsymbol{\theta}_{C_F} = [-\theta_{1s},\ \theta_{1c}]^T \text{ and } \boldsymbol{\beta}_{CP} = [\beta_{1c},\ \beta_{1s}]^T_{CP} \tag{4.6}$$

wherein $\boldsymbol{\theta}_{C_F}$ can be measured, but $\boldsymbol{\beta}_{CP}$ cannot. This therefore requires an additional state estimation technique to determine the flapping states with respect to the control plane. However, it will be shown that this is actually not necessary as the final control law will depend on the incremental change in flapping angle, that is $\Delta\boldsymbol{\beta}_{CP}$. The incremental change in flapping angle is rather small and can therefore be neglected. It should be noted that this approach does assume time-scale separation between the flapping modes and angular body modes of motion. This is because $\boldsymbol{\beta}_{CP}$ will be ignored in the final control law, therefore the cyclic control inputs have become identical to the rotor disc tilt angles, which can only happen when neglecting rotor disc-tilt dynamics [16]. Most importantly is that control effectiveness has been enhanced using this control strategy. This means that the IBS TSS condition will be less likely violated. This shows that this particular strategy is fairly similar to the previous strategy. However, the main difference between both methods is that the *method of residualised dynamics* can consider residualisation of more internal dynamics (e.g. flap-lag-inflow), whereas the *flapping angle equivalence method* only considers residualisation of flapping dynamics. It will be shown in the next chapter that the control effectiveness obtained by means of the *flapping angle equivalence method* is approximately the same as considering flap residualisation using the *method of residualised dynamics*. Moreover it should be noted that the *flapping angle equivalence method* considers steady-state flapping dynamics, therefore rotor synchronisation must also be considered.

III Another option would be to incorporate a *central finite difference method*, wherein the derivatives of the moments with respect to the control inputs are being determined [46, 47]. This method will therefore rely on measurements of moments generated by the main rotor of the rotorcraft, which cannot be obtained. In Eq. 4.7 the expression for the central finite difference is provided [46, 47]. It can be observed that it depends on the moments generated by the main rotor m_{mr}, current control inputs u_0, current state x_0 and three perturbations, namely τ_{θ_0}, $\tau_{\theta_{1s}}$ and $\tau_{\theta_{1c}}$. In [46] additional information is provided about this method.

$$\left.\frac{\partial m_{mr}(\underline{x},\underline{u})}{\partial \underline{u}}\right|_{\underline{x}_0,\underline{u}_0} = \begin{bmatrix} \frac{m^T_{mr}\left(\underline{x}_0,\underline{u}_0+\left[\tau_{\theta_0}\ 0\ 0\ 0\right]^T\right)-\underline{m}^T_{mr}\left(\underline{x}_0,\underline{u}_0-\left[\tau_{\theta_0} 0\ 0\ 0\right]^T\right)^T}{2\tau_{\theta_0}} \\ \frac{\underline{m}^T_{mr}\left(\underline{x}_0,\underline{u}_0+\left[0\ \tau_{\theta_{1s}}\ 0\ 0\right]^T\right)-\underline{m}^T_{mr}\left(\underline{x}_0,\underline{u}_0-\left[0\tau_{\theta_{1s}}\ 0\ 0\ \right]^T\right)}{2\tau_{\theta_{1s}}} \\ \frac{m^T_{mr}\left(\underline{x}_0,\underline{u}_0+\left[0\ 0\ \tau_{\theta_{1c}}\ 0\right]^T\right)-\underline{m}^T_{mr}\left(\underline{x}_0,\underline{u}_0-\left[0\ 0\ \tau_{\theta_{1c}}\ 0\right]^T\right)}{2\tau_{\theta_{1c}}} \\ 0_{1\times 3} \end{bmatrix} \tag{4.7}$$

It should be noted that this method is not feasible, because it requires measurements of main rotor moments. The strategy may work for simulation models, but not for actual implementation.

IV The last method that will be touched upon is the *active flapping control method* [18]. This control strategy differs from the previous ones as it does incorporate two subsystems for controlling the angular rates, rather than one. It includes an inner flapping subsystem and an outer angular rate subsystem [8]. The discussion shall focus on pitch and roll rates, cyclic flapping angles and cyclic control inputs. The *virtual* control inputs for the angular subsystem are the cyclic flapping angles with respect to the shaft plane ($\boldsymbol{\beta}_{SP}$), whereas the inputs to the flapping subsystem are the cyclic control inputs $\boldsymbol{\theta}_C$. This method requires IBS for both the angular rate subsystem as well as for the flapping subsystem. The *time-scale separation principle* must be incorporated in order to apply this approach [54]. This means that for the angular rate subsystem the angular body modes and flapping (regressive) modes should be well-separated in the complex plane to adhere to the IBS TSS condition. The first step towards designing the controller is by defining the first-order *Taylor* of the angular rates, which is found to be equal to

$$\dot{\boldsymbol{\omega}}_{pq} = \dot{\boldsymbol{\omega}}_{pq,0} + \boldsymbol{F}_{\omega_{pq},\beta_{SP}} \Delta\boldsymbol{\beta}_{SP}, \quad \text{with} \quad \boldsymbol{\omega}_{pq} = [p,\ q]^T \quad \text{and} \quad \boldsymbol{\beta}_{SP} = [\beta_{1c},\ \beta_{1s}]^T_{SP}. \tag{4.8}$$

The control effectiveness matrix is the state-depended term $\boldsymbol{F}_{\omega_{pq},\beta_{SP}}$, which is usually determined by hub stiffness K_β. It can be observed that this is actually fairly similar to the *flapping angle equivalence method*. As mentioned previously, the validity of the first-order *Taylor* series of Eq. 4.9 depends on whether the *virtual* control input can be reached instanteneous. As outlined in the first two methods, this does primarily hold for rotorcraft models which are associated with well-separated body and flapping modes of motion. It does therefore run into the same problem as the first two methods. Next to this the first-order *Taylor* series for the flapping subsystem can be written as

$$\dot{\boldsymbol{\beta}}_{SP} = \dot{\boldsymbol{\beta}}_{SP0} + \boldsymbol{G}_{\beta_{SP}} \Delta\boldsymbol{\theta}_C, \quad \text{with} \quad \boldsymbol{\theta_c} = [\theta_{1s},\ \theta_{1c}]^T. \tag{4.9}$$

This first-order *Taylor* series does rely on time-scale separation between cyclic control inputs and flapping states, which generally holds [18]. The problem with this control strategy is the need of having accurate and reliable knowledge of the flapping states and its derivatives. Moreover, Eq. 4.8 assumes TSS between the angular body dynamics and flapping dynamics, but this does not necessarily hold.

4.2. Main discrepancies control strategies

Previously the various control strategies have been outlined for which the main discrepancies shall be outlined in this section. This shall be done for all methods except for the *central finite difference method*, because it was previously already mentioned that this particular method is not feasible.

4.2.1. Discrepancies of method of residualised dynamics

First the discrepancies for the *method of residualised dynamics* shall be considered. The main discrepancies that do arise are: control effectiveness mismatch, angular acceleration measurement induced delay and rotor dynamics induced delay. Below the aforementioned discrepancies shall be touched upon in a bit more detail.

I The actuator measurement must be synchronised with the feedback signal of the angular acceleration measurement. Since angular accelerations need to be estimated by means of a washout filter, a similar filter must be placed in the feedback loop to enable synchronisation of both signals [53, 55]. Numerical differentiation of angular rates would amplify noise, which is not desirable [57].

II The difference between *idealised* and *actual* rotorcraft model requires adjustment of the feedback-loop of the actuator measurement. A rotor synchronisation filter is required, which is a lag filter that will slow down the feedback of the actuator measurement to synchronise it with the angular rate derivative measurement. Since steady-state flapping dynamics is considered, a flap synchronisation is required. This shows that this method requires additional effort for establishing a well-synchronised IBS controller.

III The control effectiveness matrix $\boldsymbol{G}_{\omega_{pq,R}}$ which appears in the first-order *Taylor* series expression for the angular accelerations cannot be considered fully known. This implies that additional estimation techniques are required for determining the control effectiveness. Estimation techniques cannot assure that the estimated control effectiveness is equal to the true control effectiveness ($\hat{\boldsymbol{G}}_{\omega_{pq,R}} \neq \boldsymbol{G}_{\omega_{pq,R}}$). This may can affect controller performance, however a small mismatch is allowed [53].

IV For establishing the stabilising control law it was assumed that sampling rate is sufficiently high such that control action is instantaneous. This would imply that all other state-depended terms can be neglected, with the exception of the body-flap coupling. This is a necessary condition for the incremental-based control law to be robust to uncertainties in system dynamics [54].

4.2.2. Discrepancies of flapping angle equivalence method

Next the discrepancies of the *flapping angle equivalence method* shall be considered.

I The feedback of the actuator measurements must be synchronised with the angular acceleration measurements. Since angular accelerations need to be estimated by means of a washout filter, a similar filter must be placed in the feedback loop to enable synchronisation of both signals [53, 55]. Numerical differentiation of angular rates would amplify noise, which is highly undesirable [57].

II The difference between *idealised* and *actual* rotorcraft model requires adjustment of the feedback-loop of the actuator measurement. A rotor synchronisation filter is required, which is a lag filter that will slow down the feedback of the actuator measurement to synchronise it with the angular rate derivative measurement. Since steady-state flapping dynamics is considered, a flap synchronisation is required. This shows that this method requires additional effort for establishing a well-synchronised IBS controller.

III The control effectiveness matrix $\boldsymbol{F}_{\omega_{pq},\beta_{SP}}$ which appears in the first-order *Taylor* series expression for the angular accelerations cannot be considered fully known. This implies that additional estimation techniques are required for determining the control effectiveness. Estimation techniques cannot assure that the estimated control effectiveness is equal to the true control effectiveness ($\hat{\boldsymbol{F}}_{\omega_{pq},\beta_{SP}} \neq \boldsymbol{F}_{\omega_{pq},\beta_{SP}}$). This may can affect controller performance, however a small mismatch is allowed [53].

IV For establishing the stabilising control law it was assumed that sampling rate is sufficiently high such that control action is instantaneous. This would imply that all other state-depended terms can be neglected, with the exception of the body-flap coupling. This is a necessary condition for the incremental-based control law to be robust to uncertainties in system dynamics [54].

4.2.3. Discrepancies of active flapping control method

Lastly, the discrepancies of the *active flapping control method* will be considered.

I State-dependency in the first-order *Taylor* series for the angular rate and flapping rate dynamics are being ignored, which is because high sampling rate and instantaneous control action are being assumed. When such an assumption holds then the incremental control law also can be considered robust to uncertainties in system dynamics. On the other hand when state-depended terms are large, the assumption would not hold, therefore adversely affecting controller performance [53]. This would require to redefine the first-order *Taylor* series such that it would not violate this condition.

II For establishing the first-order *Taylor* series for the angular rates, it must be assumed that the flapping angles $\boldsymbol{\beta}_{SP}$ are the *virtual* control inputs. Since it will be used to establish an IBS control law, a necessary condition would be that the desired flapping angles are reached instantaneous (steady-state flapping dynamics). This may hold for rotorcraft associated for which the angular body and flapping modes of motion are well-separated in the complex plane. If steady-state flapping dynamics cannot be assumed then state-dependency will very likely be large. This could harm the IBS TSS condition. It is therefore very likely that rotor synchronisation is also required for this control strategy.

III The stabilising control law for the angular rate and flapping subsystem requires the measurement of the angular rate and flapping derivative respectively. These are obtained making use of a second-order washout filter in the feedback of the corresponding state-derivatives. However, such a filter does introduce a delay, which could pose synchronisation issues [24, 57], therefore counter measures need to be taken. For the angular rate subsystem this would mean that the feedback of the flapping measurement (*virtual control input*) would also be fed through the exact same washout filter by which the angular accelerations are being obtained with. In a similar fashion of the flapping subsystem the feedback of the actuator measurement would also be fed through the exact same washout filter by which the flapping rate estimates are being obtained with. Normally delay compensation is only performed for the angular rate subsystem, because the flapping rates are directly governed by the control inputs.

IV The control effectiveness matrices $\boldsymbol{G}_{\beta_{SP}}$ and $\boldsymbol{F}_{\omega_{pq},\beta_{SP}}$ cannot be considered fully known. This implies that additional parameter estimation techniques are required for determining the control derivatives. Estimation techniques cannot assure that the estimated control effectiveness is equal to the true control effectiveness. This means that it may can also affect controller performance. However, a small mismatch will not significantly affect controller performance [53].

V Inclusion of an additional flapping loop increases the complexity of the control design. This makes it more prone to mistakes in established a well-defined controller.

4.3. Advanced flight control by means of flapping angle equivalence

The previous control strategy did require two subsystems to control the angular rates p and q of the rotorcraft. This strategy would enable active flapping control when command-filtered IBS was considered. On the other hand it did come at cost of requiring accurate knowledge of the flapping states and its derivatives, flapping synchronisation, mismatch of control effectiveness of inner and outer loop subsystems and the adverse effect of excluding state-dependency in the first-order *Taylor* series of the flapping rates. It is therefore a natural choice to seek for other strategies for controlling the angular rates such that some of the discrepancies can be obviated. In this section the *flapping angle equivalence method* shall be considered for establishing a stabilising control law for the angular rate subsystem. The method shall only be considered for pitch and roll rate ($\boldsymbol{\omega}_{pq}$) because of reasons given earlier.

4.3.1. Establishing first-order Taylor series by means of flapping angle equivalence

Since the angular rate dynamics of the rotorcraft does depend upon complex aerodynamics, it is a natural choice to consider an incremental-based control strategy [18, 55]. The first-order *Taylor* series is established by only considering the body-flap coupling, where after a geometric transformation is applied. The approach thus purely accounts for the fact that the angular accelerations $\dot{p}$ and $\dot{q}$ are primarily governed by flapping dynamics, which is generally true [8, 18, 55]. In Eq. 4.10 the first-order *Taylor* series for the angular accelerations is provided. In the first expression it can be observed that $\dot{\boldsymbol{\omega}}_{pq}$ does depend on the the flapping angles with respect to the shaft plane. In the second expression $\boldsymbol{\beta}_{SP}$ ($= \boldsymbol{\beta}_{CP} + \boldsymbol{\theta}_{C_F}$) has been transformed into an equivalent form, wherein the cyclic control inputs $\boldsymbol{\theta}_{C_F}$ ($= [-\theta_{1s},\ \theta_{1c}]^T$) and flapping angles with respect to the control plane $\boldsymbol{\beta}_{CP}$ ($= [\beta_{1c},\ \beta_{1s}]^T_{CP}$) explicitly appear. Moreover, the last term from Eq. 4.10 is neglected, because $\boldsymbol{F}_{\omega_{pq},\beta_{SP}} >> \boldsymbol{H}_{\omega_{pq}}$. Moreover $\boldsymbol{F}_{\omega_{pq},\beta_{SP}}$ primarily depends on K_β, which is generally well-known.

$$\begin{aligned}\dot{\boldsymbol{\omega}}_{pq} &= \dot{\boldsymbol{\omega}}_{pq,0} + \boldsymbol{F}_{\omega_{pq},\beta_{SP}}\Delta\boldsymbol{\beta}_{SP} + \boldsymbol{H}_{\omega_{pq}}\Delta\boldsymbol{\theta}_C \\ &= \dot{\boldsymbol{\omega}}_{pq,0} + \boldsymbol{F}_{\omega_{pq},\beta_{SP}}\Delta\left[\boldsymbol{\theta}_{C_F} + \boldsymbol{\beta}_{CP}\right] \\ &= \dot{\boldsymbol{\omega}}_{pq,0} + \boldsymbol{F}_{\omega_{pq},\beta_{SP}}\Delta\boldsymbol{\beta}_{CP} + \boldsymbol{F}_{\omega_{pq},\beta_{SP}}\Delta\boldsymbol{\theta}_{C_F}\end{aligned} \tag{4.10}$$

The flapping angle equivalence is given in Fig. 4.1 from which it can be observed that the flapping angles with respect to the shaft plane are related to flapping angles with respect to the control plane and cyclic control inputs. The control plane (CP) and no-feathering plane (NFP) are assumed to coincidence with each other.

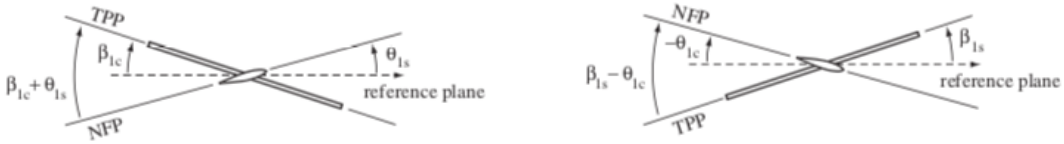

(a) Longitudinal flapping angle equivalence. **(b)** Lateral flapping angle equivalence.

Figure 4.1: Equivalence between longitudinal and lateral flapping angles with respect to the SP and CP (NFP) [20].

The flapping equivalence given in Fig. 4.1 holds for a positive *Fourier* series when transforming from the rotating frame of reference to the non-rotating frame of reference [20]. The longitudinal and lateral flapping equivalence can be written respectively as

$$\beta_{1c,cp} = \beta_{1c,sp} + \theta_{1s}, \tag{4.11}$$

$$\beta_{1s,cp} = \beta_{1s,sp} - \theta_{1c}. \tag{4.12}$$

The cyclic flapping angles and cyclic control inputs can be written into a more compact form. The aforementioned was already considered in Eq. 4.10 for writing the first-order *Taylor* series of the angular acceleration. The two above mentioned expressions can be written into the following form

$$\boldsymbol{\beta}_{SP} = \boldsymbol{\beta}_{CP} + \boldsymbol{\theta}_{C_F}, \quad \text{with } \boldsymbol{\theta}_{C_F} = [-\theta_{1s},\ \theta_{1c}]^T,\ \boldsymbol{\beta}_{CP} = [\beta_{1c},\ \beta_{1s}]^T_{CP} \text{ and } \boldsymbol{\beta}_{SP} = [\beta_{1c},\ \beta_{1s}]^T_{SP}. \tag{4.13}$$

4.3.2. Lyapunov-based control law for angular rate subsystem (p & q)

The main objective is to establish a stabilising control law for the angular rate subsystem, wherein the rotorcraft shall track a predefined angular rate trajectory. The previously defined first-order *Taylor* series shall be incorporated for deriving the IBS control law. The stabilising control law shall be derived for roll and pitch rates only. The first step towards deriving a stabilising control law for the angular rate subsystem is by defining the angular rate tracking error, which is found to be equal to the following

$$\boldsymbol{z}_{\omega_{pq}} = \boldsymbol{\omega}_{pq} - \boldsymbol{\omega}_{pq,\text{ref}}, \tag{4.14}$$

wherein $\boldsymbol{\omega}_{pq,\text{ref}}$ is the desired trajectory that needs to be followed by the vehicle. The expression for $\dot{\boldsymbol{z}}_{\omega_{pq}}$ is

$$\dot{\boldsymbol{z}}_{\omega_{pq}} = \dot{\boldsymbol{\omega}}_{pq} - \dot{\boldsymbol{\omega}}_{pq,\text{ref}} = \dot{\boldsymbol{\omega}}_{pq,0} + \boldsymbol{F}_{\omega_{pq},\beta_{SP}} \Delta\big(\boldsymbol{\theta}_{C_F} + \boldsymbol{\beta}_{CP}\big) - \dot{\boldsymbol{\omega}}_{pq,\text{ref}}, \tag{4.15}$$

wherein $(\boldsymbol{\theta}_{C_F} + \boldsymbol{\beta}_{CP})$ is equivalent to $\boldsymbol{\beta}_{SP}$. However, the former expression is more desirable, because of the cyclic control inputs explicitly showing up. A quadratic CLF shall be incorporated for deriving the stabilising control law for the angular rate subsystem. The expression for $\mathcal{V}_{\omega_{pq}}(\boldsymbol{z}_{\omega_{pq}})$ and $\dot{\mathcal{V}}_{\omega_{pq}}(\dot{\boldsymbol{z}}_{\omega_{pq}})$ are respectively

$$\mathcal{V}_{\omega_{pq}}(\boldsymbol{z}_{\omega_{pq}}) = 0.5 \boldsymbol{z}_{\omega_{pq}}^T \boldsymbol{z}_{\omega_{pq}}, \tag{4.16}$$

$$\dot{\mathcal{V}}_{\omega_{pq}}(\dot{\boldsymbol{z}}_{\omega_{pq}}) = \boldsymbol{z}_{\omega_{pq}}^T \Big\{ \dot{\boldsymbol{\omega}}_{pq,0} + \boldsymbol{F}_{\omega_{pq},\beta_{SP}} \Delta\big(\boldsymbol{\theta}_{C_F} + \boldsymbol{\beta}_{CP}\big) - \dot{\boldsymbol{\omega}}_{pq,\text{ref}} \Big\}. \tag{4.17}$$

In order to obtain the stabilising control law for the angular rate subsystem, it is necessary to let $\dot{\mathcal{V}}_{\omega_{pq}}(\dot{\boldsymbol{z}}_{\omega_{pq}})$ become negative definite along the trajectories of the error dynamics. The expressions for the stabilising control law in accordance with the standard IBS procedure is

$$\boldsymbol{\theta}_{C_F} + \boldsymbol{\beta}_{CP} = \boldsymbol{\theta}_{C_F,0} + \boldsymbol{\beta}_{CP,0} + \boldsymbol{F}^{-1}_{\omega_{pq},\beta_{SP}} \Big\{ -\dot{\boldsymbol{\omega}}_{pq,0} - \boldsymbol{c}_{\omega_{pq}} \boldsymbol{z}_{\omega_{pq}} + \dot{\boldsymbol{\omega}}_{pq,\text{ref}} \Big\}, \tag{4.18}$$

from which it can be observed that the incremental control vector $\boldsymbol{F}^{-1}_{\omega_{pq},\beta_{SP}} \Big\{ -\dot{\boldsymbol{\omega}}_{pq,0} - \boldsymbol{c}_{\omega_{pq}} \boldsymbol{z}_{\omega_{pq}} + \dot{\boldsymbol{\omega}}_{pq,\text{ref}} \Big\}$ has been added to the previous inputs $\boldsymbol{\theta}_{C_F,0} + \boldsymbol{\beta}_{CP,0}$. It should however be noted that this is not something that can be fed back to the actuator, as it still contains the explicit dependency on the flapping angles with respect to the control plane on the left hand side. This can be accounted for by putting this to the right hand side. It can thus be rewritten into an equivalent form, wherein the cyclic control inputs are isolated. The rewritten form is given in Eq. 4.19.

$$\boldsymbol{\theta}_{C_F} = \boldsymbol{\theta}_{C_F,0} - \boldsymbol{\beta}_{CP} + \boldsymbol{\beta}_{CP,0} + \boldsymbol{F}^{-1}_{\omega_{pq},\beta_{SP}} \Big\{ -\dot{\boldsymbol{\omega}}_{pq,0} - \boldsymbol{c}_{\omega_{pq}} \boldsymbol{z}_{\omega_{pq}} + \dot{\boldsymbol{\omega}}_{pq,\text{ref}} \Big\} \tag{4.19}$$

From Eq. 4.19 it can be observed that the stabilising control law depends on the incremental change in $\boldsymbol{\beta}_{CP}$. This incremental change is small and can be neglected, yielding the following stabilising control law

$$\boldsymbol{\theta}_{C_F} = \boldsymbol{\theta}_{C_F,0} + \boldsymbol{F}^{-1}_{\omega_{pq},\beta_{SP}} \Big\{ -\dot{\boldsymbol{\omega}}_{pq,0} - \boldsymbol{c}_{\omega_{pq}} \boldsymbol{z}_{\omega_{pq}} + \dot{\boldsymbol{\omega}}_{pq,\text{ref}} \Big\}. \tag{4.20}$$

Lastly, it should be noted that $\boldsymbol{\theta}_{C_F} = [-\theta_{1s} \;\; \theta_{1c}]^T$, therefore a small correction is required to transform it into $\boldsymbol{\theta}_C = [\theta_{1s} \;\; \theta_{1c}]^T$. This shall be achieved by means of $\boldsymbol{I}_{\text{cor}}$, which is $2x2$ matrix with -1 in it is first entry. This does yield the following stabilising control law.

$$\boldsymbol{\theta}_C = \boldsymbol{\theta}_{C,0} + \boldsymbol{I}_{\text{cor}} \boldsymbol{F}^{-1}_{\omega_{pq},\beta_{SP}} \Big\{ -\dot{\boldsymbol{\omega}}_{pq,0} - \boldsymbol{c}_{\omega_{pq}} \boldsymbol{z}_{\omega_{pq}} + \dot{\boldsymbol{\omega}}_{pq,\text{ref}} \Big\}. \tag{4.21}$$

It can be observed from Eq. 4.21 that there is no need for incorporating state estimation techniques for determining the flapping angles, which is thus favourable. The CLF derivative using Eq. 4.21 in accordance with the standard IBS procedure is equal to the following

$$\dot{\mathcal{V}}_{\omega_{pq}}(\dot{\boldsymbol{z}}_{\omega_{pq}}) = -\boldsymbol{z}_{\omega_{pq}}^T \boldsymbol{c}_{\omega_{pq}} \boldsymbol{z}_{\omega_{pq}}. \tag{4.22}$$

In accordance with the theorem of *LaSalle-Yoshizawa*, the equilibrium $\boldsymbol{z}_{\omega_{pq}} = \boldsymbol{0}$ can be considered globally uniformly asymptotically stable when $\boldsymbol{c}_{\omega_{pq}} > 0$ given that the sampling frequency f_s is sufficiently high. This would imply that the tracking error from Eq. 4.14 would go towards zero for $t \to \infty$.

4.3.3. Equivalent PI stabilising control law for angular rate subsystem (p & q)

The stabling control law from Eq. 4.21 can be written as classical proportional-integral (PI) control law. This can only be considered for systems of relative degree one. This means that it can only be applied to single subsystems. The two-cascaded system considered in section **??** is of relative degree two, therefore it cannot be rewritten as classical PI-controller. For analysis purposes the control strategy being proposed in this section is therefore more favourable than the previous one, because it can relate non-linear control design with linear control design. The classical PI-controller without actuator dynamics shall be considered. The derivation of the PI-controller is given in Eq. 4.24, wherein f_s and t_s are the sampling frequency and time respectively. The former must be chosen sufficiently high enough to assume the incremental law acts as a continuous integrator of the form given in 4.23.

$$\boldsymbol{\theta}_C(t) = f_s \int_0^t \Delta\boldsymbol{\theta}_C d\tau. \tag{4.23}$$

Substitution of the stabilising control law from Eq. 4.21 into Eq. 4.23 does yield the first expression of Eq. 4.24. To arrive at the final form of Eq. 4.24 it is necessary to assume that $\boldsymbol{\omega}_{pq}$ does change slow compared to t_s such that $\boldsymbol{\omega}_{pq}(t-t_s) - \boldsymbol{\omega}_{pq,\mathrm{ref}}(t)$ can be set equal to $\boldsymbol{z}_{\omega_{pq}}(t)$.

$$\begin{aligned}
\boldsymbol{\theta}_C(t) &= \int_0^t f_s \boldsymbol{I}_{\mathrm{cor}} \boldsymbol{F}^{-1}_{\omega_{pq},\beta_{SP}} \left[-\boldsymbol{c}_{\omega_{pq}} \boldsymbol{z}_{\omega_{pq}}(\tau) - \dot{\boldsymbol{\omega}}_{pq}(\tau - t_s) + \dot{\boldsymbol{\omega}}_{pq,\mathrm{ref}}(\tau) \right] d\tau \\
&= f_s \boldsymbol{I}_{\mathrm{cor}} \boldsymbol{F}^{-1}_{\omega_{pq},\beta_{SP}} \left[-\boldsymbol{c}_{\omega_{pq}} \int_0^t \boldsymbol{z}_{\omega_{pq}}(\tau) d\tau - \boldsymbol{\omega}_{pq}(t - t_s) + \boldsymbol{\omega}_{pq,\mathrm{ref}}(t) \right] \\
&= f_s \boldsymbol{I}_{\mathrm{cor}} \boldsymbol{F}^{-1}_{\omega_{pq},\beta_{SP}} \left[-\boldsymbol{c}_{\omega_{pq}} \int_0^t \boldsymbol{z}_{\omega_{pq}}(\tau) d\tau - \boldsymbol{z}_{\omega_{pq}}(t) \right]
\end{aligned} \tag{4.24}$$

The proportional and integral gains can be identified as $f_s \boldsymbol{I}_{\mathrm{cor}} \boldsymbol{F}^{-1}_{\omega_{pq}\beta_{SP}}$ and $\boldsymbol{c}_{\omega_{pq}} f_s \boldsymbol{I}_{\mathrm{cor}} \boldsymbol{F}^{-1}_{\omega_{pq}\beta_{SP}}$ respectively. The main difference between the stabilising control law from Eq. 4.24 and 4.21 is that the former does not depend on the feedback of the angular acceleration measurements $\dot{\boldsymbol{\omega}}_0$. By means of the above transformation it is possible to correlate findings from previous research, wherein linear controllers were used with the non-linear control strategy proposed here. The derivation can be extended by also considering actuator dynamics, which is explained in great detail in [53].

4.3.4. Closed-loop system of nominal controller defined in Laplace-domain

In order to establish the closed-loop system it is necessary to define the incremental control law and first-order *Taylor* series in the *Laplace*-domain. The closed-loop system that is being established without actuators, sensors or filters will be designated as the *nominal* controller. The stabilising control law from Eq. 4.21 in the *Laplace*-domain is

$$\begin{aligned}
&\boldsymbol{\theta}_C(s) = \boldsymbol{\theta}_C(s) e^{-\Delta t s} + \boldsymbol{I}_{\mathrm{cor}} \boldsymbol{F}^{-1}_{\omega_{pq},\beta_{SP}} \left\{ -s\boldsymbol{\omega}_{pq}(s) e^{-\Delta t s} + \boldsymbol{\nu}_{pq}(s) \right\} \\
&\left[\boldsymbol{I}_{2x2} - e^{-\Delta t s} \boldsymbol{I}_{2x2} \right] \boldsymbol{\theta}_C(s) = \boldsymbol{I}_{\mathrm{cor}} \boldsymbol{F}^{-1}_{\omega_{pq},\beta_{SP}} \left\{ -s\boldsymbol{\omega}_{pq}(s) e^{-\Delta t s} + \boldsymbol{\nu}_{pq}(s) \right\} \\
&\qquad \text{with} \quad \boldsymbol{\nu}_{pq}(s) = -\boldsymbol{c}_{\omega_{pq}} \boldsymbol{z}_{\omega_{pq}}(s) + s\boldsymbol{\omega}_{pq,\mathrm{ref}}(s).
\end{aligned} \tag{4.25}$$

The first-order *Taylor* series of the angular accelerations from Eq. 4.10 can written in the *Laplace*-domain as

$$s\boldsymbol{\omega}_{pq}(s) = s\boldsymbol{\omega}_{pq}(s) e^{-\Delta t s} + \boldsymbol{F}_{\omega_{pq},\beta_{SP}} \boldsymbol{I}^{-1}_{\mathrm{cor}} \left[\boldsymbol{I}_{2x2} - e^{-\Delta t s} \boldsymbol{I}_{2x2} \right] \boldsymbol{\theta}_C(s), \tag{4.26}$$

wherein $\boldsymbol{\beta}_{CP}$ was ignored and the correction factor was applied. The aforementioned would yield the same stabilising control law as given in Eq. 4.21. In order to determine the closed-loop response it is deemed necessary to rewrite Eq. 4.25 by isolating $\boldsymbol{\theta}_C(s)$ on the left hand side, where after it is being substituted into the first-order *Taylor* series from Eq. 4.26. Doing the aforementioned yields Eq. 4.27. It can be observed that $\boldsymbol{I}_{2x2} - e^{-\Delta t s} \boldsymbol{I}_{2x2}$, $\boldsymbol{I}_{\mathrm{cor}}$, $\boldsymbol{F}_{\omega_{pq},\beta_{SP}}$ and $s\boldsymbol{\omega}_{pq}(s) e^{-\Delta t s}$ cancel out, which eventually yields the closed-loop expression for the *nominal* controller. It can be observed that for the *nominal* case $s\boldsymbol{\omega}_{pq}(s)$ is equal to $\boldsymbol{\nu}_{pq}(s)$.

$$\begin{aligned} s\boldsymbol{\omega}_{pq}(s) &= s\boldsymbol{\omega}_{pq}(s)e^{-\Delta t s} + \boldsymbol{F}_{\omega_{pq},\beta_{SP}}\boldsymbol{I}_{\text{cor}}^{-1}\left[\boldsymbol{I}_{2x2} - e^{-\Delta t s}\boldsymbol{I}_{2x2}\right]\boldsymbol{\theta}_C(s) \\ &= \boldsymbol{F}_{\omega_{pq},\beta_{SP}}\boldsymbol{I}_{\text{cor}}^{-1}\left[\boldsymbol{I}_{2x2} - e^{-\Delta t s}\boldsymbol{I}_{2x2}\right]^{-1}\left[\boldsymbol{I}_{2x2} - e^{-\Delta t s}\boldsymbol{I}_{2x2}\right]\boldsymbol{I}_{\text{cor}}\boldsymbol{F}_{\omega_{pq},\beta_{SP}}^{-1}\left\{-s\boldsymbol{\omega}_{pq}(s)e^{-\Delta t s} + \boldsymbol{\nu}_{pq}(s)\right\} \\ &\quad + s\boldsymbol{\omega}_{pq}(s)e^{-\Delta t s} \\ &= s\boldsymbol{\omega}_{pq}(s)e^{-\Delta t s} + \boldsymbol{F}_{\omega_{pq},\beta_{SP}}\boldsymbol{F}_{\omega_{pq},\beta_{SP}}^{-1}\left\{-s\boldsymbol{\omega}_{pq}(s)e^{-\Delta t s} + \boldsymbol{\nu}_{pq}(s)\right\} \\ &= \boldsymbol{\nu}_{pq}(s) \end{aligned} \tag{4.27}$$

4.3.5. Angular acceleration measurement compensation

From the stabilising control law for the angular rate subsystem it can be observed that $\dot{\boldsymbol{\omega}}_{pq,0}$ is required. Currently reliable and accurate angular accelerometers do not yet exist, therefore the angular accelerations could be obtained by numerical differentiation of the angular rates. Since numerical differentiation would yield amplification of noise and delay of the angular accelerations of one time-step, this approach is not desirable [24, 55, 57]. Another choice would be by letting the angular rate measurements pass through a second-order washout filter , which is characterised with damping ratio ζ_{filt} and natural frequency $\omega_{\text{n,filt}}$ [24, 55, 57]. In addition to this there will also be an added zero-mean noise signal (indicated by $\mathcal{N}\left(0,\sigma_{\text{filt}}^2\right)$ with $\sigma_{\text{filt}} = 0.006°/s$), which accounts for sensor noise. The angular accelerations can be obtained by

$$\begin{aligned} s\boldsymbol{\omega}_{pq,\text{meas}}(s) &= s\boldsymbol{H}_{\text{filt}}(s)\left(\boldsymbol{\omega}_{pq}(s) + \mathcal{N}\left(0,\sigma_{\text{filt}}^2\right)\right) = \frac{\omega_{n,\text{filt}}^2 s}{s^2 + 2\zeta_{\text{filt}}\omega_{n,\text{filt}}s + \omega_{n,\text{filt}}^2}\left(\boldsymbol{\omega}_{pq}(s) + \mathcal{N}\left(0,\sigma_{\text{filt}}^2\right)\right) \\ &= s\boldsymbol{H}_{\text{filt}}(s)\boldsymbol{\omega}_{pq}(s) = \frac{s}{s}\boldsymbol{H}_{\text{filt}}(s)s\boldsymbol{\omega}_{pq}(s) = \boldsymbol{H}_{\text{filt}}(s)s\boldsymbol{\omega}_{pq}(s), \end{aligned} \tag{4.28}$$

where $\omega_{\text{n,filt}}$ and ζ_{filt} are set equal to 100 rad/s and 1 respectively. It can be observed that $s\boldsymbol{\omega}_{pq,\text{meas}}(s)$ is equivalent to $s\boldsymbol{\omega}_{pq}(s)$ being multiplied $\boldsymbol{H}_{\text{filt}}(s)$. It should be noted that $\boldsymbol{H}_{\text{filt}}(s)$ is a 2x2 matrix with the sensor dynamics on its diagonal. With the sensor dynamics being defined, the IBS control law shall be rewritten in order to take the sensor dynamics into account and is found to be equal to

$$\left[\boldsymbol{I}_{2x2} - e^{-\Delta t s}\boldsymbol{I}_{2x2}\right]\boldsymbol{\theta}_C(s) = \boldsymbol{I}_{\text{cor}}\boldsymbol{F}_{\omega_{pq},\beta_{SP}}^{-1}\left\{-s\boldsymbol{H}_{\text{filt}}(s)\boldsymbol{\omega}_{pq}(s)e^{-\Delta t s} + \boldsymbol{\nu}_{pq}(s)\right\}. \tag{4.29}$$

In order to obtain the closed-loop response it is necessary to substitute Eq. 4.29 into Eq. 4.26, which yields

$$\begin{aligned} s\boldsymbol{\omega}_{pq}(s) &= \boldsymbol{F}_{\omega_{pq},\beta_{SP}}\boldsymbol{I}_{\text{cor}}^{-1}\left[\boldsymbol{I}_{2x2} - e^{-\Delta t s}\boldsymbol{I}_{2x2}\right]^{-1}\left[\boldsymbol{I}_{2x2} - e^{-\Delta t s}\boldsymbol{I}_{2x2}\right]\boldsymbol{I}_{\text{cor}}\boldsymbol{F}_{\omega_{pq},\beta_{SP}}^{-1}\left\{-s\boldsymbol{H}_{\text{filt}}(s)\boldsymbol{\omega}_{pq}(s)e^{-\Delta t s} + \boldsymbol{\nu}_{pq}(s)\right\} \\ &\quad + s\boldsymbol{\omega}_{pq}(s)e^{-\Delta t s} \\ &= s\boldsymbol{\omega}_{pq}(s)e^{-\Delta t s} - s\boldsymbol{H}_{\text{filt}}(s)\boldsymbol{\omega}_{pq}(s)e^{-\Delta t s} + \boldsymbol{\nu}_{pq}(s), \end{aligned} \tag{4.30}$$

which after rearranging does yield the following closed loop response

$$s\boldsymbol{\omega}_{pq}(s) = \frac{\boldsymbol{\nu}_{pq}(s)}{\boldsymbol{I}_{2x2} + \boldsymbol{H}_{\text{filt}}(s)e^{-\Delta t s} - e^{-\Delta t s}\boldsymbol{I}_{2x2}}. \tag{4.31}$$

It can be observed that the closed-loop system From Eq. 4.31 differs from the *nominal case*. Inadequate closed-loop behaviour can be achieved for frequencies at which $|s\boldsymbol{\omega}_{pq}(s)/\boldsymbol{\nu}_{pq}(s)| > 1$ (oscillating behaviour). In addition to this, delays have also been introduced. The main terms responsible for affecting phase are: $e^{-\Delta t s}$ and $\boldsymbol{H}_{\text{filt}}(s)$. In order to counteract the adverse effects introduced by the second-order washout filter, it is deemed necessary to also introduce the filter in the feedback loop [53, 55]. This means that $\boldsymbol{\theta}_C(s)e^{-\Delta t s}$ shall be multiplied by $\boldsymbol{H}_{\text{filt}}(s)$. It will be shown that by doing this, sensor dynamics will not adversely affect closed-loop response. The stabilising control law for the angular rate subsystem can be written as

$$\boldsymbol{\theta}_C(s) = \boldsymbol{H}_{\text{filt}}(s)\boldsymbol{\theta}_C(s)e^{-\Delta t s} + \boldsymbol{I}_{\text{cor}}\boldsymbol{F}_{\omega_{pq},\beta_{SP}}^{-1}\left\{-s\boldsymbol{H}_{\text{filt}}(s)\boldsymbol{\omega}_{pq}(s)e^{-\Delta t s} + \boldsymbol{\nu}_{pq}(s)\right\} \tag{4.32}$$

The closed-loop transfer function can be determined by substituting the previously defined control law into the first-order *Taylor* series expression from Eq. 4.26. This does yield the first expression given in Eq. 4.33.

There after $s\boldsymbol{H}_{\text{filt}}(s)\boldsymbol{\omega}_{pq}(s)e^{-\Delta ts}$ is brought to the left hand side in the second expression. In the third expression, all the terms containing $\boldsymbol{F}_{\omega_{pq},\beta_{SP}}(s)\boldsymbol{I}_{\text{cor}}^{-1}\boldsymbol{\theta}_C(s)$ on the right hand side have been isolated. The last expression is obtained by noting that $\boldsymbol{F}_{\omega_{pq},\beta_{SP}}\boldsymbol{I}_{\text{cor}}^{-1}\boldsymbol{\theta}_C(s)$ is equal to $s\boldsymbol{\omega}_{pq}(s)$, which causes terms $s\boldsymbol{\omega}_{pq}(s)e^{-\Delta ts}$ and $s\boldsymbol{H}_{\text{filt}}(s)\boldsymbol{\omega}_{pq}(s)e^{-\Delta ts}$ to cancel. It can be observed from the last expression of Eq. 4.33 that the closed-loop system is equal to the *nominal* case. The adjustment will improve closed-loop behaviour.

$$\begin{aligned}
s\boldsymbol{\omega}_{pq}(s)\left[\boldsymbol{I}_{2x2}-e^{-\Delta ts}\boldsymbol{I}_{2x2}\right] &= \boldsymbol{F}_{\omega_{pq},\beta_{SP}}\boldsymbol{I}_{\text{cor}}^{-1}\left[\boldsymbol{H}_{\text{filt}}(s)\boldsymbol{\theta}_C(s)e^{-\Delta ts}+\boldsymbol{I}_{\text{cor}}\boldsymbol{F}_{\omega_{pq},\beta_{SP}}^{-1}\left\{-s\boldsymbol{H}_{\text{filt}}(s)\boldsymbol{\omega}_{pq}(s)e^{-\Delta ts}+\boldsymbol{\nu}_{pq}(s)\right\}\right] \\
&\quad -\boldsymbol{F}_{\omega_{pq},\beta_{SP}}\boldsymbol{I}_{\text{cor}}^{-1}\boldsymbol{\theta}_c(s)e^{-\Delta ts} \\
s\boldsymbol{\omega}_{pq}(s)\left[\boldsymbol{I}_{2x2}-e^{-\Delta ts}\boldsymbol{I}_{2x2}+e^{-\Delta ts}\boldsymbol{H}_{\text{filt}}(s)\right] &= \boldsymbol{F}_{\omega_{pq},\beta_{SP}}\boldsymbol{I}_{\text{cor}}^{-1}\boldsymbol{\theta}_C(s)\left[\boldsymbol{H}_{\text{filt}}(s)e^{-\Delta ts}-e^{-\Delta ts}\boldsymbol{I}_{2x2}\right]+\boldsymbol{\nu}_{pq}(s) \\
s\boldsymbol{\omega}_{pq}(s)\left[\boldsymbol{I}_{2x2}-e^{-\Delta ts}\boldsymbol{I}_{2x2}+e^{-\Delta ts}\boldsymbol{H}_{\text{filt}}(s)\right] &= s\boldsymbol{\omega}_{pq}(s)\left[\boldsymbol{H}_{\text{filt}}(s)e^{-\Delta ts}-e^{-\Delta ts}\boldsymbol{I}_{2x2}\right]+\boldsymbol{\nu}_{pq}(s) \\
s\boldsymbol{\omega}_{pq}(s) &= \boldsymbol{\nu}_{pq}(s)
\end{aligned} \tag{4.33}$$

From this it follows that when angular accelerations are being obtained by means of a second-order washout filter, a similar filter needs to be placed in the feedback-loop of the actuator measurements. From Eq. 4.33 it can be observed that closed-loop response is similar to the one given in Eq. 4.27. This will improve system stability and controller performance. In Fig. 4.2 the feedback loop of the angular rate subsystem is provided, wherein the feedback-loop of the actuator measurement has been adapted.

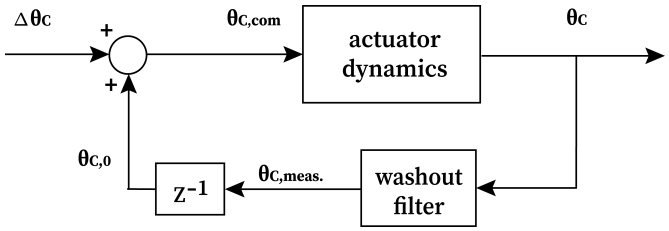

Figure 4.2: Second-order washout filter placed in feedback-loop of actuator measurement.

4.3.6. Control effectiveness mismatch in IBS control law

For establishing the stabilising control law from Eq. 4.21 it is necessary to have a well-defined control effectiveness matrix. In the derivation of the control law it was assumed that the control derivatives are fully known. In other words $\boldsymbol{F}_{\omega_{pq},\beta_{SP}}$ is assumed to be the actual control effectiveness matrix of the angular rate subsystem. In reality it is very unlikely that the exact control derivatives are fully known. This naturally implies that the control effectiveness matrix needs to be estimated and will exhibit an estimation error. In order to understand how the estimated control effectiveness matrix affects controller performance, it will be of great interest to redefine the tracking error of the angular rate subsystem in terms of the estimated control effectiveness matrix. This strategy was proposed by [32, 53].

The control effectiveness matrix in the stabilising control law for the angular rate subsystem differs from the true control effectiveness matrix, thus $\hat{\boldsymbol{F}}_{\omega_{pq},\beta_{SP}} \neq \boldsymbol{F}_{\omega_{pq},\beta}$. In Eq. 4.34 the relation between the estimated and true control effectiveness of the angular rate subsystem is shown. It can be observed that the difference is indicated by means of $\tilde{\boldsymbol{F}}_{\omega_{pq},\beta_{SP}}$. The relation between the estimated and true control effectiveness is provided in Eq. 4.35, in which $\boldsymbol{\Gamma}_{\omega_{pq}}$ is the control effectiveness scaling factor.

$$\boldsymbol{F}_{\omega_{pq},\beta_{SP}} = \tilde{\boldsymbol{F}}_{\omega_{pq},\beta_{SP}} + \hat{\boldsymbol{F}}_{\omega_{pq},\beta_{SP}} \tag{4.34}$$

$$\hat{\boldsymbol{F}}_{\omega_{pq},\beta_{SP}} = \boldsymbol{\Gamma}_{\omega_{pq}}\boldsymbol{F}_{\omega_{pq},\beta_{SP}} \tag{4.35}$$

The tracking error derivative of the angular rate subsystem is given in Eq. 4.36. It should be noted that the first-order *Taylor* series with cyclic flapping angles with respect to the shaft plane are being considered, because it simplifies the derivation. In the first expression $\boldsymbol{F}_{\omega_{pq},\beta_{SP}}$ has been replaced with Eq. 4.34. In the second expression the stabilising control law for the angular rate subsystem from Eq. 4.18 is being substituted. It should be noted that $\boldsymbol{\beta}_{SP}$ is equal to $\boldsymbol{\theta}_C + \boldsymbol{\beta}_{CP}$ when incorporating this stabilising control law. In the

third expression the terms $\dot{\boldsymbol{\omega}}_0$ and $\dot{\boldsymbol{\omega}}_{\text{ref}}$ have cancelled. In the fourth expression $\tilde{\boldsymbol{F}}_{\omega_{pq},\beta_{SP}}\hat{\boldsymbol{F}}^{-1}_{\omega_{pq},\beta_{SP}}$ has been replaced by $\left(\boldsymbol{I}_{2x2}-\boldsymbol{\Gamma}_{\omega_{pq}}\right)\boldsymbol{\Gamma}^{-1}_{\omega_{pq}}$. The last expression is obtained by cancellation of $\boldsymbol{c}_{\omega_{pq}}\boldsymbol{z}_{\omega_{pq}}$.

$$
\begin{aligned}
\dot{\boldsymbol{z}}_{\omega_{pq}} &= \dot{\boldsymbol{\omega}}_{pq,0}+\left(\tilde{\boldsymbol{F}}_{\omega_{pq},\beta_{SP}}+\hat{\boldsymbol{F}}_{\omega_{pq},\beta_{SP}}\right)\Delta\boldsymbol{\beta}_{SP}-\dot{\boldsymbol{\omega}}_{pq,\text{ref}}\\
&= \dot{\boldsymbol{\omega}}_{pq,0}+\tilde{\boldsymbol{F}}_{\omega_{pq},\beta_{SP}}\hat{\boldsymbol{F}}^{-1}_{\omega_{pq},\beta_{SP}}\left[-\dot{\boldsymbol{\omega}}_{pq,0}+\dot{\boldsymbol{\omega}}_{pq,\text{ref}}-\boldsymbol{c}_{\omega_{pq}}\boldsymbol{z}_{\omega_{pq}}\right]+\\
&\quad \hat{\boldsymbol{F}}_{\omega_{pq},\beta_{SP}}\hat{\boldsymbol{F}}^{-1}_{\omega_{pq},\beta_{SP}}\left[-\dot{\boldsymbol{\omega}}_{pq,0}+\dot{\boldsymbol{\omega}}_{pq,\text{ref}}-\boldsymbol{c}_{\omega_{pq}}\boldsymbol{z}_{\omega_{pq}}\right]-\dot{\boldsymbol{\omega}}_{pq,\text{ref}}\\
&= \tilde{\boldsymbol{F}}_{\omega_{pq}}\hat{\boldsymbol{F}}^{-1}_{\omega_{pq}}\left[-\dot{\boldsymbol{\omega}}_{pq,0}+\dot{\boldsymbol{\omega}}_{pq,\text{ref}}-\boldsymbol{c}_{\omega_{pq}}\boldsymbol{z}_{\omega_{pq}}\right]-\boldsymbol{c}_{\omega_{pq}}\boldsymbol{z}_{\omega_{pq}}\\
&= \left(\boldsymbol{I}_{2x2}-\boldsymbol{\Gamma}_{\omega_{pq}}\right)\boldsymbol{\Gamma}^{-1}_{\omega_{pq}}\left[-\dot{\boldsymbol{\omega}}_{pq,0}+\dot{\boldsymbol{\omega}}_{pq,\text{ref}}-\boldsymbol{c}_{\omega_{pq}}\boldsymbol{z}_{\omega_{pq}}\right]-\boldsymbol{c}_{\omega_{pq}}\boldsymbol{z}_{\omega_{pq}}\\
&= \left(\boldsymbol{I}_{2x2}-\boldsymbol{\Gamma}_{\omega_{pq}}\right)\boldsymbol{\Gamma}^{-1}_{\omega_{pq}}\left[-\dot{\boldsymbol{\omega}}_{pq,0}+\dot{\boldsymbol{\omega}}_{pq,\text{ref}}\right]-\boldsymbol{\Gamma}^{-1}_{\omega_{pq}}\boldsymbol{c}_{\omega_{pq}}\boldsymbol{z}_{\omega_{pq}}
\end{aligned}
\tag{4.36}
$$

From Eq. 4.36 it can be observed that the scaling factor $\boldsymbol{\Gamma}_{\omega_{pq}}$ does affect the tracking error $\dot{\boldsymbol{z}}_{\omega_{pq}}$ of the angular rate subsystem. The analysis can be simplified by assuming that the control effectiveness scaling matrix $\boldsymbol{\Gamma}_{\omega_{pq}}$ is a diagonal matrix with constant $\gamma^{-1}_{\omega_{pq}}$ on its diagonal. When multiplying Eq. 4.36 with the aforementioned scalar and only considering roll acceleration, the following expression can be obtained

$$
\begin{aligned}
\dot{z}_p &= \left(\gamma_p^{-1}-1\right)\gamma_p\left[\dot{p}_0-\dot{p}_{\text{ref}}\right]-\gamma_p c_p z_p\\
&= \left(1-\gamma_p\right)\left[\dot{p}_0-\dot{p}_{\text{ref}}\right]-\gamma_p c_p z_p
\end{aligned}
\tag{4.37}
$$

It must be noted that $\gamma_p > 1$ represents underestimation of the control effectiveness. From Eq. 4.37 two distinct terms can be identified, which shall be discussed.

I $\left(1-\gamma_p\right)\left[\dot{p}_0-\dot{p}_{\text{ref}}\right]$: is the difference between the actual and desired angular acceleration scaled by $\left(1-\gamma_p\right)$. For $\gamma_p > 1$ it does represent the overcompensated accelerations, whereas for $\gamma_p < 1$ it does represent the untracked accelerations.

II $-\gamma_p c_p z_p$: indication for the rate at which the angular rate tracking error decays. Since the term is being multiplied by the control effectiveness scaling factor it can either be beneficial or disadvantageous. When $\gamma_p > 0$ (control effectiveness underestimation) the term becomes greater in magnitude and is therefore associated with a quicker convergence of the tracking error.

In [53, 55] it was pointed out that online parameter estimation techniques could be incorporated in order to adapt the control effectiveness matrix $\boldsymbol{F}_{\omega_{pq},\beta_{SP}}$. Adaption of $\boldsymbol{F}_{\omega_{pq},\beta_{SP}}$ could be achieved by means of integrated or modular adaptive techniques. This is however beyond the scope of the analysis and shall therefore not considered here. The main purpose was to illustrate that the proposed control strategy is more favourable over the previous one as it relies upon a single control effectiveness matrix for controlling the angular rates of the rotorcraft, rather than two. Moreover the control effectiveness $\boldsymbol{F}_{\omega_{pq},\beta_{SP}}$ is easier to establish than $\boldsymbol{G}_{\beta_{SP}}$. On top of this the control laws established for the final controller will be based upon the best off-line estimate of the control effectiveness matrix.

4.3.7. Rotor synchronisation filter - lag filter to compensate for difference between idealised and actual rotorcraft model

Previously the feedback signal of the actuator measurements had to be adjusted such that it was synchronised with the measurements of the angular accelerations. This was achieved by placing a second-order washout filter in the feedback-loop of the actuator measurement. However, it did not yet take into account the difference between the *actual* and *idealised* rotorcraft model. An additional modification needs to be applied to this feedback signal to compensate for this difference. The latter model is the one that is being used for establishing the IBS control law, because it is associated with an enhanced control- to state-dependency ratio. The *idealised* model is based upon residualisation of internal dynamics, especially flapping dynamics.

This is because the body-flap coupling is large and residualisation of flapping dynamics would diminish this coupling term and use it to enhance the control-dependency. The aforementioned especially holds for the angular accelerations ($\dot{p}$ and $\dot{q}$) as these are primarily governed by the cyclic flapping angles (β_{1s} and β_{1c}). The difference between the *idealised* model based upon flap residualisation (steady-state flapping dynamics) and the *actual* rotorcraft model can be accounted for by means of a synchronisation filter. This filter does essentially reconstruct the *actual* open-loop frequency response, because $H_{\text{acutal}}(s)$ should be approximately equal to $H_{\text{sync}}(s)$ multiplied with $H_{\text{ideal}}(s)$. The synchronisation filter will assure that $\boldsymbol{\theta}_{C,\text{meas}}$ is effectively delayed by the same amount as by which angular accelerations are being delayed due to the *actual* rotorcraft dynamics.

In order to establish the rotor synchronisation filter it is first necessary to determine the *idealised* and *actual* expressions for the angular accelerations. For the derivation only flapping dynamics shall be considered as internal dynamics. The *actual* expression for the angular accelerations can be written as follows

$$\dot{\boldsymbol{\omega}}_{pq} = \boldsymbol{F}_{\omega_{pq},\beta_{SP}}\boldsymbol{\beta}_{SP} + \boldsymbol{H}_{\omega_{pq}}\boldsymbol{\theta}_{C,\text{meas}}, \tag{4.38}$$

wherein $\boldsymbol{\theta}_{C,\text{meas}}$ are the delayed actuator measurements after being fed through the second-order washout filter. Moreover, $\boldsymbol{\beta}_{SP}$ are the cyclic flapping angles with respect to the shaft plane. On top of this, $\boldsymbol{F}_{\omega_{pq},\beta_{SP}}$ and $\boldsymbol{H}_{\omega_{pq}}$ are the body-flap coupling and control-depended term of the angular accelerations respectively. It should be noted that it was assumed that the body-flap coupling is significantly greater than other coupling terms. When the body-lag or body-inflow coupling terms are large, then Eq. 4.38 should actually be augmented by taking these state-dependencies into account. The *idealised* rotorcraft model is assumed to be purely governed by cyclic control inputs only, therefore the angular accelerations can be written as

$$\dot{\boldsymbol{\omega}}_{pq} = \hat{\boldsymbol{G}}_{\omega_{pq}}\boldsymbol{\theta}_{C,\text{sync}}. \tag{4.39}$$

It should be noted from the previous equation that $\hat{\boldsymbol{G}}_{\omega_{pq}}$ needs to be established by means of the *method of residualised dynamics*, since it would yield the most direct relation between the angular accelerations and cyclic control inputs. The synchronised control inputs can there after be obtained by inverting Eq. 4.39 and substituting the expression from Eq. 4.38 into it. The synchronised control inputs are

$$\boldsymbol{\theta}_{C,\text{sync}} = \hat{\boldsymbol{G}}^{-1}_{\omega_{pq}}\left[\boldsymbol{F}_{\omega_{pq},\beta_{SP}}\boldsymbol{\beta}_{SP} + \boldsymbol{H}_{\omega_{pq}}\boldsymbol{\theta}_{C,\text{meas}}\right]. \tag{4.40}$$

From Eq. 4.40 it can be observed that $\boldsymbol{\beta}_{SP}$ is also required, which can be considered the synchronised flapping angles. These synchronised flapping angles will differ from the *actual* flapping angles. The aforementioned synchronised flapping angles can be determined using the expression given in Eq. 4.41. It can be observed that $\dot{\boldsymbol{\beta}}_{SP}$ is purely governed by the measured cyclic control inputs.

$$\dot{\boldsymbol{\beta}}_{SP} = \boldsymbol{F}_{\beta_{SP},\beta_{SP}}\boldsymbol{\beta}_{SP} + \boldsymbol{H}_{\beta_{SP}}\boldsymbol{\theta}_{C,\text{meas}}. \tag{4.41}$$

The synchronisation filter can be defined in the *Laplace*-domain. This requires Eq. 4.40 and Eq. 4.41 to be rewritten into *Laplace*-domain as well. The synchronisation filter defined in the *Laplace*-domain is

$$\boldsymbol{H}_{\text{sync}}(s) = \frac{\boldsymbol{\theta}_{C,\text{sync}}(s)}{\boldsymbol{\theta}_{C,\text{meas}}(s)} = \frac{\hat{\boldsymbol{G}}^{-1}_{\omega_{pq}}\boldsymbol{F}_{\omega_{pq},\beta_{SP}}\boldsymbol{H}_{\beta_{SP}} + \hat{\boldsymbol{G}}^{-1}_{\omega_{pq}}\boldsymbol{H}_{\omega_{pq}}s - \hat{\boldsymbol{G}}^{-1}_{\omega_{pq}}\boldsymbol{F}_{\beta_{SP},\beta_{SP}}\boldsymbol{H}_{\omega_{pq}}}{s\boldsymbol{I}_{2x2} - \boldsymbol{F}_{\beta_{SP},\beta_{SP}}}. \tag{4.42}$$

From Eq. 4.42 it can be observed that accurate knowledge of the control effectiveness matrix $\hat{\boldsymbol{G}}_{\omega_{pq}}$ is required. It also depends on the synchronised flapping angles $\boldsymbol{\beta}_{SP}$, which require an accurate model of the flapping dynamics. This means that $\boldsymbol{F}_{\beta_{SP},\beta_{SP}}$ and $\boldsymbol{H}_{\beta_{SP}}$ must be well-known as well. Moreover there must also be accurate and reliable knowledge of $\boldsymbol{H}_{\omega_{pq}}$ and $\boldsymbol{F}_{\omega_{pq},\beta_{SP}}$ for establishing the synchronisation filter. This would require parameter estimation techniques for determining the control- and state-depended terms of interest. For the purpose of the analysis it does suffice to opt for a model-based strategy. Next to this, $\boldsymbol{\theta}_{C,\text{meas}}$ can be measured and is therefore not of prime concern.

In Fig. 4.3 the flapping synchronisation filter is provided in the feedback-loop of the actuator measurement. It should be noted that only flapping dynamics was considered for the synchronisation filter design. However, as outlined earlier, the filter is incorporated to account for the difference in frequency response

between the *idealised* and *actual* rotorcraft model. When other internal dynamics such as inflow or lead-lag dynamics needs to be residualised as well to enhance the control- to state-dependency ratio for improving the TSS condition, then it shall also be accounted for in synchronisation filter design.

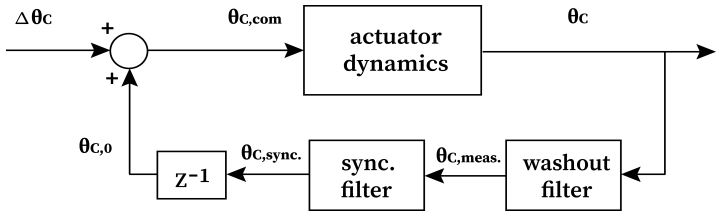

Figure 4.3: Synchronisation filter placed in feedback-loop of actuator measurement.

4.3.8. Closed-loop system with synchronisation filter defined in Laplace-domain

Previously it has been outlined that rotor synchronisation is required to synchronise actuator measurements with angular acceleration measurements, because of rotor dynamics. Moreover it was also necessary to put a second-order washout filter in the feedback-loop of the actuator measurement. This subsequently means that the closed-loop system will be adjusted with respect to the *nominal* case. Not including the synchronisation filter will most likely affect closed-loop system response/stability. In previous research it was found that delaying the state derivative measurements with respect to the actuator measurements will yield magnified control inputs, which subsequently could yield inadequate system response or even fast system instability [57]. Moreover delaying the actuator measurements with respect to state derivative measurements will yield damped control inputs, which results in slow system response and therefore also slow system instability [57].

The closed-loop system shall be considered for the angular rate controller using the stabilising control law from Eq. 4.21 for which the *Laplace* transform is provided in the first expression of Eq. 4.43. It should be noted that the continuous *Laplace* transformation is being incorporated for representing the closed-loop system. Since the controller is actually a discrete system it would be more appropriate to incorporate the discrete-time equivalent of the *Laplace* transformation, namely the *Z-transform* [57]. For this particular research the continuous-time variant shall be used as discrete effects are not of prime interest. The second expression of Eq. 4.43 is obtained by substituting the expression for $\boldsymbol{\nu}_{pq}(s)$ into it. Next to this, the third expression is obtained by substituting the expression for $\boldsymbol{z}_{\omega pq}(s)$ into it. The last expression does isolate the terms $\boldsymbol{\omega}_{pq}(s)$ and $\boldsymbol{\omega}_{pq,\text{ref}}(s)$.

$$
\begin{aligned}
\boldsymbol{\theta}_C(s) &= \boldsymbol{\theta}_C(s)e^{-\Delta t s} + \boldsymbol{I}_{\text{cor}}\hat{\boldsymbol{F}}^{-1}_{\omega_{pq},\beta_{SP}}\left[\boldsymbol{\nu}(s) - s\boldsymbol{\omega}_{pq}(s)e^{-\Delta t s}\right] \\
&= \boldsymbol{\theta}_C(s)e^{-\Delta t s} + \boldsymbol{I}_{\text{cor}}\hat{\boldsymbol{F}}^{-1}_{\omega_{pq},\beta_{SP}}\left[-\boldsymbol{c}_{\omega_{pq}}\boldsymbol{z}_{\omega_{pq}}(s) + s\boldsymbol{\omega}_{pq,\text{ref}}(s) - s\boldsymbol{\omega}_{pq}(s)e^{-\Delta t s}\right] \\
&= \boldsymbol{\theta}_C(s)e^{-\Delta t s} + \boldsymbol{I}_{\text{cor}}\hat{\boldsymbol{F}}^{-1}_{\omega_{pq},\beta_{SP}}\left[-\boldsymbol{c}_{\omega_{pq}}\boldsymbol{\omega}_{pq}(s) + \boldsymbol{c}_{\omega_{pq}}\boldsymbol{\omega}_{pq,\text{ref}}(s) + s\boldsymbol{\omega}_{pq,\text{ref}}(s) - s\boldsymbol{\omega}_{pq}(s)e^{-\Delta t s}\right] \\
&= \left[\boldsymbol{I}_{2x2} - e^{-\Delta t s}\boldsymbol{I}_{2x2}\right]^{-1}\boldsymbol{I}_{\text{cor}}\hat{\boldsymbol{F}}^{-1}_{\omega_{pq},\beta_{SP}}\left[-\boldsymbol{c}_{\omega_{pq}}\boldsymbol{\omega}_{pq}(s) - s\boldsymbol{\omega}_{pq}(s)e^{-\Delta t s}\right] + \\
&\quad \left[\boldsymbol{I}_{2x2} - e^{-\Delta t s}\boldsymbol{I}_{2x2}\right]^{-1}\boldsymbol{I}_{\text{cor}}\hat{\boldsymbol{F}}^{-1}_{\omega_{pq},\beta_{SP}}\left[\boldsymbol{c}_{\omega_{pq}}\boldsymbol{\omega}_{pq,\text{ref}}(s) + s\boldsymbol{\omega}_{pq,\text{ref}}(s)\right]
\end{aligned}
\tag{4.43}
$$

In Eq. 4.44 the closed-loop system is augmented by accounting for sensor ($\boldsymbol{H}_{\text{filt}}(s)$) and actuator ($\boldsymbol{H}_{\text{act}}(s)$) dynamics. These are both diagonal matrices with the sensor and actuator dynamics on their diagonal.

$$
\begin{aligned}
\boldsymbol{\theta}_C(s) = \left[\boldsymbol{I}_{2x2} - \boldsymbol{H}_{\text{act}}(s)\boldsymbol{H}_{\text{filt}}(s)e^{-\Delta t s}\right]^{-1}\Big(&\boldsymbol{I}_{\text{cor}}\hat{\boldsymbol{F}}^{-1}_{\omega_{pq},\beta_{SP}}\left[-\boldsymbol{H}_{\text{act}}(s)\boldsymbol{c}_{\omega_{pq}}\boldsymbol{\omega}_{pq}(s) - s\boldsymbol{H}_{\text{act}}(s)\boldsymbol{H}_{\text{filt}}(s)\boldsymbol{\omega}_{pq}(s)e^{-\Delta t s}\right] + \\
&\boldsymbol{I}_{\text{cor}}\hat{\boldsymbol{F}}^{-1}_{\omega_{pq},\beta_{SP}}\left[\boldsymbol{H}_{\text{act}}(s)\boldsymbol{c}_{\omega_{pq}}\boldsymbol{\omega}_{pq,\text{ref}}(s) + s\boldsymbol{H}_{\text{act}}(s)\boldsymbol{\omega}_{pq,\text{ref}}(s)\right]\Big)
\end{aligned}
\tag{4.44}
$$

In addition to actuator and sensor dynamics, system dynamics $\boldsymbol{H}_{\omega_{pq}}(s)$ ($\boldsymbol{\omega}_{pq}(s) = \boldsymbol{H}_{\omega_{pq}}(s)\boldsymbol{\theta}_C(s)$) must also be accounted for, thus Eq. 4.44 needs to be rewritten into the following form

$$\boldsymbol{\omega}_{pq}(s) = \left[\boldsymbol{I}_{2x2} - \boldsymbol{H}_{\text{act}}(s)\boldsymbol{H}_{\text{filt}}(s)e^{-\Delta ts}\right]^{-1}\left(\boldsymbol{I}_{\text{cor}}\hat{\boldsymbol{F}}^{-1}_{\omega_{pq},\beta_{SP}}\left[-\boldsymbol{H}_{\text{act}}(s)\boldsymbol{c}_{\omega_{pq}}\boldsymbol{\omega}_{pq}(s) - s\boldsymbol{H}_{\text{act}}(s)\boldsymbol{H}_{\text{filt}}(s)\boldsymbol{\omega}_{pq}(s)e^{-\Delta ts}\right] + \boldsymbol{I}_{\text{cor}}\hat{\boldsymbol{F}}^{-1}_{\omega_{pq},\beta_{SP}}\left[\boldsymbol{H}_{\text{act}}(s)\boldsymbol{c}_{\omega_{pq}}\boldsymbol{\omega}_{pq,\text{ref}}(s) + s\boldsymbol{H}_{\text{act}}(s)\boldsymbol{\omega}_{pq,\text{ref}}(s)\right]\right)\boldsymbol{H}_{\omega_{pq}}(s). \tag{4.45}$$

To account for the difference in *idealised* and *actual* rotorcraft model it is necessary to include the rotor synchronisation filter $\boldsymbol{H}_{\text{sync}}(s)$ in the feedback loop of the actuator measurements. Inclusion of $\boldsymbol{H}_{\text{sync}}(s)$ does require Eq. 4.45 to be rewritten into

$$\boldsymbol{\omega}_{pq}(s) = \left[\boldsymbol{I}_{2x2} - \boldsymbol{H}_{\text{sync}}(s)\boldsymbol{H}_{\text{act}}(s)\boldsymbol{H}_{\text{filt}}(s)e^{-\Delta ts}\right]^{-1}\left(\boldsymbol{I}_{\text{cor}}\hat{\boldsymbol{F}}^{-1}_{\omega_{pq},\beta_{SP}}\left[-\boldsymbol{H}_{\text{act}}(s)\boldsymbol{c}_{\omega_{pq}}\boldsymbol{\omega}_{pq}(s) - s\boldsymbol{H}_{\text{act}}(s)\boldsymbol{H}_{\text{filt}}(s)\boldsymbol{\omega}_{pq}(s)e^{-\Delta ts}\right] + \boldsymbol{I}_{\text{cor}}\hat{\boldsymbol{F}}^{-1}_{\omega_{pq},\beta_{SP}}\left[\boldsymbol{H}_{\text{act}}(s)\boldsymbol{c}_{\omega_{pq}}\boldsymbol{\omega}_{pq,\text{ref}}(s) + s\boldsymbol{H}_{\text{act}}(s)\boldsymbol{\omega}_{pq,\text{ref}}(s)\right]\right)\boldsymbol{H}_{\omega_{pq}}(s). \tag{4.46}$$

Isolating all $\boldsymbol{\omega}_{pq}(s)$-terms on the left hand side and all $\boldsymbol{\omega}_{pq,\text{ref}}(s)$-terms on the right hand side enables to rewrite Eq. 4.46 as follows

$$\boldsymbol{\omega}_{pq}(s) - \left[\boldsymbol{I}_{2x2} - \boldsymbol{H}_{\text{sync}}(s)\boldsymbol{H}_{\text{act}}(s)\boldsymbol{H}_{\text{filt}}(s)e^{-\Delta ts}\right]^{-1}\boldsymbol{I}_{\text{cor}}\hat{\boldsymbol{F}}^{-1}_{\omega_{pq},\beta_{SP}}\left[-\boldsymbol{c}_{\omega_{pq}}\boldsymbol{H}_{\text{act}}(s) - se^{-\Delta ts}\boldsymbol{H}_{\text{sens}}(s)\boldsymbol{H}_{\text{act}}(s)\right]\boldsymbol{H}_{\omega_{pq}}(s)\boldsymbol{\omega}_{pq}(s) = \left[\boldsymbol{I}_{2x2} - \boldsymbol{H}_{\text{sync}}(s)\boldsymbol{H}_{\text{act}}(s)\boldsymbol{H}_{\text{filt}}(s)e^{-\Delta ts}\right]^{-1}\boldsymbol{I}_{\text{cor}}\hat{\boldsymbol{F}}^{-1}_{\omega_{pq},\beta_{SP}}\left[\boldsymbol{H}_{\text{act}}(s)\boldsymbol{c}_{\omega_{pq}} + s\boldsymbol{H}_{\text{act}}(s)\right]\Big)\boldsymbol{H}_{\omega_{pq}}(s)\boldsymbol{\omega}_{pq,\text{ref}}(s). \tag{4.47}$$

The closed loop response $\frac{\boldsymbol{\omega}_{pq}(s)}{\boldsymbol{\omega}_{pq,\text{ref}}(s)}$ can thus be written as follows

$$\frac{\boldsymbol{\omega}_{pq}(s)}{\boldsymbol{\omega}_{pq,\text{ref}}(s)} = \frac{\left[\boldsymbol{I}_{2x2} - \boldsymbol{H}_{\text{sync}}(s)\boldsymbol{H}_{\text{act}}(s)\boldsymbol{H}_{\text{filt}}(s)e^{-\Delta ts}\right]^{-1}\boldsymbol{I}_{\text{cor}}\hat{\boldsymbol{F}}^{-1}_{\omega_{pq},\beta_{SP}}\left[\boldsymbol{H}_{\text{act}}(s)\boldsymbol{c}_{\omega_{pq}} + s\boldsymbol{H}_{\text{act}}(s)\right]\Big)\boldsymbol{H}_{\omega_{pq}}(s)}{\boldsymbol{I}_{2x2} - \left[\boldsymbol{I}_{2x2} - \boldsymbol{H}_{\text{sync}}(s)\boldsymbol{H}_{\text{act}}(s)\boldsymbol{H}_{\text{filt}}(s)e^{-\Delta ts}\right]^{-1}\boldsymbol{I}_{\text{cor}}\hat{\boldsymbol{F}}^{-1}_{\omega_{pq},\beta_{SP}}\left[-\boldsymbol{c}_{\omega_{pq}}\boldsymbol{H}_{\text{act}}(s) - se^{-\Delta ts}\boldsymbol{H}_{\text{sens}}(s)\boldsymbol{H}_{\text{act}}(s)\right]\boldsymbol{H}_{\omega_{pq}}(s)}, \tag{4.48}$$

Important to note is that the *flapping angle equivalence method* was incorporated for establishing the stabilising control law, therefore the control effectiveness used in the closed-loop frequency response from Eq. 4.48 is in accordance with that method. The *method of residualised dynamics* could also be used for defining the control effectiveness of the IBS control law. However, the synchronisation filter must be established by means of the *method of residualised dynamics*, because it would yield the most direct relationship between the angular accelerations and the cyclic control inputs. The *flapping angle equivalence method* only accounts for the body-flap coupling for establishing the control effectiveness, whereas the *method of residualised dynamics* can account for other body-rotor couplings for enhancing the control- to state-dependency ratio. This implies that when the synchronisation filter is established by means of flap residualisation only, the control effectiveness based upon the *flapping angle equivalence method* and *method of residualised dynamics* should be approximately the same. However, when the control effectiveness is found to be insufficient by only considering steady-state flapping dynamics, it is deemed necessary to consider residualisation of additional internal dynamics such as inflow or lead-lag to enhance the control- to state-dependency ratio. This would subsequently yield a synchronisation filter based upon residualisation of all the aforementioned rotor dynamics (flap, lag and/or inflow) for which the control effectiveness would be different from the one obtained by *flapping angle equivalence method*. This shows that there are some restrictions for this method. In the end it must be realised that the main objective is to assure a well-established controller for which TSS holds, otherwise the controller cannot be considered robust to uncertainties in system dynamics.

5

Rotor Synchronisation applied to varying DOF rotorcraft Models

In previous chapters the theoretical framework was established, therefore the next step is to apply a *Lyapunov*-based controller to a set of simplified rotorcraft models established earlier. As outlined in the previous chapter the main crux in control design does finds its roots in the design of the angular rate controller, therefore the analysis to be conducted in this chapter shall focus on this controller. The main objective of this chapter can be formulated as follows: analysing the necessity of feedback synchronisation for rotorcraft models associated with rotor dynamics and in particular flapping dynamics. The analysis will involve determining the natural modes of motion and open-loop *Bode* frequency response, executing an ADS-33E-PRF tracking task, determining closed-loop stability and closed-loop frequency response.

With the general procedure being outlined and the motivation for performing being explained, it is deemed necessary to briefly mention the rotorcraft models that will be analysed. In section 5.1 a 2-DOF steady-state flapping model will be considered in hover condition. It will be shown that rotorcraft models associated with steady-state flapping dynamics do not require flapping synchronisation. Steady-state flapping dynamics may suffice for some rotorcraft models, but for others it will not adequately mimic disc tilt motion. This naturally requires the need to analyse the effect of flapping dynamics on *Lyapunov*-based control design and in particular IBS. In section 5.2 a 2-DOF τ_β-based rotorcraft model with flapping dynamics will be considered, wherein τ_β is an indication of disc-tilt quickness. It will be shown that the problem lies therein that *Lyapunov*-based controllers are based upon steady-state flapping dynamics (residualisation of flapping dynamics), whereas the *actual* rotorcraft model is associated with non-instantaneous disc-tilt motion. Accounting for this discrepancy can be achieved by adjusting the feedback loop of the actuator measurements. Residualisation of the internal dynamics is necessary to diminish state-dependency in a first-order *Taylor* series and to increase state-dependency such that the time-scale separation condition of IBS is not or less likely violated. If the aforementioned condition would be violated, the stabilising control law should take into account system dynamics, which might not be favourable. It will be shown that for some rotorcraft models flapping synchronisation is a requisite to assure adequate controller performance.

From the obtained results obtained from the simple rotorcraft models a conclusion can be drawn of the necessity of accounting for flapping when designing the rotor synchronisation filter. This will provide adequate priori knowledge to build a *Lyapunov*-based controller for rotorcraft consisting of more DOF. Inclusion of lead-lag dynamics might affect the design of an IBS controller as well, therefore the knowledge obtained from the simple rotorcraft models will yield a prediction whether that indeed will be the case.

5.1. First order steady-state flapping model specified for hover condition

In this section a 2-DOF BF model with steady-state flapping dynamics will be considered. This model does consists of body state q and flapping state β_{1c}. Moreover hub stiffness K_β can be varied, whereas γ and Ω are set equal to 6 and 30 rad/s respectively. When rotor disc-tilt dynamics is being neglected then cyclic control inputs will become identical to rotor disc-tilt angles yielding instantaneous tilting of the rotor disc [16]. This is favourable in control design as it yields a direct relation between angular rates and cyclic control inputs. Most importantly the BF model on which the controller is based upon (*idealised* model) will be identical to the *actual* rotorcraft model. Compensating for differences in *idealised* and *actual* BF rotorcraft model (e.g.flapping dynamics) will not be necessary.

5.1.1. Natural modes of motion for varying K_β

First the natural modes of motion of the rotorcraft for varying hub stiffness K_β will be considered. For each K_β there will only be one mode of motion which is situated at $-\frac{16K_{\text{lon}}}{\gamma\Omega}$. In Fig. 5.1 the pitch subsidence mode is shown for varying K_β. All modes are situated on the real axis and can be regarded as an exponentially decaying component. The rate of decay is entirely determined by pole location [35]. The pitch subsidence mode moves closer to the origin for smaller K_β and will therefore be associated with slower response.

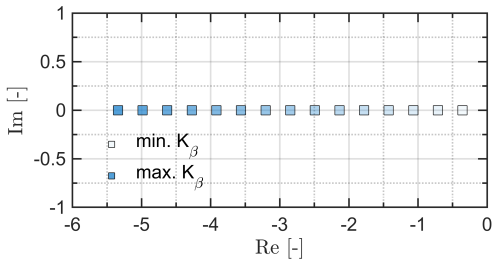

Figure 5.1: Natural modes of motion of 2-DOF steady-state flapping model for $K_\beta \in [10, 20, ..., 150]$ kNm/rad.

5.1.2. Control effectiveness established by means of method of residualised dynamics or flapping angle equivalence principle

In order to establish an IBS control law it is necessary to determine the control effectiveness of $\dot{q}$ with respect to θ_{1c}. In order to determine $\hat{G}_q$ the *method of residualised dynamics* or *flapping angle equivalence principle* could be used. The former method requires the use of steady-state flapping dynamics for which the expression is provided in Eq. 5.1. It can be observed that $\hat{G}_q$ must be equal to K_{lon}, which is because $F_{q,\beta_{1c}} F^{-1}_{\beta_{1c},\beta_{1c}} G_{\beta_{1c}}$ is equal to 0. The estimated control effectiveness must therefore be equal to the control-depended term of $\dot{q}$.

$$\hat{G}_q = G_q - F_{q,\beta_{1c}} F^{-1}_{\beta_{1c},\beta_{1c}} G_{\beta_{1c}} = K_{\text{lon}} \tag{5.1}$$

The *flapping angle equivalence principle* can also be incorporated for determining $\hat{G}_q$, which requires knowledge of $F_{q,\beta_{1c}}$ and transformation from IBCs to MBCs. This transformation is given in Eq. 4.11 and is necessary to obtain the correct sign for the control effectiveness. It should be noted that a positive *Fourier* series was used for this transformation. From this method it also would follow that $\hat{G}_q$ must be equal to K_{lon}, as $\beta_{1c_{SP}} = \beta_{1c_{CP}} - \theta_{1s}$. From both methods it can be observed that $\hat{G}_q \propto K_{\text{lon}}$. It is important to note that the control effectiveness of the steady-state BF model was established based upon the *actual* model, rather than an *idealised* model. Control effectiveness mismatch is indicated as $\hat{G}_q = \gamma_q G_q$, wherein $\gamma_q > 1$ and $\gamma_q < 1$ imply over- and underestimation respectively.

5.1.3. Stabilising control law for angular rate subsystem using IBS

To control the pitch rate of the rotorcraft it is necessary to establish a stabilising control law. Here an incremental-based control strategy is being pursued as such a strategy will also be considered for the full rotorcraft model. A *Taylor* series of the following form shall be used

$$\dot{q} \cong \dot{q}_0 + F_{q,q}\Delta q + \hat{G}_q \Delta\theta_{1s}, \quad \text{with} \quad \Delta q = q - q_0 \quad \text{and} \quad \Delta\theta_{1s} = \theta_{1s} - \theta_{1s,0}, \tag{5.2}$$

wherein $\dot{q}_0$ and $\theta_{1s,0}$ are the current pitch rate derivative and longitudinal cyclic control input measurement respectively. Moreover, Δq and $\Delta\theta_{1s}$ are the incremental state and control input respectively. The *Taylor* series from Eq. 5.2 can be simplified by assuming *time-scale separation*. This implies that $F_{q,q}\Delta q$ can be neglected with respect to $\Delta\dot{q}$ and $\hat{G}_q\Delta\theta_{1s}$ [1, 45, 46, 54]. The *time-scale separation* condition is

$$\hat{G}_q\Delta\theta_{1s} >> F_{q,q}\Delta q, \quad \text{with} \quad F_{q,q} = -\frac{16K_{\text{lon}}}{\gamma\Omega} \quad \text{and} \quad \hat{G}_q = \gamma_q K_{\text{lon}}. \tag{5.3}$$

This is equivalent by stating that control action is instantaneous given that sampling rate f_s is sufficiently high [54]. When Eq. 5.3 does not hold then it will not be robust to system dynamics. The above TSS condition will very likely hold as $\hat{G}_q >> F_{q,q}$. However, actuator limitations may affect the condition. The control law is

$$\theta_{1s} = \theta_{1s,0} + \hat{G}_q^{-1}\left[-\dot{q}_0 + \dot{q}_{\text{ref}} - c_q z_q\right]. \tag{5.4}$$

Validation of Eq. 5.3 shall be considered when performing the longitudinal *ADS-33E-PRF* tracking task.

5.1.4. Open-loop frequency response for varying K_β, Ω and γ_q

It is also of great interest to get insight in the *Bode* frequency response of the rotorcraft model with steady-state flapping dynamics. The pitch rate to longitidinal cyclic transfer function is

$$H_q(s) = \frac{q(s)}{\theta_{1s}(s)} = \left(\frac{\gamma\Omega}{16}\right)\frac{1}{\frac{\gamma\Omega}{16K_{\text{lon}}}s + 1}, \tag{5.5}$$

which is written in standard *Bode* form. It does consists of a gain and first-order lag term.

In Fig. 5.2 *Bode* frequency response is provided for different combinations of K_β, Ω and γ. It can be observed that magnitude bandwidth reduces when K_β is being reduced and is therefore associated with slower response. Reducing K_β is also apparent from the phase response as it drops quicker towards $-90°$. From Fig. 5.2 it can also be observed that increasing γ does yield an increase in magnitude at low frequencies, but on the other hand it also reduces magnitude bandwidth. Moreover phase angle did drop quicker towards $-90°$ for smaller γ. Furthermore increasing Ω did have the same effect on magnitude and phase response when increasing Ω, which can be observed from Eq. 5.5.

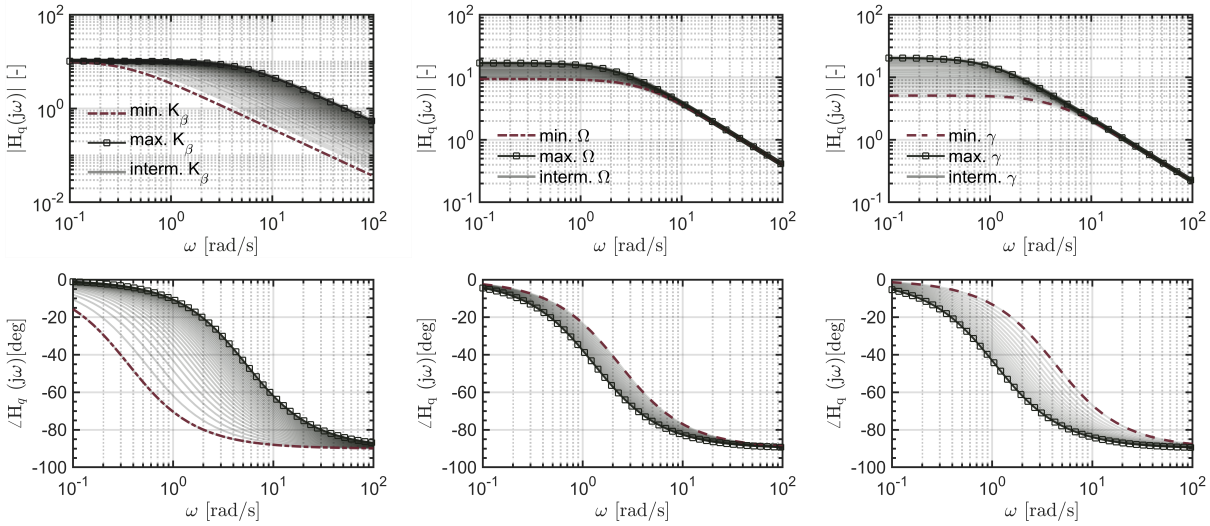

Figure 5.2: *Bode* frequency response of steady-flapping model showing the effect of variations in K_β, Ω and γ (from left to right). Variation in K_β is considered for $K_\beta \in [10, 20, ..., 150]$ kNm/rad, $\gamma = 6$ and $\Omega = 30$rad/s. Moreover variation in Ω is provided for $\Omega \in [25, 26, ..., 45]$ rad/s, $\gamma = 6$ and $K_\beta = 110$kNm/rad. Lastly variation in γ is given for $\gamma \in [3, 3.5, ..., 12]$, $\Omega = 30$ rad/s and $k_\beta = 110$ kNm/rad.

5.1.5. Longitudinal ADS-33E-PRF tracking task for varying K_β and γ_q

Lyapunov-based control performance shall be assessed by means of a longitudinal tracking task wherein the main objective is to let the rotorcraft track a predefined pitch rate of ±30°. This is in accordance with regulations stipulated by the ADS-33E-PRF [5]. The main objective is to determine whether the *Lyapunov*-based controller is robust to uncertainties in control effectiveness and to assess whether the IBS condition from Eq. 5.3 will be violated. It is very unlikely that this condition will be violated as $\Omega\gamma >> 16$. The longitudinal tracking task shall be executed using either full and accurate knowledge of $\hat{G}_q$ or partial and inaccurate knowledge of $\hat{G}_q$. Moreover an aggressive controller is considered for which $c_q = 15$. On top of this hub stiffness will be varied between 10 kNm/rad and 150 kNm/rad in steps of 10 kNm/rad. The following cases will be considered

- $\gamma_q = 1$ (no control effectiveness mismatch).
- $\gamma_q = 0.5$ (control effectiveness underestimation).
- $\gamma_q = 3$ (control effectiveness overestimation).

In Fig. 5.3-5.4 the results of the above mentioned cases are provided respectively.

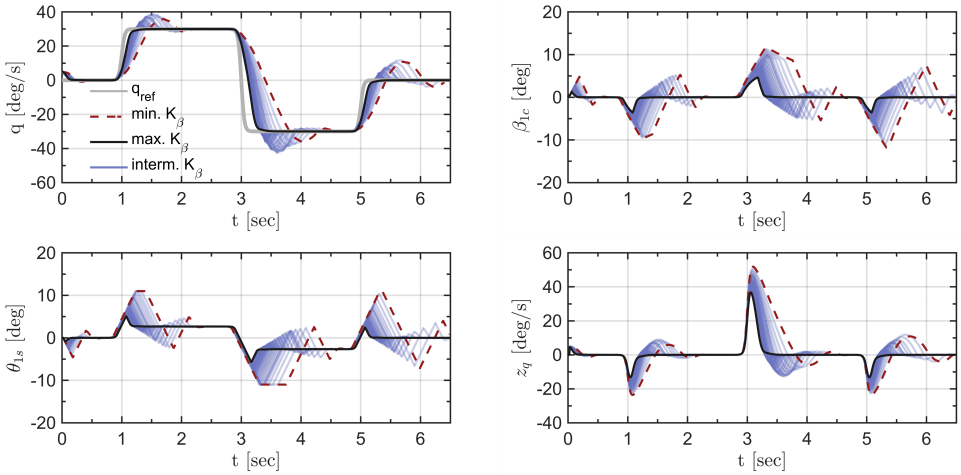

Figure 5.3: Results of longitudinal tracking tasks for steady-state BF model with $\gamma_q = 1$, $K_\beta \in [10, 20.., 150]$kNm/rad and $c_q = 15$. Rotorcraft states q and β_{1c}, control input θ_{1s} and tracking error z_q are provided.

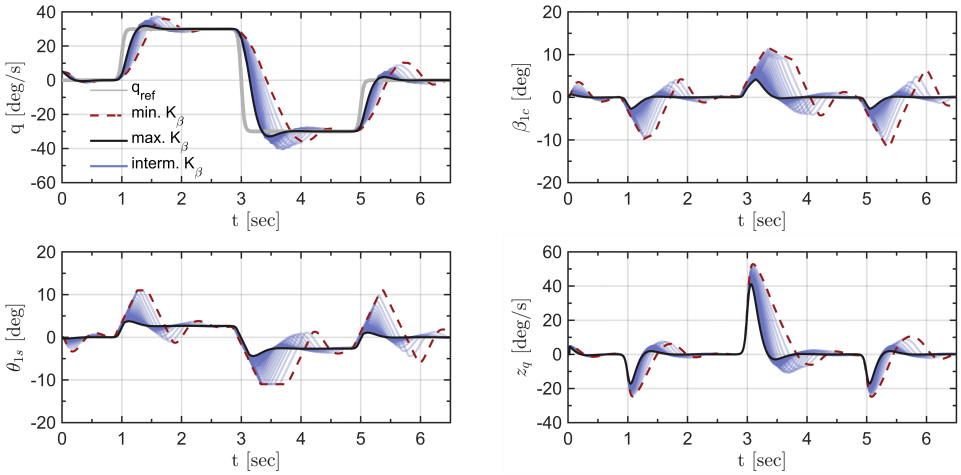

Figure 5.4: Results of longitudinal tracking tasks for steady-state BF model with $\gamma_q = 3$, $K_\beta \in [10, 20.., 150]$kNm/rad and $c_q = 15$. Rotorcraft states q and β_{1c}, control input θ_{1s} and tracking error z_q are provided.

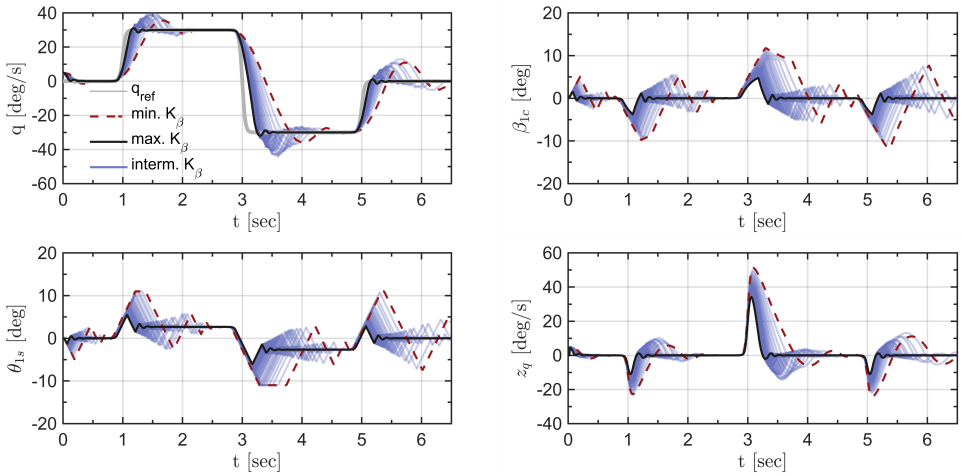

Figure 5.5: Results of longitudinal tracking tasks for steady-state BF model with $\gamma_q = 0.5$, $K_\beta \in [10, 20.., 150]$kNm/rad and $c_q = 15$. Rotorcraft states q and β_{1c}, control input θ_{1s} and tracking error z_q are provided.

It can be observed from the results that for all K_β the longitudinal tracking task can be executed. Moreover, for larger K_β it is easier to execute the aggressive manoeuvre. This is in line with observations from the frequency analysis as larger K_β is associated with quicker response. Decreasing K_β does yield more overreaction and difficulty in following q_{ref}. Most importantly the controller is robust to uncertainties in control effectiveness as the longitudinal tracking task could still be executed with adequate performance. In Fig. 5.6 control and state-dependency are provided of the previous conducted longitudinal tracking task.

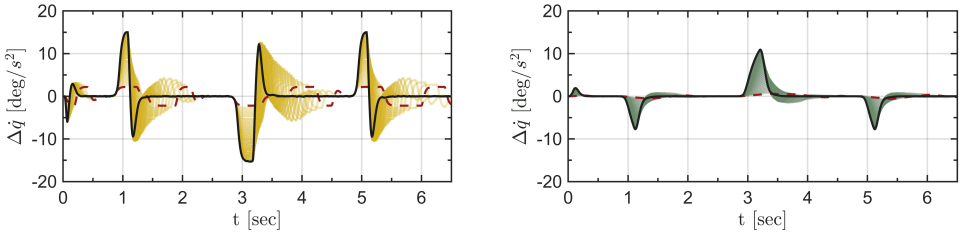

(a) Control- and state-dependency for $\gamma_q = 1$ respectively.

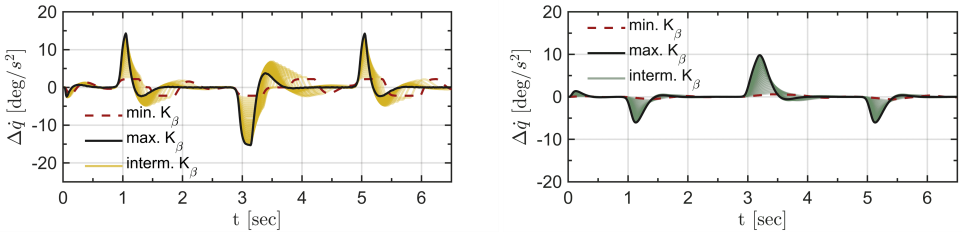

(b) Control- and state-dependency for $\gamma_q = 3$ respectively.

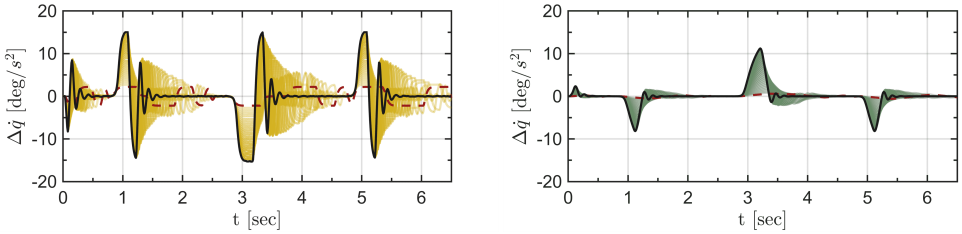

(c) Control- and state-dependency for $\gamma_q = 0.5$ respectively.

Figure 5.6: Control- and state-dependency are provided for longitudinal tracking tasks using steady-state BF model with $K_\beta \in [10, 20.., 150]$ kNm/rad, $\gamma_q \in [0.5, 1, 3]$ and $c_q = 15$.

It can be observed that control dependency is greater than state-dependency, thus not violating the IBS condition from Eq. 5.3. The aforementioned even holds for $\gamma_q < 1$. This shows that incremental-based control design such as IBS can be incorporated for rotorcraft models with steady-state flapping dynamics. It should also be noted that control-dependency is limited due to actuator limitations. This shows that physical limitations of rotorcraft can be problematic regarding the TSS condition. In this example large actuator deflections were considered, namely $\theta_{1s,\max} = 11°$, $\theta_{1s,\min} = -11°$ and $\dot{\theta}_{1s,\max} = \pm 28°/s$

Previously it has been mentioned that decreasing K_β will yield performance degradation. This is apparent from the $RMSE_q$ given in Fig. 5.7 as it indeed increases for decreasing K_β. Moreover, it can also be observed that the controller is robust to uncertainties in control effectiveness as performance is fairly similar among the three control effectiveness mismatch factors.

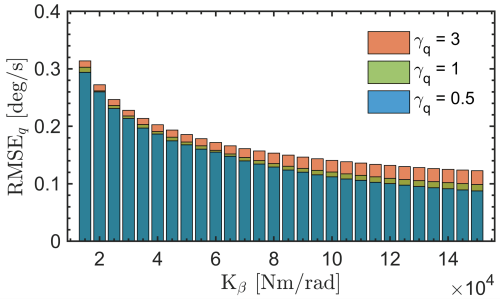

Figure 5.7: $RMSE_q$ of longitudinal tracking task using steady-state BF model with $\gamma_q \in [0.5, 1, 3]$, $K_\beta \in [10, 20, ..., 150]$ kNm/rad and $c_q = 15$.

Based on the results of the ADS-33E-PRF tracking task the following conclusions can be drawn

- The IBS controller is robust to uncertainties in control effectiveness as performance is not severely affected for control effectiveness mismatch. This can be observed from the tracking response given in Fig. 5.3 - 5.6 as well as from the $RMSE_q$ in Fig. 5.7.
- Actuator limitations do limit BF models with low K_β of achieving high desired pitch rates. Moreover the slow and overreacting response is characteristic for these type of rotorcraft when conducting an aggressive manoeuvre.
- The time-scale separation condition from Eq. 5.3 is not violated for the cases considered. This shows that incremental-based control design can be pursued for these type of rotorcraft models. However, actuator limitations can be regarded problematic for the TSS condition, because it limits the product $\hat{G}_q \Delta\theta_{1s}$. This shows that the TSS condition could be violated when an aggressive manoeuvre is being executed as actuator limitations will be very likely reached.

5.1.6. Closed-loop frequency response for varying K_β, γ_q and c_q

Next it is necessary to determine closed-loop frequency response (without actuator limitations). The closed-loop system consists of the IBS controller, actuator dynamics, sensors dynamics and steady-state BF model. The main objective is to determine the effect of uncertainties in control effectiveness on closed-loop frequency response. It was previously shown that varying $\hat{G}_q$ still enabled adequate controller performance, which should therefore also be apparent from the closed-loop frequency response. Based on the above mentioned it will be deemed necessary to consider closed-loop frequency response for different combinations of K_β, c_q and γ_q. The following cases shall be analysed

- $\gamma_q = 1$, $c_q \in [5, 10, 15]$ and $K_\beta \in [10, 20, ..., 150]$ kNm/rad.
- $\gamma_q = 3$, $c_q \in [5, 10, 15]$ and $K_\beta \in [10, 20, ..., 150]$ kNm/rad.
- $\gamma_q = 0.5$, $c_q \in [5, 10, 15]$ and $K_\beta \in [10, 20, ..., 150]$ kNm/rad.

In Fig. 5.8 - 5.10 the *Bode* frequency results are provided for $\gamma_q = 1$, $\gamma_q = 0.5$ and $\gamma_q = 3$ respectively. Moreover the region f overreaction ($|H_{CL}(j\omega)| > 1.01$) is provided as well given a tolerance of 1%.

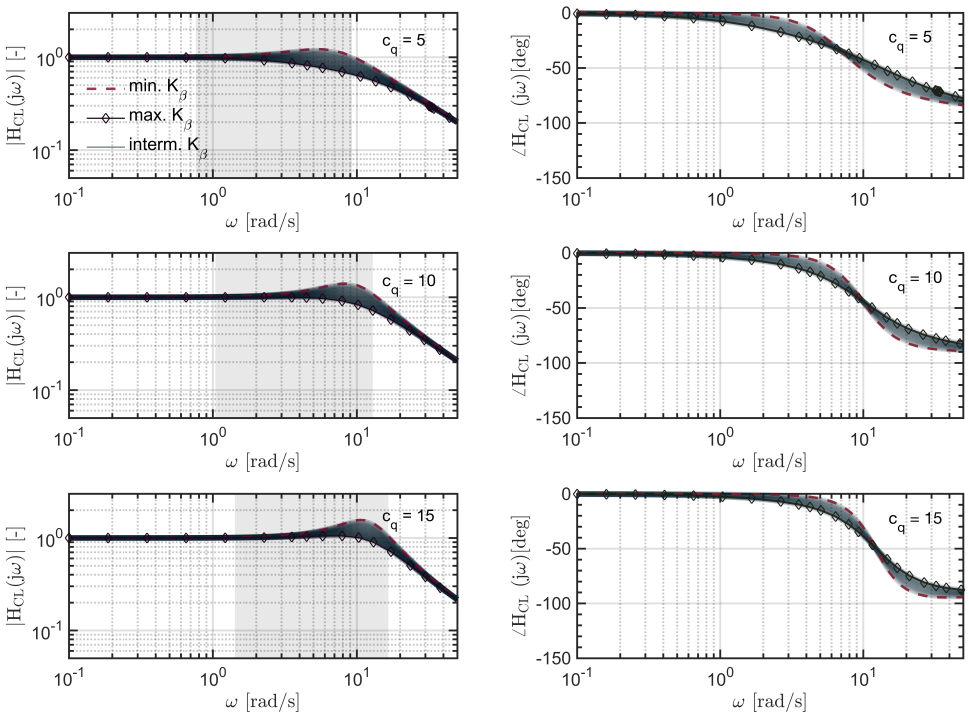

Figure 5.8: Results of closed-loop frequency response of 2-DOF steady-state BF model for $\gamma_q = 1.0$, $K_\beta \in [10, 20, ..., 150]$ kNm/rad, $c_q \in [5, 10, 15]$, $\gamma = 6$ and $\Omega = 30$ rad/s. Moreover the region of overreaction is also indicated.

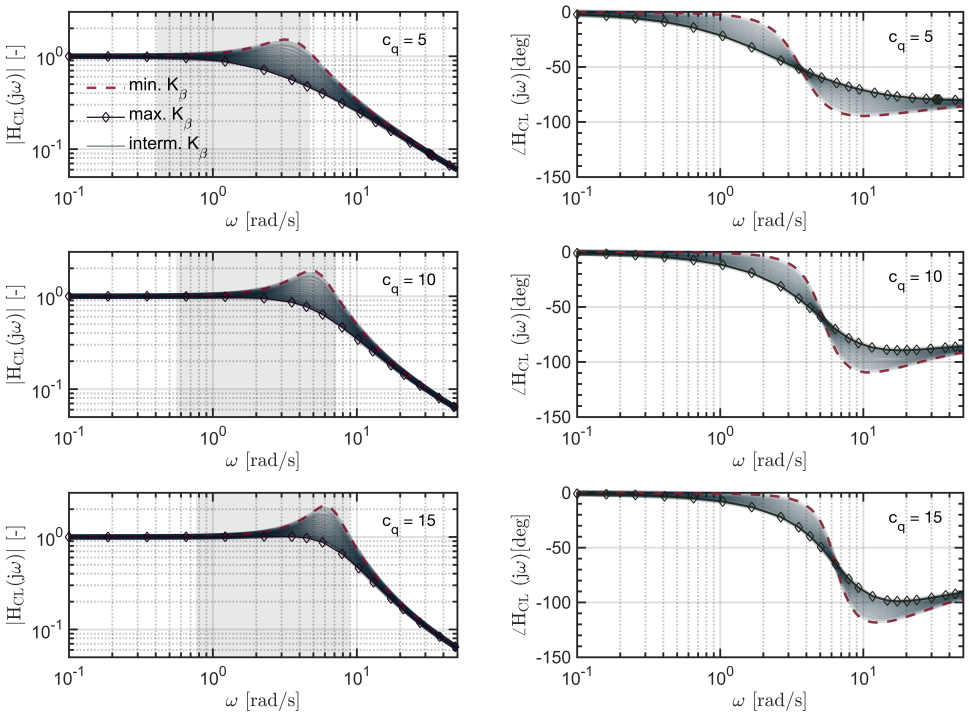

Figure 5.9: Results of closed-loop frequency response of 2-DOF steady-state BF model for $\gamma_q = 3.0$, $K_\beta \in [10, 20, ..., 150]$ kNm/rad, $c_q \in [5, 10, 15]$, $\gamma = 6$ and $\Omega = 30$ rad/s. Moreover the region of overreaction is also indicated.

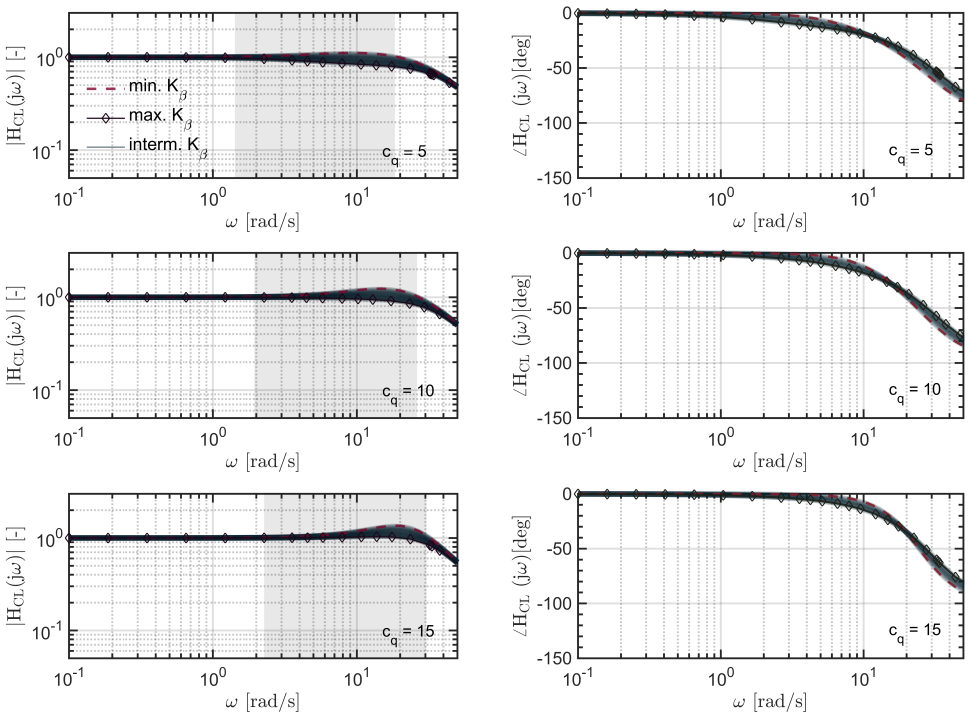

Figure 5.10: Results of closed-loop frequency response of 2-DOF steady-state BF model for $\gamma_q = 0.5$, $K_\beta \in [10, 20, ..., 150]$ kNm/rad, $c_q \in [5, 10, 15]$, $\gamma = 6$ and $\Omega = 30$ rad/s. Moreover the region of overreaction is also indicated.

From the closed-loop frequency analysis it can be observed that increasing IBS gain c_q and/or decreasing hub stiffness K_β does increase the resonance peak. This is also apparent from phase response as the drop in phase is greater for larger c_q and/or smaller K_β. The above observation does hold for all γ_q, but is more apparent for larger γ_q. Next to this increasing c_q does also increase the region of overreaction, which is not favourable. It should be noted that only the maximum region of overreaction is provided, which is determined by the minimum value of K_β. Increasing c_q does not only adversely affect closed-loop frequency response. From the results obtained it can be seen that when c_q is increased, bandwidth will also increase. In other words the frequency range for which $|H_{\text{CL}}(j\omega)| \approx 1$ will increase for increasing c_q (grey area shifts to the right).

From Fig. 5.8 - 5.10 it can be observed that adjusting γ_q results in a change in closed-loop frequency response. The first and most important observation is that the IBS controller is robust to changes in control effectiveness as bandwidth of the closed-loop frequency response does only change slightly for $\gamma_q \neq 1$. Next to this decreasing γ_q does yield a greater frequency range for which $|H_{\text{CL}}(j\omega)| \approx 1$, whereas increasing γ_q does yield a smaller frequency range for which $H_{\text{CL}}(j\omega)| \approx 1$. This is in line with observations from the longitudinal ADS-33E-PRF tracking task as performance increased slightly when γ_q decreased. The above observation can be best understood by realising that decreasing γ_q does also yield a decrease in $\hat{G}_q$ (thus $\hat{G}_q^{-1}$ increases). This means that larger incremental changes in control input (given in the stabilising control law from Eq. 5.4) can be realised within shorter amount of time. Quick changes in θ_{1s} will be demanded when the manoeuvre is aggressive (e.g. sudden changes in q_{ref}). From this it follows that a demanding control task can be easier achieved when $\hat{G}_q$ is small (γ_q is small). However, this will come at the cost of overreaction and/or violation of the TSS condition as $\hat{G}_q \Delta\theta_{1s}$ decreases, which is not favourable. This means that there will be only a small region of control effectiveness underestimation for which the above holds [53]. It can be concluded that:

- the IBS controller is robust to uncertainties in control effectiveness as bandwidth of the closed-loop frequency response only changes slightly. For $\gamma_q \neq 1$ there will still be a significant large frequency range for which $|H_{\text{CL}}(j\omega)| \approx 1$.
- Increasing IBS gain c_q and/or decreasing hub stiffness K_β does increase the resonance peak and region of overreaction. This should be avoided as this is undesirable when performing a tracking task.
- Decreasing γ_q does increase the frequency region for which $|H_{\text{CL}}(j\omega)| \approx 1$ and region of overreaction. This means that better performance may can be achieved for lower γ_q but at the cost of overreaction.

5.1.7. Closed-loop stability analysed using Routh-Hurwitz stability criterion

Next it will be of great interest to determine the analytical closed-loop stability when using the incremental-based controller. From the closed-loop frequency analysis it has become clear that the *Lyapunov*-based controller is capable of adequately tracking the reference signal even for control effectiveness mismatch.

Stability will be considered for a continuous *Laplace* transfer function. This subsequently means that the *Routh-Hurwitz* stability criterion shall be considered for assessing closed-loop stability. This criterion determines stability using the characteristic polynomial of the closed-loop transfer function. The system is found to be asymptotically stable if and only when the real parts of the closed-loop eigenvalues are situated in the LHP. Actuator dynamics (first-order lag filter with $\tau_{act} = 0.1$ s) and sensor dynamics (second-order washout filter with $\zeta_{\text{sens}} = 1$ and $\omega_{\text{n}} = 100$ rad/s) are incorporated in the closed-loop system. Moreover f_{s} was set sufficiently high to not violate Eq. 5.3 such that the stabilising control law from Eq. 5.4 could be used. The effect of actuator saturation will not be considered. In Fig. 5.11 stability regions are provided for different combinations of K_β, γ_q and c_q. These regions of stability are established using the cases outlined previously with the except of c_q, which does range from 1 to 20. It can be observed that all regions are found to be stable. In the rotorcraft models that follow here after, similar stability regions will be provided, from which it will become obvious that adjustments will be required to assure adequate closed-loop stability.

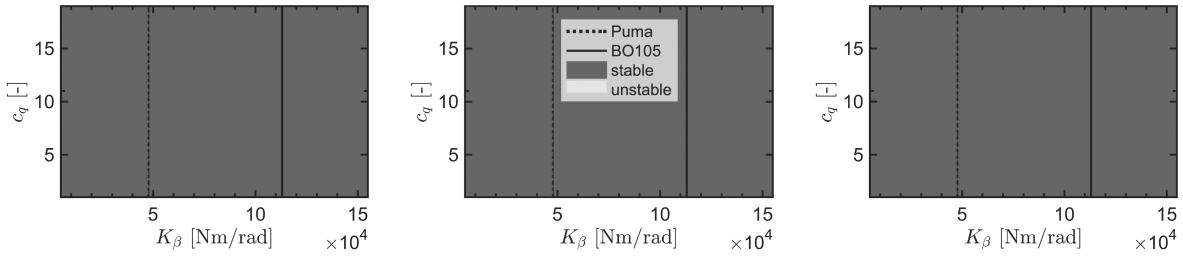

(a) Closed-loop stability with $\gamma_q = 1$, $\gamma_q = 0.5$ and $\gamma_q = 3$ respectively.

Figure 5.11: Results of closed-loop stability analysis using controller with $\gamma_q \in [0.5, 1, 3]$, $c_q \in [1, 2, ..., 20]$ and $K_\beta \in [10, 15, ..., 150]$ kNm/rad. Lines of constant hub stiffness are provided for articulated and hingeless rotorcraft.

5.2. First order τ_β-based body-flap model

With a steady-state BF model considered previously, it is necessary to consider a model with flapping dynamics. Neglecting rotor dynamics can be justified when there is large separation of the characteristic rotor and fuselage rigid body frequencies [10]. In [10] it was mentioned that for articulated rotorcraft the body modes and flapping modes are weakly coupled to each other, as the later is associated with a much faster time scale than the former. This implies that the uncoupled modes are close to the coupled modes, therefore steady-state flapping dynamics would suffice for these models (small τ_β and small K_β). When the uncoupled modes differ significantly from the coupled modes (e.g. hingeless rotor configurations), flapping dynamics must be included in the rotorcraft model [10]. This will be of prime concern in this section. Here a rotorcraft model will be considered, wherein disc tilt constant $\tau_\beta (= \frac{16}{\gamma})$ and hub stiffness K_β can be adjusted. It will be shown that flapping synchronisation will be important for rotorcraft models with slow disc-tilt response (large τ_β). In other words synchronisation must be considered for rotorcraft models for which the *idealised* (based upon steady-state flapping dynamics) and *actual* rotorcraft model differ significantly. This can be determined by means of the modes of motion and open-loop frequency response of both models. When the difference between the *idealised* and *actual* modes of motion and open-loop frequency is large, flapping synchronisation is necessary to assure adequate synchronisation of the actuator and angular acceleration measurement.

5.2.1. Natural modes of motion for varying K_β and τ_β

First, the modes of motion of the τ_β-based model without controller will be considered for the *idealised* and *actual* BF model, wherein the former was obtained by means of the *method of residualised dynamics*. This method does set $\dot{\beta}_{1c}$ equal to 0 (=steady-state flapping dynamics) and substitutes the expression for β_{1c} into the expression of $\dot{q}$. This does yield an expression, wherein $F_{q,\beta_{1c}} = 0$ and $F_{q,q}$ equal to $F_{q,q} - F_{q,\beta_{1c}} F^{-1}_{\beta_{1c},\beta_{1c}} F_{\beta_{1c},q}$. The *idealised* body mode will be decoupled from flapping. In Fig. 5.12 the modes of

motion for the *idealised* and the *actual* model are provided.

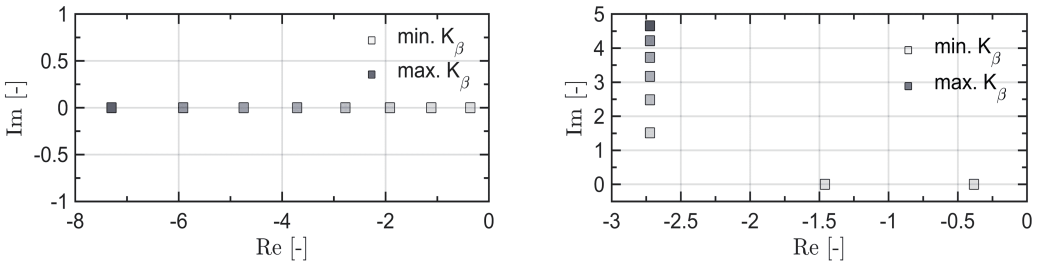

(a) *Actual* modes of motion (coupled pitch-flap) for $\tau_\beta = 1.0$ (left) and $\tau_\beta = 5.0$ (right).

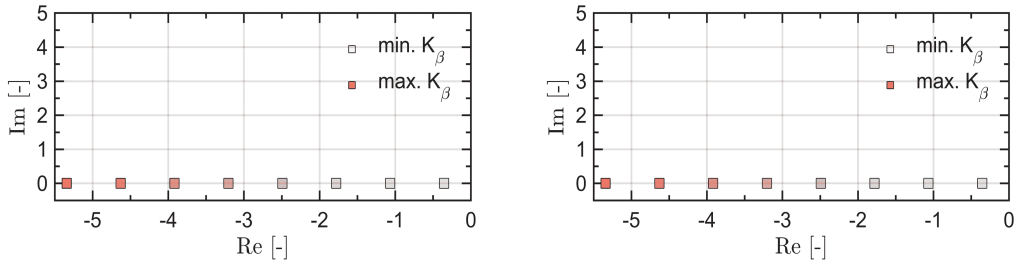

(b) *idealised* modes of motion (decoupled pitch) for $\tau_\beta = 1.0$ (left) and $\tau_\beta = 5.0$ (right).

Figure 5.12: Modes of motion of *actual* (coupled pitch-flap) and *idealised* (decoupled pitch) rotorcraft model for two instances of τ_β and $K_\beta \in [10, 30, ..., 150]$ kNm/rad.

It can be observed from Fig. 5.12 that the modes of motion for the *idealised* and *actual* rotorcraft model differ for large τ_β and K_β. The modes of motion for the *actual* rotorcraft model are situated at

$$\lambda_{1,2} = -\frac{\Omega}{2\tau_\beta} \pm \sqrt{\frac{1}{4}\left(\frac{\Omega}{\tau_\beta}\right)^2 - \frac{16K_{\text{lon}}}{\gamma\tau_\beta}} \tag{5.6}$$

and will couple for $\tau_\beta K_{\text{lon}} > \frac{\gamma\Omega^2}{64}$. The *idealised* pitch mode of motion is decoupled from flapping and situated at $-\frac{16K_{\text{lon}}}{\gamma\Omega}$. For large τ_β, the dynamic response of q will be different for *actual* and *idealised* rotorcraft model.

5.2.2. Open-loop Frequency response of angular body dynamics

Next, it is necessary to consider the open-loop frequency response without controller. The *Bode* frequency response shall be considered as it enables to determine the natural response for a wide range of frequencies given a control input [35]. The transfer function in standard *Bode* form with and without *artificial* control effectiveness coefficient are given in Eq. 5.7 and Eq. 5.8 respectively.

$$\text{for } \alpha_{G_q} \neq 0: \quad H_q(s) = \left(\frac{\gamma\Omega}{16}\left(1+\alpha_{G_q}\right)\right) \frac{\left(1 + \frac{\alpha_{G_q}\tau_\beta}{\Omega}(1+\alpha_{G_q})^{-1}s\right)}{\left(\frac{\gamma\tau_\beta}{16K_{\text{lon}}}s^2 + \frac{\Omega\gamma}{16K_{\text{lon}}}s + 1\right)} \tag{5.7}$$

$$\text{for } \alpha_{G_q} = 0: \quad H_q(s) = \frac{\left(\frac{\gamma\Omega}{16}\right)}{\left(\frac{\gamma\tau_\beta}{16K_{\text{lon}}}s^2 + \frac{\Omega\gamma}{16K_{\text{lon}}}s + 1\right)} \tag{5.8}$$

For $\alpha_{G_q} \neq 0$ it can be stated that $H_q(s)$ does consist of a first-order lead, second-order lag and gain term. However, for $\alpha_{G_q} = 0$ it can be observed that $H_q(s)$ does consist of a second-order lag and gain term only. The second-order lag term for $\alpha_{G_q} \neq 0$ and $\alpha_{G_q} = 0$ is exactly the same. In Fig. 5.13 and Fig. 5.14 the frequency response of $H_q(s)$ is provided for varying τ_β and α_{G_q} respectively. Moreover, the frequency response of $H_q(s)$ with steady-state flapping dynamics (*idealised* model) is provided as well. The difference in frequency response between the *actual* and *idealised* rotorcraft model will be of great interest.

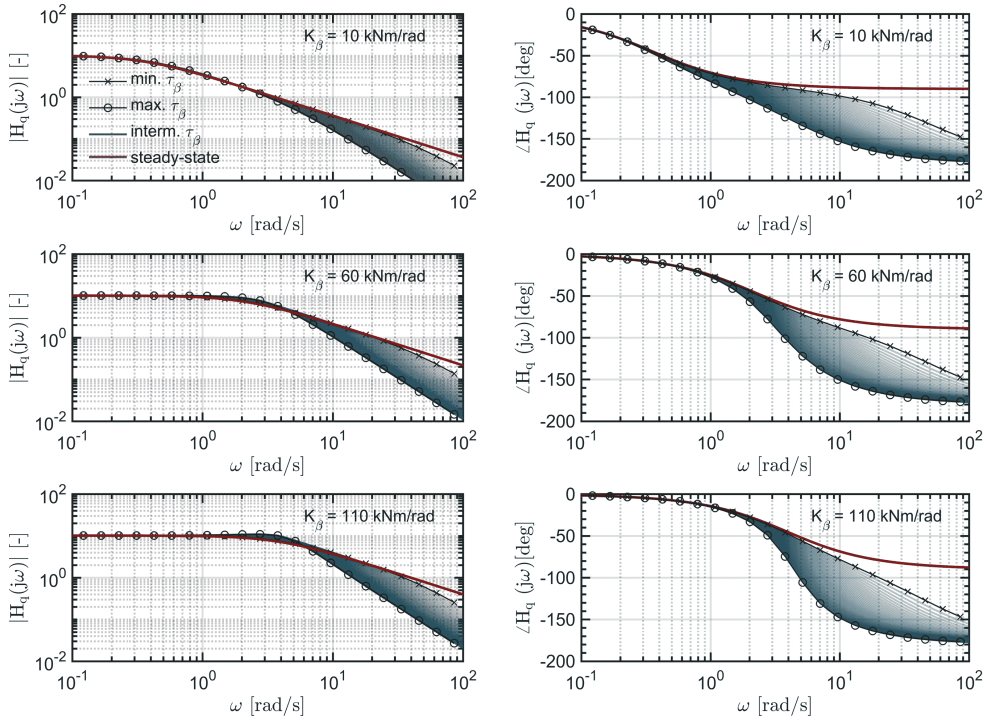

Figure 5.13: *Bode* frequency response of $H_q(s)$ for $\tau_\beta \in [0.5, 0.6, ..., 5.5]$, $K_\beta \in [10, 60, 110]$ kNm/rad and $\alpha_{G_q} = 0$.

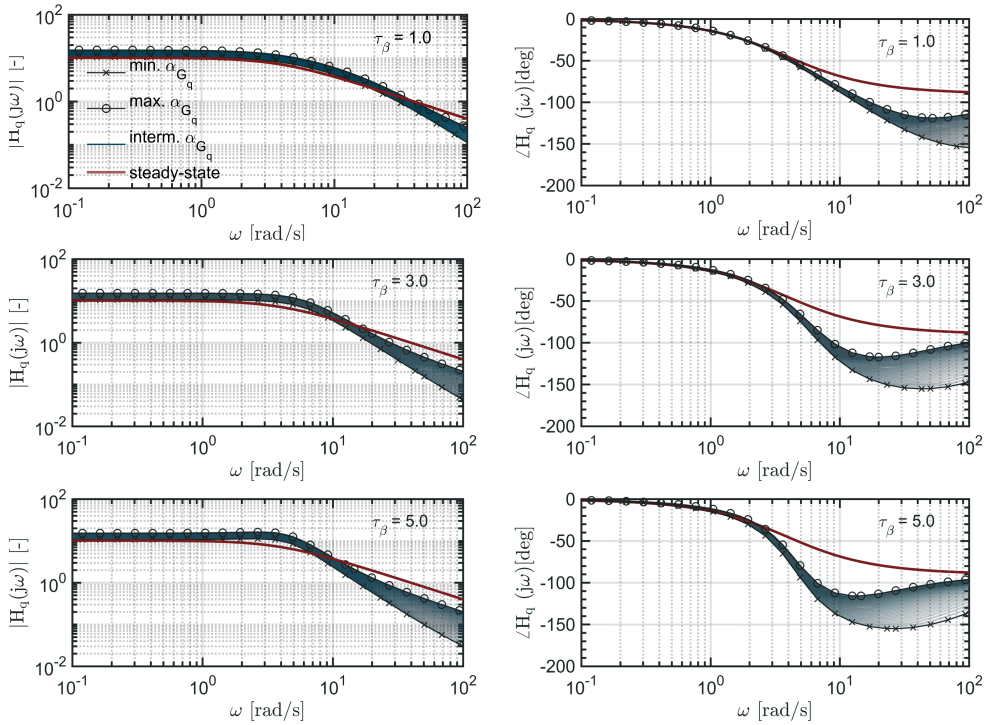

Figure 5.14: *Bode* frequency response of $H_q(s)$ for $\tau_\beta \in [1.0, 3.0, 5.0]$, $K_\beta = 110$ kNm/rad and $\alpha_{G_q} \in [0.05, 0.06, ..., 0.5]$.

In Fig. 5.13 the frequency response of $H_q(s)$ is provided for varying τ_β, three instances of K_β and $\alpha_{G_q} = 0$. It can be observed that for smaller τ_β the difference in frequency response between *idealised* (steady-state) and *actual* (τ_β-based) model becomes less. This is in line with expectation as decreasing τ_β does yield quicker disc-tilt response. It should also be noted that adjusting K_β did not influence the difference between *actual* and *idealised* rotorcraft model. This shows that τ_β is primarily responsible for the difference in frequency

response between both models. Lastly, the influence of α_{G_q} on angular body frequency response is provided in Fig. 5.14 for three instances of τ_β and one value for K_β. Increasing α_{G_q} does make the difference in frequency response between *idealised* and *actual* rotorcraft response to become greater at lower frequencies, but smaller are larger frequencies. This shows that adjusting the *artificial* control effectiveness coefficient can affect the angular body frequency response. The importance of the *artificial* control effectiveness coefficient will be considered later on.

5.2.3. Control effectiveness established using idealised rotorcraft model

For establishing the IBS controller it is necessary to determine the control effectiveness of $\dot{q}$ with respect to θ_{1s}. Two methods were incorporated for establishing the control effectiveness. The *flapping angle equivalence method* is the least complicated method as it only requires knowledge of $F_{q,\beta_{1c}}$, which is $-K_{\text{lon}}$, and the IBC to MBC transformation. Since a positive *Fourier* series was incorporated for establishing the body-flap EOM ($\beta_{1c_{SP}} = \beta_{1c_{CP}} - \theta_{1s}$), the control effectiveness G_q must be equal to K_{lon}. Another technique that can be incorporated is the *method of residualised dynamics*. This method requires more and accurate knowledge of the *actual* model. Using the previously mentioned method, the control effectiveness must be equal to

$$G_q = H_q - F_{q,\beta_{1c}} F^{-1}_{\beta_{1c},\beta_{1c}} H_{\beta_{1c}} = \alpha_{G_q} K_{\text{lon}} - -K_{\text{lon}} \cdot -\frac{\tau_\beta}{\Omega} \cdot -\frac{\Omega}{\tau_\beta} = K_{\text{lon}} \left(1 + \alpha_{G_q}\right). \tag{5.9}$$

It can be observed from Eq. 5.9 that G_q is approximately the same as the control effectiveness when using the *flapping angle equivalence method*. The only difference lies therein that the *method of residualised dynamics* also accounts for the control-depended term of the original BF model. The aforementioned would only hold when $\alpha_{G_q} \neq 0$. Important to note is that both methods are incorporated to establish an enhanced control effectiveness. It will be shown that this is required to not violate the IBS TSS condition. For the proceeding analysis it will be assumed that one does not always have full and accurate knowledge of control effectiveness. This implies that $\hat{G}_q = \gamma_q G_q$, wherein γ_q is the control effectiveness mismatch factor.

5.2.4. Stabilising control law for angular rate subsystem using IBS

With the control effectiveness determined it is necessary to establish an IBS control law for q. A *Taylor* series must be used for defining the control law. Two first-order *Taylor* series will be introduced, namely one that is based upon the *actual* rotorcraft model and another one that is based upon the *idealised* rotorcraft model. The *idealised Taylor* series will be established using the *method of residualised dynamics*. The first-order *Taylor* series using the *idealised* and *actual* rotorcraft model is given in Eq. 5.10 and Eq. 5.11 respectively.

$$\begin{aligned} \text{idealised}: \quad \dot{q} &\cong \dot{q}_0 + F_{q,\beta_{1c}} \Delta\beta_{1c} + \left(F_{q,q} - F_{q,\beta_{1c}} F^{-1}_{\beta_{1c},\beta_{1c}} F_{\beta_{1c},q}\right) \Delta q + \left(H_q - F_{q,\beta_{1c}} F^{-1}_{\beta_{1c},\beta_{1c}} H_{\beta_{1c}}\right) \Delta\theta_{1s} \\ &\cong \dot{q}_0 + 0 \cdot \Delta\beta_{1c} + \left(0 - -K_{\text{lon}} \cdot -\frac{\tau_\beta}{\Omega} \cdot \frac{16}{\gamma\tau_\beta}\right) \Delta q + \left(\alpha_{G_q} K_{\text{lon}} - -K_{\text{lon}} \cdot -\frac{\tau_\beta}{\Omega} \cdot -\frac{\Omega}{\tau_\beta}\right) \Delta\theta_{1s} \\ &\cong \dot{q}_0 - \frac{16}{\gamma\Omega} K_{\text{lon}} \Delta q + (1 + \alpha_{G_q}) K_{\text{lon}} \Delta\theta_{1s} \end{aligned} \tag{5.10}$$

$$\begin{aligned} \text{Actual}: \quad \dot{q} &\cong \dot{q}_0 + F_{q,\beta_{1c}} \Delta\beta_{1c} + F_{q,q} \Delta q + H_q \Delta\theta_{1s} \\ &\cong \dot{q}_0 - K_{\text{lon}} \Delta\beta_{1c} + \alpha_{G_q} K_{\text{lon}} \Delta\theta_{1s} \end{aligned} \tag{5.11}$$

It should be noted that $\dot{q}_0$ and $\theta_{1s,0}$ are the current pitch rate derivative and longitudinal cyclic control input respectively. Moreover, Δq, $\Delta\beta_{1c}$ and $\Delta\theta_{1s}$ are the incremental change in pitch rate, cyclic flapping angle and longitudinal control input respectively. The main difference between the *idealised* and *actual Taylor* series can be clearly identified from Eq. 5.10 and Eq. 5.11. Most importantly, is that state-dependency has diminished and control-dependency has been increased for the *idealised* first-order *Taylor* series. The previous first-order *Taylor* series can be simplified by neglecting the state-depended terms by assuming *time-scale* separation [1, 45, 46, 54]. This condition does reduce dependency on system dynamics. A necessary condition for a time-scale separated system is

$$\text{TSS condition for idealised Taylor series}: \quad (1 + \alpha_{G_q}) K_{\text{lon}} \Delta\theta_{1s} >> -\frac{16}{\gamma\Omega} K_{\text{lon}} \Delta q, \tag{5.12}$$

$$\text{TSS condition for actual Taylor series}: \quad \alpha_{G_q} K_{\text{lon}} \Delta\theta_{1s} >> -K_{\text{lon}} \Delta\beta_{1c}, \tag{5.13}$$

which is equivalent by assuming instantaneous control action given that sampling rate f_s is sufficiently high [54]. When Eq. 5.12 and Eq. 5.13 hold, then it will be robust to uncertainties in system dynamics. It can be observed that the TSS condition for the *idealised Taylor* series will hold since $\gamma\Omega >> 16$. On the other hand the TSS condition for the *actual Taylor* series will be violated as $\alpha_{G_q} << 1$. This can be regarded the crux in control design for rotorcraft control (this was also observed for the main rotorcraft model [55]). Establishing a stabilising control law using Eq. 5.11 can be achieved by including system dynamics, here flapping dynamics. This is not desirable as this requires accurate and reliable knowledge of flapping dynamics and flapping angles. The following stabilising control law will be used

$$\theta_{1s} = \theta_{1s,0} + \hat{G}_q^{-1}\left[-\dot{q}_0 + \dot{q}_{\text{ref}} - c_q z_q\right]. \tag{5.14}$$

5.2.5. Flapping synchronisation filter for synchronising actuator and angular rate derivative measurements

A flapping synchronisation filter shall be introduced to account for the fact that the controller is based upon an *idealised* model using steady-state flapping dynamics, whereas the *actual* BF model is associated with disc-tilt dynamics. The flapping synchronisation filter can be established by looking at the difference in IO response of the *idealised* and *actual* BF model. The difference can be identified as the synchronisation filter ($H_{\text{actual}}(s) = H_{\text{sync}}(s) H_{\text{ideal}}(s)$). It is important to note that the control effectiveness $\hat{G}_q$ used in the synchronisation filter must be based upon the *method of residualised dynamics* since it establishes the control effectiveness using the exact expression for steady-state flapping dynamics. Flapping synchronisation shall first be introduced in the time-domain, there after in the *Laplace*-domain. The expression for the synchronised control input and flapping angle are given in Eq. 5.15 and Eq. 5.16 respectively.

$$\left.\begin{aligned} \dot{q} &= \hat{G}_q \theta_{1s,\text{sync}} \\ \dot{q} &= F_{q,\beta_{1c}} \beta_{1c,\text{sync}} + H_q \theta_{1s,\text{meas}} \end{aligned}\right\} \quad \theta_{1s,\text{sync}} = \hat{G}_q^{-1} F_{q,\beta_{1c}} \beta_{1c,\text{sync}} + \hat{G}_q^{-1} H_q \theta_{1s,\text{meas}} \tag{5.15}$$

$$\dot{\beta}_{1c,\text{sync}} = F_{\beta_{1c},\beta_{1c}} \beta_{1c,\text{sync}} + H_{\beta_{1c}} \theta_{1s,\text{meas}} \tag{5.16}$$

The synchronisation filter can be written into the following state-space system

$$\begin{bmatrix} \dot{\beta}_{1c,\text{sync}} \\ \theta_{1s,\text{sync}} \end{bmatrix} = \begin{bmatrix} -\frac{\Omega}{\tau_\beta} \\ \gamma_q (K_{\text{lon}} + \alpha_{G_q} K_{\text{lon}})^{-1} \cdot -K_{\text{lon}} \end{bmatrix} \beta_{1c,\text{sync}} + \begin{bmatrix} -\frac{\Omega}{\tau_\beta} \\ \gamma_q (K_{\text{lon}} + \alpha_{G_q} K_{\text{lon}})^{-1} \cdot \alpha_{G_q} K_{\text{lon}} \end{bmatrix} \theta_{1s,\text{meas}}, \tag{5.17}$$

wherein $\theta_{1s,\text{meas}}$ and $\beta_{1c,\text{sync}}$ are the measured control input (fed through a second-order washout filter) and synchronised flapping angle respectively. It can be observed from Eq. 5.17 that it purely depends on $\theta_{1s,\text{meas}}$ as input. Next to this, it should be noted that Eq. 5.17 is not a function of K_β. This confirms the fact that the difference between the *idealised* and *actual* rotorcraft model is not created due to K_β. From Eq. 5.17 it can be observed that τ_β, γ_q and α_{G_q} will be of prime concern regarding rotor synchronisation. Next, it is necessary to consider the flapping synchronisation filter in the *Laplace*-domain. The transfer function for the flapping synchronisation is provided in Eq. 5.18 and Eq. 5.19 for $\alpha_{G_q} \neq 0$ and $\alpha_{G_q} = 0$ respectively.

$$\text{for } \alpha_{G_q} \neq 0: \quad H_{\text{sync}}(s) = \frac{\theta_{1s,\text{sync}}(s)}{\theta_{1s,\text{meas}}(s)} = \gamma_q^{-1}\left(1 + \alpha_{G_q}\right) \frac{\left(1 + \frac{\alpha_{G_q}\tau_\beta}{\Omega}\left(1 + \alpha_{G_q}\right)^{-1} s\right)}{\left(\frac{\tau_\beta}{\Omega} s + 1\right)} \tag{5.18}$$

$$\text{for } \alpha_{G_q} = 0: \quad H_{\text{sync}}(s) = \frac{\theta_{1s,\text{sync}}(s)}{\theta_{1s,\text{meas}}(s)} = \left(\gamma_q^{-1}\right) \frac{1}{\left(\frac{\tau_\beta}{\Omega} s + 1\right)} \tag{5.19}$$

The synchronisation filter from Eq. 5.18 is characterised by a gain, first-order lag and first-order lead term. On the other hand, for $\alpha_{G_q} = 0$ the synchronisation filter can be written into the form given in Eq. 5.19, consisting of a gain and first-order lag term. Of great interest are the effects of changes in γ_q, τ_β and α_{G_q} on synchronisation filter frequency response. In Fig. 5.15 the results are provided.

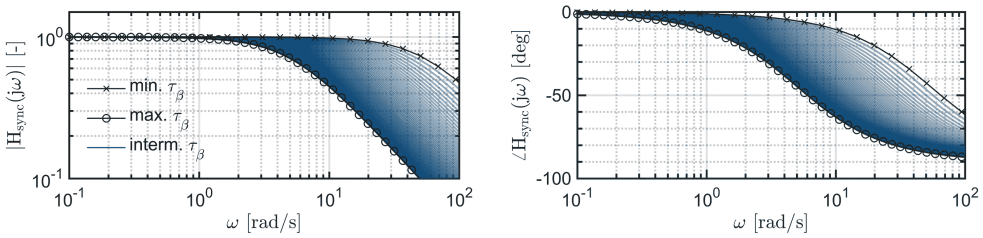

(a) Magnitude and phase response for $\tau_\beta \in [0.5, 0.6, ..., 5.5]$, $\gamma_q = 1$ and $\alpha_{G_q} = 0$.

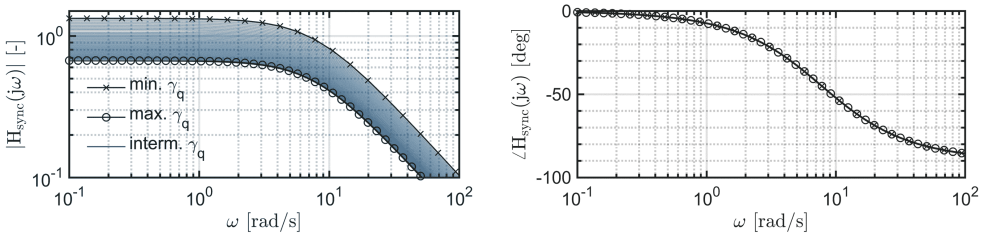

(b) Magnitude and phase response for $\gamma_q \in [0.75, 0.76, ..., 1.25]$, $\tau_\beta = 3$ and $\alpha_{G_q} = 0$.

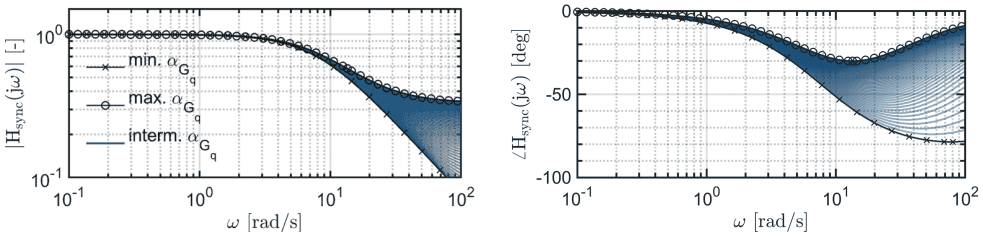

(c) Magnitude and phase response for $\alpha_{G_q} \in [0.0, 0.025, ..., 0.5]$, $\tau_\beta = 3$ and $\gamma_q = 1$.

Figure 5.15: Frequency response of flapping synchronisation filter of τ_β-based rotorcraft model for varying τ_β, γ_q and α_{G_q}. Synchronisation filters from Eq. 5.18 and Eq. 5.19 are incorporated for assessing these changes.

Based on the results of the rotor synchronisation frequency analysis the following can be stated

- increasing τ_β will decrease rotor synchronisation filter bandwidth such that $\theta_{1s,\text{meas}}$ will be slowed down more. This shows that when the difference between the *idealised* and *actual* model increases, the feedback of the actuator measurement must be slowed down more to match the feedback of the angular acceleration measurement.
- K_β will not affect the frequency response of the rotor synchronisation filter (see Eq. 5.18 and Eq. 5.19).
- frequency response of the synchronisation filter depends on control effectiveness mismatch factor. To be more specific γ_q^{-1} does act as a pure gain and will therefore affect magnitude response. Control effectiveness under- or overestimation will yield magnified and diminished control inputs respectively.
- It can be observed from Fig. 5.15 that greater α_{G_q} will be associated with greater magnitude at higher frequencies. This implies that for larger α_{G_q} the synchronisation will delay $\theta_{1s,\text{meas}}$ less. This is in line with expectation as control-dependency increases thus relatively there will be less attenuation of flapping dynamics. In other words, $\dot{q}$ will be increasingly more directly governed by θ_{1s}, while the indirect channel ($\theta_{1s} \rightarrow \beta_{1c} \rightarrow \dot{q}$) remains the same.

5.2.6. Longitudinal ADS-33E-PRF tracking task for varying τ_β

The main point of interest of the analysis is to understand the effect of rotor dynamics on IBS. The next step is to assess controller robustness. The necessity of incorporating an enhanced control effectiveness and adequate synchronisation of actuator and angular acceleration measurement will be of prime concern. In order to assess the above mentioned it will be necessary to determine IBS controller performance with and without rotor synchronisation filter. A longitudinal tracking task will be executed in accordance with the regulations stipulated by the ADS-33E-PRF for aggressive agility [4]. This means that the rotorcraft shall reach a pitch rate of $\pm 30°/s$. The following cases will be considered

- without flapping synchronisation filter ($H_{\text{sync}}(s) = 1$), $y_q = 1$, $\hat{G}_q = \alpha_{G_q} K_{\text{lon}}$ with $\alpha_{G_q} \in [0.150, 0.175, ..., 0.4]$ as control effectiveness coefficient, $\tau_\beta = 5.0$, $c_q = 5$ and $K_\beta = 110$ kNm/rad. This illustrates the main crux in control design for rotorcraft control.
- without flapping synchronisation filter, enhanced control effectiveness established using the *method of residualised dynamics* with $y_q = 1$, $\tau_\beta \in [0.5, 1.0, ..., 5.5]$, $\alpha_{G_q} = 0$, $c_q = 2.5$ and $K_\beta = 110$ kNm/rad. This is the Reduced inverse of control effectiveness matrix INDI (RINDI) method mentioned in [42].
- with flapping synchronisation filter, enhanced control effectiveness using the *method of residualised dynamics* with $y_q = 1$ for control effectiveness of IBS control law and synchronisation filter, $\tau_\beta \in [0.5, 1.0, ..., 5.5]$, $c_q = 15$, $K_\beta = 110$ kNm/rad and $\alpha_{G_q} = 0$.
- with flapping synchronisation filter, enhanced control effectiveness established using the *method of residualised dynamics*, $y_q = 0.75$ for control effectiveness of synchronisation filter, $\gamma_q = 1$ for control effectiveness of IBS control law, $\tau_\beta \in [0.5, 1.0, ..., 5.5]$, $c_q = 10$, $K_\beta = 110$ kNm/rad and $\alpha_{G_q} = 0$.

In Fig. 5.16 - 5.18 the results of the first case are provided. It can be observed that tracking response is erratic for decreasing control effectiveness. Moreover, it can also be observed that control-dependency is significantly less than state-dependency, thus violating the IBS TSS condition. System dynamics should be accounted for to not violate the condition, which would require the need for accurate and reliable knowledge of flapping dynamics and cyclic flapping angles. This is exactly what is trying to be avoided when using the IBS control strategy. From Fig. 5.18 it can be observed that controller performance is affected the most when control effectiveness decreases. This does well illustrate the crux in control design for rotorcraft control as control effectiveness based upon the control-depended term of the angular accelerations is simply insufficient. Most importantly, it would not enable IBS.

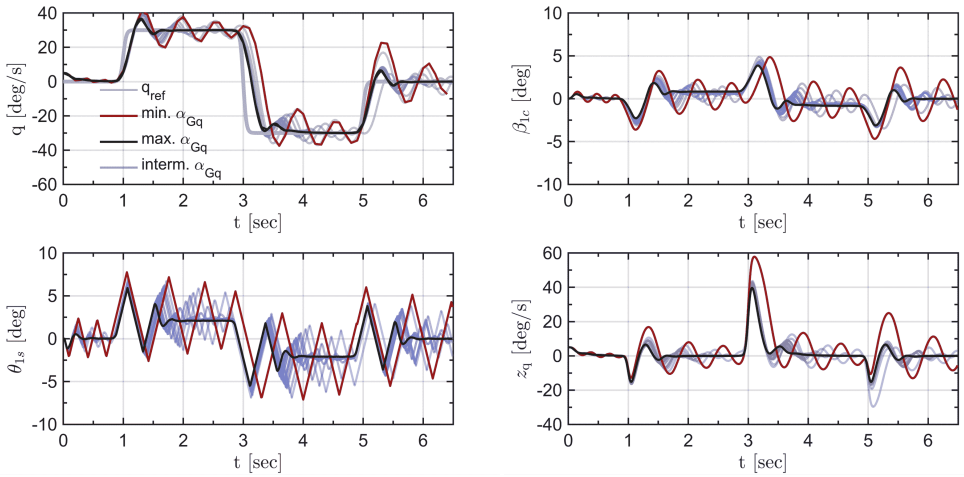

Figure 5.16: Results of longitudinal tracking task of τ_β-based rotorcraft model without synchronisation filter. Rotorcraft states q and β_{1c} are provided along with cyclic control input θ_{1s}. Also tracking error z_q is provided. Effect of varying α_{G_q} on tracking performance is analysed for $\alpha_{G_q} \in [0.15, 0.175, ..., 0.4]$, $\tau_\beta = 5.0$, $c_q = 5$ and $K_\beta = 110$ kNm/rad.

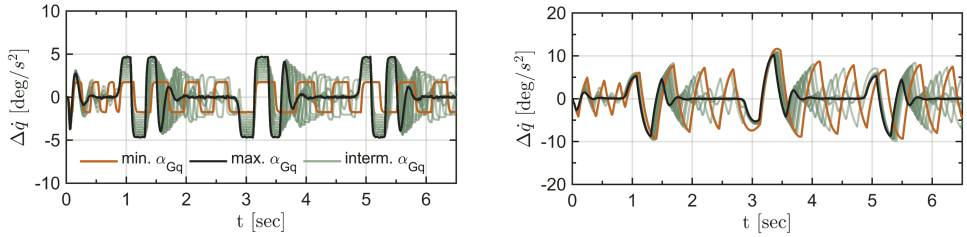

(a) $F_{q,q}\Delta q + F_{q,\beta_{1c}}\Delta\beta_{1c}$ **(b)** $H_q\Delta\theta_{1s}$

Figure 5.17: Control- and state-dependency of longitudinal tracking task of τ_β-based rotor model for which controller performance was assessed for varying α_{G_q} given that $\alpha_{G_q} \in [0.15, 0.175, ..., 0.4]$, $\tau_\beta = 5.0$, $c_q = 5$ and $K_\beta = 110$ kNm/rad.

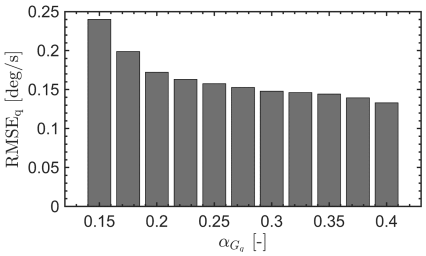

Figure 5.18: $RMSE_q$ of longitudinal tracking task of τ_β-based rotor model for which controller performance was assessed for varying α_{G_q} given that $\alpha_{G_q} \in [0.15, 0.175, ..., 0.4]$, $\tau_\beta = 5.0$, $c_q = 5$ and $K_\beta = 110$ kNm/rad.

Previously, it was mentioned that the TSS condition was violated when using the control-depended term as control effectiveness for the stabilising control law. This problem can be accounted for by means of the *method of residualised dynamics*, wherein steady-state flapping dynamics is assumed. This does enhance control-dependency and reduces state-dependency. In previous research from Pavel et al. [42] it was also found that enhancing control effectiveness (reduction of control effectiveness inverse) was necessary to assure adequate controller performance. In Fig. 5.19 - 5.21 the results are provided. It can be observed from Fig. 5.20 that control-dependency is indeed greater than state-dependency. However, from Fig. 5.19 it can be observed that tracking response is not desirable since it is quiet erratic. Moreover, in Fig. 5.21 it can be observed that $RMSE_q$ increases when disc-tilt response becomes slower.

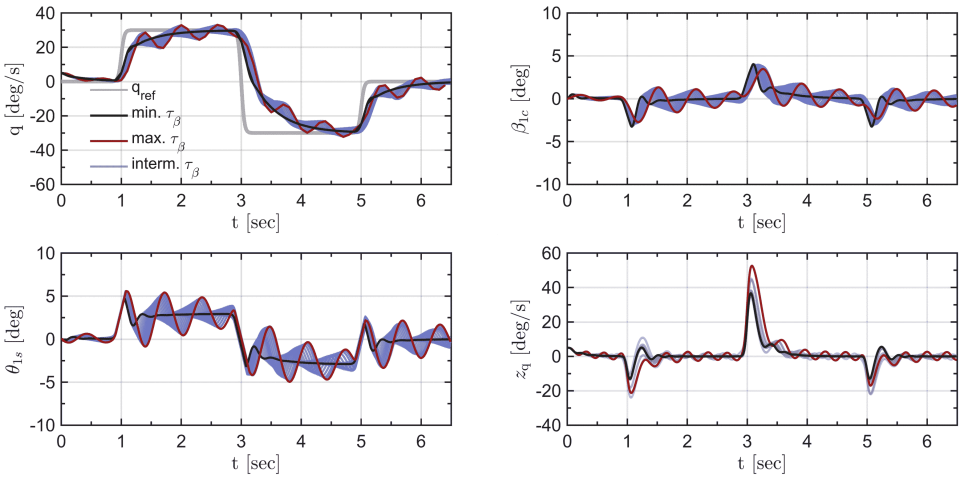

Figure 5.19: Results of longitudinal tracking task of τ_β-based rotorcraft model without synchronisation filter. Rotorcraft states q and β_{1c} are provided along with cyclic control input θ_{1s}. Moreover tracking error z_q is provided as well. Effects of varying τ_β on tracking performance is analysed for $\alpha_{G_q} = 0$, $\tau_\beta \in [0.5, 1.0, ..., 5.5]$, $c_q = 2.5$ and $K_\beta = 110$ kNm/rad.

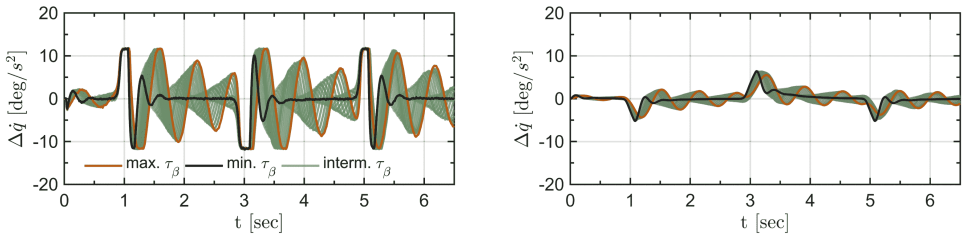

(a) $(H_q - F_{q,\beta_{1c}} F^{-1}_{\beta_{1c},\beta_{1c}} H_{\beta_{1c}})\Delta\theta_{1s}$ **(b)** $(F_{q,q} - F_{q,\beta_{1c}} F^{-1}_{\beta_{1c},\beta_{1c}} F_{\beta_{1c},q})\Delta q$

Figure 5.20: Control- and state-dependency of longitudinal tracking task of τ_β-based rotor model for which controller performance was assessed for varying τ_β given that $\alpha_{G_q} = 0$, $\tau_\beta \in [0.5, 1.0, ..., 5.5]$, $c_q = 2.5$ and $K_\beta = 110$ kNm/rad.

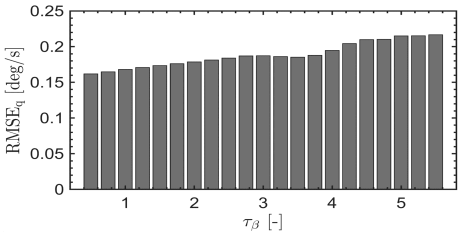

Figure 5.21: $RMSE_q$ of longitudinal tracking task of τ_β-based rotor model for which controller performance was assessed for varying τ_β given that $\alpha_{G_q} = 0$, $\tau_\beta \in [0.5, 1.0, ..., 5.5]$, $c_q = 2.5$ and $K_\beta = 110$ kNm/rad.

The previous IBS controller did not yield the desired performance even though TSS condition was not violated. The problem lies therein that $\dot{q}_0$ was not well-synchronised with $\theta_{1s,0}$, which can be accounted for by means of the flapping synchronisation filter. From Fig. 5.22 - 5.24 it can be observed that controller performance has improved and TSS condition is not violated. On top of this, the response is not erratic. Based on the difference in synchronised and unsynchronised actuator measurement it can be stated that for increasing τ_β there will be more synchronisation effort required.

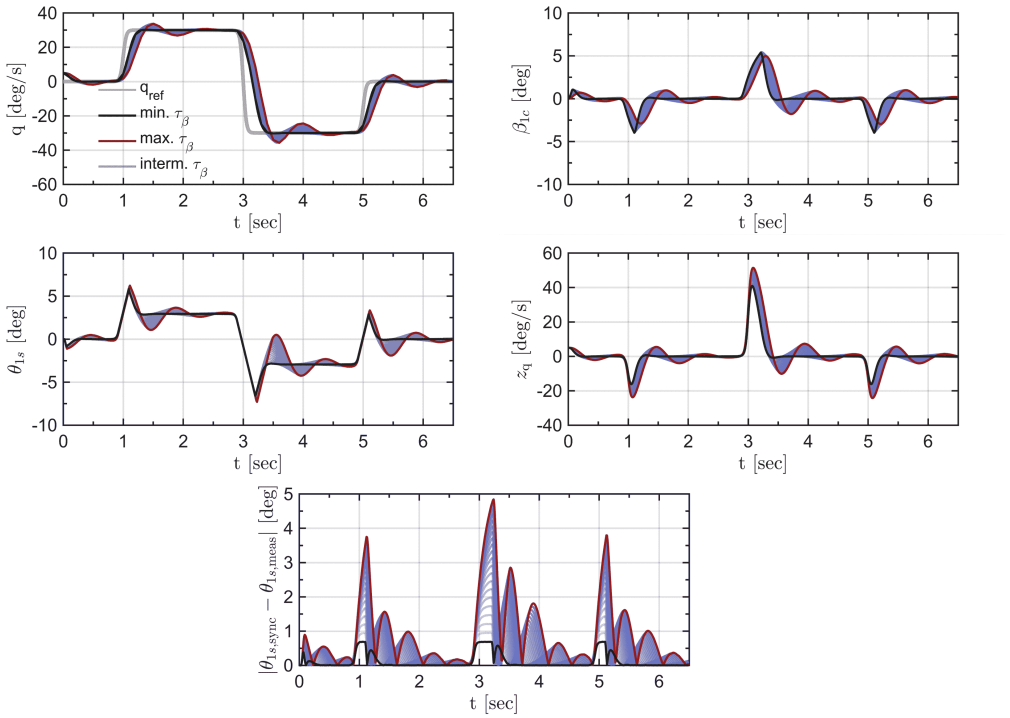

Figure 5.22: Results of longitudinal tracking task of τ_β-based rotorcraft model with rotor synchronisation. Rotorcraft states q and β_{1c} are provided along with control input θ_{1s}. In addition to this tracking z_q and absolute difference in synchronised and unsynchronised actuator measurement are provided. Effects of varying τ_β on tracking performance is analysed for $\tau_\beta \in [0.5, 1.0, ..., 5.5]$, $c_q = 15$, $\alpha_{G_q} = 0$, $\gamma_q = 1$ and K_β equal to 110 kNm/rad.

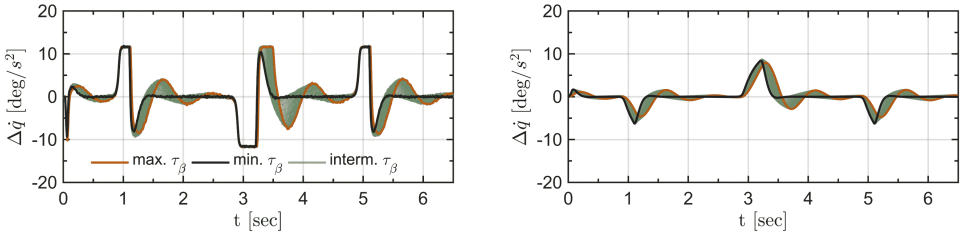

(a) $(H_q - F_{q,\beta_{1c}} F^{-1}_{\beta_{1c},\beta_{1c}} H_{\beta_{1c}})\Delta\theta_{1s}$ **(b)** $(F_{q,q} - F_{q,\beta_{1c}} F^{-1}_{\beta_{1c},\beta_{1c}} F_{\beta_{1c},q})\Delta q$

Figure 5.23: Control- and state-dependency of longitudinal tracking task of τ_β-based rotorcraft model with rotor synchronisation controller, wherein $\alpha_{G_q} = 0$, $\tau_\beta \in [0.5, 1.0, ..., 5.5]$, $\gamma_q = 1$, $c_q = 15$ and K_β equal to 110 kNm/rad.

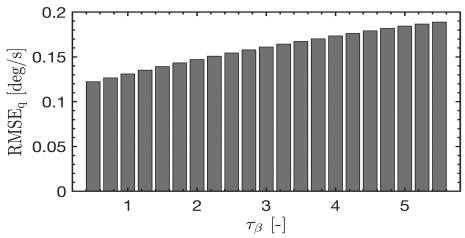

Figure 5.24: $RMSE_q$ of longitudinal tracking task of τ_β-based rotorcraft model with rotor synchronisation filter, wherein $\alpha_{G_q} = 0$, $\tau_\beta \in [0.5, 1.0, ..., 5.5]$, $\gamma_q = 1$, $c_q = 15$ and K_β equal to 110 kNm/rad.

A control effectiveness mismatch of $\gamma_q = 0.75$ is considered for the control effectiveness in the rotor synchronisation filter, while $\gamma_q = 1$ will be considered for the control effectiveness of the IBS control law. In Fig. 5.25 - 5.27 the results are provided. It can be observed that controller performance is severely affected as tracking response has become more erratic. Moreover, q has an offset with respect to q_{ref} as a result of inadequate signal synchronisation. This shows that the controller is not robust to uncertainties in control effectiveness of the synchronisation filter.

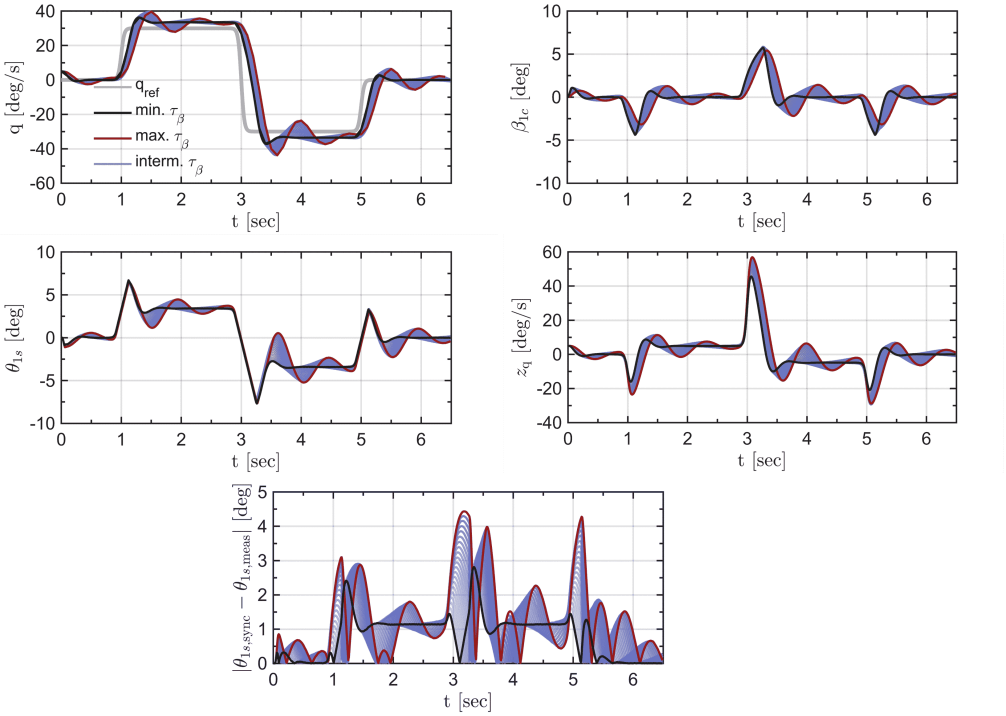

Figure 5.25: Results of longitudinal tracking task of τ_β-based rotorcraft model with rotor synchronisation. Rotorcraft states q and β_{1c} are provided along with control input θ_{1s}. In addition to this tracking z_q and absolute difference in synchronised and unsynchronised actuator measurement are provided. Effects of varying τ_β on tracking performance is analysed for $\tau_\beta \in [0.5, 1.0, ..., 5.0]$, $c_q = 10$, $\alpha_{G_q} = 0$, $\gamma_q = 0.75$ for synchronisation filter and K_β equal to 110 kNm/rad.

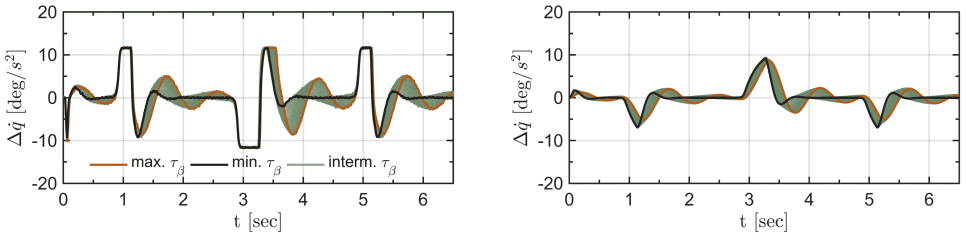

(a) $(H_q - F_{q,\beta_{1c}} F^{-1}_{\beta_{1c},\beta_{1c}} H_{\beta_{1c}})\Delta\theta_{1s}$ **(b)** $(F_{q,q} - F_{q,\beta_{1c}} F^{-1}_{\beta_{1c},\beta_{1c}} F_{\beta_{1c},q})\Delta q$

Figure 5.26: Control- and state-dependency of longitudinal tracking task of τ_β-based rotorcraft model with rotor synchronisation, $\tau_\beta \in [0.5, 1.0, ..., 5.0]$, $\gamma_q = 0.75$ for synchronisation filter, $c_q = 10$ and $K_\beta = 110$ kNm/rad.

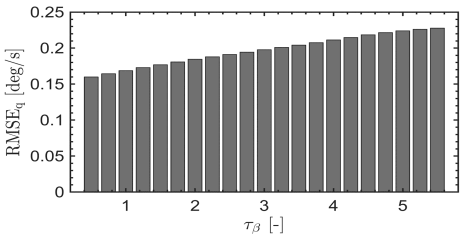

Figure 5.27: $RMSE_q$ of longitudinal tracking task of τ_β-based rotorcraft model with rotor synchronisation filter, wherein $\tau_\beta \in [0.5, 1.0, ..., 5.0]$, $\gamma_q = 0.75$ rotor synchronisation filter, $c_q = 10$ and K_β equal to 110 kNm/rad.

It can be stated that violation of the TSS condition did require modification of the original BF model to enable enhanced control effectiveness and diminished state-dependency. This was realised by means of the *method of residualised dynamics*. This did yield a difference in *idealised* and *actual* rotorcraft model and especially for those models with large τ_β (see Fig. 5.12 and Fig. 5.13). This discrepancy was overlooked in the second case (see Fig. 5.19 - Fig. 5.21), which resulted in unsynchronised actuator and state derivative measurement. The following conclusions can be drawn:

- a stabilising control law using the (*artificial*) control-depended term of $\dot{q}$ as control effectiveness will yield violation of the TSS condition from Eq. 5.12.
- incorporating the *method of residualised dynamics* for enhancing control-dependency and diminishing state-dependency did not violate the TSS condition from Eq. 5.13. However, it did not account for the difference in *actual* and *idealised* rotorcraft model, yielding poor synchronisation of actuator and state-derivative measurement. This resulted in erratic behaviour of the controlled and uncontrolled states.
- synchronisation of actuator and angular acceleration measurement by means of a synchronisation filter can be regarded a requisite for BF models with significant difference in *actual* and *idealised* model.
- control effectiveness mismatch for the control effectiveness in the rotor synchronisation filter can severely affect controller performance as vehicle response is associated with steady-state error. It is therefore not robust to uncertainties in control effectiveness.
- actuator limits do pose a problem regarding the TSS condition, as the product $(H_{q,q} - F_{q,\beta_{1c}} F^{-1}_{\beta_{1c},\beta_{1c}} H_{\beta_{1c}})\Delta\theta_{1s}$ or $H_q \Delta\theta_{1s}$ can only reach a certain maximum depending on the actuator limits.

5.2.7. Closed-loop frequency response of IBS controller with or without synchronisation

Having performed a time-domain analysis, it will be necessary to consider a closed-loop frequency analysis. Findings from the time-domain analysis should also be apparent from the closed-loop frequency analysis. The main objective is to show that a flapping synchronisation filter is necessary to assure adequate closed-loop frequency response and to proof that the controller is more robust to uncertainties in control effectiveness mismatch for the IBS control law than for the flapping synchronisation filter. The main parameters of interest for the analysis are: γ_q, α_{G_q} and τ_β. Below a set of cases will be outlined which are all considered with or without rotor synchronisation filter, $c_q \in [3, 9]$ and $K_\beta = 110$ kNm/rad. Moreover, control effectiveness is established using the *method of residualised dynamics* such that it will be equal to K_{lon} for $\alpha_{G_q} = 0$ or $K_{\text{lon}}(1 + \alpha_{G_q})$ when $\alpha_{G_q} \neq 0$. The following cases will be considered:

- variation in τ_β with $\gamma_q = 1$ ($\hat{G}_q = K_{\text{lon}}$) for IBS control law and synchronisation filter and $\alpha_{G_q} = 0$.
- variation in α_{G_q} with $\gamma_q = 1$ ($\hat{G}_q = (1 + \alpha_{G_q})K_{\text{lon}}$) for IBS control law and synchronisation filter, $\alpha_{G_q} \in [0.1, 0.11, ..., 0.5]$ and $\tau_\beta = 3.5$.
- variation in γ_q ($\hat{G}_q = \gamma_q K_{\text{lon}}$) with $\gamma_q \in [0.75, 0.775, .., 1.0]$ or $\gamma_q \in [1.0, 1.05, ..., 3]$ for the stabilising control law, $\gamma_q = 1$ for the synchronisation filter, $\alpha_{G_q} = 0$ and $\tau_\beta = 3$.
- variation in γ_q ($\hat{G}_q = \gamma_q K_{\text{lon}}$) given that $\gamma_q \in [0.75, 0.775, .., 1.0]$ or $\gamma_q \in [1.0, 1.05, ..., 3]$ for the rotor synchronisation filter, $\gamma_q = 1$ for the IBS control law, $\alpha_{G_q} = 0$ and $\tau_\beta = 3$.
- variation in γ_q ($\hat{G}_q = \gamma_q K_{\text{lon}}$) given that $\gamma_q \in [0.75, 0.775, .., 1.0]$ or $\gamma_q \in [1.0, 1.05, ..., 3]$ for the rotor synchronisation filter and IBS control law, $\alpha_{G_q} = 0$ and $\tau_\beta = 3$.

Below the above mentioned cases are provided respectively. The maximum region of overreaction (with 1% margin) of closed-loop response is indicated. For the IBS controller with and without rotor synchronisation this is indicated in dark and light grey respectively. In Fig. 5.28 the closed-loop frequency response is provided for varying τ_β. It can be observed that the IBS controller without rotor synchronisation does yield undesirable closed-loop frequency response, because of the resonance peak. This peak is more apparent when τ_β and/or IBS gain c_q are being increased. This shows that inclusion of the rotor synchronisation filter is of paramount importance to assure adequate closed-loop frequency response. This especially holds for aggressive manoeuvres for which large gains are required and/or when the rotorcraft is associated with slow disc-tilt response. In Fig. 5.29 the closed-loop frequency response is provided for varying α_{G_q}. Increasing α_{G_q} is beneficial for the closed-loop response of the IBS controller without synchronisation filter as the resonance peak decreases. This shows that when the control-dependency increases more desirable response can be achieved.

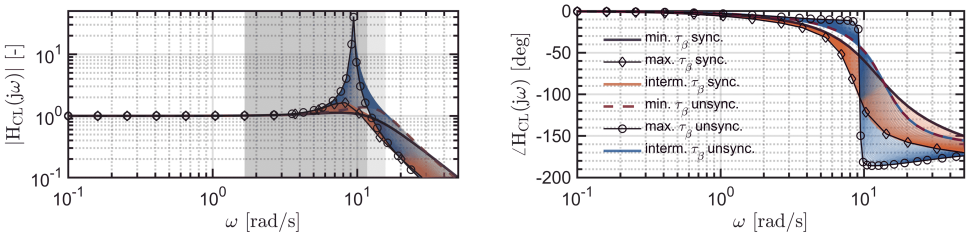

(a) Closed-loop frequency response for $c_q = 9$.

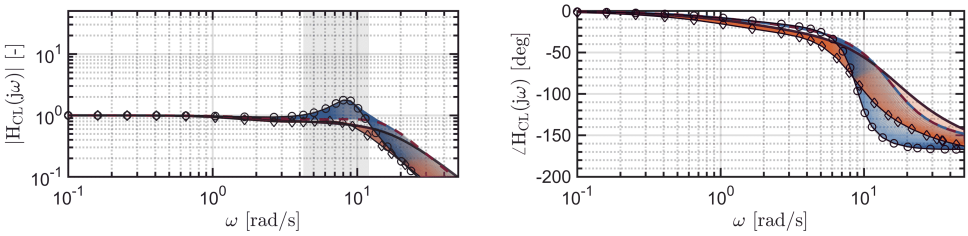

(b) Closed-loop frequency response for $c_q = 3$.

Figure 5.28: Closed-loop frequency response for IBS controller with and without flapping synchronisation filter, $\gamma_q = 1$ for IBS control law and synchronisation filter, $\tau_\beta \in [0.5, 0.575, ..., 4]$, $K_\beta = 110$ kNm/rad and $\alpha_{G_q} = 0$.

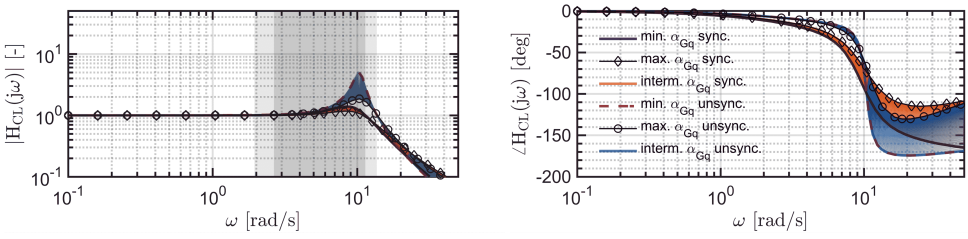

(a) Closed-loop frequency response for $c_q = 9$.

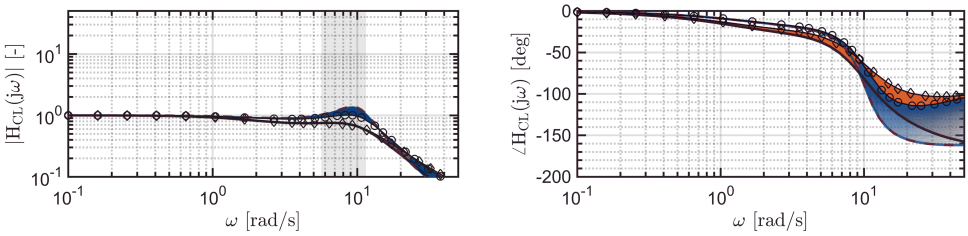

(b) Closed-loop frequency response for $c_q = 3$.

Figure 5.29: Closed-loop frequency response for IBS controller with and without flapping synchronisation filter, $\gamma_q = 1$ for IBS control law and synchronisation filter, $\tau_\beta = 3.5$, $K_\beta = 110$ kNm/rad and $\alpha_{G_q} \in [0.1, 0.11, ..., 0.5]$.

In Fig. 5.30 and Fig. 5.31 the closed-loop frequency response is provided for control effectiveness over- and underestimation in the IBS control law respectively. The first and foremost observation is that the resonance peak is smaller when control effectiveness is being overestimated. However, bandwidth is greater for control effectiveness underestimation, thus associated with quicker response. Most importantly, adequate closed-loop response could still be achieved when control effectiveness was over- or underestimated. This is because the closed-loop bandwidth has only changed slightly (magnitude is 1 for low and mid frequencies). This shows that the IBS controller is robust enough to uncertainties in control effectiveness in the IBS control law. Moreover, it can also be observed that when γ_q is overestimated and IBS gain is sufficiently high then adequate closed-loop response can be achieved for the IBS controller without synchronisation filter. This similar to the RINDI method from Pavel et al. [42].

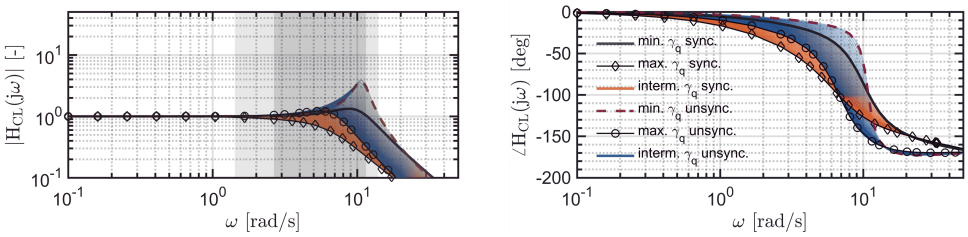

(a) Closed-loop frequency response for $c_q = 9$.

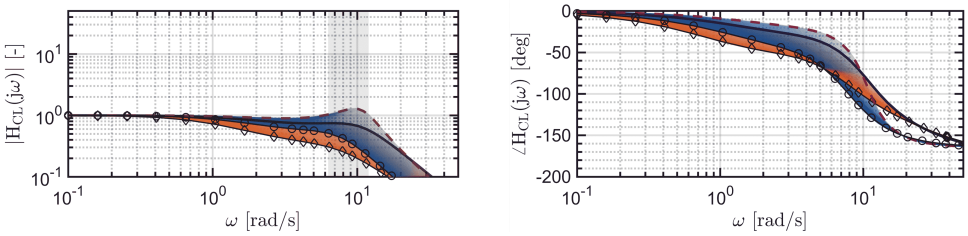

(b) Closed-loop frequency response for $c_q = 3$.

Figure 5.30: Closed-loop frequency response for IBS controller with and without rotor synchronisation filter, $\gamma_q \in [1, 1.05, ..., 3]$ for IBS control law, $\gamma_q = 1$ for rotor synchronisation filter, $\tau_\beta = 3$, $K_\beta = 110$kNm/rad and $\alpha_{G_q} = 0$..

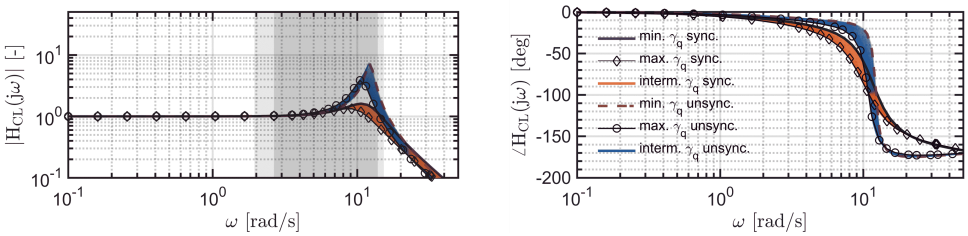

(a) Closed-loop frequency response for $c_q = 9$.

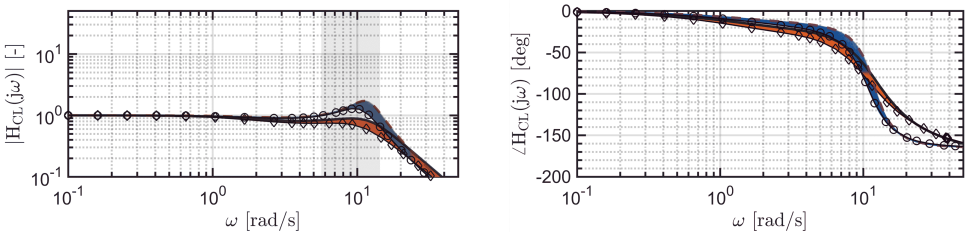

(b) Closed-loop frequency response for $c_q = 3$.

Figure 5.31: Closed-loop frequency response for IBS controller with and without rotor synchronisation filter, $\gamma_q \in [0.75, 0.775, ..., 1]$ for IBS control law, $\gamma_q = 1$ for synchronisation filter, $\tau_\beta = 3$, $K_\beta = 110$ kNm/rad and $\alpha_{G_q} = 0$.

Aside from considering control effectiveness mismatch for the IBS control it was also found necessary to consider it for the synchronisation filter. In Fig. 5.32 and Fig. 5.33 the results are provided of the robustness analysis on the synchronisation filter. Only the results of the IBS controller with synchronisation shall be considered for the discussion. It can be observed that the closed-loop frequency response is not desirable when control effectiveness is over- or under-estimated. When control effectiveness is over- or underestimated, there will be a significant region of under- and overestimation respectively. This is also in line with observations from the ADS-33E-PRF tracking from which it was found that controller performance was inadequate when control effectiveness was not well estimated. This shows that the controller is not robust to uncertainties in control effectiveness in the synchronisation filter.

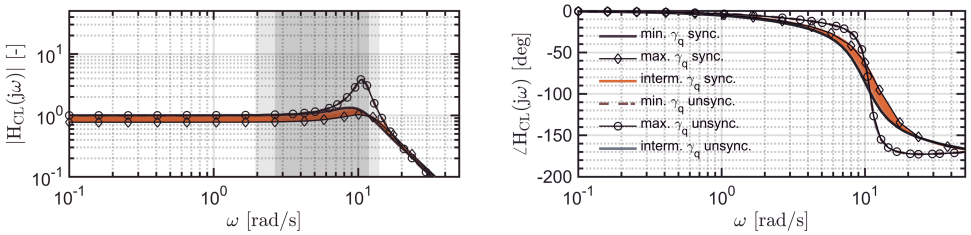

(a) Closed-loop frequency response for $c_q = 9$.

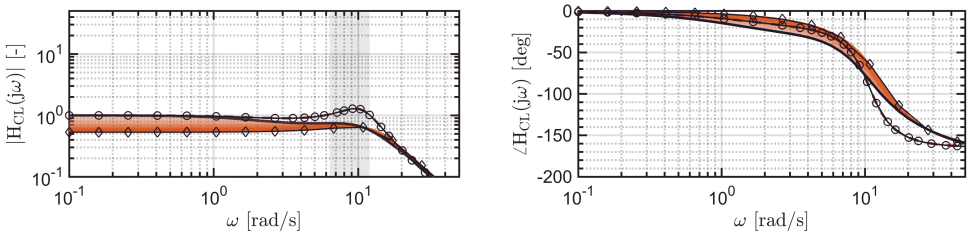

(b) Closed-loop frequency response for $c_q = 3$.

Figure 5.32: Closed-loop frequency response for IBS controller with and without rotor synchronisation filter, $\gamma_q \in [1, 1.05, ..., 3]$ for rotor synchronisation filter, $\gamma_q = 1$ for IBS control law, $\tau_\beta = 3$, $K_\beta = 110$kNm/rad and $\alpha_{G_q} = 0$.

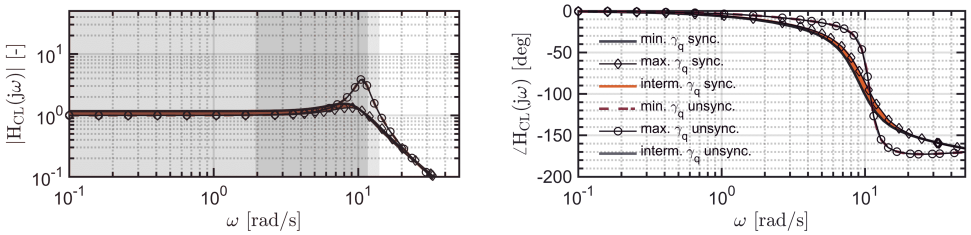

(a) Closed-loop frequency response for $c_q = 9$.

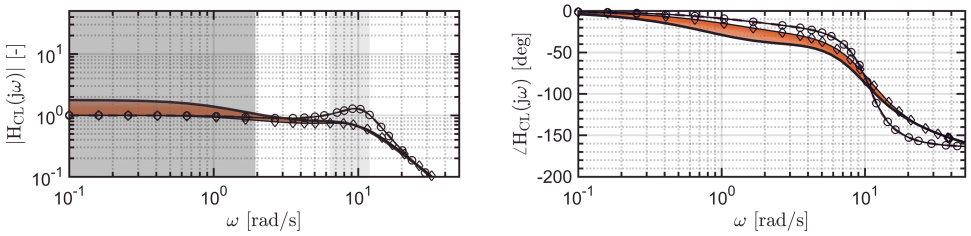

(b) Closed-loop frequency response for $c_q = 3$.

Figure 5.33: Closed-loop frequency response for IBS controller with and without rotor synchronisation filter, $\gamma_q \in [0.75, 0.775, ..., 1]$ for synchronisation filter, $\gamma_q = 1$ for IBS control law, $\tau_\beta = 3$, $K_\beta = 110$kNm/rad and $\alpha_{G_q} = 0$.

Previously, only control effectiveness mismatch was considered for either the IBS control law or synchronisation filter. In the next case, control effectiveness mismatch shall be considered for both the IBS control law and synchronisation filter. In Fig. 5.34 and Fig. 5.35 the closed-loop frequency response is provided for control effectiveness over- and underestimation respectively. It can be observed that closed-loop frequency response is not desirable as magnitude significantly deviates from 1. For control effectiveness over- and underestimation it can be observed that the region of under- and overestimation for low and mid frequencies is significant. Moreover, there is also a resonance peak for both cases. This is especially apparent for control effectiveness underestimation. This shows that controller performance can be severely affected when control effectiveness mismatch exists for both synchronisation filter and IBS control law.

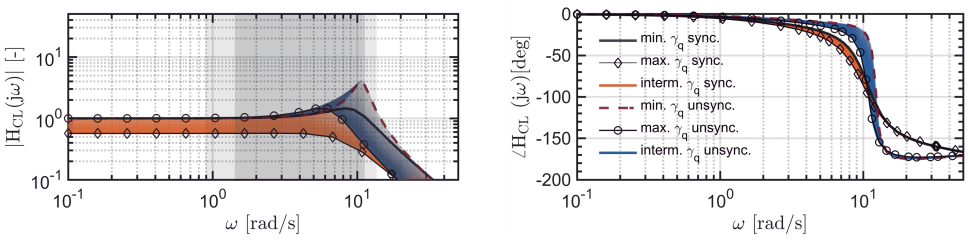

(a) Closed-loop frequency response for $c_q = 9$

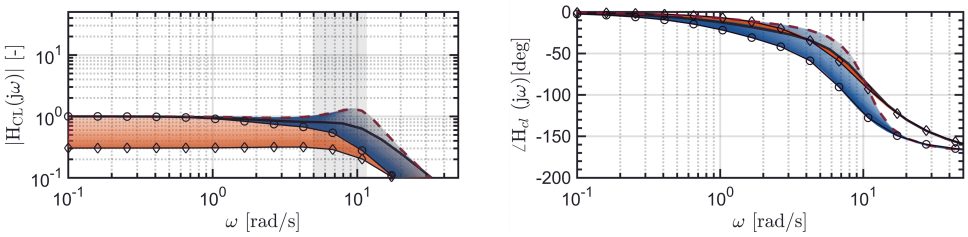

(b) Closed-loop frequency response for $c_q = 3$

Figure 5.34: Closed-loop frequency response for IBS controller with and without rotor synchronisation filter, $\gamma_q \in [1, 1.05, ..., 3]$ for rotor synchronisation filter and IBS control law, $\tau_\beta = 3$, $K_\beta = 110$kNm/rad and $\alpha_{G_q} = 0$..

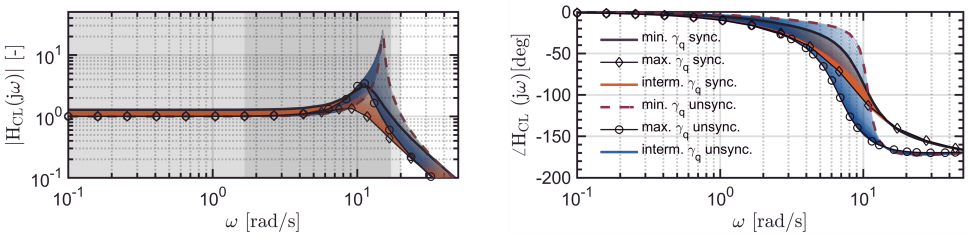

(a) Closed-loop frequency response for $c_q = 9$

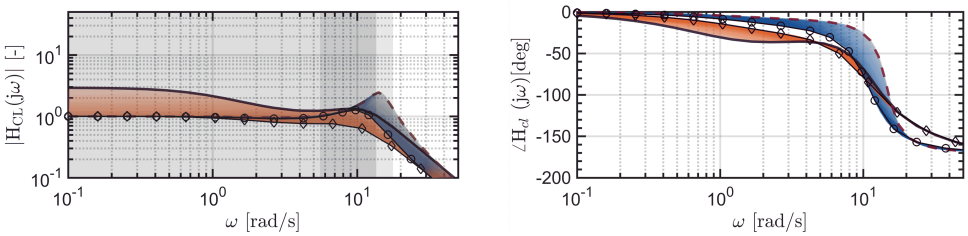

(b) Closed-loop frequency response for $c_q = 3$

Figure 5.35: Closed-loop frequency response for IBS controller with and without rotor synchronisation filter, $\gamma_q \in [0.75, 0.775, ..., 1]$ for rotor synchronisation filter and IBS control law, $\tau_\beta = 3$, $K_\beta = 110$kNm/rad and $\alpha_{G_q} = 0$.

Based on the closed-loop frequency analysis the following can be concluded:

- inclusion of a flapping synchronisation filter is necessary to avoid or reduce the resonance peak in the closed-loop frequency response. This subsequently means that when a flapping synchronisation filter is not included, closed-loop response will be erratic and characterised with significant overestimation of the reference signal. The above especially holds for an aggressive controller for which IBS gain is large and/or when disc-tilt response is slow. This can be observed from Fig. 5.28.
- increasing τ_β will yield a greater resonance peak. This is due to a greater difference in *idealised* and *actual* model, which translates into a significant delay between actuator and angular acceleration measurement. The former is based upon the *idealised* BF model, whereas the latter comes for the *actual* BF model. Since the angular acceleration measurements are used in a negative feedback loop, there will be magnified control inputs when it is delayed with respect to the actuator measurement [57].
- increasing IBS gain c_q will increase the resonance peak, yielding overreaction of the closed-loop system. For an aggressive tracking tasks (fast changing signal with large amplitude) this can be troublesome.
- the IBS controller is robust to uncertainties in control effectiveness of the IBS control law. This is based upon observations from Fig. 5.30 and Fig. 5.31. For $\gamma_q > 1$ or $\gamma_q < 1$, adequate closed-loop response was still achieved as closed-loop bandwidth was still sufficient. For control effectiveness over- or underestimation bandwidth would be reduced and increased respectively. From this it follows that, underestimation of control effectiveness could be favourable when performing a tracking task. However, this would be at cost of significant overreaction because of the large resonance peak. On the other hand, control effectiveness overestimation is characterised with a diminished resonance peak yielding less overreaction, but at the cost of slower closed-loop response.
- the IBS controller is not robust to uncertainties in control effectiveness in the synchronisation filter. This is apparent from Fig. 5.32 and Fig. 5.33, wherein control effectiveness over- and underestimation are considered. It can be clearly observed that the closed-loop frequency response is highly undesirable, because magnitude significantly deviates from 1 for a large frequency range.
- when the ratio $\frac{H_q}{Fq,\beta_{1c}}$ increases then $\dot{q}$ will be increasingly more directly governed by the cyclic control inputs, which subsequently decreases the resonance peak.

5.2.8. Closed-loop stability analysed using Routh-Hurwitz stability criterion

Next, it will be of interest to determine the analytical closed-loop stability. A continuous *Laplace* transfer function ($H_{CL}(s)$) is being used to represent the closed-loop system, therefore the *Routh-Hurwitz* stability criterion shall be incorporated. This criterion does assess closed-loop stability by means of the characteristic polynomial of the closed-loop transfer function [35]. The system is asymptotically stable when the real parts of the closed-loop eigenvalues are situated in the LHP. Actuator (first-order lag filter with $\tau_{\text{act}} = 0.1$ s) and sensor dynamics (second-order washout filter with $\zeta_{\text{filt}} = 1$ and $\omega_{\text{n,filt}} = 100$ rad/s) are taken into account when performing the analysis. Moreover, sampling time was set sufficiently low (dt = 0.01 s) and control saturation was not accounted for. The analysis shall be considered for the closed-loop system with and without flapping synchronisation filter. Full and accurate knowledge of system dynamics is assumed when constructing the filters. However, control effectiveness shall be changed for the IBS control law and/or synchronisation filter and are established by means of the *method of residualised dynamics*. The analysis shall be considered for $c_q \in [15, 20]$, $\tau_\beta \in [0.5, 1.0, \ldots, 5.0]$, $K_\beta \in [10, 15, \ldots, 150]$ kNm/rad and $\alpha_{G_q} = 0$. The objective is to show that without flapping synchronisation filter, closed-loop stability will be affected for high gains and to proof that the controller is more robust to uncertainties in control effectiveness for the IBS control law than for the synchronisation filter. All cases to be analysed will consider variation in τ_β and K_β. The cases of interest are:

- without flapping synchronisation filter and $\gamma_q \in [0.5, 1, 3]$ for control effectiveness in IBS control law.
- with flapping synchronisation filter given that $\gamma_q = 1$ for control effectiveness in flapping synchronisation filter and $\gamma_q \in [0.5, 1, 3]$ for control effectiveness in IBS control law.
- with flapping synchronisation filter given that $\gamma_q \in [0.5, 1, 3]$ for control effectiveness in flapping synchronisation filter and $\gamma_q = 1$ for control effectiveness in IBS control law.
- with flapping synchronisation filter given that $\gamma_q \in [0.5, 1, 3]$ for control effectiveness in synchronisation filter and IBS control law.

In Fig. 5.36 and Fig. 5.37 the results of the closed-loop stability analysis are provided for the closed-loop system without and with flapping synchronisation filter respectively. It can be observed that the closed-loop system without flapping synchronisation filter is less stable than the closed-loop system with flapping synchronisation filter. Moreover, the closed-loop system without rotor synchronisation and $\gamma_q > 1$ does have a greater region of stability than for $\gamma_q \leq 1$. This means that for specific combinations of K_β and τ_β it is still possible to have closed-loop stability even though rotor synchronisation is not considered. Control effectiveness overestimation is therefore favourable regarding closed-loop system response, which is in line with observations from [42]. From Fig. 5.37 it can be observed that rotor synchronisation significantly improves system stability, which shows the importance of signal synchronisation.

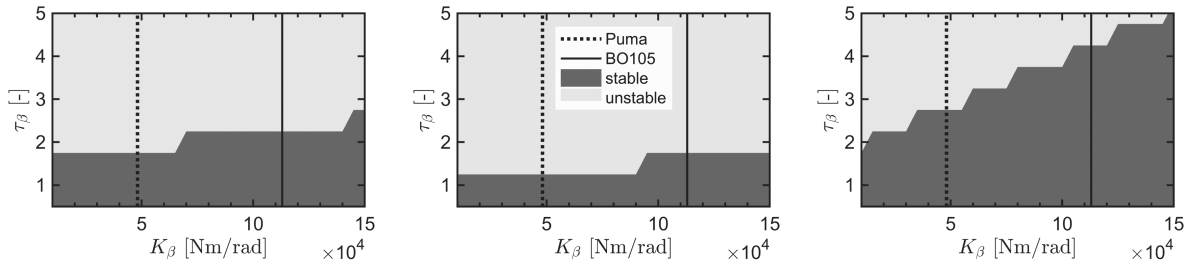

(a) Closed-loop stability with $c_q = 15$ and for $\gamma_q = 1$, $\gamma_q = 0.5$ and $\gamma_q = 3$ respectively.

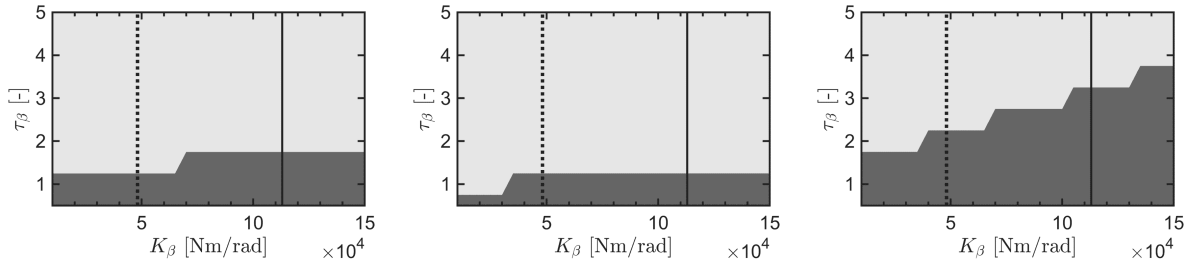

(b) Closed-loop stability with $c_q = 20$ and for $\gamma_q = 1$, $\gamma_q = 0.5$ and $\gamma_q = 3$ respectively.

Figure 5.36: Results closed-loop stability analysis using IBS controller without flapping synchronisation filter given that $\gamma_q \in [0.5, 1, 3]$ for control effectiveness in IBS control law, $c_q \in [15, 20]$, $\tau_\beta \in [0.5, 1, .., 5]$ and $K_\beta \in [10, 15, ..., 150]$ kNm/rad.

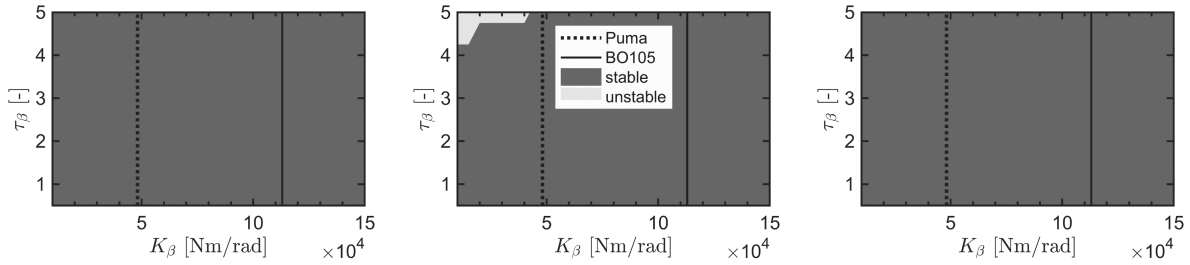

(a) Closed-loop stability with $c_q = 15$ and for $\gamma_q = 1$, $\gamma_q = 0.5$ and $\gamma_q = 3$ respectively.

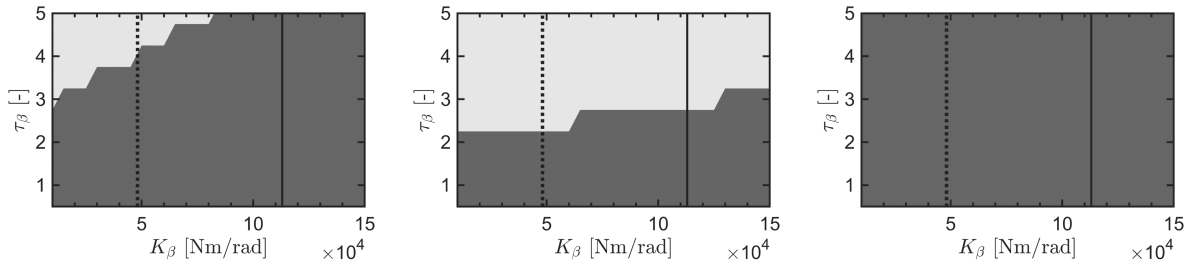

(b) Closed-loop stability with $c_q = 20$ and for $\gamma_q = 1$, $\gamma_q = 0.5$ and $\gamma_q = 3$ respectively.

Figure 5.37: Results closed-loop stability analysis for IBS controller with flapping synchronisation filter given that $\gamma_q \in [0.5, 1, 3]$ for control effectiveness in IBS control law, $\gamma_q = 1$ for control effectiveness in synchronisation filter, $c_q \in [15, 20]$, $\tau_\beta \in [0.5, 1, .., 5]$ and $K_\beta \in [10, 15, ..., 150]$ kNm/rad.

In Fig. 5.38 the results of the closed-loop stability analysis are provided for the IBS controller with control effectiveness mismatch in the flapping synchronisation filter only. It can be observed that closed-loop stability is affected when $\gamma_q < 1$, since the region of instability is significant. Moreover, the region of instability increases when c_q increases. On the other hand, closed-loop stability is not affected for large γ_q. In Fig. 5.39 the results of the closed-loop stability analysis are provided for the IBS controller with control effectiveness mismatch for the control effectiveness in the IBS control law and synchronisation filter. It can be observed that stability is affected when the control effectiveness is underestimated. The region of stability differs from the previous case, since it has been rotated clockwise.

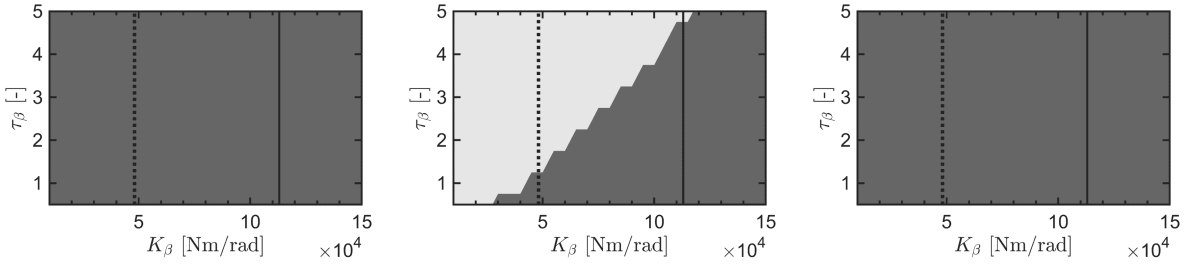

(a) Closed-loop stability with $c_q = 15$ and for $\gamma_q = 1$, $\gamma_q = 0.5$ and $\gamma_q = 3$ respectively.

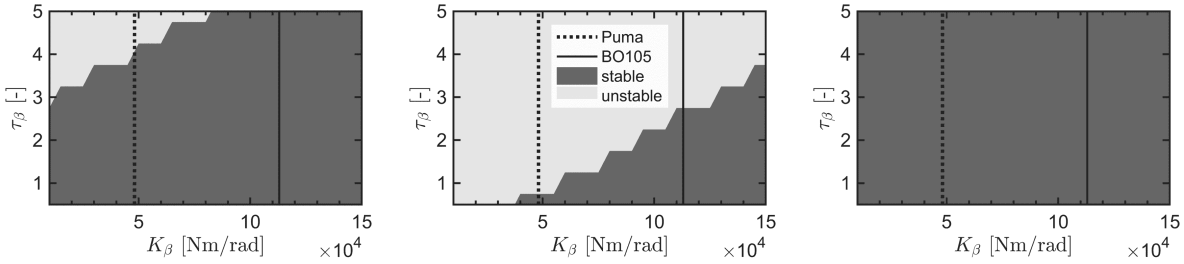

(b) Closed-loop stability with $c_q = 20$ and for $\gamma_q = 1$, $\gamma_q = 0.5$ and $\gamma_q = 3$ respectively.

Figure 5.38: Results closed-loop stability analysis for IBS controller with flapping synchronisation filter given that $\gamma_q \in [0.5, 1, 3]$ for control effectiveness in synchronisation filter, $\gamma_q = 1$ for control effectiveness in IBS control law, $c_q \in [15, 20]$, $\tau_\beta \in [0.5, 1, .., 5]$ and $K_\beta \in [10, 15, ..., 150]$ kNm/rad.

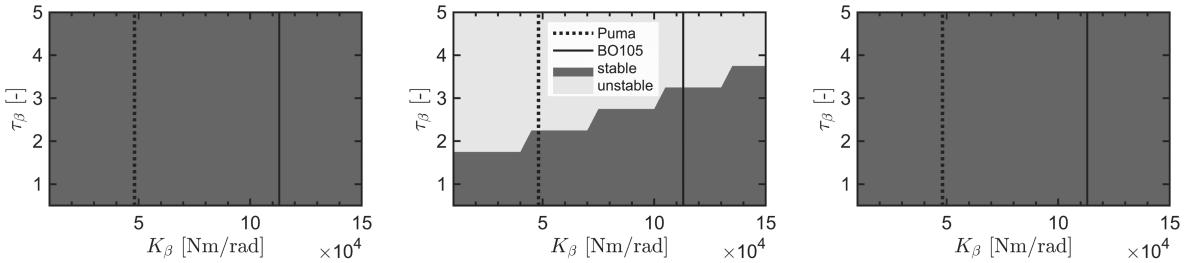

(a) Closed-loop stability with $c_q = 15$ and for $\gamma_q = 1$, $\gamma_q = 0.5$ and $\gamma_q = 3$ respectively.

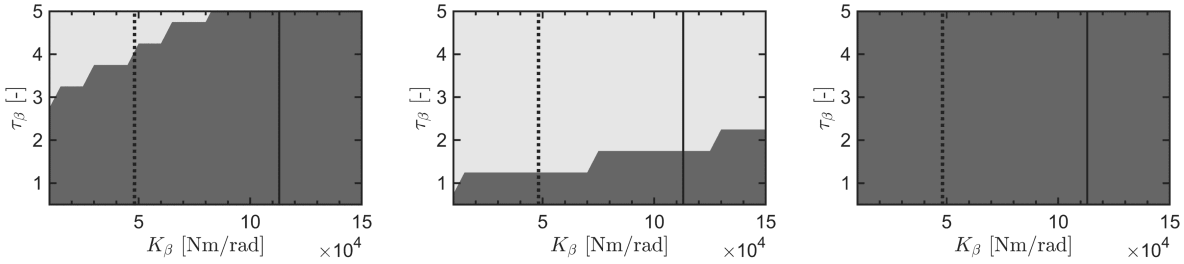

(b) Closed-loop stability with $c_q = 20$ and for $\gamma_q = 1$, $\gamma_q = 0.5$ and $\gamma_q = 3$ respectively.

Figure 5.39: Results closed-loop stability analysis for IBS controller with flapping synchronisation filter given that $\gamma_q \in [0.5, 1, 3]$ for control effectiveness in IBS control law and synchronisation filter, $c_q \in [15, 20]$, $\tau_\beta \in [0.5, 1, .., 5]$ and $K_\beta \in [10, 15, ..., 150]$ kNm/rad.

Based on the closed-loop stability analysis the following can be stated:

- Closed-loop stability is significantly affected when $\dot{q}_0$ and $\theta_{1s,\text{meas}}$ are not well-synchronised with each other. This can be observed from Fig. 5.36 as the region of instability is significantly greater than for the synchronised case from Fig. 5.37. Without flapping synchronisation, angular acceleration measurements will be lagging behind the actuator measurements. Since the angular acceleration measurements are used in a negative feedback loop, see Eq. 5.14, control inputs will be magnified, yielding quicker instability of the closed-loop system. For slower disc tilt response (large τ_β), there will be a greater time-delay between the angular acceleration and actuator measurements, yielding even quicker system instability. Without rotor synchronisation it is still possible to improve system stability, namely by increasing the control effectiveness. Rotor synchronisation will improve closed-loop stability as $\dot{q}_0$ and $\theta_{1s,\text{meas}}$ will be synchronised with each other. This can be observed from Fig. 5.37 as the region of stability has significantly improved. Only when control effectiveness is highly underestimated and control gain is high, there will be a significant region of instability for the synchronised case.
- For the IBS controller with control effectiveness mismatch of the synchronisation filter control effectiveness, it can be stated that control effectiveness underestimation is most concerning. This is based on the significant region of instability, which can be observed from Fig. 5.38. This can be related to findings from Fig. 5.15, wherein control effectiveness underestimation did yield magnified control inputs. This could yield quicker instability of the closed-loop system. The aforementioned also holds when both the control effectiveness of the IBS control law and synchronisation filter are underestimated. However, the regions of stability/instability differ for both cases. It must be stated that the controller is more affected by control effectiveness mismatch of the synchronisation filter control effectiveness than by control effectiveness mismatch of the IBS control effectiveness.
- Another general observation that can be made is that stability can be assured for a greater range of τ_β for the hingeless MBB Bo 105 (K_β = 113330 Nm/rad from [40]) than for the articulated Aérospatiale SA 330 Puma (K_β = 48149 Nm/rad from [40]). This is because the former is associated with greater K_β.

5.2.9. Conclusion on Lyapunov-based control design for τ_β-based rotorcraft model

With the analysis performed on the τ_β-based rotorcraft model it is necessary to sum up findings. These findings can be of great importance when considering the inclusion of lead-lag dynamics to a BF model in terms of *Lyapunov*-based control design. A special focus will be on IBS for which certain assumptions, such as TSS, shall not be violated. Angular accelerations are primarily governed by cyclic flapping angles, rather than by cyclic control inputs, thus $\boldsymbol{F}_{q,\beta_{1c}} > \boldsymbol{H}_\Omega$. This can be regarded problematic as this does violate a necessary condition for establishing an incremental-based stabilising control law, namely the TSS condition [54]. This could be circumvented by means of the *method of residualised dynamics*, which assumes residualisation of the internal dynamics. In this specific case, this would mean residualisation of flapping dynamics. The *idealised* rotorcraft model would therefore be based upon steady-state flapping dynamics. The *actual* rotorcraft model is actually associated with flapping dynamics, which implies that there is some discrepancy between both models. This discrepancy can be accounted for by means of the so-called synchronisation filter. Which is a lag filter that delays the actuator measurement effectively by the same amount as by which the *actual* angular body response is delayed with. This will assure that both the actuator and pitch acceleration measurements are synchronised with each other. Synchronisation can be of prime concern for those rotorcraft models which are associated with slow discs-tilt response (large τ_β), because body and flap are heavily coupled with each other. When the controller is based upon a decoupled model, then there will also be a large difference between the *actual* and *idealised* model. This implies that rotor synchronisation can be considered a requisite for those rotorcraft models which are associated with large τ_β. Moreover, another important conclusion form the analysis is that residualisation of rotor dynamics will be of prime concern when the body-rotor coupling and control-depended term of that specific rotor dynamics (e.g. lead-lag/inflow etc.) is significant. This is based on the fact that residualisation will remove the body-rotor coupling term and enhance the control-dependency using that coupling term. The aforementioned will yield an improvement in the TSS condition. On the other hand actuator limitations were found to be problematic regarding the aforementioned, because it did limit $\hat{\boldsymbol{G}}_q \Delta\theta_{1c}$, therefore making it more prone to violating the TSS condition.

6
Rotorcraft Control Modes

In this chapter the control modes of the main MBB Bo 105 rotorcraft model from chapter 2 are being provided. The Rate Command/Attitude Hold (RCAH) and Attitude Command/Attitude Hold (ACAH) mode are the control modes that will be discussed. The rotorcraft model is actually also equipped with the Translational Rate Command/Position Hold mode, but shall not be considered in this research and therefore also not discussed in this chapter. In Section 6.1 the control structure of the rotorcraft is shortly touched upon. In Section 6.2 the RCAH shall be discussed, wherein the derivation of this control mode is provided and additional modifications to assure adequate actuator and state measurement synchronisation. A CFIBS control strategy is realised for this control mode. In addition to this, it will also be shown that the RCAH control mode can be equivalent to a PI controller when considering standard IBS. In Section 6.3 the derivation of the ACAH control is being discussed. This control mode incorporates a CFBS control strategy for defining its control law.

6.1. Rotorcraft control architecture

Before considering the control modes individually it is first necessary to understand the general architecture of the flight control system, which can be observed in Fig. 6.1. It does consist of three subsystems, which are naturally separated because of time-scale separation between their dynamics [46]. The most inner subsystem is associated with the fastest dynamics, whereas the outer subsystems are associated with slower dynamics. The angular rate subsystem can be identified as the most inner subsystem of the flight control system. This subsystem provides the required cyclic and tail rotor control inputs for achieving a desired tracking task. The attitude subsystem can be considered an outer loop of the angular rate subsystem. This means that the angular rate subsystem provides the *virtual* control inputs for the attitude subsystem. The navigational subsystem can be considered an outer loop with respect to the attitude subsystem, which means that the attitude subsystem provides the *virtual* control inputs to the navigational subsystem. Based on the previous discussion it is obvious that inadequate synchronisation in the most inner subsystem can be problematic, because it will propagate through all the other subsystems yielding poor controller performance.

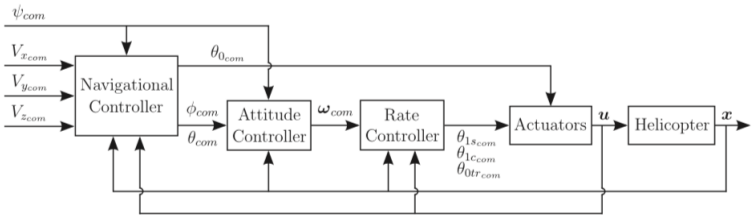

Figure 6.1: Flight control system of rotorcraft [47].

6.2. Rate Command/Attitude Hold (RCAH) mode

The first control mode to be considered is the RCAH mode. The main objective of this mode is to let the rotorcraft track a desired angular rate while achieving bounded response of the remaining body states. The desired angular rates are commanded by the system and set by the human operator. The RCAH control mode is integral part of the on-board flight computers which receive inputs from the human operator and subsequently translate these electrical signals into control inputs such that the desired actions can be executed

[46]. Execution of these commands must be within the space of possibilities of the controller, which e.g. implies that natural limitations of the actuators must be respected. The RCAH mode does consist of a single subsystem, namely the angular rate subsystem. The angular rate subsystem is directly connected to the cyclic control inputs, therefore constructing a RCAH controller is more convenient than an ACAH controller. The aforementioned is actually not completely true as flapping dynamics forms a delaying channel between the angular accelerations and the control inputs. This is especially true for the pitch and roll accelerations, which are primarily governed by the cyclic flapping angles. The control strategy adopted for the ACAH is (CF)IBS, because its obviates the need of having accurate model, which implies that it can be more robust to uncertainties in system dynamics [53].

6.2.1. First-order Taylor series for angular accelerations

The RCAH mode does require a stabilising control law for the angular rate subsystem, which can be established by means of the *method of residualised dynamics* or the *flapping angle equivalence method*. The *flapping angle equivalence method* is a geometric transformation wherein the flapping angles with respect to the shaft plane are transformed to a combination of flapping angles with respect to the control plane and cyclic control inputs (it assumes instantaneous disc-tilt). The other method considers residualisation of internal dynamics (e.g. steady-state flap-lag dynamics) for increasing control-dependency and diminishing state-dependency. Both strategies will yield an expression for the angular accelerations wherein control-dependency has been enhanced to enable an IBS control law for which TSS holds. This can be considered of prime concern when considering incremental-based control design. The main difference between the two above mentioned methods, is that the *flapping angle equivalence method* only considers steady-state flapping dynamics (flapping residualisation), whereas the *method of residualised dynamics* can consider residualisation of more internal dynamics (e.g. flap-lag-inflow) to enhance the control- to state-dependency more. On the other hand, the former method requires more model knowledge, which is not favourable. However, the strategies do not yet account for the delay introduced by rotor dynamics. Accounting for the delay introduced by rotor dynamics shall be considered in the feedback of the actuator measurements by means of a synchronisation filter and shall be considered later on.

Both above mentioned strategies will be considered for the derivation of the stabilising control law for the angular rate subsystem. These shall be considered in parallel with each other. The first step towards deriving the stabilising control law for the angular rate subsystem, starts by defining the first-order *Taylor* series. For the *flapping angle equivalence method* and *method of residualised dynamics* these can be identified as

$$\dot{\boldsymbol{\omega}} = \dot{\boldsymbol{\omega}}_0 + \hat{\boldsymbol{G}}_{\omega,F}\Delta \begin{bmatrix} \boldsymbol{\beta}_{SP} \\ \theta_{0,tr} \end{bmatrix}, \tag{6.1}$$

$$\dot{\boldsymbol{\omega}} = \dot{\boldsymbol{\omega}}_0 + \hat{\boldsymbol{G}}_{\omega,R}\boldsymbol{U}, \tag{6.2}$$

wherein $\dot{\boldsymbol{\omega}}$ is the vector containing the angular accelerations, namely $[\dot{p}\ \dot{q}\ \dot{r}]^T$. Moreover $\dot{\boldsymbol{\omega}}_0$ is the time-delayed measurement of the angular accelerations. The control vector of the first-order *Taylor* series from Eq. 6.1 is $[\beta_{1c}\ \beta_{1s}\ \theta_{0,tr}]^T$, which shows explicit dependency on the flapping angles with respect to the shaft plane. This differs from the control vector $\boldsymbol{U}$ from Eq. 6.2, which is $[\theta_{1s}\ \theta_{1c}\ \theta_{0,tr}]^T$. In order for the *flapping angle equivalence method* to have an function explicitly depending on the cyclic control inputs, it is necessary to incorporate a transformation. This transformation converts $\boldsymbol{\beta}_{SP}$ to $\boldsymbol{\beta}_{CP} + \boldsymbol{\theta}_{C_F}$, with $\boldsymbol{\beta}_{CP}$ being the flapping angles with respect to the control plane ($[\beta_{1c}\ \beta_{1s}]^T_{CP}$) and $\boldsymbol{\theta}_{C_F}$ being a vector containing the cyclic control inputs ($[-\theta_{1s}\ \theta_{1c}]^T$). Moreover, is should be noted that the $\boldsymbol{\theta}_C$ will be considered the vector containing the cyclic control inputs of the following form $[\theta_{1s}\ \theta_{1c}]^T$. From this it follows that $\boldsymbol{\theta}_{C_F} \neq \boldsymbol{\theta}_C$, which means that a transformation is required to arrive from one to another, which shall be touched upon later on. This means that $[\boldsymbol{\beta}_{SP}\ \theta_{0,tr}]$ from Eq. 6.1 can be written as $[\beta_{1c} - \theta_{1s}\ \beta_{1s} + \theta_{1c}\ \theta_{0,tr}]^T$, wherein the flapping angles are now with respect to the control plane.

6.2.2. Control effectiveness matrix

Next, it is deemed necessary to consider the control effectiveness of the first-order *Taylor* series from Eq. 6.1 and Eq. 6.2. The control effectiveness of the first-order *Taylor* series using the *flapping angle equivalence method* is partially based on the state-depended relationship between the angular accelerations $\dot{p}$ and $\dot{q}$ and the cyclic flapping angles β_{1s} and β_{1c} with respect to the shaft plane. The aforementioned does account

for the fact that these angular accelerations are more governed by cyclic flapping angles than cyclic control inputs. The relation between $\dot{p}$ and $\dot{q}$ and the cyclic flapping angles β_{1s} and β_{1c} can be obtained using the expression for the dynamics of the rotational motion given in Eq. 2.113 and the the expressions for the hub moments given in Eq. 2.85 and Eq. 2.86. Substitution of the latter two expression into Eq. 2.113 will yield an expression explicitly depending on the cyclic flapping angles with respect to the shaft plane and therefore provide the state-depended terms $\boldsymbol{F}_{p,\beta_{1s}}$, $\boldsymbol{F}_{p,\beta_{1c}}$, $\boldsymbol{F}_{q,\beta_{1s}}$ and $\boldsymbol{F}_{q,\beta_{1c}}$. Furthermore the control effectiveness of $\dot{r}$ can be established using the expression for the dynamics of the rotational motion given in Eq. 2.113 and the global moment contribution of the tail rotor as given in Eq. 2.98. The aforementioned will yield an expression for $\dot{r}$, which depends explicitly on the tail rotor collective $\theta_{0,\text{tr}}$, which shall be denoted as $\boldsymbol{H}_{r,\theta_{0\text{tr}}}$. Using Eq. 2.113, it is possible to account for the entries indicated by $\square$. Based on the above mentioned the following control effectiveness matrix $\hat{\boldsymbol{G}}_{\omega,F}$ using the method of *flapping angle equivalence method* can be established

$$\hat{\boldsymbol{G}}_{\omega,F} = \begin{bmatrix} * & \boldsymbol{F}_{p,\beta_{1s}} & \square \\ -\boldsymbol{F}_{q,\beta_{1c}} & * & * \\ * & \square & \boldsymbol{H}_{r,\theta_{0\text{tr}}} \end{bmatrix}, \tag{6.3}$$

wherein the empty entries $(*)$ can be neglected. On the other hand, the control effectiveness using the *method of residualised dynamics* is determined by means of residualisation of internal dynamics. This implies that $\hat{\boldsymbol{G}}_R$ can be established by considering flap/flap-lag/flap-lag-inflow residualisation. For obtaining $\hat{\boldsymbol{G}}_{\omega,R}$ it will therefore be deemed necessary to consider steady-state condition for the internal dynamics. For this particular research it will be of prime interest to consider residualisation of flap or flap-lag dynamics. In Eq. 6.4 and Eq. 6.5 the control effectiveness is provided when considering flap or flap-lag residualisation given that the model is associated with second-order flap-lag dynamics respectively.

$$\hat{\boldsymbol{G}}_{\omega,R} = \boldsymbol{H}_{\omega} - \boldsymbol{F}_{\omega,\beta_{SP}} \boldsymbol{F}^{-1}_{\dot{\beta}_{SP},\beta_{SP}} \boldsymbol{H}_{\dot{\beta}_{SP}} \tag{6.4}$$

$$\hat{\boldsymbol{G}}_{\omega,R} = \boldsymbol{H}_{\omega} - \begin{bmatrix} \boldsymbol{F}_{\omega,\beta_{SP}} & \boldsymbol{F}_{\omega,\zeta} \end{bmatrix} \begin{bmatrix} \boldsymbol{F}_{\dot{\beta}_{SP},\beta_{SP}} & \boldsymbol{F}_{\dot{\beta}_{SP},\zeta} \\ \boldsymbol{F}_{\dot{\zeta},\beta_{SP}} & \boldsymbol{F}_{\dot{\zeta},\zeta} \end{bmatrix}^{-1} \begin{bmatrix} \boldsymbol{H}_{\dot{\beta}_{SP}} \\ \boldsymbol{H}_{\dot{\zeta}} \end{bmatrix} \tag{6.5}$$

From Eq. 6.4 and Eq. 6.5 it can be observed that these do depended on a couple of state- and control-depended terms. The following control-depended terms were considered

$$\boldsymbol{H}_{\omega} = \begin{bmatrix} H_p \\ H_q \\ H_r \end{bmatrix}, \quad \boldsymbol{H}_{\dot{\beta}_{SP}} = \begin{bmatrix} H_{\dot{\beta}_0} \\ H_{\dot{\beta}_{1s}} \\ H_{\dot{\beta}_{1c}} \end{bmatrix} \text{ and } \boldsymbol{H}_{\dot{\zeta}} = \begin{bmatrix} H_{\dot{\zeta}_0} \\ H_{\dot{\zeta}_{1s}} \\ H_{\dot{\zeta}_{1c}} \end{bmatrix}. \tag{6.6}$$

Moreover the body-flap and body-lag matrices can be identified respectively as

$$\boldsymbol{F}_{\omega,\beta_{SP}} = \begin{bmatrix} F_{p,\beta_0} & F_{p,\beta_{1s}} & F_{p,\beta_{1c}} \\ F_{q,\beta_0} & F_{q,\beta_{1s}} & F_{q,\beta_{1c}} \\ F_{r,\beta_0} & F_{r,\beta_{1s}} & F_{r,\beta_{1c}} \end{bmatrix} \text{ and } \boldsymbol{F}_{\omega,\zeta} = \begin{bmatrix} F_{p,\zeta_0} & F_{p,\zeta_{1s}} & F_{p,\zeta_{1c}} \\ F_{q,\zeta_0} & F_{q,\zeta_{1s}} & F_{q,\zeta_{1c}} \\ F_{r,\zeta_0} & F_{r,\zeta_{1s}} & F_{r,\zeta_{1c}} \end{bmatrix}. \tag{6.7}$$

Lastly, the following state-depended terms can also be identified as

$$\begin{aligned} \boldsymbol{F}_{\dot{\beta},\beta_{SP}} &= \begin{bmatrix} F_{\dot{\beta}_0,\beta_0} & F_{\dot{\beta}_0,\beta_{1s}} & F_{\dot{\beta}_0,\beta_{1c}} \\ F_{\dot{\beta}_{1s},\beta_0} & F_{\dot{\beta}_{1s},\beta_{1s}} & F_{\dot{\beta}_{1s},\beta_{1c}} \\ F_{\dot{\beta}_{1c},\beta_0} & F_{\dot{\beta}_{1c},\beta_{1s}} & F_{\dot{\beta}_{1c},\beta_{1c}} \end{bmatrix} \quad \boldsymbol{F}_{\dot{\zeta},\zeta} = \begin{bmatrix} F_{\dot{\zeta}_0,\zeta_0} & F_{\dot{\zeta}_0,\zeta_{1s}} & F_{\dot{\zeta}_0,\zeta_{1c}} \\ F_{\dot{\zeta}_{1s},\zeta_0} & F_{\dot{\zeta}_{1s},\zeta_{1s}} & F_{\dot{\zeta}_{1s},\zeta_{1c}} \\ F_{\dot{\zeta}_{1c},\zeta_0} & F_{\dot{\zeta}_{1c},\zeta_{1s}} & F_{\dot{\zeta}_{1c},\zeta_{1c}} \end{bmatrix} \\ \boldsymbol{F}_{\dot{\beta}_{SP},\zeta} &= \begin{bmatrix} F_{\dot{\beta}_0,\zeta_0} & F_{\dot{\beta}_0,\zeta_{1s}} & F_{\dot{\beta}_0,\zeta_{1c}} \\ F_{\dot{\beta}_{1s},\zeta_0} & F_{\dot{\beta}_{1s},\zeta_{1s}} & F_{\dot{\beta}_{1s},\zeta_{1c}} \\ F_{\dot{\beta}_{1c},\zeta_0} & F_{\dot{\beta}_{1c},\zeta_{1s}} & F_{\dot{\beta}_{1c},\zeta_{1c}} \end{bmatrix} \quad \boldsymbol{F}_{\dot{\zeta},\beta_{SP}} = \begin{bmatrix} F_{\dot{\zeta}_0,\beta_0} & F_{\dot{\zeta}_0,\beta_{1s}} & F_{\dot{\zeta}_0,\beta_{1c}} \\ F_{\dot{\zeta}_{1s},\beta_0} & F_{\dot{\zeta}_{1s},\beta_{1s}} & F_{\dot{\zeta}_{1s},\beta_{1c}} \\ F_{\dot{\zeta}_{1c},\beta_0} & F_{\dot{\zeta}_{1c},\beta_{1s}} & F_{\dot{\zeta}_{1c},\beta_{1c}} \end{bmatrix} \end{aligned} \tag{6.8}$$

From Eq. 6.4 and Eq. 6.5 it can be observed that residualisation of flap is more favourable, because it does depend less on system dynamics. On the other hand, flap-lag residualisation can be more favourable when it enhances control effectiveness even more such that the TSS is less likely of being violated.

6.2.3. Stabilising control law for angular rate subsystem using standard IBS procedure

For establishing a stabilising control law for the angular rate subsystem it is first necessary to determine the tracking error $\boldsymbol{z}_\omega$. The expression for $\boldsymbol{z}_\omega$ is equal to

$$\boldsymbol{z}_\omega = \boldsymbol{\omega} - \boldsymbol{\omega}_{\text{ref}}, \tag{6.9}$$

wherein $\boldsymbol{\omega}$ and $\boldsymbol{\omega}_{\text{ref}}$ are the actual and desired angular rates respectively. The next design step is to take the derivative of Eq. 6.9 and substituting the expression for the first-order *Taylor* series from either Eq. 6.1 or Eq. 6.2 into it. The expression for $\dot{\boldsymbol{z}}_\omega$ using the first-order *Taylor* series from Eq. 6.1 or Eq. 6.2 is respectively

$$\dot{\boldsymbol{z}}_\omega = \dot{\boldsymbol{\omega}} - \dot{\boldsymbol{\omega}}_{\text{ref}} = \dot{\boldsymbol{\omega}}_0 + \hat{\boldsymbol{G}}_{\omega,F}\Delta\begin{bmatrix}\boldsymbol{\theta}_{C_F} + \boldsymbol{\beta}_{CP}\\ \theta_{\text{tr}}\end{bmatrix} - \dot{\boldsymbol{\omega}}_{\text{ref}}, \tag{6.10}$$

$$\dot{\boldsymbol{z}}_\omega = \dot{\boldsymbol{\omega}} - \dot{\boldsymbol{\omega}}_{\text{ref}} = \dot{\boldsymbol{\omega}}_0 + \hat{\boldsymbol{G}}_{\omega,R}\Delta\boldsymbol{U} - \dot{\boldsymbol{\omega}}_{\text{ref}}. \tag{6.11}$$

A quadratic CLF $\mathcal{V}_\omega(\boldsymbol{z}_\omega)$ shall be used for the angular rate subsystem, which can be written as follows

$$\mathcal{V}_\omega(\boldsymbol{z}_\omega) = 0.5\boldsymbol{z}_\omega^T\boldsymbol{z}_\omega. \tag{6.12}$$

Taking the derivative of $\mathcal{V}_\omega(\boldsymbol{z}_\omega)$ and substituting Eq. 6.10 or 6.11 into it, respectively yields

$$\dot{\mathcal{V}}_\omega(\dot{\boldsymbol{z}}_\omega) = \boldsymbol{z}_\omega^T\Big\{\dot{\boldsymbol{\omega}}_0 + \hat{\boldsymbol{G}}_{\omega,F}\Delta\begin{bmatrix}\boldsymbol{\theta}_{C_F} + \boldsymbol{\beta}_{CP}\\ \theta_{\text{tr}}\end{bmatrix} - \dot{\boldsymbol{\omega}}_{\text{ref}}\Big\}, \tag{6.13}$$

$$\dot{\mathcal{V}}_\omega(\dot{\boldsymbol{z}}_\omega) = \boldsymbol{z}_\omega^T\Big\{\dot{\boldsymbol{\omega}}_0 + \hat{\boldsymbol{G}}_{\omega,R}\Delta\boldsymbol{U} - \dot{\boldsymbol{\omega}}_{\text{ref}}\Big\}. \tag{6.14}$$

In order to obtain the stabilising control law for the angular rate subsystem, it is necessary to let $\dot{\mathcal{V}}_\omega(\dot{\boldsymbol{z}}_\omega)$ become negative definite along the trajectories of the error dynamics. The stabilising control law for the angular rate subsystem in accordance with the standard IBS strategy using Eq. 6.13 is

$$\begin{aligned}
\begin{bmatrix}\boldsymbol{\beta}_{SP}\\ \theta_{\text{tr}}\end{bmatrix} &= \begin{bmatrix}\boldsymbol{\beta}_{SP,0}\\ \theta_{\text{tr},0}\end{bmatrix} + \hat{\boldsymbol{G}}_{\omega,F}^{-1}\Big\{-\dot{\boldsymbol{\omega}}_0 - \boldsymbol{c}_\omega\boldsymbol{z}_\omega + \dot{\boldsymbol{\omega}}_{\text{ref}}\Big\}\\
\begin{bmatrix}\boldsymbol{\theta}_{C_F} + \boldsymbol{\beta}_{CP}\\ \theta_{\text{tr}}\end{bmatrix} &= \begin{bmatrix}\boldsymbol{\theta}_{C_F,0} + \boldsymbol{\beta}_{CP,0}\\ \theta_{\text{tr},0}\end{bmatrix} + \hat{\boldsymbol{G}}_{\omega,F}^{-1}\Big\{-\dot{\boldsymbol{\omega}}_0 - \boldsymbol{c}_\omega\boldsymbol{z}_\omega + \dot{\boldsymbol{\omega}}_{\text{ref}}\Big\}\\
\begin{bmatrix}\boldsymbol{\theta}_{C_F}\\ \theta_{\text{tr}}\end{bmatrix} &= \begin{bmatrix}-\boldsymbol{\beta}_{CP} + \boldsymbol{\theta}_{C_F,0} + \boldsymbol{\beta}_{CP,0}\\ \theta_{\text{tr},0}\end{bmatrix} + \hat{\boldsymbol{G}}_{\omega,F}^{-1}\Big\{-\dot{\boldsymbol{\omega}}_0 - \boldsymbol{c}_\omega\boldsymbol{z}_\omega + \dot{\boldsymbol{\omega}}_{\text{ref}}\Big\}.
\end{aligned} \tag{6.15}$$

The stabilising control law from Eq. 6.15 can be written into a form, wherein the incremental change of the flapping angles with respect to the control plane ($\Delta\boldsymbol{\beta}_{CP}$) explicitly appear, namely

$$\begin{bmatrix}\boldsymbol{\theta}_{C_F}\\ \theta_{\text{tr}}\end{bmatrix} = \begin{bmatrix}-\Delta\boldsymbol{\beta}_{CP} + \boldsymbol{\theta}_{C_F,0}\\ \theta_{\text{tr},0}\end{bmatrix} + \hat{\boldsymbol{G}}_{\omega,F}^{-1}\Big\{-\dot{\boldsymbol{\omega}}_0 - \boldsymbol{c}_\omega\boldsymbol{z}_\omega + \dot{\boldsymbol{\omega}}_{\text{ref}}\Big\}. \tag{6.16}$$

It can be assumed that the contribution of $\Delta\boldsymbol{\beta}_{C_{CP}}$ is neglectable, thus Eq. 6.16 can be rewritten into

$$\begin{bmatrix}\boldsymbol{\theta}_{C_F}\\ \theta_{\text{tr}}\end{bmatrix} = \begin{bmatrix}\boldsymbol{\theta}_{C_F,0}\\ \theta_{\text{tr},0}\end{bmatrix} + \hat{\boldsymbol{G}}_{\omega,F}^{-1}\Big\{-\dot{\boldsymbol{\omega}}_0 - \boldsymbol{c}_\omega\boldsymbol{z}_\omega + \dot{\boldsymbol{\omega}}_{\text{ref}}\Big\}. \tag{6.17}$$

The previous control law must be corrected, since $\boldsymbol{\theta}_{C_F} = [-\theta_{1s}\ \theta_{1c}]^T$. A transformation is required, which transforms $\boldsymbol{\theta}_{C_F} = [-\theta_{1s}\ \theta_{1c}]^T$ to $\boldsymbol{\theta}_C = [\theta_{1s}\ \theta_{1c}]^T$. This can be achieved by means of a correction matrix $\boldsymbol{I}_{\text{cor}}$, which is a 3 by 3 identity matrix with -1 in the first entry of the diagonal. Incorporating the aforementioned correction matrix does yield the following stabilising control law

$$\boldsymbol{U} = \boldsymbol{U}_0 + \boldsymbol{I}_{\text{cor}}\hat{\boldsymbol{G}}_{\omega,F}^{-1}\Big\{-\dot{\boldsymbol{\omega}}_0 - \boldsymbol{c}_\omega\boldsymbol{z}_\omega + \dot{\boldsymbol{\omega}}_{\text{ref}}\Big\}, \tag{6.18}$$

wherein $\boldsymbol{U} = [\theta_{1s}\ \theta_{1c}\ \theta_{0,\text{tr}}]^T$ and $\boldsymbol{U} = I_{\text{cor}}[\boldsymbol{\theta}_{C_F}\ \boldsymbol{\theta}_{0,\text{tr}}]^T$. It can now be observed that the stabilising control vector is written as $\boldsymbol{U}$, which is more convenient. Next to this the stabilising control law for the angular rate subsystem based upon the *method of residualised dynamics* using Eq. 6.14 is

$$\boldsymbol{U} = \boldsymbol{U}_0 + \hat{\boldsymbol{G}}_{\omega,R}^{-1}\{-\dot{\boldsymbol{\omega}}_0 - \boldsymbol{c}_\omega \boldsymbol{z}_\omega + \dot{\boldsymbol{\omega}}_{\text{ref}}\}. \tag{6.19}$$

It can be observed that the stabilising control laws from Eq. 6.18 and 6.19 are almost exactly the same, except for the difference in control effectiveness and correction factor for the former stabilising control law. The stabilising control law from Eq. 6.18 and 6.19 enable to rewrite the CLF derivative from Eq. 6.12 into

$$\dot{\mathcal{V}}_\omega(\dot{\boldsymbol{z}}_\omega) = -\boldsymbol{z}_\omega^T \boldsymbol{c}_\omega \boldsymbol{z}_\omega. \tag{6.20}$$

The equilibrium $\boldsymbol{z}_\omega = 0$ can be regarded globally uniformly asymptotically stable when given that $\boldsymbol{c}_\omega > 0$ such that that the desired angular rates $\boldsymbol{\omega}_{\text{ref}}$ can be tracked for $t \to \infty$. The above mentioned is in accordance with the theorem of *LaSalle-Yoshizawa* [50].

6.2.4. Command-filtered IBS approach for imposing limits on commanded signals

Instead of directly applying one of the previous stabilising control laws a new raw reference signal could be defined and led through a command filter. This will enable to impose rate, magnitude and bandwidth limitations on this raw reference signal $\boldsymbol{U}^0$ yielding the command $\boldsymbol{U}$ and command derivative $\dot{\boldsymbol{U}}$ signal. Since an incremental-based control strategy is adopted for the angular rate subsystem, the command filter shall be applied to the total raw reference signal in order to limit sensitivity to delays [54]. This means that the raw reference signal $\boldsymbol{U}^0$ shall be led through a command filter, yielding $\boldsymbol{U}$ and $\dot{\boldsymbol{U}}$. The effect of the command filter on $\boldsymbol{z}_\omega$ is being estimated by means of a stable linear filter. The expressions for $\dot{\boldsymbol{\chi}}_\omega$ using the *flapping equivalence principle* or *method of residualised dynamics* is respectively equal to

$$\dot{\boldsymbol{\chi}}_\omega = -\boldsymbol{c}_\omega \boldsymbol{\chi}_\omega + \boldsymbol{I}_{\text{cor}} \hat{\boldsymbol{G}}_{\omega,F}\left(\boldsymbol{U} - \boldsymbol{U}^0\right), \tag{6.21}$$

$$\dot{\boldsymbol{\chi}}_\omega = -\boldsymbol{c}_\omega \boldsymbol{\chi}_\omega + \hat{\boldsymbol{G}}_{\omega,R}\left(\boldsymbol{U} - \boldsymbol{U}^0\right), \tag{6.22}$$

wherein $\boldsymbol{\chi}_\omega = \boldsymbol{0}$. Moreover the correction factor was also applied for defining the first stable linear filter. The auxiliary system compensates for the constraint effects of the command filter. The compensated tracking error of the angular rate subsystem can be defined as

$$\bar{\boldsymbol{z}}_\omega = \boldsymbol{z}_\omega - \boldsymbol{\chi}_\omega. \tag{6.23}$$

The following second-order command filter with initial condition will be incorporated

$$\begin{bmatrix} \dot{\boldsymbol{U}} \\ \ddot{\boldsymbol{U}} \end{bmatrix} = \begin{bmatrix} \dot{\boldsymbol{U}} \\ 2\zeta\omega_n\left(\boldsymbol{S}_R\left\{\frac{\omega_n^2}{2\zeta\omega_n}\left[\boldsymbol{S}_M\left(\boldsymbol{U}^0\right) - \boldsymbol{U}\right]\right\} - \dot{\boldsymbol{U}}\right) \end{bmatrix}, \quad \text{with} \quad \begin{matrix} \boldsymbol{U}(0) = \boldsymbol{U}(\boldsymbol{z}_\omega(0)) \\ \dot{\boldsymbol{U}}(0) = 0 \end{matrix} \tag{6.24}$$

A second-order filter could be obtained by combining two first-order filters. Such a filter is characterised with increased noise suppression at the cost of an increased time-delay between $\boldsymbol{U}$ and $\boldsymbol{U}^0$. Imposing magnitude and rate limitations on the raw reference signal is desirable as it mimics the properties of the actuators well. However, these limitations can be ignored by setting $\boldsymbol{S}_R$ and $\boldsymbol{S}_M$ equal to 1 such that only the commanded signal and its derivative are generated. This filter is characterised with damping ratio ζ_n and natural frequency ω_n. The magnitude limitations $\boldsymbol{S}_{\text{M}}$ define the allowable actuator deflections of the rotorcraft, whereas the rate limitations $\boldsymbol{S}_{\text{R}}$ define the actuator rate deflections of the rotorcraft. The magnitude and rate limitations can be defined respectively as

$$\boldsymbol{S}_M(\boldsymbol{U}^0) = \begin{cases} \boldsymbol{U}_{\max} & \text{if} \quad \boldsymbol{U}^0 \geq \boldsymbol{U}_{\max} \\ \boldsymbol{U}^0 & \text{if} \quad \boldsymbol{U}_{\min} < \boldsymbol{U}^0 < \boldsymbol{U}_{\max} \\ \boldsymbol{U}_{\min} & \text{if} \quad \boldsymbol{U}^0 \leq \boldsymbol{U}_{\min} \end{cases} \tag{6.25}$$

$$\boldsymbol{S}_R\left[\left(\frac{\omega_n^2}{2\zeta\omega_n}\right)\left(\boldsymbol{S}_M\left(\boldsymbol{U}^0\right) - \boldsymbol{U}\right)\right] = \begin{cases} \dot{\boldsymbol{U}}_{\max} & \text{if} \quad \dot{\boldsymbol{U}}^0 \geq \dot{\boldsymbol{U}}_{\max} \\ \dot{\boldsymbol{U}}^0 & \text{if} \quad \dot{\boldsymbol{U}}_{\min} < \dot{\boldsymbol{U}}^0 < \dot{\boldsymbol{U}}_{\max} \\ \dot{\boldsymbol{U}}_{\min} & \text{if} \quad \dot{\boldsymbol{U}}^0 \leq \dot{\boldsymbol{U}}_{\min} \end{cases} \tag{6.26}$$

The actuator magnitude and rate limitations are provided in Table E.6. In Fig. 6.2 the second-order command-filter of the RCAH control mode is provided.

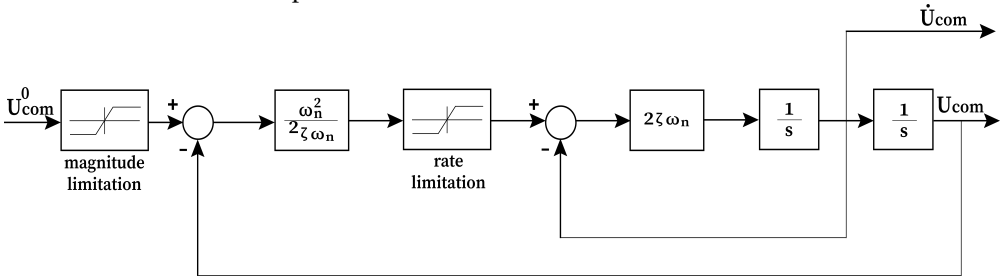

Figure 6.2: Second-order command-filter used in the angular rate subsystem.

With the stable linear filter being defined, it is necessary to determine the derivative of the compensated tracking error given in Eq. 6.23. The aforementioned shall first be considered for the *equivalent flapping angle* method, which requires the use of the stabilising control law from Eq. 6.18. In addition to this the first order *Taylor* series from Eq. 6.1 shall be used as well, but must be corrected. To be more specific $\hat{\boldsymbol{G}}_F$ shall be multiplied with $\boldsymbol{I}_{\text{cor}}$, because of reasons given earlier. Secondly, the flapping angles with respect to the control plane are neglected as these are being discarded in the stabilising control law from Eq. 6.17. This enables the control vector $\boldsymbol{U}$ to explicitly appear in the first-order *Taylor* series when using this method (see first expression from Eq. 6.27). The second expression from Eq. 6.27 is obtained by substituting Eq. 6.21 into it. The third expression is obtained by noticing that $\Delta\boldsymbol{U}$ can be written as $\boldsymbol{U}-\boldsymbol{U}_0$.

$$\begin{aligned}\dot{\tilde{\boldsymbol{z}}}_\omega = \dot{\boldsymbol{z}}_\omega - \dot{\boldsymbol{\chi}}_\omega &= \dot{\boldsymbol{\omega}}_0 + \boldsymbol{I}_{\text{cor}}\hat{\boldsymbol{G}}_{\omega,F}\Delta\boldsymbol{U} - \dot{\boldsymbol{\omega}}_{\text{ref}} - \dot{\boldsymbol{\chi}}_\omega \\ &= \dot{\boldsymbol{\omega}}_0 + \boldsymbol{I}_{\text{cor}}\hat{\boldsymbol{G}}_{\omega,F}\Delta\boldsymbol{U} - \dot{\boldsymbol{\omega}}_{\text{ref}} + \boldsymbol{c}_\omega\boldsymbol{\chi}_\omega - \boldsymbol{I}_{\text{cor}}\hat{\boldsymbol{G}}_{\omega,F}\left(\boldsymbol{U}-\boldsymbol{U}^0\right) \\ &= \dot{\boldsymbol{\omega}}_0 + \boldsymbol{I}_{\text{cor}}\hat{\boldsymbol{G}}_{\omega,F}\left(\boldsymbol{U}^0-\boldsymbol{U}_0\right) - \dot{\boldsymbol{\omega}}_{\text{ref}} + \boldsymbol{c}_\omega\boldsymbol{\chi}_\omega\end{aligned} \tag{6.27}$$

The expression for $\dot{\tilde{\boldsymbol{z}}}_\omega$ using the *method of residualised dynamics* can be obtained using the stable linear filter from Eq. 6.21 and first-order *Taylor* series from Eq. 6.2. The expression for $\dot{\tilde{\boldsymbol{z}}}_\omega$ using this method is

$$\begin{aligned}\dot{\tilde{\boldsymbol{z}}}_\omega = \dot{\boldsymbol{z}}_\omega - \dot{\boldsymbol{\chi}}_\omega &= \dot{\boldsymbol{\omega}}_0 + \hat{\boldsymbol{G}}_{\omega,R}\Delta\boldsymbol{U} - \dot{\boldsymbol{\omega}}_{\text{ref}} - \dot{\boldsymbol{\chi}}_\omega \\ &= \dot{\boldsymbol{\omega}}_0 + \hat{\boldsymbol{G}}_{\omega,R}\Delta\boldsymbol{U} - \dot{\boldsymbol{\omega}}_{\text{ref}} + \boldsymbol{c}_\omega\boldsymbol{\chi}_\omega - \hat{\boldsymbol{G}}_{\omega,R}\left(\boldsymbol{U}-\boldsymbol{U}^0\right) \\ &= \dot{\boldsymbol{\omega}}_0 + \hat{\boldsymbol{G}}_{\omega,R}\left(\boldsymbol{U}^0-\boldsymbol{U}_0\right) - \dot{\boldsymbol{\omega}}_{\text{ref}} + \boldsymbol{c}_\omega\boldsymbol{\chi}_\omega.\end{aligned} \tag{6.28}$$

The expression of the CLF using compensated tracking errors can be identified as

$$\mathcal{V}_\omega(\tilde{\boldsymbol{z}}_\omega) = \frac{1}{2}\tilde{\boldsymbol{z}}_\omega^T\tilde{\boldsymbol{z}}_\omega. \tag{6.29}$$

Next, it is deemed necessary to define the CLF derivative using the compensated tracking errors from Eq. 6.27 and Eq. 6.28. This shall first be considered for the *flapping angle equivalence* method, where after the method of *residualised dynamics* will be considered. The derivative of the compensated tracking error from Eq. 6.27 enables to define the first expression of the CLF derivative given in Eq. 6.30. The second expression is obtained by substitution of the stabilising control law for the angular rate subsystem from Eq. 6.18 into it. This enables simplification of $\dot{\mathcal{V}}_\omega(\dot{\tilde{\boldsymbol{z}}}_\omega)$, eventually yielding the last expression.

$$\begin{aligned}\dot{\mathcal{V}}_\omega(\dot{\tilde{\boldsymbol{z}}}_\omega) &= \tilde{\boldsymbol{z}}_\omega^T\left[\dot{\boldsymbol{\omega}}_0 + \boldsymbol{I}_{\text{cor}}\hat{\boldsymbol{G}}_{\omega,F}\left(\boldsymbol{U}^0-\boldsymbol{U}_0\right) - \dot{\boldsymbol{\omega}}_{\text{ref}} + \boldsymbol{c}_\omega\boldsymbol{\chi}_\omega\right] \\ &= \tilde{\boldsymbol{z}}_\omega^T\left[\dot{\boldsymbol{\omega}}_0 + \boldsymbol{I}_{\text{cor}}\hat{\boldsymbol{G}}_{\omega,F}\left(\boldsymbol{U}_0 + \boldsymbol{I}_{\text{cor}}\hat{\boldsymbol{G}}_{\omega,F}^{-1}\left[-\boldsymbol{c}_\omega\boldsymbol{z}_\omega - \dot{\boldsymbol{\omega}}_0 + \dot{\boldsymbol{\omega}}_{\text{ref}}\right] - \boldsymbol{U}_0\right) - \dot{\boldsymbol{\omega}}_{\text{ref}} + \boldsymbol{c}_\omega\boldsymbol{\chi}_\omega\right] \\ &= \tilde{\boldsymbol{z}}_\omega^T\left[-\boldsymbol{c}_\omega\boldsymbol{z}_\omega + \boldsymbol{c}_\omega\boldsymbol{\chi}_\omega\right] \\ &= -\tilde{\boldsymbol{z}}_\omega^T\boldsymbol{c}_\omega\tilde{\boldsymbol{z}}_\omega\end{aligned} \tag{6.30}$$

Next the CLF derivative shall be defined using the *method of residualised dynamics*. Using the derivative of the compensated tracking error from Eq. 6.28 yields the first expression of Eq. 6.31. The second expression

is obtained by substitution of the stabilising control law from Eq. 6.19 into it. This enables simplification of $\dot{\mathcal{V}}_\omega(\dot{\tilde{\boldsymbol{z}}}_\omega)$, eventually yielding the last expression.

$$\begin{aligned}\dot{\mathcal{V}}_\omega(\dot{\tilde{\boldsymbol{z}}}_\omega) &= \tilde{\boldsymbol{z}}_\omega^T\left[\dot{\boldsymbol{\omega}}_0 + \hat{\boldsymbol{G}}_{\omega,R}\left(\boldsymbol{U}^0 - \boldsymbol{U}_0\right) - \dot{\boldsymbol{\omega}}_{\text{ref}} + \boldsymbol{c}_\omega\boldsymbol{\chi}_\omega\right] \\ &= \tilde{\boldsymbol{z}}_\omega^T\left[\dot{\boldsymbol{\omega}}_0 + \hat{\boldsymbol{G}}_{\omega,R}\left(\boldsymbol{U}_0 + \hat{\boldsymbol{G}}_{\omega,R}^{-1}\left[-\boldsymbol{c}_\omega\boldsymbol{z}_\omega - \dot{\boldsymbol{\omega}}_0 + \dot{\boldsymbol{\omega}}_{\text{ref}}\right] - \boldsymbol{U}_0\right) - \dot{\boldsymbol{\omega}}_{\text{ref}} + \boldsymbol{c}_\omega\boldsymbol{\chi}_\omega\right] \\ &= \tilde{\boldsymbol{z}}_\omega^T\left[-\boldsymbol{c}_\omega\boldsymbol{z}_\omega + \boldsymbol{c}_\omega\boldsymbol{\chi}_\omega\right] \\ &= -\tilde{\boldsymbol{z}}_\omega^T\boldsymbol{c}_\omega\tilde{\boldsymbol{z}}_\omega\end{aligned} \tag{6.31}$$

In accordance with the theorem of *LaSalle-Yoshizawa* the equilibrium $\tilde{\boldsymbol{z}}_\omega = 0$ can be regarded uniformly asymptotically stable [54]. The CFIBS approach assures desirable properties for $\tilde{\boldsymbol{z}}_\omega$ and not for $\boldsymbol{z}_\omega$ [54]. Without inclusion of magnitude, rate and bandwidth limitations the control strategy falls back on the IBS control strategy for which convergence of $\boldsymbol{z}_\omega$ can be assured. For aggressive rotorcraft manoeuvring there will be magnitude and rate limitations for which $\boldsymbol{\chi}_\omega$ and $\boldsymbol{z}_\omega$ will be non-zero and remain bounded [54]. In Fig. 6.3 the RCAH control mode with command-filters is provided.

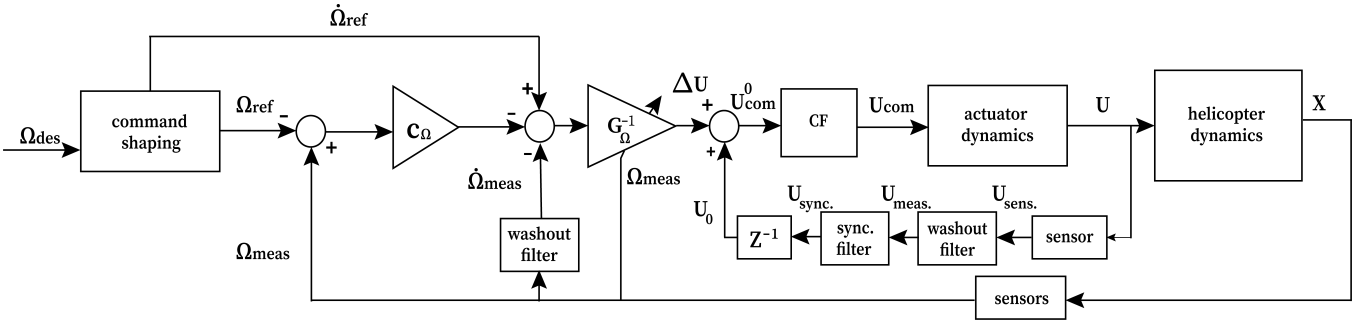

Figure 6.3: RCAH control mode structure.

6.2.5. Synchronising actuator and state derivative measurement by accounting for the second-order washout filter

The angular accelerations need to be obtained by means of a second order washout filter [53]. It has already been outlined that inclusion of such filters does yield delays to the signal, which may can harm controller performance [53, 55]. In order to account for the washout filter, it is deemed necessary to adjust the feedback loop of the actuator measurements by placing the exact same washout filter in this loop. This means that $\boldsymbol{U}_0$ is effectively being delayed by the same amount by which the angular accelerations are being delayed with. This will assure that both signals are equally delayed and therefore synchronised with each other. This will be apparent from the tracking response as steady-state errors will vanish when the aforementioned counter measure is included [53].

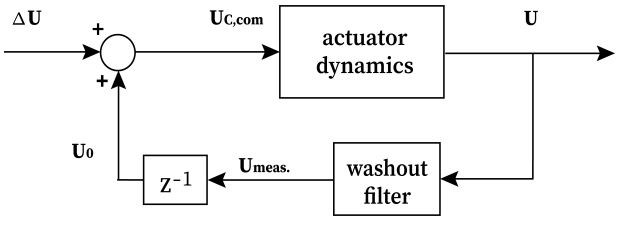

Figure 6.4: Second-order washout filter placed in feedback-loop of actuator measurement.

6.2.6. Rotor synchronisation filter: time-delayed auxiliary system

Previously the feedback signal of the actuator measurements had to be adjusted by placing a second-order washout filter inside this loop. However, it did not yet take into account the difference between the *actual* and *idealised* rotorcraft model. An additional modification needs to be applied to the actuator feedback signal to compensate for this difference. The latter model is the one that is being used for establishing the IBS control law, because it is associated with an enhanced control- to state-dependency ratio. The *idealised* model is based upon residualisation of internal dynamics, especially flapping dynamics. This is because the body-flap coupling is large and residualisation of flapping dynamics would diminish this coupling term and use it to enhance the control-dependency. Previously it has already been outlined that the *flapping angle equivalence method* and *method of residualised dynamics* are attractive control strategies for controlling the angular rates of the rotorcraft. The former method incorporates steady-state flapping dynamics for establishing its control effectiveness, therefore flap synchronisation is required. On the other hand, the *method of residualised dynamics* enables residualisation of more internal dynamics such as lead-lag and/or inflow to further enhancing control effectiveness and reducing state-dependency. This implies that e.g. residualisation of flap-lag dynamics would require a flap-lag synchronisation filter.

To close the gap between the model on which controller has been based (*idealised* model) and the *actual* rotorcraft model, one needs to account for the delaying nature of rotor dynamics. Based on the previous discussion it can be stated that signal synchronisation due to internal dynamics can be realised by adjusting the feedback loop of the actuator measurements by means of the rotor synchronisation filter. In order to establish the rotor synchronisation filter it is first necessary to determine the *idealised* and *actual* expressions for the angular accelerations. For a flap or flap-lag synchronisation filter, it is necessary to define the *actual* expressions of the angular accelerations such that these do account for flap and flap-lag dynamics respectively. In Eq. 6.32 and Eq. 6.33 the aforementioned expressions are provided respectively

$$\dot{\boldsymbol{\omega}} = \boldsymbol{F}_{\omega,\beta_{SP}}\boldsymbol{\beta}_{SP} + \boldsymbol{H}_{\omega}\boldsymbol{U}_{\text{meas}}, \tag{6.32}$$

$$\dot{\boldsymbol{\omega}} = \begin{bmatrix}\boldsymbol{F}_{\omega,\beta_{SP}} & \boldsymbol{F}_{\omega,\zeta}\end{bmatrix}\begin{bmatrix}\boldsymbol{\beta}_{SP}\\ \boldsymbol{\zeta}\end{bmatrix} + \boldsymbol{H}_{\omega}\boldsymbol{U}_{\text{meas}}, \tag{6.33}$$

wherein $\boldsymbol{U}_{\text{meas}}$ are the delayed actuator measurements after being fed through the second-order washout filter. Moreover, $\boldsymbol{\beta}_{SP}$ and $\boldsymbol{\zeta}$ are the synchronised cyclic flapping angles with respect to the shaft plane and synchronised lead-lag angles respectively. Next to this, it can be observed that Eq. 6.33 requires more model knowledge than Eq. 6.32. Based on the above mentioned it can be stated that a model-based strategy is inevitable and shall therefore pursued. For the sake of the analysis this is not disturbing as the main objective is not to have the most optimal controller, but rather one that can be manipulated such that the effect of the internal dynamics on the controller can be analysed. The angular accelerations can be written into a form wherein it is directly affected by the physical control inputs, namely Eq. 6.34. The synchronised control inputs are denoted as $\boldsymbol{U}_{\text{sync}}$. The equation assumes that that the delay introduced by the flapping dynamics is not there. This is exactly on which the controller is based upon.

$$\dot{\boldsymbol{\omega}} = \hat{\boldsymbol{G}}_{\omega}\boldsymbol{U}_{\text{sync}} \tag{6.34}$$

The control effectiveness matrix from Eq. 6.34 must be derived using the method of residualised dynamics. This method relates the control inputs to the steady-state angular accelerations by considering steady-state internal dynamics. For a flap synchronisation filter this would require a control effectiveness based upon flap residualisation, which is provided in Eq. 6.4. On the other hand the control effectiveness for flap-lag residualisation is provided in Eq. 6.5. The synchronised control input $\boldsymbol{U}_{\text{sync}}$ can be obtained by substitution of Eq. 6.32 into Eq. 6.34 and the isolating $\boldsymbol{U}_{\text{sync}}$. Performing the aforementioned does yield

$$\boldsymbol{U}_{\text{sync}} = \hat{\boldsymbol{G}}_{\omega}^{-1}\left[\boldsymbol{F}_{\omega,\beta_{SP}}\boldsymbol{\beta}_{SP} + \boldsymbol{H}_{\omega}\boldsymbol{U}_{\text{meas}}\right], \tag{6.35}$$

$$\boldsymbol{U}_{\text{sync}} = \hat{\boldsymbol{G}}_{\omega}^{-1}\left[\begin{bmatrix}\boldsymbol{F}_{\omega,\beta_{SP}} & \boldsymbol{F}_{\omega,\zeta}\end{bmatrix}\begin{bmatrix}\boldsymbol{\beta}_{SP}\\ \boldsymbol{\zeta}\end{bmatrix} + \boldsymbol{H}_{\omega}\boldsymbol{U}_{\text{meas}}\right], \tag{6.36}$$

from which it can be observed that the synchronised flapping angles $\boldsymbol{\beta_{SP}}$ are required for the both synchronisation filters. These synchronised flapping angles will differ from the actual flapping angles. On the other hand, the synchronised lead-lag angles are required for the flap-lag synchronisation filter from Eq. 6.36. The synchronised flapping angles for the flapping syncrhonisaiton filter can be determined using Eq. 6.37. On

the other hand, the synchronised flapping and lead-lag angles for the flap-lag syncrhonisaiton filter can be determined using Eq. 6.38.

$$\begin{bmatrix} \dot{\boldsymbol{\beta}}_{SP} \\ \ddot{\boldsymbol{\beta}}_{SP} \end{bmatrix} = \begin{bmatrix} \boldsymbol{F}_{\beta_{SP},\beta_{SP}} & \boldsymbol{F}_{\beta_{SP},\dot{\beta}_{SP}} \\ \boldsymbol{F}_{\dot{\beta}_{SP},\beta_{SP}} & \boldsymbol{F}_{\dot{\beta}_{SP},\dot{\beta}_{SP}} \end{bmatrix} \begin{bmatrix} \boldsymbol{\beta}_{SP} \\ \dot{\boldsymbol{\beta}}_{SP} \end{bmatrix} + \begin{bmatrix} \boldsymbol{H}_{\beta} \\ \boldsymbol{H}_{\dot{\beta}} \end{bmatrix} \boldsymbol{U}_{\text{meas}} \tag{6.37}$$

$$\begin{bmatrix} \dot{\boldsymbol{\beta}}_{SP} \\ \ddot{\boldsymbol{\beta}}_{SP} \\ \dot{\boldsymbol{\zeta}} \\ \ddot{\boldsymbol{\zeta}} \end{bmatrix} = \begin{bmatrix} \boldsymbol{F}_{\beta_{SP},\beta_{SP}} & \boldsymbol{F}_{\beta_{SP},\dot{\beta}_{SP}} & \boldsymbol{F}_{\beta_{SP},\zeta} & \boldsymbol{F}_{\beta_{SP},\dot{\zeta}} \\ \boldsymbol{F}_{\dot{\beta}_{SP},\beta_{SP}} & \boldsymbol{F}_{\dot{\beta}_{SP},\dot{\beta}_{SP}} & \boldsymbol{F}_{\dot{\beta}_{SP},\zeta} & \boldsymbol{F}_{\dot{\beta}_{SP},\dot{\zeta}} \\ \boldsymbol{F}_{\zeta,\beta_{SP}} & \boldsymbol{F}_{\zeta,\dot{\beta}_{SP}} & \boldsymbol{F}_{\zeta,\zeta} & \boldsymbol{F}_{\zeta,\dot{\zeta}} \\ \boldsymbol{F}_{\dot{\zeta},\beta_{SP}} & \boldsymbol{F}_{\dot{\zeta},\dot{\beta}_{SP}} & \boldsymbol{F}_{\dot{\zeta},\zeta} & \boldsymbol{F}_{\dot{\zeta},\dot{\zeta}} \end{bmatrix} \begin{bmatrix} \boldsymbol{\beta}_{SP} \\ \dot{\boldsymbol{\beta}}_{SP} \\ \boldsymbol{\zeta} \\ \dot{\boldsymbol{\zeta}} \end{bmatrix} + \begin{bmatrix} \boldsymbol{H}_{\beta} \\ \boldsymbol{H}_{\dot{\beta}} \\ \boldsymbol{H}_{\zeta} \\ \boldsymbol{H}_{\dot{\zeta}} \end{bmatrix} \boldsymbol{U}_{\text{meas}}. \tag{6.38}$$

In Fig. 6.5 the synchronisation filter inside the feedback loop of the angular rate subsystem is provided.

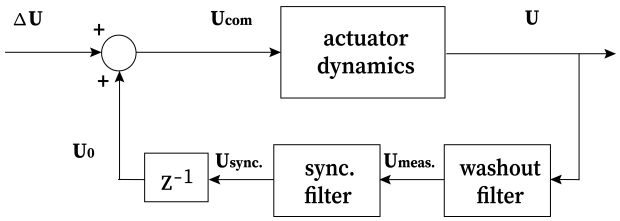

Figure 6.5: Synchronisation filter placed inside feedback-loop of actuator measurement.

6.2.7. RCAH IBS stabilising control law written into equivalent PI control law form

The stabilising control law of the RCAH control mode was established by means of a (CF)IBS control strategy, wherein two different methods were considered. For the sake of the analysis it will be of great interest to determine the equivalent *linear* controller. The IBS control laws from Eq. 6.18 and 6.19 can be written as a classical proportional-integral (PI) control law (relative degree one). The classical PI controller without actuator dynamics shall be considered. In order to perform the derivation it is deemed necessary to consider the incremental stabilising control law in discrete form, wherein the delay of the feedback loop is equal to the sampling time. For low sampling times the stabilising control laws from 6.18 and 6.19 can be considered a continuous integrator [53]. The derivation of the PI-controller is given in Eq. 6.39 for the *flapping angle equivalence* method. It should be noted that f_s and t_s are the sampling frequency and time respectively.

$$\begin{aligned} \boldsymbol{U}(t) &= \int_0^t f_s \boldsymbol{I}_{\text{cor}} \left(\hat{\boldsymbol{G}}_{\omega,F}\right)^{-1} \left[-\boldsymbol{c}_{\omega} \boldsymbol{z}_{\omega}(\tau) - \dot{\boldsymbol{\omega}}(\tau - t_s) + \dot{\boldsymbol{\omega}}_{\text{ref}}(\tau)\right] d\tau \\ &= f_s \boldsymbol{I}_{\text{cor}} \left(\hat{\boldsymbol{G}}_{\omega,F}\right)^{-1} \left[-\boldsymbol{c}_{\omega} \int_0^t \boldsymbol{z}_{\omega}(\tau) d\tau - \boldsymbol{\omega}(t - t_s) + \boldsymbol{\omega}_{\text{ref}}(t)\right] \\ &= f_s \boldsymbol{I}_{\text{cor}} \left(\hat{\boldsymbol{G}}_{\omega,F}\right)^{-1} \left[-\boldsymbol{c}_{\omega} \int_0^t \boldsymbol{z}_{\omega}(\tau) d\tau - \boldsymbol{z}_{\omega}(t)\right] \end{aligned} \tag{6.39}$$

For arriving at the final expression of Eq. 6.39 it was assumed that the angular rates change slow with respect to the the sampling time such that the tracking error $\boldsymbol{z}_{\omega}(t)$ could be approximated by $\boldsymbol{\omega}(t - t_s) - \boldsymbol{\omega}_{\text{ref}}(t)$. From Eq. 6.39 it can be observed that the proportional and integral gains are $f_s \boldsymbol{I}_{\text{cor}} \left(\hat{\boldsymbol{G}}_{\omega,F}\right)^{-1}$ and $\boldsymbol{c}_{\omega} f_s \boldsymbol{I}_{\text{cor}} \left(\hat{\boldsymbol{G}}_{\omega,F}\right)^{-1}$ respectively. This means that the gains are primarily determined by the sampling frequency and control effectiveness. Furthermore the control law does not incorporate any feedback delays as it does not depend on the feedback of the angular accelerations. The classical PI control law when using the method of *residualised dynamics* shall be considered next. This requires the use of the stabilising control law from Eq. 6.19. In Eq. 6.40 the PI-controller is provided when using the above mentioned method.

$$\begin{aligned}\boldsymbol{U}(t) &= \int_0^t f_s \hat{\boldsymbol{G}}_{\omega,R}^{-1} \left[-\boldsymbol{c}_\omega \boldsymbol{z}_\omega(\tau) - \dot{\boldsymbol{\omega}}(\tau - t_s) + \dot{\boldsymbol{\omega}}_{\text{ref}}(\tau)\right] d\tau \\ &= f_s \left(\hat{\boldsymbol{G}}_{\omega,R}\right)^{-1} \left[-\boldsymbol{c}_\omega \int_0^t \boldsymbol{z}_\omega(\tau) d\tau - \boldsymbol{\omega}(t - t_s) + \boldsymbol{\omega}_{\text{ref}}(t)\right] \\ &= f_s \left(\hat{\boldsymbol{G}}_{\omega,R}\right)^{-1} \left[-\boldsymbol{c}_\omega \int_0^t \boldsymbol{z}_\omega(\tau) d\tau - \boldsymbol{z}_\omega(t)\right],\end{aligned} \tag{6.40}$$

from which it can be observed that $f_s \left(\hat{\boldsymbol{G}}_{\omega,R}\right)^{-1}$ and $\boldsymbol{c}_\omega f_s \left(\hat{\boldsymbol{G}}_{\omega,R}\right)^{-1}$ are the proportional and integral gains respectively. Similar to the previous PI-controller it can be observed that the control law does not require the feedback of the angular acceleration. This implies that synchronising actuator and state derivative measurements are not of prime concern for such a controller. Most importantly it shows that when shifting from a linear to a non-linear controller other type of issues will arise. It must also be mentioned that for establishing the linear control laws given in Eq. 6.39 and Eq. 6.40 high sample rates had to be assumed such that the incremental control law ($U = U_0 + \Delta U$) can be written in an equivalent discrete form ($U_{k+1} = U_k + \Delta U_k$) [53].

6.3. Attitude Command/Attitude Hold (ACAH) mode

The next type of control mode that will be considered is the Attitude Command/Attitude Hold (ACAH) mode, which enables to control the attitude angles of the vehicle with respect to the body frame of reference [46]. Since the attitude angles are governed by angular rates, an additional outer loop around the angular rate subsystem would enable control of the attitude angles by means of the control inputs. The ACAH control mode can therefore be considered a two-cascaded system as it consist of an outer attitude loop and an inner angular rate loop, whereby the angular rates can be considered the *virtual* inputs to the attitude subsystem. For establishing the stabilising control law for the attitude subsystem a CFBS control approach will suffice as the relation between the attitude angles and angular rates is well-known. The ACAH controller is based upon the time-scale separation principle, wherein the evolution of angular rates can be regarded significantly faster than the corresponding change in attitude angles [46]. In other words the slow inner loop provides the commanded angular rates $\boldsymbol{\omega}_{\text{ref}}$ to be tracked by the fast inner loop such that $\boldsymbol{\Theta}_{\text{ref}}$ can be achieved. Below the derivation of the ACAH control mode is provided.

6.3.1. Standard BS control law for Attitude subsystem of ACAH mode

The derivation of the ACAH mode starts with the attitude subsystem, since this is the subsystem furthest away from the physical control inputs. The main objective is to let the rotorcraft track a smooth attitude reference signal $\boldsymbol{\Theta}_{\text{ref}}$. In order to establish the stabilising control law for the attitude subsystem, it is necessary to define the attitude and angular rate tracking errors, which are equal to

$$\boldsymbol{z}_\Theta = \boldsymbol{\Theta} - \boldsymbol{\Theta}_{\text{ref}}, \tag{6.41}$$

$$\boldsymbol{z}_{\boldsymbol{\omega}} = \boldsymbol{\omega} - \boldsymbol{\omega}_{\text{ref}}. \tag{6.42}$$

Next, it is necessary to determine the derivative of $\boldsymbol{z}_\Theta$. After taking the derivative of $\boldsymbol{z}_\Theta$, $\boldsymbol{\omega}$ is rewritten as a function of $\boldsymbol{z}_\omega$ and $\boldsymbol{\omega}_{\text{ref}}(=\boldsymbol{\alpha}_\omega)$, where after it is being substituted into $\dot{\boldsymbol{z}}_\Theta$. This yields

$$\dot{\boldsymbol{z}}_\Theta = \dot{\boldsymbol{\Theta}} - \dot{\boldsymbol{\Theta}}_{\text{ref}} = \boldsymbol{G}_\Theta\big(\boldsymbol{z}_\omega + \boldsymbol{\alpha}_\omega\big) - \dot{\boldsymbol{\Theta}}_{\text{ref}}. \tag{6.43}$$

The well-known kinematic relation was used in Eq. 6.43 (see Eq. 2.114 for the kinematic relation). A quadratic CLF $\mathcal{V}_\Theta(\boldsymbol{z}_\Theta)$ is incorporated for acquiring the stabilising control law $\boldsymbol{\alpha}_\omega$ for the attitude subsystem. The expression for $\mathcal{V}_\Theta(\boldsymbol{z}_\Theta)$ and $\dot{\mathcal{V}}_\Theta(\dot{\boldsymbol{z}}_\Theta)$ are respectively

$$\mathcal{V}_\Theta(\boldsymbol{z}_\Theta) = 0.5 \boldsymbol{z}_\Theta^T \boldsymbol{z}_\Theta, \tag{6.44}$$

$$\dot{\mathcal{V}}_\Theta(\dot{\boldsymbol{z}}_\Theta) = \boldsymbol{z}_\Theta^T \Big\{\boldsymbol{G}_\Theta\big(\boldsymbol{z}_\omega + \boldsymbol{\alpha}_\omega\big) - \dot{\boldsymbol{\Theta}}_{\text{ref}}\Big\}. \tag{6.45}$$

In order to obtain the stabilising control law $\boldsymbol{\alpha}_\omega$ it is necessary to let $\mathcal{V}_\Theta(\dot{\boldsymbol{z}}_\Theta)$ become negative definite along the trajectories of the error dynamics. The stabilising control law using the standard BS procedure is

$$\boldsymbol{\alpha}_{\omega} = \boldsymbol{G}_{\Theta}^{-1}\left[\dot{\boldsymbol{\Theta}}_{\text{ref}} - \boldsymbol{c}_{\Theta}\boldsymbol{z}_{\Theta}\right], \quad \text{with } \boldsymbol{c}_{\Theta} > 0. \tag{6.46}$$

Substitution of the stabilising control law from Eq. 6.46 into the quadratic CLF derivative from Eq. 6.45 yields

$$\dot{\mathcal{V}}_{\Theta}(\dot{\boldsymbol{z}}_{\Theta}) = -\boldsymbol{z}_{\Theta}^{T}\boldsymbol{c}_{\Theta}\boldsymbol{z}_{\Theta} + \boldsymbol{z}_{\Theta}^{T}\boldsymbol{G}_{\Theta}\boldsymbol{z}_{\omega}. \tag{6.47}$$

It can be observed that $\dot{\mathcal{V}}_{\Theta}(\dot{\boldsymbol{z}}_{\Theta})$ incorporates a cross-term, which shall be removed in the next design step. When incorporating the standard BS procedure then Eq. 6.46 must be used as stabilising control law for the attitude subsystem.

6.3.2. Command-filtered BS approach for imposing limits on commanded signals

Instead of directly applying the stabilising control law from Eq. 6.46 a new signal could defined, namely $\boldsymbol{\omega}_{\text{ref}}^{0}$. This raw reference signal could be led through a command filter yielding $\boldsymbol{\omega}_{\text{ref}}$ and $\dot{\boldsymbol{\omega}}_{\text{ref}}$. The effect of the command filter on $\boldsymbol{z}_{\omega}$ is estimated by means of a stable linear filter. The expressions for $\boldsymbol{\omega}_{\text{ref}}^{0}$ and $\dot{\boldsymbol{\chi}}_{\Theta}$ are respectively equal to

$$\boldsymbol{\omega}_{\text{ref}}^{0} = \boldsymbol{\alpha}_{\omega} - \boldsymbol{\chi}_{\omega}, \tag{6.48}$$

$$\dot{\boldsymbol{\chi}}_{\Theta} = -\boldsymbol{c}_{\Theta}\boldsymbol{\chi}_{\Theta} + \boldsymbol{G}_{\Theta}\left(\boldsymbol{\omega}_{\text{ref}} - \boldsymbol{\omega}_{\text{ref}}^{0}\right), \tag{6.49}$$

wherein $\boldsymbol{\chi}_{\Theta} = \boldsymbol{0}$. Magnitude, rate and bandwidth limitations for attitude control are taken into account by the command filter. The following second-order command filter with initial condition will be incorporated:

$$\begin{bmatrix} \dot{\boldsymbol{\omega}}_{\text{ref}} \\ \ddot{\boldsymbol{\omega}}_{\text{ref}} \end{bmatrix} = \begin{bmatrix} \dot{\boldsymbol{\omega}}_{\text{ref}} \\ 2\zeta\omega_n\left(\boldsymbol{S}_R\left\{\frac{\omega_n^2}{2\zeta\omega_n}\left[\boldsymbol{S}_M\left(\boldsymbol{\omega}_{\text{ref}}^{0}\right) - \boldsymbol{\omega}_{\text{ref}}\right]\right\} - \dot{\boldsymbol{\omega}}_{\text{ref}}\right) \end{bmatrix}, \text{ with } \begin{matrix} \boldsymbol{\omega}_{\text{ref}}(0) = \boldsymbol{\alpha}_{\omega}\left(\boldsymbol{z}_{\Theta}(0), \boldsymbol{\Theta}_{\text{ref}}(0)\right) \\ \dot{\boldsymbol{\omega}}_{\text{ref}}(0) = 0 \end{matrix} \tag{6.50}$$

The magnitude limitations $\boldsymbol{S}_M$ defines the allowable angular rates of the rotorcraft. Since there are no limitations on angular accelerations, $\boldsymbol{S}_R = 1$. Magnitude and rate limitations can be defined respectively as

$$\boldsymbol{S}_M(\boldsymbol{\omega}_{\text{ref}}^{0}) = \begin{cases} \boldsymbol{\omega}_{\max} & \text{if} \quad \boldsymbol{\omega}_{\text{ref}}^{0} \geq \boldsymbol{\omega}_{\max} \\ \boldsymbol{\omega}_{\text{ref}}^{0} & \text{if} \quad \boldsymbol{\omega}_{\min} < \boldsymbol{\omega}_{\text{ref}}^{0} < \boldsymbol{\omega}_{\max} \\ \boldsymbol{\omega}_{\min} & \text{if} \quad \boldsymbol{\omega}_{\text{ref}}^{0} \leq \boldsymbol{\omega}_{\min} \end{cases} \tag{6.51}$$

$$\boldsymbol{S}_R\left(\left[\left(\frac{\omega_n^2}{2\zeta\omega_n}\right)\left(\boldsymbol{S}_M\left(\boldsymbol{\omega}_{\text{ref}}^{0}\right) - \boldsymbol{\omega}_{\text{ref}}\right)\right]\right) = 1 \tag{6.52}$$

The maximum allowable angular rates for the main simulation model could be set equal to $\pm 50°/s$, $\pm 30°/s$ and $\pm 60°/s$ for p_{ref}^{0}, q_{ref}^{0} and r_{ref}^{0} respectively. These are the maximum angular rates as demanded by the ADS-33E-PRF. Similar magnitude limitations were used by [55]. Moreover $\zeta \geq 1$ to assure that ω_{ref} will not overshoot $\boldsymbol{S}_M$ [54]. In this particular case ζ and ω_n could be set equal to 1 and 100 rad/s for all channels. In order to proceed further with the CFBS control strategy it is necessary to define the compensated tracking errors, which account for the stable linear filter. The compensated tracking errors $\bar{\boldsymbol{z}}_{\Theta}$ and $\bar{\boldsymbol{z}}_{\omega}$ are equal to

$$\bar{\boldsymbol{z}}_{\Theta} = \boldsymbol{z}_{\Theta} - \boldsymbol{\chi}_{\Theta}, \tag{6.53}$$

$$\bar{\boldsymbol{z}}_{\omega} = \boldsymbol{z}_{\omega} - \boldsymbol{\chi}_{\omega}. \tag{6.54}$$

The derivative of the compensated tracking error $\boldsymbol{z}_{\Theta}$ can be written as follows

$$\dot{\bar{\boldsymbol{z}}}_{\Theta} = \dot{\boldsymbol{z}}_{\Theta} - \dot{\boldsymbol{\chi}}_{\Theta} = \boldsymbol{G}_{\Theta}\left(\boldsymbol{z}_{\omega} + \boldsymbol{\alpha}_{\omega}\right) - \dot{\boldsymbol{\Theta}}_{\text{ref}} + \boldsymbol{c}_{\Theta}\chi_{\Theta} - \boldsymbol{G}_{\Theta}\left(\boldsymbol{\omega}_{\text{ref}} - \boldsymbol{\omega}_{\text{ref}}^{0}\right). \tag{6.55}$$

The objective is to let $\dot{\mathcal{V}}_{\Theta}(\dot{\bar{\boldsymbol{z}}}_{\Theta})$ become negative definite along the trajectories of the compensated error dynamics. The aforementioned can be observed in Eq. 6.56. In order to simplify the first expression it is deemed necessary to add and subtract $\boldsymbol{G}_{\Theta}\boldsymbol{\omega}_{\text{ref}}^{0}$ from it. The positive term $\boldsymbol{G}_{\Theta}\boldsymbol{\omega}_{\text{ref}}^{0}$ is transformed such that $\boldsymbol{\omega}_{\text{ref}}^{0}$ is replaced by $\left(\boldsymbol{\alpha}_{\omega} - \boldsymbol{\chi}_{\omega}\right)$. This does cancel out both $\boldsymbol{G}_{\Theta}\boldsymbol{\omega}_{\text{ref}}$ and $\boldsymbol{G}_{\Theta}\boldsymbol{\omega}_{\text{ref}}^{0}$. It should be noted that $\boldsymbol{\omega}_{\text{ref}}$ is equivalent to $\boldsymbol{\alpha}_{\omega}$. After cancelling the aforementioned terms, the stabilising control law $\boldsymbol{\alpha}_{\omega}$ is being substituted into the expressions. This enables cancellation of the term $\dot{\boldsymbol{\Theta}}_{\text{ref}}$. There after the compensated tracking errors $\bar{\boldsymbol{z}}_{\omega}$ and $\bar{\boldsymbol{z}}_{\theta}$ can be substituted into it. This eventually does yield the last expression.

$$
\begin{aligned}
\dot{\mathcal{V}}_\Theta(\dot{\bar{\boldsymbol{z}}}_\Theta) &= \bar{\boldsymbol{z}}_\Theta^T\Big\{\boldsymbol{G}_\Theta\big(\boldsymbol{z}_\omega+\boldsymbol{\alpha}_\omega\big)-\dot{\boldsymbol{\Theta}}_{\text{ref}}+\boldsymbol{c}_\Theta\boldsymbol{\chi}_\Theta-\boldsymbol{G}_\Theta\Big(\boldsymbol{\omega}_{\text{ref}}-\boldsymbol{\omega}_{\text{ref}}^0\Big)\Big\}\\
&= \bar{\boldsymbol{z}}_\Theta^T\Big\{\boldsymbol{G}_\Theta\big(\boldsymbol{z}_\omega+\boldsymbol{\alpha}_\omega\big)-\boldsymbol{G}_\Theta\boldsymbol{\omega}_{\text{ref}}^0+\boldsymbol{G}_\Theta\boldsymbol{\omega}_{\text{ref}}^0-\dot{\boldsymbol{\Theta}}_{\text{ref}}+\boldsymbol{c}_\Theta\boldsymbol{\chi}_\Theta-\boldsymbol{G}_\Theta\Big(\boldsymbol{\omega}_{\text{ref}}-\boldsymbol{\omega}_{\text{ref}}^0\Big)\Big\}\\
&= \bar{\boldsymbol{z}}_\Theta^T\Big\{\boldsymbol{G}_\Theta\big(\boldsymbol{z}_\omega+\boldsymbol{\alpha}_\omega\big)-\boldsymbol{G}_\Theta\boldsymbol{\omega}_{\text{ref}}^0+\boldsymbol{G}_\Theta\Big(\boldsymbol{\alpha}_\omega-\boldsymbol{\chi}_\omega\Big)-\dot{\boldsymbol{\Theta}}_{\text{ref}}+\boldsymbol{c}_\Theta\boldsymbol{\chi}_\Theta-\boldsymbol{G}_\Theta\Big(\boldsymbol{\omega}_{\text{ref}}-\boldsymbol{\omega}_{\text{ref}}^0\Big)\Big\}\\
&= \bar{\boldsymbol{z}}_\Theta^T\Big\{\boldsymbol{G}_\Theta\big(\boldsymbol{z}_\omega+\boldsymbol{G}_\Theta^{-1}\big[\dot{\boldsymbol{\Theta}}_{\text{ref}}-\boldsymbol{c}_\Theta\boldsymbol{z}_\Theta\big]\big)-\boldsymbol{G}_\Theta\boldsymbol{\chi}_\omega-\dot{\boldsymbol{\Theta}}_{\text{ref}}+\boldsymbol{c}_\Theta\boldsymbol{\chi}_\Theta\Big\}\\
&= \bar{\boldsymbol{z}}_\Theta^T\Big\{\boldsymbol{G}_\Theta\big(\boldsymbol{z}_\omega-\boldsymbol{\chi}_\omega\big)-\boldsymbol{c}_\Theta\big(\boldsymbol{z}_\Theta-\chi_\Theta\big)\Big\}\\
&= \bar{\boldsymbol{z}}_\Theta^T\Big\{\boldsymbol{G}_\Theta\bar{\boldsymbol{z}}_\omega-\boldsymbol{c}_\Theta\bar{\boldsymbol{z}}_\Theta\Big\}\\
&= \bar{\boldsymbol{z}}_\Theta^T\boldsymbol{G}_\Theta\bar{\boldsymbol{z}}_\omega-\bar{\boldsymbol{z}}_\Theta^T\boldsymbol{c}_\Theta\bar{\boldsymbol{z}}_\Theta,\quad\text{with}\quad c_\Theta>0.
\end{aligned}
\tag{6.56}
$$

It can be observed that Eq. 6.56 is not completely negative definite because of the cross-term $\bar{\boldsymbol{z}}_\Theta^T\boldsymbol{G}_\Theta\bar{\boldsymbol{z}}_\omega$ which shall be removed in the next design step. The control effectiveness matrix $\boldsymbol{G}_\Theta$ is a square matrix, thus virtual control allocation is not deemed necessary. It should be noted that the stabilising control law was established by means of regular CFBS, because of the well-known *kinematic* relationship between attitude derivatives and angular rates. Since the attitude subsystem is not directly governed by the control inputs, it must be linked to the angular rate subsystem.

6.3.3. Stabilising control law for angular rate subsystem of ACAH mode

In section 6.2 the stabilising control law for the angular rate subsystem was already derived, however it did not yet account for the additional additional cross-term $\bar{\boldsymbol{z}}_\Theta^T\boldsymbol{G}_\Theta\bar{\boldsymbol{z}}_\omega$. With the tracking error for the angular rate subsystem being defined, it is necessary to take the derivative of it and substitute the expression for the first-order *Taylor* series into it. Both the the *flapping angle equivalence method* and *method of residualised dynamics* will be considered for the derivation. The first-order *Taylor* series of both aforementioned methods are given in Eq. 6.1 and Eq. 6.2 respectively. The expression for $\dot{\boldsymbol{z}}_\omega$ using the first-order *Taylor* series for the *flapping angle equivalence method* and *method of residualised dynamics* are respectively equal to

$$
\dot{\boldsymbol{z}}_\omega=\dot{\boldsymbol{\omega}}-\dot{\boldsymbol{\omega}}_{\text{ref}}=\dot{\boldsymbol{\omega}}_0+\hat{\boldsymbol{G}}_{\omega,F}\Delta\begin{bmatrix}\boldsymbol{\theta}_{C_F}+\boldsymbol{\beta}_{CP}\\ \theta_{0,\text{tr}}\end{bmatrix}-\dot{\boldsymbol{\omega}}_{\text{ref}},
\tag{6.57}
$$

$$
\dot{\boldsymbol{z}}_\omega=\dot{\boldsymbol{\omega}}-\dot{\boldsymbol{\omega}}_{\text{ref}}=\dot{\boldsymbol{\omega}}_0+\hat{\boldsymbol{G}}_{\omega,R}\Delta\boldsymbol{U}-\dot{\boldsymbol{\omega}}_{\text{ref}}.
\tag{6.58}
$$

The quadratic CLF $\mathcal{V}_\Theta(\bar{\boldsymbol{z}}_\Theta)$ from the attitude subsystem shall be augmented to penalise the angular rate tracking error. The expression for $\mathcal{V}_\omega(\bar{\boldsymbol{z}}_\Theta,\boldsymbol{z}_\omega)$ is

$$
\mathcal{V}_\omega(\bar{\boldsymbol{z}}_\Theta,\boldsymbol{z}_\omega)=\mathcal{V}_\Theta(\bar{\boldsymbol{z}}_\Theta)+0.5\boldsymbol{z}_\omega^T\boldsymbol{z}_\omega,
\tag{6.59}
$$

from which it can be observed that the command-filters from the previous subsystem are taken into account. When the standard IBS control law from Eq. 6.46 would have been considered, that is without the command-filters, then $\mathcal{V}_\omega(\boldsymbol{z}_\Theta,\boldsymbol{z}_\omega)$ should have been used. The derivation wherein the attitude subsystem is augmented with command filters shall be provided. Taking the derivative of $\mathcal{V}_\omega(\bar{\boldsymbol{z}}_\Theta,\boldsymbol{z}_\omega)$ and substituting the tracking error derivatives from Eq. 6.57 or Eq. 6.58 into it, yields the following expression for $\dot{\mathcal{V}}_\omega(\dot{\bar{\boldsymbol{z}}}_\Theta,\dot{\boldsymbol{z}}_\omega)$ using the *flapping angle equivalence method* and *method of residualised dynamics* respectively

$$
\dot{\mathcal{V}}_\omega(\dot{\bar{\boldsymbol{z}}}_\Theta,\dot{\boldsymbol{z}}_\omega)=\dot{\mathcal{V}}_\Theta+\boldsymbol{z}_\omega^T\Big\{\dot{\boldsymbol{\omega}}_0+\hat{\boldsymbol{G}}_{\omega,F}\Delta\begin{bmatrix}\boldsymbol{\theta}_{C_F}+\boldsymbol{\beta}_{CP}\\ \theta_{0,\text{tr}}\end{bmatrix}-\dot{\boldsymbol{\omega}}_{\text{ref}}\Big\},
\tag{6.60}
$$

$$
\dot{\mathcal{V}}_\omega(\dot{\bar{\boldsymbol{z}}}_\Theta,\dot{\boldsymbol{z}}_\omega)=\dot{\mathcal{V}}_\Theta+\boldsymbol{z}_\omega^T\Big\{\dot{\boldsymbol{\omega}}_0+\hat{\boldsymbol{G}}_{\omega,R}\Delta\boldsymbol{U}-\dot{\boldsymbol{\omega}}_{\text{ref}}\Big\}.
\tag{6.61}
$$

In order to obtain the stabilising control law for the angular rate subsystem, it is necessary to let $\dot{\mathcal{V}}_\omega(\dot{\bar{\boldsymbol{z}}}_\Theta,\dot{\boldsymbol{z}}_\omega)$ from Eq. 6.60 or Eq. 6.61 to become negative definite along the trajectories of the error dynamics. The expression for the stabilising control law using the *flapping angle equivalence method* requires the use of Eq. 6.60 and is found to be equal to

$$\boldsymbol{U} = \boldsymbol{U}_0 + \boldsymbol{I}_{\text{cor}}\hat{\boldsymbol{G}}_{\omega,F}^{-1}\Big\{-\dot{\boldsymbol{\omega}}_0 - \boldsymbol{c}_\omega \boldsymbol{z}_\omega + \dot{\boldsymbol{\omega}}_{\text{ref}} - \boldsymbol{G}_\Theta \bar{\boldsymbol{z}}_\Theta\Big\}, \tag{6.62}$$

wherein $\boldsymbol{I}_{\text{cor}}$ is the correction matrix. The stabilising control law in accordance with the *method of residualised dynamics* requires the use of Eq. 6.61 and is found to be equal to

$$\boldsymbol{U} = \boldsymbol{U}_0 + \hat{\boldsymbol{G}}_{\omega,R}^{-1}\{-\dot{\boldsymbol{\omega}}_0 - \boldsymbol{c}_\omega \boldsymbol{z}_\omega + \dot{\boldsymbol{\omega}}_{\text{ref}} - \boldsymbol{G}_\Theta \bar{\boldsymbol{z}}_\Theta\}. \tag{6.63}$$

Using the stabilising control law from Eq. 6.62 or Eq. 6.63 enables the CLF derivative from Eq. 6.60 and Eq. 6.61 to be rewritten into

$$\dot{\mathcal{V}}_\omega(\dot{\bar{\boldsymbol{z}}}_\Theta, \dot{\boldsymbol{z}}_\omega) = -\bar{\boldsymbol{z}}_\Theta^T \boldsymbol{c}_\Theta \bar{\boldsymbol{z}}_\Theta - \boldsymbol{z}_\omega^T \boldsymbol{c}_\omega \boldsymbol{z}_\omega - \bar{\boldsymbol{z}}_\Theta^T \boldsymbol{G}_\Theta (\boldsymbol{z}_\omega - \bar{\boldsymbol{z}}_\omega). \tag{6.64}$$

It must be noted that $\bar{\boldsymbol{z}}_\Theta^T \boldsymbol{G}_\Theta \bar{\boldsymbol{z}}_\omega \neq \bar{\boldsymbol{z}}_\Theta^T \boldsymbol{G}_\Theta \boldsymbol{z}_\omega$, because command filters were not considered yet for the angular rate subsystem, therefore $\boldsymbol{z}_\omega$ can be greater than $\bar{\boldsymbol{z}}_\omega$. In other words the terms do not always fully cancel out. The equilibrium $\boldsymbol{z}_\omega = 0$ can be regarded as globally uniformly asymptotically stable when given that $\boldsymbol{c}_\omega > 0$ and $\boldsymbol{c}_\Theta > 0$ such that that the desired attitude angles $\boldsymbol{\Theta}_{\text{ref}}$ can be tracked for $t \to \infty$. The above mentioned is in accordance with the theorem of *LaSalle-Yoshizawa* [50]. The ACAH control mode shall incorporate a CFIBS control strategy for the angular rate subsystem, which shall be considered here after as it will enables completely removal of cross-term $\bar{\boldsymbol{z}}_\Theta^T \boldsymbol{G}_\Theta \bar{\boldsymbol{z}}_\omega$.

6.3.4. Command-filtered IBS approach for imposing limits on commanded signals

Instead of directly applying one of the stabilising control laws from Eq. 6.62 or Eq. 6.63, a new raw reference could be defined and led through a command filter. This would enable to impose rate, magnitude and bandwidth limitations on the commanded cyclic and tail rotor collective inputs. In addition to this, since an incremental-based control strategy is adopted for the angular rate subsystem, it is a natural choice to apply the command filter to the total raw reference signal in order to limit sensitivity to delays [54]. This means that the raw reference signal $\boldsymbol{U}^0$ will be led through a command filter, yielding $\boldsymbol{U}$ and $\dot{\boldsymbol{U}}$. The effect of the command filter on $\boldsymbol{z}_\omega$ is being estimated by means of a stable linear filter. The expressions for $\dot{\boldsymbol{\chi}}_\omega$ using the *flapping angle equivalence method* and *method of residualised dynamics* were already provided in Eq. 6.21 and Eq. 6.22 respectively. In addition to this the compensated tracking error $\bar{\boldsymbol{z}}_\omega$ was provided in in Eq. 6.23. Magnitude, rate and bandwidth limitations are taken into account by the command filter. A second-order command filter with initial conditions was provided in Eq. 6.24 for the angular rate subsystem. The magnitude and rate limitations of the cyclic deflections of the main rotor and tail rotor collective were provided in Eq. 6.25 and 6.26 respectively. In Fig. 6.2 the command filter of the angular subsystem was provided. With the stable linear filters being defined, it is necessary to define the derivative of the compensated tracking error given in Eq. 6.23. The expression for $\dot{\bar{\boldsymbol{z}}}_\omega$ in accordance with the *flapping angle equivalence method* and *method of residualised dynamics* are provided in Eq. 6.65 and Eq. 6.66 respectively.

$$\dot{\bar{\boldsymbol{z}}}_\omega = \dot{\boldsymbol{\omega}}_0 + \boldsymbol{I}_{\text{cor}}\hat{\boldsymbol{G}}_{\omega,F}\left(\boldsymbol{U}^0 - \boldsymbol{U}_0\right) - \dot{\boldsymbol{\omega}}_{\text{ref}} + \boldsymbol{c}_\omega \boldsymbol{\chi}_\omega \tag{6.65}$$

$$\dot{\bar{\boldsymbol{z}}}_\omega = \dot{\boldsymbol{\omega}}_0 + \hat{\boldsymbol{G}}_{\omega,R}\left(\boldsymbol{U}^0 - \boldsymbol{U}_0\right) - \dot{\boldsymbol{\omega}}_{\text{ref}} + \boldsymbol{c}_\omega \boldsymbol{\chi}_\omega \tag{6.66}$$

It should be noted that the first-order *Taylor* series of the *flapping angle equivalence* method was adjusted slightly to arrive at the form given in Eq. 6.65. Normally it should be $\boldsymbol{I}_{\text{cor}}^{-1}\hat{\boldsymbol{G}}_{\omega,F}\left(\boldsymbol{U}^0 - \boldsymbol{U}_0\right)$, but since I_{cor} is a diagonal matrix the following will hold: $\boldsymbol{I}_{\text{cor}}^{-1} = \boldsymbol{I}_{\text{cor}}$. The CLF derivative using the compensated tracking errors from Eq. 6.65 and Eq. 6.66 shall be determined. The expression for $\mathcal{V}_\omega(\bar{\boldsymbol{z}}_\Theta, \bar{\boldsymbol{z}}_\omega)$ and its derivative are

$$\mathcal{V}_\omega(\bar{\boldsymbol{z}}_\Theta, \bar{\boldsymbol{z}}_\omega) = \mathcal{V}_\Theta(\bar{\boldsymbol{z}}_\Theta) + 0.5\bar{\boldsymbol{z}}_\omega^T \bar{\boldsymbol{z}}_\omega, \tag{6.67}$$

$$\dot{\mathcal{V}}_\omega(\dot{\bar{\boldsymbol{z}}}_\Theta, \dot{\bar{\boldsymbol{z}}}_\omega) = \dot{\mathcal{V}}_\Theta(\dot{\bar{\boldsymbol{z}}}_\Theta) + \bar{\boldsymbol{z}}_\omega \dot{\bar{\boldsymbol{z}}}_\omega. \tag{6.68}$$

The CLF derivative shall first be determined for the *flapping angle equivalence method* where after the it will be considered for the *method of residualised dynamics*. Substitution of Eq. 6.65 into the CLF derivative yields the first expression from Eq. 6.69. The second expression is obtained by substitution of the stabilising control law from Eq. 6.62 into it. This enables simplification of $\dot{\mathcal{V}}_\omega(\dot{\bar{\boldsymbol{z}}}_\Theta, \dot{\bar{\boldsymbol{z}}}_\omega)$, eventually yielding the last expression.

$$\begin{aligned}
\dot{\mathcal{V}}_\omega(\dot{\bar{\boldsymbol{z}}}_\Theta, \dot{\bar{\boldsymbol{z}}}_\omega) &= -\bar{\boldsymbol{z}}_\Theta^T \boldsymbol{c}_\Theta \bar{\boldsymbol{z}}_\Theta + \bar{\boldsymbol{z}}_\Theta^T \boldsymbol{G}_\Theta \bar{\boldsymbol{z}}_\omega + \bar{\boldsymbol{z}}_\omega^T \Big[\dot{\boldsymbol{\omega}}_0 + \boldsymbol{I}_{\text{cor}} \hat{\boldsymbol{G}}_{\omega,F} \left(\boldsymbol{U}^0 - \boldsymbol{U}_0 \right) - \dot{\boldsymbol{\omega}}_{\text{ref}} + \boldsymbol{c}_\omega \boldsymbol{\chi}_\omega \Big] \\
&= -\bar{\boldsymbol{z}}_\Theta^T \boldsymbol{c}_\Theta \bar{\boldsymbol{z}}_\Theta + \bar{\boldsymbol{z}}_\Theta^T \boldsymbol{G}_\Theta \bar{\boldsymbol{z}}_\omega + \bar{\boldsymbol{z}}_\omega^T \Big[\dot{\boldsymbol{\omega}}_0 + \boldsymbol{I}_{\text{cor}} \hat{\boldsymbol{G}}_{\omega,F} \Big(\boldsymbol{U}_0 + \boldsymbol{I}_{\text{cor}} \hat{\boldsymbol{G}}_{\omega,F}^{-1} \Big[-\boldsymbol{c}_\omega \boldsymbol{z}_\omega - \dot{\boldsymbol{\omega}}_0 + \dot{\boldsymbol{\omega}}_{\text{ref}} - \boldsymbol{G}_\Theta \bar{\boldsymbol{z}}_\Theta \Big] - \boldsymbol{U}_0 \Big) \\
&\quad - \dot{\boldsymbol{\omega}}_{\text{ref}} + \boldsymbol{c}_\omega \boldsymbol{\chi}_\omega \Big] \\
&= -\bar{\boldsymbol{z}}_\Theta^T \boldsymbol{c}_\Theta \bar{\boldsymbol{z}}_\Theta + \bar{\boldsymbol{z}}_\Theta^T \boldsymbol{G}_\Theta \bar{\boldsymbol{z}}_\omega + \bar{\boldsymbol{z}}_\omega^T \left[-\boldsymbol{c}_\omega \boldsymbol{z}_\omega + \boldsymbol{c}_\omega \boldsymbol{\chi}_\omega - \boldsymbol{G}_\Theta \bar{\boldsymbol{z}}_\Theta \right] \\
&= -\bar{\boldsymbol{z}}_\Theta^T \boldsymbol{c}_\Theta \bar{\boldsymbol{z}}_\Theta - \bar{\boldsymbol{z}}_\omega^T \boldsymbol{c}_\omega \bar{\boldsymbol{z}}_\omega
\end{aligned} \tag{6.69}$$

Next the CLF derivative shall be determined using for *the method of residualised dynamics*. Substituting the stabilising control law of Eq. 6.63 into the CLF derivative does yield the second expression of Eq. 6.70. This enables simplification of $\dot{\mathcal{V}}_\omega(\dot{\bar{\boldsymbol{z}}}_\Theta, \dot{\bar{\boldsymbol{z}}}_\omega)$, eventually yielding the last expression.

$$\begin{aligned}
\dot{\mathcal{V}}_\omega(\dot{\bar{\boldsymbol{z}}}_\Theta, \dot{\bar{\boldsymbol{z}}}_\omega) &= -\bar{\boldsymbol{z}}_\Theta^T \boldsymbol{c}_\Theta \bar{\boldsymbol{z}}_\Theta + \bar{\boldsymbol{z}}_\Theta^T \boldsymbol{G}_\Theta \bar{\boldsymbol{z}}_\omega + \bar{\boldsymbol{z}}_\omega^T \Big[\dot{\boldsymbol{\omega}}_0 + \hat{\boldsymbol{G}}_{\omega,R} \left(\boldsymbol{U}^0 - \boldsymbol{U}_0 \right) - \dot{\boldsymbol{\omega}}_{\text{ref}} + \boldsymbol{c}_\omega \boldsymbol{\chi}_\omega \Big] \\
&= -\bar{\boldsymbol{z}}_\Theta^T \boldsymbol{c}_\Theta \bar{\boldsymbol{z}}_\Theta + \bar{\boldsymbol{z}}_\Theta^T \boldsymbol{G}_\Theta \bar{\boldsymbol{z}}_\omega + \bar{\boldsymbol{z}}_\omega^T \Big[\dot{\boldsymbol{\omega}}_0 + \hat{\boldsymbol{G}}_{\omega,R} \Big(\boldsymbol{U}_0 + \hat{\boldsymbol{G}}_{\omega,R}^{-1} \Big[-\boldsymbol{c}_\omega \boldsymbol{z}_\omega - \dot{\boldsymbol{\omega}}_0 + \dot{\boldsymbol{\omega}}_{\text{ref}} - \boldsymbol{G}_\Theta \bar{\boldsymbol{z}}_\Theta \Big] - \boldsymbol{U}_0 \Big) \\
&\quad - \dot{\boldsymbol{\omega}}_{\text{ref}} + \boldsymbol{c}_\omega \boldsymbol{\chi}_\omega \Big] \\
&= -\bar{\boldsymbol{z}}_\Theta^T \boldsymbol{c}_\Theta \bar{\boldsymbol{z}}_\Theta + \bar{\boldsymbol{z}}_\Theta^T \boldsymbol{G}_\Theta \bar{\boldsymbol{z}}_\omega + \bar{\boldsymbol{z}}_\omega^T \left[-\boldsymbol{c}_\omega \boldsymbol{z}_\omega + \boldsymbol{c}_\omega \boldsymbol{\chi}_\omega - \boldsymbol{G}_\Theta \bar{\boldsymbol{z}}_\Theta \right] \\
&= -\bar{\boldsymbol{z}}_\Theta^T \boldsymbol{c}_\Theta \bar{\boldsymbol{z}}_\Theta - \bar{\boldsymbol{z}}_\omega^T \boldsymbol{c}_\omega \bar{\boldsymbol{z}}_\omega
\end{aligned} \tag{6.70}$$

In accordance with the theorem of *LaSalle-Yoshizawa* the equilibrium $\bar{\boldsymbol{z}} = \boldsymbol{0}$ can be regarded globally uniformly asymptotically stable when $\boldsymbol{c}_\Theta > 0$, $\boldsymbol{c}_\omega > 0$ and when sampling rate is sufficiently high [50, 54]. The aforementioned therefore implies that $\boldsymbol{\Theta}_{\text{ref}}$ can be tracked for $t \to \infty$.

7

Conclusions and Recommendations

7.1. Conclusions

First the effect of flapping dynamics on IBS control design, performance and robustness shall be considered. Rotor dynamics are found to be fundamental when establishing an angular rate controller of a rotorcraft. This is based on the fact that control effectiveness of the angular accelerations was found to be insufficient, but could be enhanced by considering a modified rotorcraft model, which was designated as the *idealised* rotorcraft model. This particular rotorcraft model was established by means of residualisation of rotor dynamics. The first and foremost way of enhancing control effectiveness for BF(L) models was by considering steady-state flapping dynamics, because flapping dynamics is significantly excited by main rotor cyclic control inputs and because the coupling between angular accelerations and flapping angles is significant as well. Residualisation would remove the aforementioned coupling term and enhance the control effectiveness. This would subsequently yield an *idealised* rotorcraft model, for which control-dependency had been increased, whereas state-dependency decreased. However, this rotorcraft model did differ from the *actual* rotorcraft model. The extent by which these differ, depends on whether the *actual* rotorcraft model could incorporate steady-state flapping dynamics for mimicking flapping motion. The aforementioned appeared not to be the case for the hingeless MBB Bo 105 model, because of the strong coupling between the angular body modes, such as pitch and roll subsidence, and the regressive flapping modes. This discrepancy had to be accounted for by means of a flapping synchronisation filter in the feedback-loop of the actuator measurements. This would enable to effectively delay the actuator measurement by the same amount as by which the angular acceleration measurements are being delayed with due to flapping dynamics. Not accounting for flapping synchronisation would yield magnified control inputs and thus overreaction of the closed-loop system. This implies that closed-loop stability could not be assured when flapping synchronisation was left out of the control design. The above mentioned was of prime concern for rotorcraft models with slow disc-tilt motion, because the *idealised* and *actual* rotorcraft model would significantly differ from each other. Performance was significantly affected when the flapping synchronisation filter was not accounted for in control design. This could be observed when conducting a tracking tasks, because RMSE significantly increased for the case wherein flapping synchronisation was not considered. Based on the above mentioned it can be stated that when the IBS controller is based upon an *idealised* rotorcraft model, modifications are required to account for the difference between *actual* and *idealised* rotorcraft model. In other words, it will affect the control design of the IBS controller. Moreover, controller performance was also affected when the IBS controller based upon the *idealised* rotorcraft model did not account for the flapping synchronisation filter. Next to this, it was also found that control effectiveness mismatch of the control effectiveness in the synchronisation filter can affect controller performance as well. This is because it adversely affects the synchronisation between the actuator and angular acceleration measurement. For over- and underestimation of the control effectiveness in the synchronisation filter, it was found that a steady-state tracking error would be present when executing a tracking task. This shows that there is also a lack of robustness for the flapping synchronisation filter.

Having considered the effects of flapping dynamics on IBS control design, performance and robustness, it will also be necessary to consider it for lead-lag dynamics. Based on findings, it can be stated that establishing a modified rotorcraft model for BFL models based upon residualisation of flap-lag dynamics is redundant. The aforementioned does hold for all BFL models analysed (with and without body-lag coupling). First, it must be acknowledged that accounting for the coupling between the angular body dynamics and lead-lag dynamics is deemed necessary to improve the open-loop frequency response. The aforementioned especially holds for the roll-rate-to-lateral-cyclic transfer function, which showed better correlation with frequency responses found in other research. The *idealised* rotorcraft model based upon flap-lag or flap residualisation

did not significantly differ from each other. This shows that the greatest discrepancy between both rotorcraft models is due to flapping dynamics. The control and state-dependency of the *idealised* rotorcraft model, did not significantly change with the residualisation of flap-lag dynamics. This shows that accounting for lead-lag dynamics in IBS control design is redundant. When comparing the performance of an IBS controller based upon an *idealised* flap-lag or flap residualised rotorcraft model, it can be stated that the improvement in performance was neglectable. The RMSE did not significantly differ for both controllers. On top of this, flap-lag residualisation did not significantly affect the TSS assumption. This is because the increments in system dynamics and control-depended increments were not significantly different between the IBS controller based upon flap and flap-lag residualisation. Based on the above mentioned it must be concluded that accounting for lead-lag dynamics in control design is not deemed necessary. This is favourable, because it obviates the need of having accurate and reliable knowledge of lead-lag dynamics. This subsequently also implies that the rotor synchronisation filter shall be established by not considering lead-lag dynamics. Likewise, the control effectiveness shall be established by only considering residualisation of flapping dynamics. It can therefore be stated that the IBS controller is robust to uncertainties in lead-lag dynamics.

It can therefore be concluded that accounting for flapping dynamics is still necessary to assure a well-established control effectiveness such that the IBS TSS is not violated or less violated. The controller was not robust to uncertainties in control effectiveness of the synchronisation filter, because it would yield inadequate synchronisation of actuator and angular acceleration measurement. To be more specific, control effectiveness over- or underestimation would yield diminished or magnified control inputs and therefore affecting closed-loop response. This shows that rotor synchronisation is a good way to deal with the discrepancy between *idealised* and *actual* rotorcraft model, but it still requires accurate model knowledge for establishing it. A well-established synchronisation filter is therefore of prime concern to assure adequate controller performance.

7.2. Recommendations for future work

Next, it is will be of great importance to consider recommendations for future work. Based on the conclusion it can be stated that the results of the analysis are satisfying and did answer the research questions. On the other hand, there is still room for improvement. Below recommendations are provided.

1. Currently, only the effect of flapping and lead-lag dynamics on control design is being analysed. However, it will also be interesting to see whether other internal dynamics, such as inflow dynamics will influence control design. Of particular interest would be its effect on the *idealised* rotorcraft model. Residualisation of for example flap-inflow dynamics could may yield an *idealised* rotorcraft model that would improve the control effectiveness. When found that inflow dynamics does play an important factor to assure a well-established control effectiveness for the IBS control law, then the synchronisation filter needs to be adapted as well. This would require more model knowledge, which is not favourable. It will therefore be of great interest to determine whether accounting for inflow dynamics in IBS control design could improve controller performance, while maintaining good controller robustness as well.
2. It is recommended to have a better established BFL model, wherein all coupling terms are accounted for. The main rotorcraft model has been established based on different models, which makes it difficult to integrate these into one good simulation model. Currently, the main rotorcraft model introduced in Chapter 2 incorporates a second-order flapping model and first-order *Pitt-Peters* inflow model [37]. On the other hand, lead-lag dynamics was obtained from Nguyen [34]. The flap-lag EOM from Nguyen [34] did lack traceability, because it had not been simplified yet. It is therefore highly recommended to reduce the flap-lag EOM from Nguyen [34], such that the traceability of the independent variables does increase. On top of this, lead-lag dynamics was not accounted for when establishing the force and moment equations for the main rotor. This can be regarded as a major drawback of the current MBB Bo 105 simulation model, because the coupling between the angular body dynamics and lead-lag dynamics is not present. This implies that when assessing the TSS condition for the first-order *Taylor* series of the angular accelerations, little can be said about the increments due to lead-lag dynamics. It is therefore highly recommenced to account for lead-lag dynamics in force and moment calculation of the main rotor.
3. The robustness analysis on the synchronisation filter could be more extensive. In this research only control effectiveness mismatch of the synchronisation filter was considered. It was namely found that

controller is not robust to uncertainties in control effectiveness of the rotor synchronisation filter. This showed that accurate and reliable knowledge of control effectiveness was needed for the synchronisation filter. Other model mismatches can be considered for the synchronisation filter. The main objective is to assure that actuator measurement and state derivative measurement are synchronised with each other, which is more difficult to assure when there are other deficiencies in the synchronisation filter.

Bibliography

[1] BPJ Acquatella. Robust nonlinear spacecraft attitude control: An incremental backstepping approach. 2011.

[2] Mohammad Al-Sharman, Mohammad Amin Al-Jarrah, and Mamoun Abdel-Hafez. Auto takeoff and precision terminal-phase landing using an experimental optical flow model for gps/ins enhancement. *ASCE-ASME Journal of Risk and Uncertainty in Engineering Systems, Part B: Mechanical Engineering*, 5 (1):011001–1, 2018.

[3] Bimal Aponso, Duc Tran, Jeffery Schroeder, and Steven Beard. Rotorcraft research at the nasa vertical motion simulator. In *AIAA Atmospheric Flight Mechanics Conference*, page 6056, 2008.

[4] US Army Aviation and Missile Command. Aeronautical design standard performance specification handling qualities requirement for military rotorcraft. redstone arsenal, al. *Redstone Arsenal, AL*, 2000.

[5] Barry J Baskett. Aeronautical design standard performance specification handling qualities requirements for military rotorcraft. Technical report, ARMY AVIATION AND MISSILE COMMAND REDSTONE ARSENAL AL, 2000.

[6] Mohd Basri, Mohd Ariffanan, Kumeresan A Danapalasingam, and Abdul Rashid Husain. Design and optimization of backstepping controller for an underactuated autonomous quadrotor unmanned aerial vehicle. *Transactions of FAMENA*, 38(3):27–44, 2014.

[7] Y Baudoin and Maki K Habib. Using robot in hazardous environments. *Woodhead Publishing, United Kingdom*, pages 486–489, 2011.

[8] J. T. Booms. Improving helicopter handling qualities with constrained incremental backstepping. 2017.

[9] Robert TN Chen. Effects of primary rotor parameters on flapping dynamics. 1980.

[10] HC Curtiss. Stability and control modelling. 1986.

[11] HC Curtiss Jr. Physical aspects of rotor body coupling in stability and control. In *46th Annual Forum of the American Helicopter Society*, 1990.

[12] Charles W Ellis. Effects of rotor dynamics on helicopter automatic control system requirements. *Aeronaut. Eng. Rev*, 12(7), 1953.

[13] Wouter Falkena, Eddy van Oort, and Ping Chu. Towards certifiable advanced flight control systems, a sensor based backstepping approach. In *AIAA Guidance, Navigation, and Control Conference*, page 6482, 2011.

[14] Jay Farrell, Marios Polycarpou, and Manu Sharma. Adaptive backstepping with magnitude, rate, and bandwidth constraints: Aircraft longitude control. In *Proceedings of the 2003 American Control Conference, 2003.*, volume 5, pages 3898–3904. IEEE, 2003.

[15] Jay A Farrell, Marios Polycarpou, Manu Sharma, and Wenjie Dong. Command filtered backstepping. *IEEE Transactions on Automatic Control*, 54(6):1391–1395, 2009.

[16] WE Hall Jr and AE Bryson Jr. Inclusion of rotor dynamics in controller design for helicopters. *Journal of Aircraft*, 10(4):200–206, 1973.

[17] Peter G Hamel. Advances in aerodynamic modeling for flight simulation and control design. *Aeronautical Journal*, pages 169–178, 1984.

[18] J Howitt. Application of non-linear dynamic inversion to rotorcraft flight control. In *ANNUAL FORUM PROCEEDINGS-AMERICAN HELICOPTER SOCIETY*, volume 61, page 1160. AMERICAN HELICOPTER SOCIETY, INC, 2005.

[19] Liviu Gr Ixaru and Guido Vanden Berghe. Runge-kutta solvers for ordinary differential equations. In *Exponential Fitting*, pages 223–304. Springer, 2004.

[20] Wayne Johnson. *Helicopter theory*. Courier Corporation, 2012.

[21] Ioannis Kanellakopoulos, Petar V Kokotovic, and A Stephen Morse. Systematic design of adaptive controllers for feedback linearizable systems. In *1991 American Control Conference*, pages 649–654. IEEE, 1991.

[22] Ali Karimi, Amer Al-Hinai, Karl Schoder, and Ali Feliachi. Power system stability enhancement using backstepping controller tuned by particle swarm optimization technique. In *IEEE Power Engineering Society General Meeting, 2005*, pages 1388–1395. IEEE, 2005.

[23] T Keijzer. Flight testing of incremental backstepping based control laws with angular accelerometer feedback. 2017.

[24] Twan Keijzer. *Design and Flight Testing of Incremental Control Laws using Angular Accelerometer Feedback on a CS-25 Aircraft.* PhD thesis, Delft University of Technology, 2018.

[25] Hassan K Khalil and Jessy W Grizzle. *Nonlinear systems*, volume 3. Prentice hall Upper Saddle River, NJ, 2002.

[26] Petar Kokotović and Murat Arcak. Constructive nonlinear control: a historical perspective. *Automatica*, 37(5):637–662, 2001.

[27] JFR Koschorke. Advanced flight control design and evaluation: an application of time delayed incremental backstepping. 2012.

[28] M Krstić, I Kanellakopoulos, and PV Kokotović. Adaptive nonlinear control without overparametrization. *Systems & Control Letters*, 19(3):177–185, 1992.

[29] Miroslav Krstic, Ioannis Kanellakopoulos, Petar V Kokotovic, et al. *Nonlinear and adaptive control design*, volume 222. Wiley New York, 1995.

[30] Miroslav Krstic, Dan Fontaine, Petar V Kokotovic, and James D Paduano. Useful nonlinearities and global stabilization of bifurcations in a model of jet engine surge and stall. *IEEE Transactions on Automatic Control*, 43(12):1739–1745, 1998.

[31] Gordon J Leishman. *Principles of helicopter aerodynamics with CD extra*. Cambridge university press, 2006.

[32] Peng Lu, Erik-Jan Van Kampen, and Q Ping Chu. Robustness and tuning of incremental backstepping approach. In *AIAA Guidance, Navigation, and Control Conference*, page 1762, 2015.

[33] AS Mendes. Vision-based automatic landing of a quadrotor uav on a floating platform: A new approach using incremental backstepping. 2012.

[34] A.E. Nguyen. The development of a body-flap-lag model for rotorcraft-pilot couplings investigation. 2008.

[35] Katsuhiko Ogata and Yanjuan Yang. *Modern control engineering*, volume 5. Prentice hall Upper Saddle River, NJ, 2010.

[36] Stephen Osder and Donald Caldwell. Design and robustness issues for highly augmented helicopter controls. *Journal of guidance, control, and dynamics*, 15(6):1375–1380, 1992.

[37] Gareth D Padfield. *Helicopter flight dynamics*. Wiley Online Library, 2008.

[38] Gareth D Padfield, AT McCallum, H Haverdings, A-M Dequin, D Haddon, K Kampa, P-M Basset, and W Von Gruenhagen. Predicting rotorcraft flying qualities through simulation modelling. a review of key results from garteur ag06. In *European Rotorcraft Forum*, volume 22, pages 71–1. ASSOCIAZIONE ITALIANA DI AERONAUTICA ED ASTRONAUTICA, 1996.

[39] Marilena Domnica Pavel. On the necessary degrees of freedom for helicopter and wind turbine low-frequency mode modeling. 2001.

[40] MD Pavel. Modeling lead-lag dynamics for rotorcraft-pilot-couplings investigation. In *American Helicopter Society 66th Annual Forum, Phoenix Arizona*, 2010.

[41] MD Pavel, Th Holten, et al. On the prediction of the necessary rotor dynamics for helicopter flight simulation. 1997.

[42] MD Pavel, P Shanthakumaran, O Stroosma, et al. Development of advanced flight control laws for the ah-64 apache helicopter-sketches from the work of tu delft-boeing project in simona simulator. In *Proceedings of the American Helicopter Society 72th Annual Forum*, 2016.

[43] Raymond W Prouty. *Helicopter performance, stability, and control*. 1995.

[44] Raymond W Prouty and HC Curtiss. Helicopter control systems: A history. *Journal of Guidance, Control, and Dynamics*, 26(1):12–18, 2003.

[45] S Sieberling, QP Chu, and JA Mulder. Robust flight control using incremental nonlinear dynamic inversion and angular acceleration prediction. *Journal of guidance, control, and dynamics*, 33(6):1732–1742, 2010.

[46] P Simplicio. Helicopter nonlinear flight control: An acceleration measurements-based approach using incremental nonlinear dynamic inversion. 2011.

[47] P Simplício, MD Pavel, E Van Kampen, and QP Chu. An acceleration measurements-based approach for helicopter nonlinear flight control using incremental nonlinear dynamic inversion. *Control Engineering Practice*, 21(8):1065–1077, 2013.
[48] Sigurd Skogestad and Ian Postlethwaite. *Multivariable feedback control: analysis and design*, volume 2. Wiley New York, 2007.
[49] L Sonneveldt. Adaptive backstepping flight control for modern fighter aircraft. 2010.
[50] Lars Sonneveldt, QP Chu, and JA Mulder. Nonlinear flight control design using constrained adaptive backstepping. *Journal of Guidance, Control, and Dynamics*, 30(2):322–336, 2007.
[51] Lars Sonneveldt, ER Van Oort, QP Chu, and JA Mulder. Comparison of inverse optimal and tuning functions designs for adaptive missile control. *Journal of guidance, control, and dynamics*, 31(4):1176–1182, 2008.
[52] Georges Tod, Marilena D Pavel, François Malburet, Julien Gomand, and Pierre-Jean Barre. Understanding pilot biodynamical feedthrough coupling in helicopter adverse roll axis instability via lateral cyclic feedback control. *Aerospace Science and Technology*, 59:18–31, 2016.
[53] W van Ekeren. Incremental nonlinear flight control for fixed-wing aircraft. 2016.
[54] P Van Gils. Adaptive incremental backstepping flight control. 2015.
[55] RR Van Goot. Helicopter control using incremental adaptive backstepping. 2017.
[56] Eduard Richard Van Oort. Adaptive backstepping control and safety analysis for modern fighter aircraft. 2011.
[57] RC van't Veld. Incremental nonlinear dynamic inversion flight control: Stability and robustness analysis and improvements. 2016.

A

Reference Frames and Transformations

For establishing the rotorcraft simulation model a set of reference frames was required. Moreover, transformations between these frames was deemed necessary as well. In this Appendix the reference frames and intermediate transformations shall be provided. These were obtained from [55] and [46].

A.1. Body-fixed Reference Frame F_B

The first reference frame to be introduced is the body-fixed reference frame. This reference frame is fixed to the rotorcraft in which the origin is situated at the center of gravity. The rotorcraft can be associated with a plane of symmetry in which the x_B- and z_B-axis lie. The x-axis does point forward and is aligned with the centerline of the fuselage, whereas the z_B-axis does point downward and is perpendicular to the other axis. The y_B-axis is perpendicular to the two aforementioned axis and is oriented such that it yields a right-handed orthogonal axis system. In Fig. A.1 the body-fixed reference frame is provided along with the Earth reference frame. Angular and linear body velocities are commonly expressed in this reference frame [46].

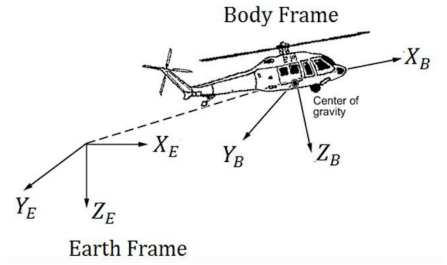

Figure A.1: Body-fixed reference frame [2].

A.2. North-East-Down Reference Frame F_{NED}

The next reference frame to be considered is the North-East-Down (NED) reference frame. This reference frame is also attached to the rotorcraft, wherein the origin is situated at the center of gravity. The orientation of this reference frame is such that the z_{NED}-axis does points downwards towards the local gravity vector. Moreover the x_{NED}-axis does point to the north and y_{NED}-axis points to the east such that a right-hand coordinate system is completed. In [46] was outlined that the orientation of this specific reference system does not significantly change for small distances. For defining this reference system it was assumed that Earth's curvature can be neglected such that flat Earth surface can be assumed. Moreover it is also assumed that Earth is non-rotating. Based on the aforementioned it can be stated that F_{NED} is an inertial reference frame. All of the above assumptions do hold when short simulations are performed as the change in orientation of the reference system is negligible.

A.3. Transformation from F_{NED} to F_B

The first transformation to be considered is the one from the F_{NED} to F_B. Since both axis-systems are situated at the center of gravity of the rotorcraft, rotations suffice to go from one frame of reference to the other.

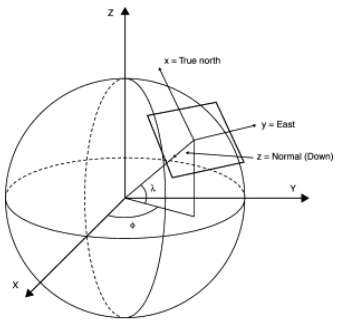

Figure A.2: NED-reference frame (without vehicle) [7].

Transformation from F_{NED} to F_B can be achieved by three successive rotations, which will involve two intermediate axis system which are denoted as $F_{NED'}$ and $F_{NED''}$. These intermediate axis-systems are reached after performing the first and second rotation respectively. The rotation can be written as

$$F_{NED} \longrightarrow F_{NED'} \longrightarrow F_{NED''} \longrightarrow F_B. \tag{A.1}$$

Transformation from F_{NED} to F_B requires the following transformations:

- yaw angle (ψ) rotation about the z_{NED}-axis
- pitch angle (θ) rotation about the $y_{NED'}$-axis
- roll angle (ϕ) rotation about the $x_{NED''}$-axis

Doing the aforementioned will yield the transformation given in Eq. A.2 [46]. It should be noted that c and s are abbreviations for cos and sin respectively.

$$T^{B}_{NED} = R_x(\phi)R_y(\theta)R_z(\psi) = \begin{bmatrix} c_\psi c_\phi & s_\psi c_\theta & -s_\theta \\ c_\psi s_\theta s_\phi - s_\psi c_\phi & s_\psi s_\theta s_\phi + c_\psi c_\phi & c_\theta c_\phi \\ c_\psi s_\theta c_\phi + s_\psi s_\phi & s_\psi s_\theta c_\phi - c_\psi s_\phi & c_\theta c_\phi \end{bmatrix} \tag{A.2}$$

Important to note is that $T^{B^{-1}}_{NED}$=$T^{B^{T}}_{NED}$ because of preserved orthogonality. Moreover it can also be stated that T^{NED}_{B}=$T^{B^{-1}}_{NED}$, which means that the transformation from F_B to F_{NED} can also easily be executed using the transformation matrix from Eq. A.2.

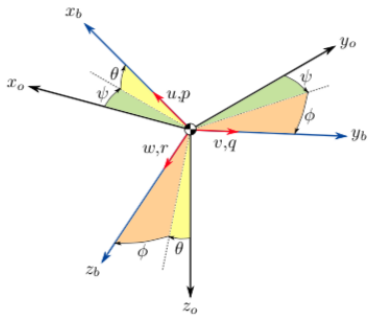

Figure A.3: Rotation between the F_{NED} and F_B from [46].(subscript o does represent that NED reference frame)

A.4. Velocity reference frame F_V

The next reference frame to be considered is the velocity reference frame. The velocity reference frame does have its origin also located at the center of gravity of the rotorcraft. The reference system is oriented in such a way that the x_V-axis is aligned with the velocity vector of the rotorcraft. Moreover, the y_V-axis is perpendicular to local gravity vector and x_V-axis. In order to complete the right-handed axis system it is necessary for the

z_V-axis to be perpendicular to the two aforementioned axis. The velocity vector in F_V is thus solely given by the x-coordinate.

A.5. Transformation from F_{NED} to F_V

The next transformation to be considered is the one from F_{NED} to F_V. Similar to the previous transformation it does not involve any translations as F_{NED} and F_V are both situated at the center of gravity. Transformation F_{NED} to F_V involves two rotations, which implies that the transformation can be written as

$$F_{\text{NED}} \longrightarrow F_{\text{NED}'} \longrightarrow F_{\text{V}}. \tag{A.3}$$

The transformation from one frame of reference to another can be achieved by incorporating the following successive rotations

- flight path angle (γ) rotation about the y_V-axis
- heading angle (θ) rotation about the $x_{V'}$-axis

The flight path angle can be defined as the angle between the velocity vector and the local horizon. This local horizon is perpendicular to the local gravity field. Moreover, the heading angle can be defined as the angle between velocity vector and the vector pointing northwards. The above transformation is given in Eq. A.4 [46].

$$T^{\text{V}}_{\text{NED}} = R_y(\gamma)R_z(\chi) = \begin{bmatrix} c_\psi c_\gamma & s_\psi c_\gamma & -s_\gamma \\ -s_\psi & c_\psi & 0 \\ c_\psi s_\gamma & s_\psi s_\gamma & c_\gamma \end{bmatrix} \tag{A.4}$$

From this transformation it also follows that the following will be equivalent: T^{V}_{NED}=$T^{NED^{-1}}_{V}$=$T^{NED^{T}}_{V}$. It should be noted that when the velocity vector is aligned with rotorcraft centerline then flight path angle and yaw angle will be equal to each other. Moreover pitch angle and flight path angle will also be equal to each other. In Fig. A.4 the relation between different reference systems can be observed. From this figure the angle of attack ($\alpha = \theta$ - γ) and sideslip ($\beta = \chi$ - ψ) angle can be identified.

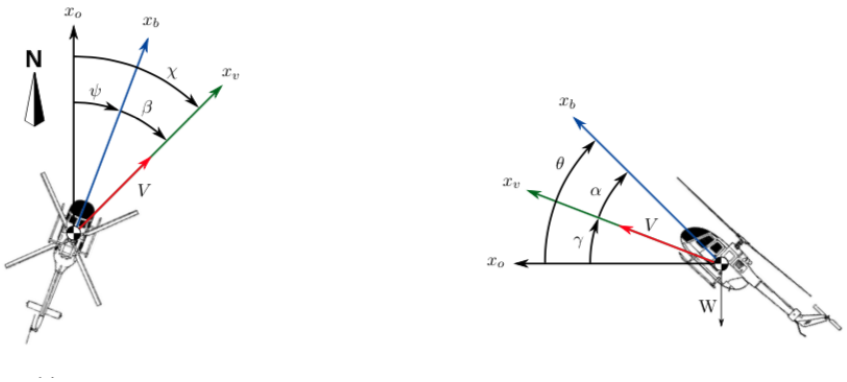

(a) Vertical plane. **(b)** Horizontal plane.

Figure A.4: Relation between coordinate system [46].

A.6. Hub Reference Frame F_h

The hub reference frame does have its origin located at the rotor shaft. This is the location where the rotor hinges do attach. The orientation of this reference frame is such that the the z_h-axis does point downward along the shaft. Next to this the x_h-axis is perpendicular to the z_h-axis and is situated in the plane of symmetry of the rotorcraft. To complete the right-handed axis system, the y_h-axis must be perpendicular to the two aforementioned axis. Important to note is that the plane perpendicular to the z_h-axis is the shaft/hub plane.

A.7. Transformation from F_B to F_h

Transforming coordinates from F_B to F_h does require a single rotation and two translations. This implies that there will not be an intermediate reference system, thus the transformation can be simply written as

$$F_{\mathrm{B}} \longrightarrow F_{\mathrm{h}}, \tag{A.5}$$

wherein the following rotation is required

- disc-tilt angle (γ_{s}) rotation about y_{B}-axis

The above mentioned transformation is given in Eq. A.6 [46].

$$T_B^h = R_y\left(-\gamma_s\right) = \begin{bmatrix} c_{\gamma_s} & 0 & s_{\gamma_s} \\ 0 & 1 & 0 \\ -s_{\gamma_\alpha} & 0 & c_{\gamma_*} \end{bmatrix} \tag{A.6}$$

Furthermore it is also necessary to account for the offset of F_B with respect to F_h. A translation is required to let F_B and F_h coincidence with each other. The following translations are required

- -x_{cg} along x_{B}-axis
- h_{R} along negative z_{B}-axis

The above mentioned rotation and translations enable to rewrite any vector from F_B to F_h. The translations and rotation can be written into the compact form given in Eq. A.7 [46].

$$\mathbf{r}_h = T_B^h\left(\mathbf{r}_b + \begin{bmatrix} -x_{cg} \\ 0 \\ h_R \end{bmatrix}\right) \tag{A.7}$$

The BF model from [37] and incorporated by [55] require the body velocities to be defined in the hub reference frame. This can be achieved by incorporating the transformation given in Eq. A.8 [46].

$$\begin{bmatrix} u_h \\ v_h \\ w_h \end{bmatrix} = T_B^h\left(\begin{bmatrix} u_B \\ v_B \\ w_B \end{bmatrix} + \begin{bmatrix} -x_{cg} \\ 0 \\ h_R \end{bmatrix} \times \begin{bmatrix} p \\ q \\ r \end{bmatrix}\right) \tag{A.8}$$

A.8. Hub-wind Reference Frame

Another hub reference frame that needs to be considered is the hub-wind reference frame [55]. This reference frame is similar to the hub reference frame except for the x_{hw}-axis being aligned with the local hub velocity vector in the hub plane.

A.9. Transformation from F_h to F_{hw}

Transformation from F_h to F_{hw} can be achieved by means of a single rotation. The transformation is therefore simple and can be written as

$$F_{\mathrm{h}} \longrightarrow F_{\mathrm{hw}}, \tag{A.9}$$

wherein the following rotation must be considered

- rotor sideslip angle ψ_{w} rotation about z_h-axis.

The rotor sideslip angles are provided in Eq. A.10 and Eq. A.11 [55].

$$\cos(\psi_{\mathrm{w}}) = \frac{u_{\mathrm{h}}}{u_{\mathrm{h}}^2 + v_{\mathrm{h}}^2}, \tag{A.10}$$

$$\sin(\psi_{\mathrm{w}}) = \frac{v_{\mathrm{h}}}{u_{\mathrm{h}}^2 + v_{\mathrm{h}}^2}. \tag{A.11}$$

The transformation matrix from F_h to F_{hw} is provided in Eq. A.12 [55].

$$T_h^{hw} = \frac{1}{\sqrt{u_h^2 + v_h^2}} \begin{bmatrix} u_h & v_h & 0 \\ -v_h & u_h & 0 \\ 0 & 0 & \sqrt{u_h^2 + v_h^2} \end{bmatrix}. \tag{A.12}$$

A.10. Blade Reference Frame

The next reference system that needs to be considered is the blade reference system, which is explained in detail in [55]. The origin of this axis system is variable as it can vary along the blade leading edge. The orientation of this reference frame is such that $\mathrm{y_{bl}}$ is parallel to the leading edge of the rotor blade. Moreover $\mathrm{x_{bl}}$ is orthogonal to $\mathrm{y_{bl}}$ in the hub plane. The right-handed reference frame is completed with $\mathrm{z_{bl}}$ being orthogonal to the two aforementioned axis.

A.11. Transformation from F_{hw} and F_{bl}

Next, it will be deemed necessary to consider the transformation from the hub-wind frame of reference to the blade frame of reference. This transformation is provided in Eq. A.13 [55].

$$T_{hw}^{bl} = R_z(-\psi)R_y(-\beta) = \begin{bmatrix} -c_\psi c_\beta & -s_\psi & -c_\psi s_\beta \\ s_\psi c_\beta & -c_\psi & s_\psi s_\beta \\ -s_\beta & 0 & c_\beta \end{bmatrix} \tag{A.13}$$

Next to this, the angular velocities in the rotating reference system are given in Eq. A.14 [55].

$$\begin{bmatrix} \omega_x \\ \omega_y \end{bmatrix} = \begin{bmatrix} \cos(\psi) & -\sin(\psi) \\ \sin(\psi) & \cos(\psi) \end{bmatrix} \begin{bmatrix} p_{hw} \\ q_{hw} \end{bmatrix} \tag{A.14}$$

The velocities in $\mathrm{F_{bl}}$ at $\mathrm{r_{bl}}$ using small angle approximation for β can be written as follows

$$\begin{aligned} u_{bl} &= -u_{hw}\cos(\psi) - w_{hw}\beta \\ v_{bl} &= -u_{hw}\sin(\psi) - r_{bl}\left(\Omega - r_{hw} + \beta\omega_x\right) \\ w_{bl} &= -u_{hw}\beta\cos(\psi) + w_{hw} + r_{bl}\left(\omega_y - \dot{\beta}\right) \end{aligned} \tag{A.15}$$

Next, it is deemed necessary to neglect hub translational accelerations and hub-blade velocity products. This will eventually yield the expression of the acceleration in $\mathrm{F_{bl}}$ at $\mathrm{r_{bl}}$ given below [55].

$$\begin{aligned} a_{xbl} &= r_b\left(-\left(\Omega - r_{hw}\right)^2 + 2\dot{\beta}\omega_y - 2\left(\Omega - r_{hw}\right)\beta\omega_x\right) \\ a_{ybl} &= r_b\left(-\dot{\Omega} + \dot{r}_{hw} - \beta\left(\dot{q}_{hw}\sin(\psi) - \dot{p}_{hw}\cos(\psi)\right) + r_{hw}\beta\omega_y\right) \\ a_{zbl} &= r_b\left(2\Omega\omega_x + \left(\dot{q}_{hw}\cos(\psi) + \dot{p}_{hw}\sin(\psi)\right) - r_{hw}\omega_x - \left(\Omega - r_{hw}\right)^2\beta - \ddot{\beta}^2\right) \end{aligned} \tag{A.16}$$

Moreover, the assumption given below was also required [55].

$$\left(\Omega - r_{hw}\right) \approx \Omega \tag{A.17}$$

$$\left(\dot{\Omega} - \dot{r}_{hw}\right) \approx -\dot{r}_{hw} \tag{A.18}$$

A.12. Disc-wind Reference Frame

The last reference frame that shall be considered is the disc-wind reference frame, for which a more detailed explanation is provided in [55]. This reference frame is defined as the plane that is being spanned by the vectors y_h-axis and x_h-axis, which are tilted with respect to $-\beta_{1s}$ and β_{1c}. Moreover, the z_{dw}-axis is perpendicular to the aforementioned plane. On top of this the z_{dw}-axis does point downward at originates at the

hub. In addition to this the x_{dp}-axis is oriented in such a way that it is defined by the hub velocity vector in the disc plane. Lastly, the y_{dw} is perpendicular to the two aforementioned axes, completing a right-handed orthogonal axis system. In order to find the orientation of the z_{dw}-axis in the hub plane, one can make use of Eq. A.19 [55].

$$\mathbf{z}_{h-dw} = \begin{bmatrix} c_{\beta_{1c}} \\ 0 \\ s_{\beta_{1c}} \end{bmatrix} \times \begin{bmatrix} 0 \\ c_{\beta_{1s}} \\ -s_{\beta_{1s}} \end{bmatrix} = \begin{bmatrix} -s_{\beta_{1c}} c_{\beta_{1s}} \\ c_{\beta_{1c}} s_{\beta_{1s}} \\ c_{\beta_{1c}} c_{\beta_{1s}} \end{bmatrix} \tag{A.19}$$

It should be noted that the vector norm is provided in Eq. A.20 [55].

$$|\mathbf{z}_{h-dw}| = \sqrt{s^2_{\beta_{1c}} c^2_{\beta_{1s}} + c^2_{\beta_{1c}} s^2_{\beta_{1s}} + c^2_{\beta_{1c}} c^2_{\beta_{1s}}} = \sqrt{s^2_{\beta_{1c}} c^2_{\beta_{1s}} + c^2_{\beta_{1c}}} \tag{A.20}$$

Next to this, the expression for the xdw-axis is provided in Eq. A.21, which is found to be the projection of a wind vector on the disc plane.

$$\begin{aligned} \mathbf{x}_{h-dw} &= \mathbf{v}_h - \frac{\mathbf{v}_h \cdot \mathbf{z}_{h-dw}}{|\mathbf{z}_{h-dw}|^2} \mathbf{z}_{h-dw} \\ &= \begin{bmatrix} u_h \\ v_h \\ w_h \end{bmatrix} + \frac{s_{\beta_{1c}} c_{\beta_{1s}} u_h - c_{\beta_{1c}} s_{\beta_1} v_h - c_{\beta_{1c}} c_{\beta_{1s}} w_h}{s^2_{\beta_{1c}} c^2_{\beta_{1s}} + c^2_{\beta_{1c}}} \begin{bmatrix} -s_{\beta_{1c}} c_{\beta_{1s}} \\ c_{\beta_{1c}} s_{\beta_{1s}} \\ c_{\beta_{1c}} c_{\beta_{1s}} \end{bmatrix} \end{aligned} \tag{A.21}$$

The orientation vectors can be normalised yielding the unit vectors from Eq. A.22 [55].

$$\begin{aligned} \mathbf{k}_{h-dw} &= \frac{\mathbf{Z}_{h-dw}}{|\mathbf{z}_{h-dw}|} \\ \mathbf{i}_{h-dw} &= \frac{\mathbf{X}_{h-dw}}{|\mathbf{x}_{h-dw}|} \\ \mathbf{j}_{h-dw} &= \mathbf{k}_{h-dw} \times \mathbf{i}_{h-dw} \end{aligned} \tag{A.22}$$

From this follows the transformation matrix

$$T_{h-dw} = \begin{bmatrix} \mathbf{i}_{h-dw} & \mathbf{j}_{h-dw} & \mathbf{k}_{h-dw} \end{bmatrix} \tag{A.23}$$

A.13. Reference Systems for establishing flap-lag EOM

In order to derive the coupled flap-lag EOM, it is found deemed necessary to define a set of rotating (3) and non-rotating (5) axis systems. These reference systems are provided and are obtained from [34, 40]. The reference systems being considered are:

I **Body fixed axis system** $\{\vec{E}_b\}$: the origin is located at the rotorcraft CG, in which The body axes are fixed to the fuselage and x-axis points forward towards the nose of the rotorcraft, the z-axis points downward being perpendicular to the x-axis and the y-axis is perpendicular to the two other axes and thus points starboard. In hover the x-axis and y-axis will be situated in the horizontal plane and the z-axis will point downward in vertical direction, which implies that the rotorcraft will have zero cyclic pitch.

II **Shaft axis system** $\{\vec{E}_s\}$: which is situated at a negative distance h in Z_b direction from the the centre of gravity, with the orientation of the shaft (or hub) being aligned with the body system of reference.

III **Rotating shaft axis system** $\{\vec{E}'_s\}$: which is situated at the same position as $\{\vec{E}_s\}$, but is now rotating with blade azimuth angle ψ in the negative direction.

IV **Blade axis system** $\{\vec{E}_b\}$: is the reference for an arbitrary point on the rotor blade situated at a distance from the flapping hinge.

V **Lead-lag axis system**$\{\vec{E}_\zeta\}$: local reference system at the lead-lag hinge of the rotor blade.

VI **Rotating Lead-lag axis system**$\{\vec{E}'_\zeta\}$: local reference system at the lead-lag hinge capable of rotating around the lead-lag hinge.

VII **Flapping axis system**$\{\vec{E}_\beta\}$: local reference system at the flapping hinge of the rotor blade.

VIII **Rotating Flapping axis system**$\{\vec{E}'_{\boldsymbol{\beta}}\}$: local reference system at the flapping hinge capable of rotating around the flapping hinge.

The different system of references can be reached when incorporating an appropriate set of transformations. For executing the derivation, the transformation given below will suffice [34, 40].

$$\begin{array}{ll} \{\vec{E}_s\} = \{\vec{E}_b\}, & \\ \{\vec{E}'_s\} = [\psi]\{\vec{E}_s\}, & \left\{\vec{E}'_\beta\right\} = \{\vec{E}_\zeta\}; \{\vec{E}_\beta\} = [\beta]\left\{\vec{E}'_\beta\right\} = [\beta][\zeta][\psi]\{\vec{E}_s\}, \\ \{\vec{E}'_s\} = \left\{\vec{E}'_\zeta\right\}; \{\vec{E}_\zeta\} = [\zeta]\left\{\vec{E}'_\zeta\right\}, & \{\vec{E}_{bl}\} = \{\vec{E}_\beta\}. \end{array} \tag{A.24}$$

The transformations are achieved by means of the transformation matrices **[$\boldsymbol{\zeta}$]**, **[$\boldsymbol{\beta}$]** and **[$\boldsymbol{\psi}$]**. These matrices are given in Eq. A.25 [34, 40].

$$[\psi] = \begin{bmatrix} \cos(\psi) & -\sin\psi & 0 \\ \sin\psi & \cos\psi & 0 \\ 0 & 0 & 1 \end{bmatrix}, \quad [\zeta] = \begin{bmatrix} \cos\zeta & -\sin\zeta & 0 \\ \sin\zeta & \cos\zeta & 0 \\ 0 & 0 & 1 \end{bmatrix} \text{and} \quad [\beta] = \begin{bmatrix} \cos\beta & 0 & \sin\beta \\ 0 & 1 & 0 \\ -\sin\beta & 0 & \cos\beta \end{bmatrix} \tag{A.25}$$

B

Assumptions Derivation of Flap-Lag model

Below a set of assumptions are provided, which were deemed necessary for deriving the Body-Flap-Lag Model in [34]. Similar assumptions are also provided in [40].

I the rotor blade can be regarded as being rigid both in torsion and bending, containing a lagging and flapping with a spring hinge of strength K_ζ and K_β respectively located at an offset e_ζ and e_β respectively

II the rotor blades rotate at a constant angular speed (Ω = const.) in counter clockwise (CCW) direction.

III the inflow, lagging and flapping angles can be regarded as sufficiently small (Taylor Series truncation)

IV the shaft axis goes through the centre of gravity of the rotorcraft and is located at distance h from the CG

V the force due to the gravitational acceleration ($\mathrm{d}m\vec{g}$) shall not be taken into consideration.

VI reversed flow region is not being considered, thus stall and compressibility effects are ignored

VII the rotor blade is assumed to have a constant chord distribution, thus being of rectangular nature

VIII the rectangular blade is assumed to have no root cut-out

IX the control axis, aerodynamic axis, blade elastic axis and centre of mass do coincide with each other.

X couplings such as pitch-lag and pitch-flap are not taken into consideration, thus this implies that the no-feathering plane and the disc plane do coincidence with each other

XI tip losses of the the rotor blade are being neglected

XII incorporating an inflow model mimicking constant inflow over the rotor disc, hence uniform inflow

XIII the hinge order is lag-flap-pitch (Sikorsky), which commonly holds for articulated rotorcraft and is also generally accepted for the hingeless BO-105 rotorcraft

C

Linearisation Procedure Flap-Lag Model

With the nonlinear coupled FL EOM being defined in the rotating frame of reference, a linearisation procedure is required to transform the EOM from the rotating to the non-rotating frame of reference. This procedure was provided in [34]. Such a linearisation procedure is justified when the small angle assumption does hold, thus when the flapping and lead-lag angles are small. Linearisation of the nonlinear system of EOM can be achieved by incorporating a first-order *Taylor* series approximation about the steady state condition. The first order *Taylor* series shall be taken around the trim condition of the rotorcraft. The *Taylor* series approximation for flapping and lead-lag are given in Eq. C.1 [34].

$$F(\beta) = \sum_{n=0}^{\infty} \frac{F^n(\beta_{tr})}{n!}\left(\beta - \beta_{tr}\right)^n \quad \text{and} \quad F(\zeta) = \sum_{n=0}^{\infty} \frac{F^n(\zeta_{tr})}{n!}\left(\zeta - \zeta_{tr}\right)^n \tag{C.1}$$

The first-order *Taylor* series expression can be obtained by only retaining the terms up till n=1. The higher-order terms are therefore neglected. The first order Taylor series expression for β and ζ are provided in Eq. C.2 [34].

$$F(\beta) = F(\beta_{tr}) + F(\beta_{tr})\left(\beta - \beta_{tr}\right) \quad \text{for n = 1} \quad \text{and} \quad F(\zeta) = F(\zeta_{tr}) + F(\zeta_{tr})\left(\zeta - \zeta_{tr}\right) \quad \text{for n = 1} \tag{C.2}$$

The first order Taylor series expressions do depend on the incremental changes, namely $(\beta - \beta_{tr})$ or $(\zeta - \zeta_{tr})$. These incremental changes can be denoted as $\Delta\beta$ or $\Delta\zeta$ respectively, and are small deviations from their corresponding trim conditions. In addition to this it should be noted that β_{tr} and ζ_{tr} do not vary over time, hence β'_{tr} and ζ'_{tr} (and higher order derivatives) are set equal to zero. As mentioned previously, the linearisation procedure can be regarded as valid when the small angle approximation does hold, thus

$$\cos(\beta) = 1, \quad \sin(\beta) = \beta, \quad \cos(\zeta) = 0 \quad \text{and} \quad \sin(\zeta) = \zeta \tag{C.3}$$

The small angle assumption shall be applied after linearising the coupled flap-lag equations of motion. This will assure that important terms will be retained, as being stressed in [34]. Applying small angle approximation principle before conducting the linearisation procedure will yield a loss in first order terms of the coupled nonlinear flap-lag EOM. Therefore it is a natural choice of first conducting the first order Taylor series expansion before incorporating the small angle approximation principle.

D

Dynamic Behaviour Rotorcraft

With the inclusion of lead-lag dynamics, it will be of great interest to determine whether the implementation is correct. Therefore, it is a natural choice to consider the dynamic behaviour of the model. In Fig. D.1 the modes of motion of the main simulation model are provided. It can be observed that for $C_\zeta = 0.02$, the modes of motion for lead-lag dynamics are located at the expected poistion in the complex plane. This is based upon reference data from [17, 34, 40]. Even though $C_\zeta = 0.02$ will be considered a variable throughout the analysis, it is still of great importance to assure that the modes of motion related of lead-lag are correct.]

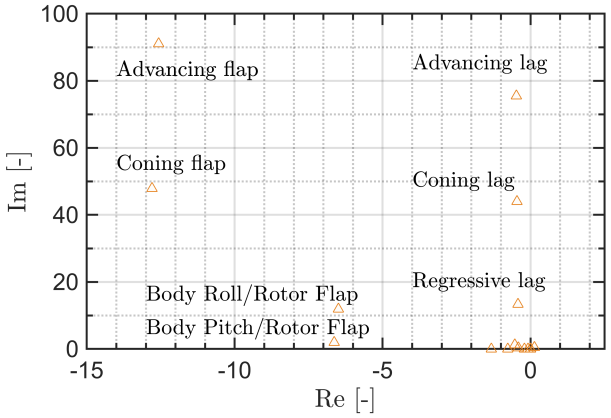

Figure D.1: Modes of motion of the MBB Bo 105 rotorcraft model trimmed at 10 m/s forward flight and 1000 m altitude.

E

Helicopter Data of MBB Bo 105

This appendix provides helicopter data of the MBB Bo 105 used for simulations. Rotorcraft data was obtained from [38, 39, 43, 44, 46, 55]. It should be noted that for the actuator limitations rate limit was used from [46], which did incorporate the rate limit of the Bell 412 helicopter.

Table E.1: Main rotor parameters of MBB Bo 105.

description of parameter	symbol	value	unit
Rotational speed	Ω	44.4	rad/s
Rotor radius	R	4.91	m
Steady-state coning angle	$\beta_{ss} = \beta_0$	2.5	deg
Number of blades	b/N	4	-
Equivalent blade chord	c_e	0.27	m
Zero lift profile drag coefficient $C_{D,0}$ in ($C_D = C_{D,0} + C_{D,1}\alpha^2$)	C_{D_0}	0.011	-
Profile drag coefficient $C_{D,1}$ in ($C_D = C_{D,0} + C_{D,1}\alpha^2$)	C_{D_1}	0.4	-
Non-dimensional inflow velocity for hover	λ_i	0.0495	-
Static blade moment (approximated $m_{\text{bl}}R/2$)	m_s	50	mkg
Blade lift curve slope	C_{L_α}	6.11	rad^{-1}
Linear blade twist	θ_{tw}	-0.1396	rad
Blade mass	m_{bl}	27.3	kg
Blade moment of inertia about its flapping hinge	I_{bl}	231.7	kgm^2
Equivalent hinge offset ratio	ϵ_β / e_β	0.14	-
Rotor shaft tilt angle	γ_s	0.0524	rad
Longitudinal position with respect to the helicopter c.g.	l	-0.00761	m
Lateral position with respect to the helicopter c.g.	l_1	0.02995	m
Vertical position with respect to the helicopter c.g.	h	0.94468	m

Table E.2: Tail rotor parameters of MBB Bo 105.

description of parameter	symbol	Value	unit
Rotational speed	Ω_{tr}	233.1	rad/s
Rotor radius	R_{tr}	0.95	m
Number of blades	N_{tr}	2	-
Equivalent blade chord	$c_{e_{tr}}$	0.18	m
Blade lift curve slope	$C_{L_{\alpha,\text{tr}}}$	5.70	rad^{-1}
Main rotor downwash factor at the tail rotor	K_{tr}	1	-
Time constant of the induced inflow	$\tau_{\lambda_{0,\text{tr}}}$	0.1	s
Longitudinal position with respect to the helicopter c.g.	l_{tr}	6.00965	m
Vertical position with respect to the helicopter c.g.	h_{tr}	1.05418	m

Table E.3: Fuselage parameters of MBB Bo 105.

description of parameter	symbol	value	unit
Parasite drag area	F_0	1.3	m^2
Eq. volume in the horizontal plane with only circular sections	V_{fus_M}	6.126	m^3
Eq. volume in the lateral plane with only circular sections	V_{fus_N}	25.525	m^3
Incidence angle for zero pitch moment	$\alpha_{fus,M=0}$	0	rad
Correction coefficient for moment calculation	K_{fus}	0.83	-

Table E.4: Horizontal tail parameters of the MBB Bo 105.

description of parameter	symbol	value	unit
Surface area	S_{ht}	0.803	m^2
Surface lift curve slope	$C_{L_\alpha,ht}$	4.0	rad^{-1}
Built-in surface incidence	α_{hto}	0.0698	rad
Correction coefficient in the pitch moment	K_{ht}	1.5	-
Longitudinal position with respect to the helicopter c.g.	l_{ht}	4.548	m

Table E.5: Vertical tail parameters of the MBB Bo 105.

description of parameter	symbol	value	unit
Surface area	S_{vt}	0.805	m^2
Surface lift curve slope	$C_{L_\alpha,vt}$	4.0	rad^{-1}
Built-in surface incidence	β_{vto}	-0.0812	rad
Correction coefficient in the pitch moment	l_{vt}	5.416	m
Longitudinal position with respect to the helicopter c.g.	h_{vt}	0.970	m

Table E.6: Actuator limitations of the MBB Bo 105.

description of parameter	symbol	Min. saturation limit [deg]	Max. saturation limit [deg]	Rate limit [deg/sec]
Collective pitch main rotor	θ_0	-0.2	20.0	16.0
Longitudinal cyclic	θ_{1s}	-6.0	11.0	28.8
Lateral cyclic	θ_{1c}	-5.7	4.2	16.0
Collective pitch tail rotor	$\theta_{0,tr}$	-8.0	20.0	32.0

Table E.7: Additional parameters of the MBB Bo 105.

description of parameter	symbol	value	unit
Normalised flapping frequency	$\lambda_\beta = 1 + \frac{3}{2}\frac{\epsilon_\beta}{1-\epsilon_\beta}$	1.12	-
Center-spring stiffnes	$K_\beta = (\lambda_\beta^2 - 1) I_\beta \Omega^2$	113	$kNm \cdot rad^{-1}$
Main rotor Lock number	$\gamma = \frac{\rho C_{L_\alpha} c_e R^4}{I_\beta}$	5.0692	rad^{-1}
Main rotor solidity	$\sigma = \frac{N c_e}{\pi R}$	0.007	-
Tail rotor solidity	$\sigma_{tr} = \frac{N_{tr} c_{e_{tr}}}{\pi R_{tr}}$	0.1206	-

Table E.8: Mass and inertia of the MBB Bo 105.

description of parameter	symbol	value	unit
Total mass	m	2200	kg
Total weight	W	21574	N
Inertia tensor	J	$\begin{bmatrix} 1433 & 0 & -660 \\ 0 & 4973 & 0 \\ -660 & 0 & 4099 \end{bmatrix}$	$kg \cdot m^2$